Sveučilište u Zagrebu

Farmaceutsko-biokemijski fakultet

Tomislav Friganović

UTJECAJ STUPNJA SIJALINIZACIJE LJUDSKOG SERUMSKOG TRANSFERINA NA TERMODINAMIKU VEZANJA ŽELJEZA

DOKTORSKI RAD

Zagreb, 2025.

Sveučilište u Zagrebu

Farmaceutsko-biokemijski fakultet

Tomislav Friganović

UTJECAJ STUPNJA SIJALINIZACIJE LJUDSKOG SERUMSKOG TRANSFERINA NA TERMODINAMIKU VEZANJA ŽELJEZA

DOKTORSKI RAD

Mentor:
izv. prof. dr. sc. Tin Weitner

Zagreb, 2025.

University of Zagreb

Faculty of Pharmacy and Biochemistry

Tomislav Friganović

INFLUENCE OF THE DEGREE OF SIALYLATION OF HUMAN SERUM TRANSFERRIN ON THE THERMODYNAMICS OF IRON BINDING

DOCTORAL DISSERTATION

Supervisor
Professor Tin Weitner, PhD

Zagreb, 2025.

Informacije o mentoru

Rad je predan na ocjenu Fakultetskom vijeću Farmaceutsko-biokemijskog fakulteta Sveučilišta u Zagrebu radi stjecanja akademskog stupnja doktora znanosti iz područja biomedicine i zdravstva, polje farmacija, grana farmacija.

Doktorski rad je izrađen na Zavodu za opću i anorgansku kemiju Farmaceutsko-biokemijskog fakulteta Sveučilišta u Zagrebu, pod mentorstvom izv. prof. dr. sc. Tina Weitnera. Rad je izrađen u okviru doktorskog studija Farmaceutsko-biokemijske znanosti Farmaceutsko-biokemijskog fakulteta Sveučilišta u Zagreb, a financiran je iz projekta Hrvatske zaklade za znanost naziva „Glikozilacija serumskog transferina kao faktor u mehanizmu prijenosa željeza“ (HRZZ-UIP-2017-05-9537).

ZAHVALE

Riječi često ne znače mnogo, ali zato djela govore sve – oni kojima sam istinski zahvalan toga su itekako svjesni.

SAŽETAK

Ljudski transferin je glikoprotein čija je glavna uloga prijenos željeza u krvi i tkivima; sastoji se od dvije domene s veznim mjestima za ione željeza(III). Željezo(III) tvori vrlo stabilan kompleks s transferinom putem koordinacije s aminokiselinama i sinergističkim karbonatnim ionom. Otpuštanje željeza iz transferina potpomognuto je sniženim pH endosoma i vezanjem na transferinski receptor. Transferin je visokoglikozilirani glikoprotein s vezanom sijalinskom kiselinom; u zdravih osoba najčešća glikoforma ima dva oligosaharidna lanca s četiri sijalinske kiseline. Smanjena sijalinizacija transferina opažena je u patološkim stanjima poput alkoholizma, genetskih poremećaja i tijekom sepse. Promjene u sijalinizaciji nisu nužno vezane uz patološka stanja; primjerice, tijekom trudnoće povećava se udio visoko sijaliniziranog transferina, što se nakon poroda normalizira. Utjecaj sijalinizacije transferina može značajno utjecati na prijenos i metabolizam željeza u ljudskom organizmu. U ovom radu optimizirana je priprava asijalotransferina i razvijena kromatografska metoda temeljena na gradijentu pH za testiranje kvalitete desijalinizacije i razdvajanje glikoformi transferina. Optimizacijom enzimske desijalinizacije dobiveno je oko 100 puta više asijalotransferina nego što deklarira proizvođač. Kromatografskom metodom uspješno je detektiran i razdvojen nativni i asijalotransferin. Viskoprotočnim fluorimetrijskim mjerenjima određene su konstante ravnoteže kojima je kvantificiran afinitet dvaju veznih mjesta nativnog i asijalotransferina prema željezu(III). Utvrđeno je da asijalotransferin ima veći afinitet prema željezu od nativnog transferina, oko tri puta veći pri fiziološkom pH i oko deset puta veći pri približnom pH endosoma. Povećana efikasnost asijalotransferina u kiselim uvjetima može biti povezana s brzom desijalinizacijom tijekom sepse, kao odgovorom organizma koji uskraćuje željezo bakterijama. Snižavanje pH smanjuje konstante ravnoteže za obje forme transferina i oba vezna mjesta. Zapažene su promjene kooperativnosti pri vezanju, posebno je zanimljiva iznimna pozitivna kooperativnost opažena pri pH = 6,8. Razvijena je i nova metoda korekcije učinka unutarnjeg filtra (IFE) za čitače mikrotitarskih pločica, nužna za kvalitetna fluorimetrijska istraživanja. Nova metoda IFE-korekcije, omogućena podešavanjem visine optičkog elementa čitača, pokazala se pogodnom za fluorimetrijske titracije transferina i kompleksa željeza(III) s nitrilotrioctenom kiselinom, bez potrebe za mjerenjem apsorbancije. Metoda je također primjenjiva i u neprozirnim mikrotitarskim pločicama.

Ključne riječi: ljudski transferin, željezo(III), glikozilacija, neuraminidaza, kromatografija, fluorimetrija, IFE-korekcije, konstante ravnoteže

SUMMARY

Introduction

Human transferrin is an essential glycoprotein present both in blood and tissues; it has an important role in iron transport within the human body. Structurally, transferrin is composed of two similar domains, each containing a single binding site for iron(III) ion (or other metal ions) which allows the protein to bind up to two iron ions simultaneously. The iron(III) ions form a distorted octahedral coordination complex with four amino acid residues of transferrin. The two oxygen atoms from a synergistic carbonate ion are bound to the remaining two binding sites. The presence of a synergistic anion is crucial for the formation of a stable complex. Under physiological conditions, transferrin forms a very stable complex with iron(III). The release of iron from this stable complex is facilitated both by the lowered pH within endosomes and by the binding of transferrin to the transferrin receptor. This mechanism ensures that iron is delivered efficiently to cells while minimizing free iron levels in circulation. Free iron, specifically in the form of hexaaquairon complexes, is known to facilitate harmful free radical reactions. Transferrin is a highly glycosylated glycoprotein, with sialic acid residues predominantly attached to the termini of its glycan branches. In healthy individuals, the most common glycoform of transferrin contains two biantennary oligosaccharide chains with a total of four sialic acid residues. Significant changes in the sialylation of transferrin, particularly decreased sialylation, have been observed in certain pathological conditions. For instance, a pronounced reduction in transferrin sialylation is a biomarker for chronic alcoholism. Decreased sialylation can also result from some specific genetic disorders known as congenital disorders of glycosylation. Acute decreases in sialylation can occur during sepsis, potentially as a rapid response mechanism of the body. Interestingly, changes in transferrin sialylation are not always associated with disease states; during pregnancy, there is a gradual increase in the proportion of highly sialylated transferrin, which quickly returns to normal levels postpartum. Transferrin sialylation is a potentially significant physiological parameter that may significantly influence iron metabolism and transport in the human body. Understanding how variations in sialylation affect transferrin's affinity towards iron(III) is important for better understanding of iron homeostasis and its disruption in various diseases.

Methods and materials

Firstly, the preparation of asialotransferrin, the desialylated form of transferrin, was optimized. An enzymatic desialylation process was employed using sialidase (neuraminidase) to selectively remove sialic acid residues from native transferrin. The goal was to significantly increase the yield of asialotransferrin product beyond what is typically provided by commercial suppliers. This was done by increasing the mass concentration of protein solutions, buffer concentrations and contact time. Two commercially available enzyme products, GlycoCleave® and SialEXO®, were used. Both products contain immobilized neuraminidase enzyme coated on the surface of agarose beads. Multiple desialylation cycles were performed in succession. A pH-gradient chromatographic method suitable for assessing the quality of enzymatic desialylation and for separating different transferrin glycoforms was developed. This method utilized pISep buffers with high buffering capacity (in wide pH range) to maintain a stable pH gradient during chromatography, which enables effective separation based on the isoelectric points of the glycoforms. The chromatographic method was initially developed using ÄKTA Start FPLC device and two HiTrap Q HP columns connected in a series. To further improve the separation, a more powerful chromatographic system consisting of ÄKTA Purifier 10 instrument paired with SOURCE™ 15Q 4.6/100 PE chromatographic column was used. In order to verify the quality of both the enzymatic sialylation optimization and the separation of native from asialotransferrin, a glycan analyses of protein samples were performed. Glycan analysis starts by releasing glycans from proteins using the enzyme PNGase F, which specifically cleaves N-glycans. After release, glycans are labeled with a fluorescent marker, such as 2-aminobenzamide (2-AB). The labeled glycans are then purified through *Hydrophilic Interaction Liquid Chromatography - Solid Phase Extraction* (HILIC-SPE) and separated using *Ultra High Performance Liquid Chromatography* (UHPLC). The glycans are then analyzed *via* mass spectrometry, thus obtaining complete glycan profiling of the protein sample. High-throughput fluorimetric measurements were conducted in microtiter plates in order to determine the equilibrium constants that quantify the affinity of the two iron-binding sites of both the native transferrin and the asialotransferrin toward iron(III) ions. Fluorimetric titrations were performed with the Opentrons OT-2 pipetting robot which was programmed using the custom Python scripts. Titrations were executed for both the native and asialotransferrin solutions at 5 distinct pH values (7,4, 6,8, 6,5, 6,2 and 5,9). In each titration, variable amounts of FeNTA complex were mixed with the constant amounts of protein. Constant amounts of NTA, PIPES buffer and potassium carbonate salt were present in each titration. However, NTA varied

throughout the titrations depending on the pH conditions. After 24 hours incubation at 25 ˚C, the fluorescence and the absorbance spectra were measured using the Tecan Spark M10 microplate reader. Fluorescence was measured with excitation wavelength set at λ = 280 nm, and the emission at λ = 335 nm. In addition, prior to the titration experiments, molar extinction coefficients of asialotransferrin were determined and molar extinction coefficients of native transferrin were redetermined using a modified Edelhoch method. A critical aspect in ensuring the quality of fluorimetric data is the correction for the *Inner Filter Effect* (IFE). IFE arises due to non-uniform attenuation of excitation and/or emission radiation within the sample. For this purpose, a novel correction method suitable for microplate readers was developed. The method involved simple adjustment of the optical element's height within the instrument. This method does not require absorbance measurements and is applicable even when using inexpensive, non-transparent microtiter plates. The intrinsic fluorescence quenching that occurs when iron binds to human transferrin was successfully modeled using a binding polynomial for two independent iron-binding sites. The applied iterative approach provided a general solution to determine both the apparent and conditional thermodynamic equilibrium constants by fitting the experimental data with only two parameters.

Results

The optimization of the enzymatic desialylation process resulted in approximately 100 times higher yield of asialotransferrin than what is declared by the manufacturer. This was primarily achieved by increasing the concentration of transferrin fourfold and by increasing the contact (reaction) time from 30 min to 24 h. The desialylation process proved to be effective even after 19 consecutive desialylation cycles. To counteract the acidification of the solution resulting from enzymatic desialylation, the buffer concentration was increased to maintain a nearly constant pH throughout the process. This optimized method allows for the preparation of substantial amounts of asialotransferrin in a relatively short time frame. The simultaneous use of multiple enzyme-containing columns appears to be an effective strategy. The pH-gradient chromatographic method proved successful in detecting and separating native transferrin and asialotransferrin. The use of pISep buffers with high buffering capacity ensured a stable pH gradient, allowing for clear resolution of transferrin forms based on their differing isoelectric points. Method proved to be especially useful for monitoring the quality of the desialylation process. The newly developed method for correcting the IFE was enabled by a straightforward adjustment of the optical element's height in the microplate reader. The method proved

generally suitable for a variety of fluorimetric uses including fluorimetric titrations involving transferrin and iron(III) complexes. Notably, the method does not necessitate absorbance measurements, which allows usage of the (affordable) non-transparent microplates. Moreover, this correction method is suitable even for very absorptive solutions. Fluorimetric titrations were performed in order to subsequently calculate the equilibrium constants quantifying the formation of iron(III)-transferrin complexes at different pH values. The results showed that asialotransferrin has a higher affinity for iron compared to native transferrin. This preference is approximately three times greater at physiological pH (7,4) and up to ten times greater at the pH near endosomal (5,9). The increased preference of asialotransferrin (compared to native transferrin) towards iron(III) was also observed in the previous calorimetric study. Lowering the pH also led to a decrease in the equilibrium constants for both forms of transferrin and for both binding sites, indicating that acidic conditions affect iron binding affinity overall. Additionally, notable changes in cooperativity during iron binding were observed. Specifically, an exceptional positive cooperativity was detected at pH 6,8.

Conclusions

The optimization of the enzymatic desialylation of human transferrin proved to be very effective, yielding a very significant increase in the total amount of asialotransferrin that can be produced with a single enzyme-containing column. The development of the pH-gradient chromatographic method allowed for effective separation and analysis of transferrin glycoforms. This also provided a useful quality control tool of the desialylation process. Preliminary results indicate that this method can even be useful for separating multitude of transferrin glycoforms, including some rare forms which were prepared by intentional incomplete desialylation. The new IFE-correction method proved to be generally suitable for a variety of fluorimetric measurements performed on microplate reader. The method was also useful in correcting the IFE in fluorimetric titration experiments containing transferrin. To the author's knowledge, this is the first method developed specifically for microplate readers, and it has proven cost-effective by allowing the use of less expensive non-transparent microplates. The findings indicated that asialotransferrin exhibits a substantially higher affinity for iron(III) compared to native transferrin, particularly under relatively acidic conditions similar to those in endosomes. This increased affinity may play a significant role in the body's acute response to infection. For instance, during sepsis, by effectively withholding iron from invading pathogens and thus inhibiting their proliferation. The apparent significant changes in binding

cooperativity, notably the significant positive cooperativity at pH 6,8, improves general understanding of how iron binds to transferrin forms through allosteric mechanisms. These results may be important for better understanding the role of transferrin sialylation in regulating iron metabolism. Better understanding the link between transferrin sialylation and iron-binding affinity may allow for an improved treatment of iron metabolism disorders.
Keywords: human transferrin, iron(III), glycosylation, neuraminidase, chromatography, fluorimetry, inner filter effect corrections, equilibrium constants

SADRŽAJ

1. UVOD

1.1. Otopinska kemija iona željeza

Željezo je element atomskog broja 26 koji pripada skupini prijelaznih metala. Element je geološki vrlo zastupljen te je iznimno značajan kako za industriju (1) tako i za gotovo sve organizme (2).

Elementarno željezo i njegovi oksidi/hidroksidi u pravilu su vrlo slabo topljivi u vodi, a dobro topljivi u vrlo kiselim vodenim otopinama (3,4). U vidu otopinske kemije, najzastupljenija oksidacijska stanja željeza su Fe(II) ([Ar] $3d^6$) i Fe(III) ([Ar] $3d^5$); viša oksidacijska stanja su uglavnom nestabilna, ali postoje iznimke poput vrlo stabilnih kavezastih kompleksa Fe(IV) (5,6). Uz elementarno željezo i prethodno spomenuta oksidacijska stanja, željezo može postojati i u −2, +1, +5 +6 i +7 oksidacijskim stanjima (6–9).

Ioni željeza tvore razne koordinacijske komplekse s mnoštvom različitih liganada. U slučajevima +2 i +3 oksidacijskih stanja centralnih metalnih iona željeza, oktaedarski i tetraedarski kompleksi vrlo su česti, a kvadratni razmjerno rjeđi (naročito visokospinski) (9–12). Osim prethodno navedenih koordinacija, različiti koordinirani ioni (ili atomi) željeza mogu biti i drugih geometrija kao što su primjerice: trigonsko bipiramidalna, kvadratno piramidalna, dodekaedarska i trigonska (9,10). Ovisno o njegovom oksidacijskom stanju i o vrsti liganda, željezo tvori visoko- i niskospinske komplekse (9). U slučaju visokospinskih kompleksa opažena je Jahn-Tellerova deformacija (13,14). Željezo tvori komplekse sa: sigma- donorskim, pi- donorskim i akceptorskim, ambidentatnim, kelatirajućim i makrocikličkim ligandima (9,15–20). Vrlo zanimljivi su i takozvani „sendvič kompleksi“ (primjerice feroceni) u kojima je željezo smješteno između dvaju planarnih liganada odnosno između dvaju aromatskih prstenova (21–23).

Vodene otopine iona Fe(II) i Fe(III) tvore heksakoordinirane oktaedarske vrste odnosno heksaakva komplekse. S obzirom na snažnu polarizacijsku moć centralnog iona željeza, uslijed smanjenja elektronske gustoće kisik-vodik veze koordinirajuće vode, navedeni kompleksi često djeluju kiselo i načelno su podložni hidrolizi (24–26). Često je potrebno održavati razmjerno niske pH vrijednosti radnih otopina kako bi se izbjegla neželjena hidroliza iona željeza. Problemi hidrolize Fe(III) iona posebno su značajni pri višim pH vrijednostima, primjerice pri fiziološkom pH koji je oko 7,4, prilikom čega može doći do nastanka netopljivih hidroksida (27). Primjenom prikladnih kelatora također je moguće stabilizirati vodene otopine Fe(III) iona

(27,28). Zanimljivo je da se primjenom odgovarajućih kelatora može značajno povećati redoks stabilnost određenih iona željeza, smanjujući tako njihovu sklonost ka redukciji ili oksidaciji (29,30).

1.2. Fiziološki značaj željeza u čovjeka

Premda željezo spada među najzastupljenije metale u prirodi, ono je često jedan od ograničavajućih faktora rasta organizama (31). Srž problema nalazi se samoj kemiji željeza odnosno u njegovoj sklonosti da vrlo lako stvara teško topljive hidrokside/okside. Takve supstancije predstavljaju biološki slabo dostupno željezo za čovjeka i glavninu viših organizama (32). Neki od načina kojim niži organizmi apsorbiraju željezo je izlučivanjem siderofora, vrlo efikasnih kelatora željeza(III) (33–35). Kvasci posjeduju razmjerno sofisticiran mehanizam prikupljanja i prijenosa željeza pomoću Fet3p i Ftr1p proteina (36–39). Fet3p inicijalno oksidira željezo(II) u željezo(III) koje zatim Ftr1p transportira u stanicu. Ferireduktaze na površini stanice reduciraju željezo(III) te ga time čine topljivim i dostupnim za transport (40–42).

Zanimljivo je da čovjek posjeduje mogućnost apsorpcije i daljnjeg iskorištenja anorganskog (nehemskog) željeza, putem različitih prehrambenih namirnica kao što su jaja i povrće. Takvo željezo se apsorbira u dvanaesniku pomoću enterocita. Proces apsorpcije uključuje redukciju željeza(III) u željezo(II) djelovanjem enzima ferireduktaze, također poznate kao citokrom b reduktaza 1 (Cybrd1 ili DcytB). Nakon redukcije, dvovalentni metalni transporter 1 (engl. *Divalent Metal Transporter 1*, DMT1) pospješuje transport željeza(II) kroz staničnu membranu (43). Ipak, glavninu željeza čovjek dobiva iz hemskog željeza. Premda je postotak unosa anorganskog željeza oko 60 %, ono se slabo apsorbira (44).

Većina željeza u ljudskom organizmu nalazi se u jetri (uglavnom oko 60 %) od čega je čak oko 95 % željeza pohranjeno kao feritin u hepatocitima, a manja količina kao hemosiderin, produkt razgradnje feritina (44). U čovjeka ne postoje regulatorni mehanizmi izlučivanja željeza; homeostaza je regulirana apsorpcijom (45). Neadekvatna apsorpcija željeza vodi ka anemiji; pretjerana apsorpcija može biti uzrokovana hemokromatozom, bolešću koja dovodi do prekomjernog nakupljanja željeza u tijelu (45–47). Kelatori poput deferoksamina i deferiprona koriste se za tretiranje preopterećenja željezom tako što se vežu za višak željeza u tijelu čime olakšavaju njegovo izlučivanje (20,48).

Željezo je ključno za prijenos i skladištenje kisika u ljudskom tijelu. Ono je sastavni dio hemoglobina, proteina prenosioca kisika prisutnog u crvenim krvnim stanicama (eritrocitima)

(49–51). Hemoglobin je građen od četiri podjedinice, od kojih svaka sadrži po jedan polipeptidni lanac i po jednu prostetičku, hemsku skupinu (51–54). Hemsko željezo (Fe(II)) kompleksirano je s četiri atoma dušika porfirinskog prstena te dušikovim atomom proksimalnog histidina. Na preostalo šesto koordinacijsko mjesto deformiranog oktaedra može se (reverzibilno) vezati molekula kisika (55,56). Hemoglobin je također i sekundarni prenositelj CO_2 u ljuskom organizmu; vezanjem CO_2 na α-amino skupine terminalnih završetka globinskih lanaca hemoglobina nastaje karbaminohemoglobin (57,58). Osim hemoglobina, željezo je i bitan konstituent mioglobina koji se nalazi u ljudskim mišićima. On pomaže u prijenosu i skladištenju kisika unutar mišićnih stanica (59,60).

Željezo je veoma bitno za pravilnu funkciju raznih enzima, ono je komponenta citokroma, enzima koji imaju ključnu ulogu u mitohondrijskoj proizvodnji energije i staničnom disanju (61,62). Željezo je također inkorporirano u katalazama i peroksidazama, enzimima koji štite stanice od oksidativnog stresa (63–65). Ono se nalazi i u ribonukleotid reduktazi, enzimu važnom za sintezu DNA redukcijom ribonukleotida u deoksiribonukleotide (66–68).

Koenzimi željeza sudjeluju u sintezi aminokiselina, sterola, kolagena i proteina općenito (69,70). Željezo je također važno za sintezu steroidnih hormona i metabolizam lipida kao i za sintezu hormona štitnjače (71–76). Bitno je za pravilnu funkciju imunološkog sustava te za sintezu neurotransmitera kao što su: dopamin, serotonin i noradrenalin (77–80).

1.3. Uloga i svojstva ljudskog transferina

1.3.1. Uloga, građa i vezanje željeza

Transferin je jedan od glavnih prijenosnika željeza u ljudskom organizmu. Ovaj transportni glikoprotein može na sebe (reverzibilno) vezati do dva iona željeza(III); on ima važnu ulogu u transportu željeza iz probavnog trakta do stanica (81). Sintetizira se primarno u jetri (82). Adekvatnom ekspresijom transferinskih receptora, stanice osiguravaju potreban unos željeza (83,84). Vrijeme poluživota glikoziliranog transferina u serumu je 7 do 10 dana (85).

Transferin je visoko glikozilirani globularni glikoprotein približne molekulske mase oko 79 kDa (28,86). Sastavljen je od dvaju domena: C- domena sadrži 343 aminokiseline, a N-domena 336. Svaka domena dodatno se dijeli na dvije poddomene (C1 i C2 odnosno N1 i N2) (81,87). Domene su povezane kratkim peptidnim slijedom; dodatno su povezane s 19 intralančanih disulfidnih veza (88). N- domena sastoji se od 14 alfa-zavojnica i 13 beta-lanaca,

a C- domena od 17 alfa-zavojnica i 13 beta-lanaca (89). Svaka domena sadrži po jedno hidrofilno mjesto na koje se može vezati ion željeza(III) (88).

Vezanje se (u obje domene) odvija preko četiriju aminokiselinskih liganada: histidina, asparaginske kiseline i dva tirozina (88). Vezanjem željeza nastaje koordinacijski kompleks geometrije deformiranog oktaedra (90). Na dva od ukupno šest koordinacijskih mjesta didentatno se preko kisikovih atoma veže karbonatni anion (detaljnije obrazloženje navedeno je u kasnijem potpoglavlju rukopisa). Histidin se veže preko dušikovog atoma (imidazolnog prstena), a asparaginska kiselina i tirozin preko atoma kisika (88,91). S obzirom da transferin (Tf) može kompleksirati do dva iona željeza(III), postoje četiri različite izoforme ovisno o sadržaju željeza: apotransferin (bez vezanog željeza), Fe_CTF ili Fe_NTF (jedno željezo vezano po transferinu na -C ili -N kraju) i Fe_2TF (holotransferin, oba vezna mjesta popunjena) (28). Važno je napomenuti da transferin nije potpuno simetrična molekula odnosno -C i -N domene nisu kemijski ekvivalentne, već se one donekle razlikuju u afinitietima i kinetici vezanja željeza, bez obzira na to što je željezo u oba slučaja koordinirano istim aminokiselinama (28,84,92,93). Osim željeza, transferin može tvoriti komplekse s raznim drugim metalnim ionima (ponekad ireverzibilno) (89,94–97). Poznato je i da kompleksiranje pojedinih iona željeza (ili drugih metala) transferinom uzrokuje značajne konformacijske promjene samog transferina (81,94,98,99).

1.3.2. Značaj karbonata i drugih (ne)sinergističkih iona

Kao što je prethodno spomenuto, dva od ukupno šest koordinacijskih mjesta deformiranog oktaedra transferinskog kompleksa željeza(III) zauzima sinergistički karbonat (100,101). Vezanje karbonata inducira značajne konformacijske promjene transferina; on prelazi iz takozvane „otvorene“ u „zatvorenu“ strukturu. Odvijanje te konformacijske promjene ključno je za posljedičnu visoku stabilnost koordinacijskog kompleksa (102). Kompleks je također dodatno stabiliziran vodikovim vezama koje tvori karbonatni ligand. Dolazak karbonata na vezno mjesto unutar N2 odnosno C2 poddomena prethodi nastanku kompleksa odnosno stvaranju veza željeza s aminokiselinama (102). Ipak, kompleks može nastati i bez prisustva karbonata ili drugih sinergističkih aniona. U tim slučajevima željezo je mnogo slabije vezano odnosno kompleks je prilično labilan (103). Važno je napomenuti da je prisustvo ili nedostatak dvostrukog negativnog naboja karbonata zasigurno značajan faktor koji utječe na ukupni naboj kompleksa i centralnog metalnog iona time posredno utječući na interakciju željeza s aminokiselinskim ligandima. Karbonat može imati ključnu ulogu i prilikom vezanja

nekih drugih metalnih iona na transferin. Primjerice, slično kao i kod željeza, stvaranje stabilnog kompleksa transferina s kromom(III) također je pogodovano sudjelovanjem karbonatnog liganda (97,102).

Osim karbonata, moguće je vezanje drugih sinergističkih aniona na centralni metalni ion transferinskog kompleksa (101). Neki od primjera sinergističkih aniona su: oksalat, salicilat, malonat, nitrilotriacetat i tioglikolat. Potencijalni sinergistički anioni u pravilu trebaju sadržavati karboksilnu skupinu preko čijih kisikovih atoma se didentatno veže željezo(III) u transferinski kompleks. Također, sinergistički anion ne smije biti velika molekula, jer je prostor oko veznog mjesta širine približno 7 Å (104). Opaženo je također da supstitucija karbonata drugim sinergističkim anionima može imati značajan utjecaj na kinetiku otpuštanja željeza iz transferinskog kompleksa (105,106). Pitanje je koliko su fiziološki značajni transferinski kompleksi različitih sinergističkih iona, s obzirom na to da su neke od tvari koje fungiraju kao potencijalni sinergistički ioni vrlo slabo zastupljene u ljudskom organizmu. Oksalat je potencijalno fiziološki relevantan, posebno u slučajevima hiperoksalemije, koja može biti posljedica bubrežne insuficijencije, akutnog trovanja antifrizom (etilenglikolom) ili neposrednog trovanja oksalatima (84,107–109).

Ioni koji direktno ne sudjeluju u tvorbi koordinacijskih kompleksa željeza s transferinom, ali imaju utjecaja na fizičko-kemijska svojstva tih kompleksa nazivaju se nesinergističkim ionima. Vezanje nesinergističkih iona odvija se razmjerno blizu veznom mjestu željeza(III). Nesinergistički ioni, poput fosfata i sulfata, vežu se na kinetički značajno anionsko vezno mjesto (engl. *KInetically Significant Anion Binding Site*, KISAB) (110,111). Nesinergistički ioni su alosterički regulatori i, kao što se može pretpostaviti prema nazivu mjesta njihovog vezanja, njihov utjecaj je primarno kinetičke prirode, poglavito u vidu kinetike otpuštanja željeza (111). Prisustvo nesinergističkih iona uvjetuje otvoreniju konformaciju transferina čime se pospješuje otpuštanje iona željeza(III) iz proteinskog kompleksa. Promjene su posljedica razlika u elektrostatskim interakcijama i tvorbi vodikovih veza. Pretpostavlja se i značajan utjecaj nesinergističkih aniona na takozvani dilizinski okidač (engl. *dilysine trigger*). Nesinergistički anioni mogu ometati ključne elektrostatske interakcije i vodikove veze između aminokiselina LYS206 i LYS296 (110,112). Nesinergistički ioni također mogu biti značajni faktori i u slučaju vezanja drugih metala osim željeza (113).

1.3.3. Značaj pH i transferinskih receptora

Poznato je da kinetički i termodinamički parametri vezanja odnosno otpuštanja transferinskog željeza(III) ovise o pH uvjetima (28,93,114,115). U ljudskom organizmu, željezo(III) izuzetno se lako veže na transferin pri fiziološkim uvjetima pH (≈ 7,4). Budući da željezo pri tim uvjetima formira vrlo stabilan kompleks s transferinom, njegovo otpuštanje iz kompleksa ne odvija se lako te ono zahtijeva promjenu fizičko-kemijskih uvjeta u otopini ili direktnu kemijsku interakciju s drugim molekulama (115,116).

Kod čovjeka, stanicama potrebno željezo otpušta se u endosomu. Proces unosa transferina u stanicu odvija se tako da se molekule transferina primarno vežu na transferinske receptore (TfR_x), koji se nalaze s vanjske strane stanične membrane. Navedeni receptorski kompleks potom prelazi kroz membranu u samu stanicu. Unutar stanice, receptorski kompleks završava u endosomu, gdje se, pri uvjetima sniženog pH (≈ 5,5), odvija otpuštanje željeza (116,117).

Postoje dvije vrste transferinskih receptora; TfR_1 i TfR_2. TfR_1 je primarno odgovoran za unos željeza u stanicu putem endocitoze transferinsko-receptorskog kompleksa. Taj receptor široko je rasprostranjen i eksprimiran na većini ljudskih stanica (118–121). Unos željeza u stanicu reguliran je ekspresijom ovog receptora; ako stanici nedostaje željeza, povećava se njegova proizvodnja i obrnuto. Ekspresija receptora regulirana je preko IRP (engl. *Iron Regulatory Protein*) proteina koji se vežu na mRNA ukosnice, tzv. željezove responzivne elemente (engl. *Iron Response Elements*, IRE), čime stabiliziraju mRNA, što posljedično povećava sintezu transferina (122,123). TfR_1 je posebno zastupljen na membranama stanica kojima su za pravilnu funkciju i razvoj potrebne velike količine željeza, poput eritroidnih prekursora i stanica posteljice (placente). Također je vrlo prisutan u hepatocitima, retikulocitima, stanicama krvno-moždane barijere i endotelnim stanicama (118,124,125). TfR_2 je značajnije zastupljen uglavnom na stanicama jetre (126,127). Njegova glavna uloga je regulacija homeostaze željeza; važan je za detekciju razina željeza i regulaciju sinteze hepcidina, hormona koji kontrolira apsorpciju i distribuciju željeza u organizmu (126,128). Važno je napomenuti da oba transferinska receptora mogu tvoriti komplekse s transferinom. Ovi kompleksi su najstabilniji u slučaju potpuno zasićenog transferina, odnosno holotransferina. TfR_1 također tvori stabilnije transferinske komplekse nego TfR_2 (129,130).

Vezanje transferinskog receptora na holotransferin značajno pospješuje otpuštanje željeza iz transferinskog koordinacijskog kompleksa. Ustanovljeno je da se u endosomu, pri kiselim uvjetima, odvija konformacijska promjena holoTf-TfR_1 kompleksa koja olakšava otpuštanje željeza(III) i stabilizira nastali apoTf-TfR_1 kompleks (129,131,132).

Kiseli uvjeti također potiču protonaciju sinergističkog karbonatnog aniona didentatno vezanog na željezo(III) u holotransferinu, što doprinosi raspadu kompleksa (102,133). S obzirom na to da je ugljična kiselina slaba, karbonat je relativno jak konjugirani anion sklon protonaciji u kiselijem mediju. Također, poznato je da se pri formiranju kompleksa željeza(III) i transferina otpušta otprilike 3 H^+ po ionu željeza, pa je za očekivati da će kiseli medij pomaknuti ravnotežu prema raspadu kompleksa (134). Utjecaj pH također je važno razmotriti kroz aspekt protonacije/deprotonacije aminokiselina proteina. Sniženjem pH, odnosno protonacijom, transferin postupno prelazi iz "zatvorene" u "otvorenu" konformaciju, što omogućava lakše otpuštanje vezanog željeza (115,135,136). Otpuštanje željeza dodatno je potpomognuto njegovom redukcijom iz oksidacijskog stanja +3 u +2 djelovanjem duodenalne reduktaze (137,138).

1.3.4. Glikozilacija transferina i značaj sijalinske kiseline

Glikozilacija je kemijski proces kojim se ugljikohidrati (glikani) kovalentno vežu na makromolekule, najčešće proteine i lipide (139). Ova posttranslacijska modifikacija primarno se odvija u endoplazmatskom retikulumu i Golgijevom aparatu unutar stanica (140,141). Glikozilacija igra ključnu ulogu u pravilnoj funkciji i stabilnosti brojnih proteina; odgovarajuća glikozilacija neophodna je za mnoge biološke procese, uključujući pravilno savijanje proteina, stanično prepoznavanje i komunikaciju, imunološki odgovor organizma, i brojne druge funkcije (142–149).

Postoji više vrsta glikozilacije, a najčešće su *N*-vezana i *O*-vezana glikozilacija. *N*-vezana glikozilacija uglavnom podrazumijeva vezanje glikana preko dušikovog (N) atoma asparagina na Asn-X-Ser/Thr sekvencu, gdje je X bilo koja aminokiselina osim prolina (150,151). Ovaj proces započinje u endoplazmatskom retikulumu, gdje se prethodno formirani oligosaharid veže na novonastali protein. Dodatne modifikacije glikanske strukture odvijaju se u Golgijevom aparatu (152–155). *N*-vezana glikozilacija vrlo je važna za pravilno savijanje proteina i njihov međustanični transport (144,156–158). *O*-vezana glikozilacija odnosi se na kovalentno vezanje glikana preko kisikovog (O) atoma serina ili treonina (159–161). Ovaj tip glikozilacije uglavnom se odvija u Golgijevom aparatu i ključan je za pravilnu funkciju mnogih membranskih proteina i mucina (161–167).

Općenito, nepravilna glikozilacija proteina povezana je s brojnim patološkim stanjima. Promjene u glikozilaciji također mogu biti dobar prediktor razvoja bolesti poput dijabetesa tipa 2 i različitih kardiovaskularnih oboljenja (168–170). Zanimljivo je napomenuti da se sastav

glikana može prilično dobro korelirati s biološkom starošću, čak i bolje nego skraćivanje telomera (170,171).

Kao što je prethodno spomenuto, ljudski transferin visoko je glikozilirani protein. On je *N*-glikoziliran na dvama aminokiselinama, Asn-432 i Asn-630 (172,173). Glikanski lanci se granaju; oni mogu biti bi- ili triantenarni. Na krajevima tih ogranaka uobičajeno se nalazi sijalinska (*N*-acetilneuraminska) kiselina, što omogućava postojanje od asijalo do heksasijalo formi (174,175). U normalnom ljudskom serumu, 85 % transferina prisutno je kao tetrasijalo, a preostalih 15 % kao penta- ili trisijalo (174,175).

Sijalinske kiseline također spadaju u glikane, a kao što i samo ime sugerira, kiselih su svojstava. Postoji više vrsta sijalinskih kiselina (oko 50 monosaharidnih derivata), a u sisavaca su daleko najzastupljenije *N*-acetilneuraminska i *N*-glikolilneuraminska kiselina (176). S obzirom da je u ljudskom transferinu prisutna samo *N*-acetilneuraminska kiselina, daljnje spominjanje "sijalinske kiseline" odnosi se na *N*-acetilneuraminsku kiselinu (177,178).

Slobodna sijalinska kiselina sadrži karboksilnu skupinu i ima pK_a vrijednost oko 2,6 (176). Pri fiziološkim uvjetima (pH ≈ 7.4) ona je stoga deprotonirana (172).

Glikanski ogranci od izuzetnog su značaja za pravilno funkcioniranje ljudskog transferina. Nepravilna sijalinizacija transferina može biti posljedica određenih genskih bolesti, ali također može biti i indikator nekih drugih patoloških stanja (179,180). Primjerice, poznat je širok spektar kongenitalnih poremećaja glikozilacije (engl. *Congenital Disorders of Glycosilation*, CDG) poput: PMM2-CDG, MPI-CDG, MGAT2-CDG, SLC35A1-CDG i ALG6-CDG, pri čemu prefiks ispred „-CDG“ specificira mutirani gen (181–188). Također su poznati kongenitalni poremećaji skladištenja sijalinske kiseline, koji su uzrokovani nakupljanjem sijalinske kiseline u lizosomima zbog mutacija u genu SLC17A5. Primjeri takvih bolesti su ISSD (engl. *Infantile Sialic acid Storage Disease*) i Salla bolest (189–192). Takvi poremećaji obično nemaju direktan utjecaj na sijalinizaciju transferina. Zanimljivo je da je utvrđeno kako poremećaj CAFSA (engl. *Cerebellar Ataxia with Free Sialic Acid*), koji uzrokuje značajnu hiposijalinizaciju transferina u cerebrospinalnoj tekućini, ispoljava puno slabiji učinak kod osoba sa Salla bolešću. Kod takvih pacijenata, iako je prisutno povišenje slobodne sijalinske kiseline u cerebrospinalnoj tekućini, hiposijalinizacija transferina nije toliko izražena, što sugerira da Salla bolest može na određeni način ublažiti simptome koji su inače uočljivi kod CAFSA sindroma (189).

Promjene u sijalinizaciji transferina nisu ograničene samo na genetske poremećaje; one se mogu opaziti i kod brojnih stečenih bolesti i akutnih stanja. Primjerice, promjene sijalinizacije mogu poslužiti kao potencijalni prognostički markeri intenziteta akutnog

pankreatitisa i ozbiljnosti sepse odnosno septičkog šoka (180,193,194). Objavljena je i studija koja povezuje niže razine ugljikohidrat-deficijentnog transferina (engl. *Carbohydrate-Deficient Transferrin*, CDT), što ukazuje na višu sijalinizaciju, s većom vjerojatnošću razvoja sinukleinopatija poput Parkinsonove bolesti (195,196). Povišene koncentracije niskosijaliniziranog transferina (poglavito disijalotransferina) povezane su s prekomjernim uživanjem u alkoholnim pićima (197–200). Ipak, transferin se ne koristi kao biomarker za detekciju akutnog stanja alkoholiziranosti; značajnije promjene sijalinizacije posljedica su isključivo kronične prekomjerne konzumacije alkohola (198). U tom aspektu, transferin se može koristit kao vrlo specifičan dijagnostički marker (201).

U normalnom serumu, vrijeme poluživota glikoziliranog transferina iznosi oko 7 do 10 dana (28,202). Desijalnizirani transferin ima znatno kraće vrijeme poluživota te doprinosi povećanoj pohrani željeza u jetri (193). Promjene u glikozilaciji transferina ne moraju nužno biti vezane uz patološka stanja. Na primjer, tijekom trudnoće dolazi do postupnog i progresivnog povećanja udjela visoko sijaliniziranog transferina, koji se nakon poroda brzo vraća na normalne razine (203).

1.4. Enzimska desijalinizacija

Za potrebe istraživanja proteinskih glikoformi, nužno je osigurati dovoljne količine proteinskih uzoraka željenog stupnja glikozilacije. U teoriji, to se može postići na dva načina: prvi je potpuna sinteza glikoproteina, a drugi je modifikacija proteinskih izolata. Glikozilacija proteina spada u najsloženije posttranslacijske dorade; procjenjuje se da je čak oko 5 % ljudskog genoma izravno odgovorno za sintezu (odnosno kodiranje) velikog broja enzima koji vrše posttranslacijske modifikacije proteina (204–206). Potpuna laboratorijska sinteza određenih glikoproteina načelno je moguća, ali je i iznimno kompleksna (207). Stoga je svrsishodnije proizvesti potrebne proteinske glikoforme pripremom proteinskih izolata i/ili njihovom doradom djelovanjem prikladnih enzima.

U slučaju transferina, određene nisko sijalizirane forme, a posebno asijalotransferin, vrlo su slabo zastupljene u serumu zdravih osoba, a posljedično su rijetke i u komercijalno dostupnim proteinskim izolatima (175). Dobivanje dovoljnih količina asijalotransferina iz takvih pripravaka bilo bi iznimno neefikasno zbog vrlo niskog udjela asijalotransferina u uzorcima. Također, potrebno je uzeti u obzir relativnu fizičko-kemijsku osjetljivost proteina te mogućnost njegove djelomične degradacije, denaturacije ili agregacije prilikom provođenja složenijih metoda pročišćavanja (208–213).

Drugi način priprave željenih proteinskih glikoformi *N*-glikoziliranih proteina može se provesti enzimskom deglikozilacijom (214–216). Za analitičke svrhe, glikani se mogu ukloniti tretiranjem hidrazinom, ali to dovodi do potpunog uništenja neglikanskog dijela proteina (217,218).

Za pripremu dovoljne količine asijalotransferina za eksperimente određivanja konstanti ravnoteže kompleksiranja željeza(III), moguće je koristiti enzim neuraminidazu (sijalidazu). Ovaj enzim uklanja *N*-acetilneuraminsku (sijalinsku) kiselinu sa završetaka glikanskih ogranaka sijaliniziranih formi transferina (28,84,175,219). Enzim je uglavnom komercijalno dostupan u obliku agaroznih kuglica na kojima je deponiran. S obzirom na visoku cijenu enzima i osjetljivost njegove aktivnosti na pH i druge fizičko-kemijske parametre, poželjna je inicijalna optimizacija eksperimentalnih uvjeta kako bi se postigli maksimalni prinosi (219).

1.5. Kromatografsko odjeljivanje i glikanska karakterizacija proteinskih glikofomi

Postoje različite tehnike tekućinske kromatografije koje se potencijalno mogu koristiti za razdvajanje i analizu proteinskih glikoformi, kao što su: afinitetna kromatografija, kromatografija ionskog sparivanja, HILIC (engl. *Hydrophilic Interaction LIquid Chromatography*) i metode pH gradijenta. Sprega kromatografskih metoda s masenom spektrometrijom osobito je korisna jer omogućuje cjelovito glikansko profiliranje proteinskih frakcija (220–224).

S obzirom na to da je sijalinska kiselina izrazito kiseli glikan, za očekivati je da će uklanjanjem sijalinske kiseline s krajeva glikanskih ogranaka doći do ukupnog smanjenja kiselosti glikoproteina. U slučaju transferina, opaženo je da se pI vrijednosti nativnog transferina (pI ≈ 5,3) i asijalotransferina (pI ≈ 6,5) znatno razlikuju. Ta značajna razlika u izoelektričnim točkama omogućava razdvajanje glikoformi metodom pH gradijenta (175).

Kromatografska metoda temeljena na pH gradijentu može se provesti tako da se prvo pozitivno ili negativno nabijene proteinske forme vežu na kromatografsku kolonu suprotnog naboja. Kromatografija se izvodi od višeg ka nižem pH, ili obrnuto, ovisno o naboju kolone. U trenutku kada se pH eluensa izjednači s pI vrijednošću proteinske frakcije, ta frakcija se počinje eluirati, odnosno odvaja se s kolone jer postaje nenabijena s obzirom da joj je pI jednak pH otopine. Na taj način moguće je razdvojiti više različitih formi, pod uvjetom da je promjena pH dovoljno postupna i da su pI vrijednosti formi međusobno dovoljno različite. Za uspješno razdvajanje potrebno je uspostaviti dobar pH gradijent primjenom prikladnih pufera širokog puferskog kapaciteta. Ako se detekcija kromatografskih frakcija temelji na mjerenju

apsorbancije pri λ = 280 nm, što odgovara približnom lokalnom apsorpcijskom maksimumu proteina, prikladno je koristiti puferske smjese koje ne apsorbiraju značajno pri toj valnoj duljini. Metodu je moguće vršiti primjenom razmjerno jeftinih niskotlačnih FPLC (engl. *Fast Protein Liquid Chromatography*) sustava (175,225–229).

Kromatografiju temeljenu na gradijentu pH, odnosno izoelektrično fokusiranje, moguće je koristiti kao preliminarni test kvalitete enzimske desijalinizacije transferina. Ova metoda zahtijeva relativno male količine proteina (dovoljno je oko desetine miligrama), a eluirani protein može se, po potrebi, djelomično regenerirati mikrocentrifugiranjem sakupljenih frakcija odnosno dijalizom. Preliminarni test većih količina desijaliniziranog transferina može se provesti kombiniranjem vrlo malih alikvota uzetih iz pojedinih proteinskih šarži dobivenih nakon provođenja višestrukih ciklusa enzimskih desijalinizacija. Ako osim glavnog signala nisu vidljivi drugi manji signali, te ako je pH maksimum signala jednak očekivanom pI asijalotransferina (do na manju eksperimentalnu pogrešku), može se pretpostaviti da je enzimska desijalinizacija bila uspješna (28,84,175,219).

S obzirom na to da se samom pH-gradijent kromatografijom uz uporabu UV-Vis detekcije ne može nedvosmisleno utvrditi glikanski sastav proteina, po potrebi se konačna potvrda potpunosti desijalinizacije može izvršiti analizom glikana uz pomoć metoda masene spektrometrije. Takve analize također su potencijalno korisne za profiliranje komercijalno nabavljivih uzoraka nativnog transferina. Naime, dostupni pripravci obično su objedinjeni iz uzoraka prikupljenih od više donora, što upućuje na mogućnost postojanja manjih razlika u glikanskim sastavima ljudskog transferina između različitih šarži i/ili proizvođača, budući da je omjer glikoformi rezultat genetskih varijacija među pojedincima, a može ovisiti o dobi, spolu te raznim drugim biokemijskim i fiziološkim čimbenicima (230–232).

Glikanska analiza može se provesti na sljedeći način. Prvo se korištenjem enzima PNGaze F (engl. *Peptide:N-Glycosidase*) glikani oslobađaju iz proteina pomoću enzima. Oznaka „F“ nalazi se u imenu jer se enzim dobiva iz gram-negativne bakterije *Flavobacterium meningosepticum* (233). Taj enzim specifično cijepa *N*-glikane s proteina (233–235). Nakon oslobađanja, glikani se označavaju fluorescentnim markerom, primjerice, 2-aminobenzamidom (2-AB). Ovaj korak omogućuje detekciju glikana tijekom kromatografske analize. Glikani obilježeni fluorescentnim markerom pročišćavaju se pomoću hidrofobne interakcijske kromatografije (HILIC-SPE, engl. *Hydrophilic Interaction LIquid Chromatography - Solid Phase Extraction*) kako bi se uklonili slobodni markeri i redukcijska sredstva. Fluorescentno označeni glikani zatim se međusobno odvajaju pomoću UHPLC (engl. *Ultra High Performance*

Liquid Chromatography) na specifičnim kolonama. Eluati se mogu analizirati fluorimetrijski, detekcijom pri određenim valnim duljinama (npr. pobuda na 250 nm i emisija na 428 nm).

Odvojeni glikani analiziraju se masenom spektrometrijom koristeći, primjerice, Synapt G2-Si ESI-QTOF-MS sustav (engl. *Electrospray Ionization Quadrupole Time-of-Flight Mass Spectrometry*). U pozitivnom ionskom modu, glikani se ioniziraju, a zatim fragmentiraju putem CID-a (engl. *Collision-Induced Dissociation*) u načinu rada koji ovisi o podacima (DAD, engl. *Data-Dependent Acquisition*). Dobiveni MS i MS/MS spektri koriste se za anotaciju glikanskih struktura, uz usporedbu s poznatim vrijednostima iz baza podataka poput GlycoStore. Programi kao što su GlycoWorkbench i GlycoMod mogu se koristiti za daljnju potvrdu glikanskih struktura (175,236–240).

1.6. Fluorescencijska spektroskopija

1.6.1. Fluorescencijska spektroskopija i fluorimetrija u mikrotitarskim pločicama

Fluorescencijska spektroskopija vrlo je široko primjenjiva analitička metoda koja se koristi za detekciju i kvantifikaciju tvari putem njihove interakcije s elektromagnetskim zračenjem. Metoda je u pravilu neinvazivna i nedestruktivna te nalazi primjenu u brojnim znanstvenim disciplinama kao što su kemija, medicina, biologija, biofizika, nanotehnologija, znanosti o okolišu i (nano)materijalima (241–247). Ona se koristi za proučavanje molekulskih struktura, interakcija i dinamike, od pojedinačnih molekula do makromolekulskih kompleksa (248–252).

Jedna od glavnih prednosti fluorescencijske spektroskopije visoka je osjetljivost, koja u pravilu omogućava detekciju i mjerenje vrlo niskih koncentracija fluorofora (253,254). To je osobito korisno pri istraživanjima vršenim na biokemijskim uzorcima visoke vrijednosti, poput izolata ljudskih proteina, jer se istraživanja često mogu vršiti uz nisku potrošnju analita (255–257). Metoda također omogućava širok koncentracijski raspon te može biti vrlo selektivna uz pravilan odabir valnih duljina pobudnog i emitiranog zračenja. Zbog Stokesovog pomaka, odnosno razlike između valnih duljina fluorescencijski emitiranog i pobudnog zračenja, interferencije pobude u vidu mjerene fluorescencije često su slabe, što uglavnom rezultira vrlo niskim vrijednostima baznih linija (258,259). Stoga je često moguće istovremeno detektirati više različitih fluorescentnih tvari u smjesi, pod uvjetom da su njihova spektralna svojstva dovoljno različita. Za preciznu istovremenu kvantifikaciju višestrukih analita, često je važna dobra izvedivost spektralne dekonvolucije djelomično preklopljenih spektara (260–263).

Za razliku od fosforescencije, fluorescencija je brz proces, što omogućava primjenu fluorescencijske spektroskopije u istraživanjima brzih kinetika. Na primjer, fluorescencija se može koristiti kao metoda detekcije u sklopu tehnika zaustavljenog protoka (engl. *stopped-flow*) (264–269).

Osim učestalo korištenog klasičnog fluorimetra, gdje se uzorak uglavnom snima u kiveti pod kutem od 90 stupnjeva u odnosu na izvor pobudnog zračenja, za istraživanja biokemijskih uzoraka vrlo su korisni čitači mikrotitarskih pločica. Prednosti ovih uređaja su višestruke. Čitači omogućuju visoku protočnost odnosno snimanje velikog broja uzoraka u kratkom vremenu (270–273). Kada se koriste uz automatski titrator i/ili robot za pipetiranje, omogućena je brza priprava uzoraka direktno unutar mikrotitarskih pločica, što rezultira vrlo brzim mjerenjima velikog broja uzoraka. Automatizacija procesa također olakšava replikaciju, što doprinosi statističkoj pouzdanosti rezultata, jer je zbog jednostavnosti postupka lako moguće pripremiti više replikata za pojedini uzorak.

Druga važna prednost čitača mikrotitarskih pločica je mogućnost mjerenja vrlo malih volumena uzoraka. Ovisno o vrsti mikrotitarske pločice, moguće je precizno mjerenje uzoraka od samo nekoliko desetaka mikrolitara (ili manje) (274,275). Nasuprot tome, glavnina kiveta primjenjivih za tipične fluorimetre uglavnom zahtijevaju volumene od barem nekoliko stotina mikrolitara. Također, kod klasičnih fluorimetara, kivetu je potrebno temeljito ispirati i sušiti između uzastopnih mjerenja, dok taj problem nije prisutan kod uporabe mikrotitarskih pločica, s obzirom da su jednokratne. Moderni čitači mikrotitarskih pločica vrlo su precizni, i uzimajući u obzir dosadašnje trendove i vlastito iskustvo, autor očekuje da će se njihova primjena u preciznim fluorimetrijskim istraživanjima u budućnosti povećati.

1.6.2. Fluorimetrijsko određivanje konstanti ravnoteže

U literaturi su poznati brojni primjeri uporabe fluorescencijske spektroskopije u svrhu određivanja konstanti ravnoteže. Eksperimenti se najčešće provode tako da se prvo izvrši titracija, pri čemu se varira koncentracija barem jednog od sudionika reakcije, dok se koncentracije preostalih sudionika održavaju konstantnima. Ključni preduvjet smislenosti mjerenja je da barem jedan konstituent reakcije fluorescira te da se njegova fluorescencija mijenja prilikom vezanja (276–283).

Prije provođenja samih mjerenja, nužno je osigurati da je kemijska ravnoteža uspostavljena. Brzina uspostavljanja ravnoteže ovisi o kinetici proučavanih reakcija, a uspostavu ravnoteže u pravilu je moguće provjeriti uzastopnim mjerenjima uzoraka u

određenim vremenskim intervalima. Ako se pri istim uvjetima snimanja ne opažaju promjene tokom vremena, može se zaključiti da je reakcija postigla ravnotežno stanje (284).

Važno je pažljivo kontrolirati eksperimentalne uvjete, poput temperature i trajanja snimanja, posebno kada se mjerenja vrše u mikrotitarskim pločicama. Fluorescencija, uz same konstante ravnoteže, ovisi o temperaturi, jer intenzitet fluorescencije može varirati zbog promjena u brzini termičke relaksacije pobuđenog fluorofora i zbog razlika u broju međumolekulskih sudara (285–288). Tijekom snimanja općenito može doći do manje promjene temperature uzoraka i određenog gubitka volumena uslijed hlapljenja. Navedene perturbacije mogu se smanjiti dobrim dizajnom eksperimenta. Temperaturna kontrola prisutna je kod mnogih čitaća mikrotitarskih pločica, i opažene temperaturne varijacije uglavnom su veoma niske.

Vrlo dugotrajna mjerenja, koja uključuju snimanje pobudnih, emisijskih i/ili 3D spektara, treba izbjegavati za veći broj uzoraka. Ako su takva mjerenja nužna, preporučuje se prvo izmjeriti (1D) fluorescenciju na emisijskom maksimumu ili relevantnoj valnoj duljini, jer su ta mjerenja brza, a tek zatim snimiti cijele spektre. Određeno smanjenje utjecaja sustavnih učinaka, poput promjene temperature ili hlapljenja, može se postići mjerenjem uzoraka u (pseudo)nasumičnom redoslijedu. Na taj način, sustavni učinci poput kontinuiranog hlapljenja ne akumuliraju se na uzastopne točke titracije, čime se izbjegava ispoljavanje dodatnog (neželjenog) trenda povezanog s kontinuiranim promjenama koncentracije titranta.

Također je važno razmotriti potencijalne nepoželjne sekundarne učinke, poput mehanizama gašenja fluorescencije koji nisu izravno povezani s promjenama uslijed vezanja odnosno kompleksiranja. Na primjer, prisutnost iona teških metala može uzrokovati gašenje fluorescencije sudarima (dinamičko gašenje), dok istovremeno prisustvo više fluorofora u otopini nerijetko dovodi do prijenosa pobude FRET (engl. *Förster Resonance Energy Transfer*) mehanizmom. FRET trnjenje može biti uzrokovano i drugim nefluorescentnim kromoforskim akceptorima. Dinamičko gašenje, primjerice, provjerljivo je Stern-Volmerovom jednadžbom pomoću koje se analizira ovisnost intenziteta fluorescencije o koncentraciji gasitelja fluorescenije. Primjenom te jednadžbe, moguće je kvantificirati učinkovitost gašenja i izračunati bimolekulsku konstantu gašenja koja direktno ovisi o frekvenciji sudara između fluorofora i gasitelja (289–296). U slučaju proteina, moguća je djelomična fotokemijska degradacija uslijed višestrukih ili dugotrajnih mjerenja. Eventualnu fotokemijsku degradaciju može se jednostavno provjeriti repliciranjem mjerenjima istog uzorka u prikladnim vremenskim intervalima. Izostanak varijabilnosti i trenda u podacima indikacija je beznačajne fotodegradacije fluorofora (297–302).

Odabir smislenih omjera koncentracija reaktanata prilikom fluorimetrijskih (i drugih) eksperimenata određivanja konstanti ravnoteže od iznimne je važnosti. Uobičajeno je održavati koncentraciju jednog reaktanta konstantnom, a koncentraciju drugog reaktanta varirati. Postizanje tzv. titracijskog režima važno je kako bi se osigurala dovoljna promjena fluorescencije uslijed vezanja. Međutim, ako je konstanta ravnoteže iznimno visoka, sav titrirani (dodani) reaktant može u svakoj točki titracije biti gotovo potpuno vezan na reaktant (koji je prisutan u konstantnoj koncentraciji). Takva situacija otežava praćenje postupnih promjena vezanja, ona smanjuje osjetljivost eksperimenta i otežava precizno određivanje konstanti ravnoteže, jer dolazi do brzog zasićenja i monotone promjene signala titracijske krivulje (28,303–305).

U specifičnim slučajevima vezanja iona željeza(III) na forme ljudskog transferina, zbog vrlo visokih konstanti ravnoteže, cjelokupno titrirano željezo praktički je u potpunosti vezano na transferin u svim točkama titracije. Ako se koncentracija transferina održava konstantnom, dodavanje željeza uzrokuje kontinuirani pad fluorescencije sve dok se ne postigne približan stehiometrijski omjer 2:1 u korist željeza. Nakon toga, daljnji dodatak željeza ne dovodi do dodatnog gašenja signala, jer je sav transferin već potpuno zasićen (28).

Takav eksperiment može biti problematičan ukoliko je svrha precizno određivanje konstanti ravnoteže. On doduše može biti koristan za preliminarnu provjeru stehiometrije reakcije. Točka pregiba krivulje javlja se blizu omjera 2:1 željeza prema transferinu, a dodatkom suviška željeza može se potvrditi da nema daljnjeg smanjenja signala, što ukazuje na izostanak neželjenog kolizijskog gašenja fluorescencije. Također, značajnije odstupanje od očekivanog omjera može indicirati pogreške nastale pri određivanju koncentracije rektan(a)ta. To može biti posljedica grube pogreške titracijskog eksperimenta i/ili netočnosti u određivanju barem jednog od molarnih apsorpcijskih koeficijenata korištenih za spektrofotometrijsku kvantifikaciju reaktanata. Znatno niži omjer od očekivanog može uputiti na eventualnu djelomičnu denaturaciju proteina ili njegovu kontaminaciju drugim metalima. S obzirom da se tijekom spomenute hipotetske titracije svo dodano željezo gotovo u potpunosti veže na protein prije postizanja zasićenja veznih mjesta transferina, količina slobodnog željeza u ravnoteži bit će vrlo niska i stoga teško odrediva, jer slobodno željezo(III) ne fluorescira pri uvjetima pobude proteina λ_{pobudna} = 280 nm (28,306,307).

Za precizno određivanje konstanti ravnoteže vezanja iona željeza(III) na transferin, potreban je dodatak kompetitivnog liganda, poput nitrilotrioctene kiseline (NTA), koja također tvori stabilan kompleks sa željezom, ali manje stabilan od transferinskog. Time se omogućuje postupnije vezanje željeza na protein, što povećava osjetljivost metode. Finim podešavanjem

fiksne količine kompetitivnog liganda prisutnog u svim točkama titracije moguće je ostvariti željeni titracijski režim i time dodatno unaprijediti osjetljivost metode (27,28,303).

U eksperimentima kompleksiranja transferina sa željezom ili drugim metalima, potrebno je pažljivo kontrolirati pH otopina, jer su te ravnoteže izrazito pH-ovisne (28,96,308). Poželjna je i upotreba prikladnih puferskih otopina u dovoljnim koncentracijama. Kvalitetu puferiranja može se provjeriti mjerenjima pH nakon titracije odnosno neposredno prije i/ili nakon mjerenja fluorescencije. Važno je koristiti pufere koji ne kompleksiraju sa željezom(III), imaju odgovarajući puferski kapacitet u željenom pH području i prikladni su za rad s proteinima.

Titriranja varijabilnih količina otopina kompleksa željeza(III) u otopine fiksnih koncentracija transferina zasigurno će imati određeni manji utjecaj na ukupnu ionsku jakost otopina. Navedeni utjecaj nije trivijalno procijeniti s obzirom na složene pH ravnoteže pufera, transferina i nitrilotrioctene kiseline (ili nekog drugog dodanog kompetitivnog kelatora). Jedan od jednostavnih načina anuliranja varijabilnost ionske jakosti između različitih uzoraka dodatak je fiksnih koncentracija inertnih soli, poput KCl-a, u sve otopine korištene tijekom titracije (28,309).

1.6.3. Značaj korekcija učinka unutarnjeg filtra – korekcije u mikrotitarskim pločicama

Jedan od ključnih izazova u fluorescencijskoj spektroskopiji korigiranje je učinka unutarnjeg filtra (engl. *Inner Filter Effect*, IFE). IFE se odnosi na smanjenje intenziteta fluorescencije zbog nezanemarive apsorpcije zračenja u analiziranom uzorku. Ako dolazi do atenuacije (prigušenja) pobudnog zračenja, radi se o primarnom učinku unutarnjeg filtra (pIFE); ako je prigušena emitirana fluorescencija, riječ je o sekundarnom učinku unutarnjeg filtra (sIFE). Oba učinka djeluju kumulativno, što rezultira redukcijom intenziteta mjerene fluorescencije (273,310). Atenuacijsko trnjenje postaje zanemarivo samo u slučajevima u kojima otopina analita gotovo uopće ne apsorbira niti pobudno niti emitirano zračenje, što je u praksi rijetko. Prethodno je opaženo da učinak unutarnjeg filtra postaje značajan čak i pri vrlo niskim apsorbancijama. Na primjer, pri apsorbanciji A = 0,06, relativna pogreška u mjerenom intenzitetu fluorescencije iznosi približno 8 %. Ta se razlika povećava na oko 12 % pri A = 0,1, te na čak 38 % pri A = 0,3 (273,311,312). Iako su ova opažanja, prema autorovom iskustvu i saznanjima, točna za čiste fluorofore, ona ne moraju nužno vrijediti u slučajevima gdje se, zbog visokih i konstantnih apsorbancija uvjetovanih fiksnim koncentracijama (nefluorescentnog) kromofora, gubici uslijed IFE-a izjednačavaju unatoč visokoj ukupnoj apsorbanciji svih uzoraka (310). Drugim riječima, premda dolazi do smanjenja ukupne fluorescencije, ukoliko je

ono jednoliko, ne dolazi do promjena omjera fluorescencija, samo do ukupnog pada intenziteta fluorescencije svih uzoraka.

IFE može biti posljedica apsorpcije samog analita (fluorofora), ali može biti uzrokovan i prisustvom drugih apsorbirajućih tvari (kromofora) u uzorku. Problem se uglavnom manifestira kroz nelinearni odziv fluorescencije kao funkcije koncentracije apsorptivnog fluorofora (273,310,311,313,314). Nelinearni odziv signala, sam po sebi, nije nužno problematičan. U slučaju otopine apsorptivnog čistog fluorofora, vjerojatno je moguće relativno precizno odrediti njegovu koncentraciju vršenjem nelinearne interpolacije baždarne krivulje. Međutim, u iznimno apsorptivnim otopinama, trnjenje fluorescencije uzrokovano IFE-om može postati toliko izraženo da dodatno povišenje koncentracije apsorptivnog fluorescentnog analita uzrokuje redukciju fluorescencije (310). U tom slučaju, problem nastaje kada se za dvije različite vrijednosti koncentracije analita (x) dobivaju jednake vrijednosti odziva (y). To posebno otežava interpretaciju rezultata, jer nije moguće jednoznačno odrediti koncentraciju analita isključivo na temelju fluorescencijskog signala (pri samo jednoj valnoj duljini emisije). Čak i pri nižim apsorbancijama, ako su u otopini prisutne i druge apsorbirajuće tvari nepoznatih (i možda nasumičnih) koncentracija, nelinearna interpolacija gubi smisao. Perturbacije uzrokovane drugim atenuatorima (apsorberima) u pravilu su neovisne o koncentraciji glavnog analita, što dodatno komplicira precizno određivanje koncentracije pomoću baždarne krivulje. Uz pretpostavku neapsorptivnog otapala, u veoma razrijeđenim sustavima problem IFE praktički nije prisutan jer vrlo niske koncentracije tvari uzrokuju vrlo nisku optičku gustoću uzorka, što rezultira slabom apsorpcijom zračenja. Drugim riječima, čak i uzorci koji su inicijalno vrlo apsorptivni neće apsorbirati značajan udio zračenja ako se sustav dovoljno razrijedi.

Stoga, možda i najjednostavnije rješenje IFE problema svodi se na razrjeđivanje sustava. Međutim, otopinu je često potrebno mnogostruko razrijediti, što može unijeti značajnu eksperimentalnu pogrešku i negativno utjecati na omjer signala i šuma. Razrjeđenjem je moguće smanjiti intenzitet signala do te mjere da postane teško razlikovati fluorescencijski signal analita od pozadinskog šuma (311,315,316). U slučaju eksperimenata koji imaju za cilj izračunavanje konstanti ravnoteže, razrjeđivanje uglavnom nije valjana opcija jer ono može značajno pomaknuti kemijsku ravnotežu u određenom smjeru. Na primjer, u hipotetskom eksperimentu mjerenja fluorescencije nastajanja dimera nekog fluorofora, u razrijeđenim sustavima (zanemariv IFE) dimer možda ne bi bio prisutan u značajnim količinama, jer razrjeđenje pogoduje raspadu kompleksa i stvaranju monomera. Osim toga, razrjeđenje može

poremetiti koloidnu stabilnost, utjecati na fizičko-kemijska svojstva sustava i općenito može imati različite nepredvidive učinke na proučavani kemijski sustav (314,317).

U literaturi su poznati brojni drugi načini korekcije IFE, ali oni se gotovo isključivo odnose na mjerenja provedena klasičnim fluorimetrima s kutom otklona od 90 stupnjeva između pobudnog i detektiranog (emitiranog) zračenja (273,310,318). U gotovo svim slučajevima, IFE učinci mogu se barem djelomično umanjiti dobrim odabirom valnih duljina pobude i emisije. U slučaju pobude, optimum vrlo često odgovara valnoj duljini lokalnog maksimuma apsorbancije. Značajniji odmak od tog maksimuma može djelomično reducirati pIFE, ali takav pomak će ujedno i smanjiti efikasnost (neatenuirane) pobude, čime može negativno utjecati na intenzitet mjerenja fluorescencije, odnosno kritično smanjiti omjer signala i šuma (319). Važno je napomenuti da pobudna zračenja različitih uređaja često nisu u potpunosti monokromatska, pa se čak i pri odmaku maksimuma pobude od snažno apsorptivne zone dio zračenja može i dalje značajno apsorbirati (253,320–322). Prilikom snimanja emisije, poželjno je odabrati valnu duljinu pri kojoj je apsorbancija minimalna, a fluorescencijski signal dovoljno snažan za postizanje dobrog omjera signala i šuma.

Ukoliko se korekcije za IFE ne provode, moguća je kriva interpretacija rezultata koja nije uvijek lako uočljiva (323,324). U titracijskim eksperimentima provedenim sa svrhom određivanja konstanti ravnoteže, rezultirajuće fluorescencijske krivulje sadrže doprinos „prave“ (neatenuirane) fluorescencije i IFE. IFE može biti manje očit nego, na primjer, u slučaju kalibriranja fluorescencijsko-koncentracijskih krivulja fluorofora, gdje je odstupanje od linearnosti jasna indikacija ispoljavanja IFE-a. Ako bi se titrirale dvije tvari koje se međusobno ne vežu, ali kod kojih je prisutan porast IFE s dodatkom titransa, mogla bi se dobiti lažna krivulja vezanja, premda vezanja zapravo nema.

Razne IFE-korekcijske metode prikladne su isključivo za klasične fluorimetre i ne mogu se uspješno primijeniti na mjerenja provedena čitačima mikrotitarskih pločica zbog razlika u geometriji snimanja. U uobičajenim fluorimetrijskim kvantifikacijama, pobudna zraka ulazi u kivetu i dopire do zone približnog središta kivete. Fluorescencija se generira cijelim putem, ali detektirano zračenje dolazi samo iz središnje zone kivete, pod kutem od 90 stupnjeva u odnosu na ulaznu zraku (314,318). Na taj način minimiziraju se potencijalne interferencije uzrokovane dolaskom pobudnog zračenja na detektor. Primarni učinak unutarnjeg filtra (pIFE) važan je faktor samo na putu zrake od ulaska u kivetu do (približnog) centra, dok je sekundarni učinak unutarnjeg filtra (sIFE) značajan na putu emitirane fluorescencije od centra kivete do detektora. To znači da su optički putevi relevantnog pobudnog i emitiranog zračenja konstantni, neovisni

o vrsti analita i njegovoj koncentraciji, ovisni isključivo o geometriji kivete. Ti optički putevi otprilike su polovine pripadajućih prostornih dimenzija kivete (314,318).

Mjerenja u mikrotitarskim pločicama provode se tako da je izvor zračenja smješten s iste strane uzorka kao i detektor, najčešće iznad tekućine, premda neki uređaji omogućavaju i mjerenje s dna (prozirne) pločice. Ovakav način snimanja sličan je takozvanoj "*front-face*" konfiguraciji klasičnog fluorimetra. Kod takvih mjerenja, prodiranje zračenja u otopinu i rezultantni optički putevi ovise o optičkoj gustoći uzorka, te stoga nisu fiksni i *a priori* poznati. Dodatni utjecaj na varijabilnost optičkih puteva prilikom snimanja na čitačima mikrotitarskih pločica ima i volumen uzorka. U mikrotitarskim pločicama, udaljenost od površine tekućine do dna pločice ovisi o volumenu uzorka koji se mjeri (273,310,313,325–327).

Velik broj poznatih korekcijskih metoda zahtijeva, uz mjerenje fluorescencije, i mjerenje apsorbancije. Primjerice, možda najčešće korištena Lakowiczeva metoda zahtijeva mjerenje apsorbancije i pogodna je samo u rasponu do otprilike 0,7 apsorbancijskih jedinica (253,273,310,314).

Adekvatna primjenjivost drugih metoda baziranih na mjerenjima apsorbancije upitna je u slučaju mjerenja provedenih u mikrotitarskim pločicama zbog specifičnosti geometrije iluminacije uzorka, odnosno razlika u načinu propagacije pobudnog i emitiranog zračenja kroz uzorak. Osim toga, neke poznate metode zahtijevaju posebne aparature, primjerice mehanizam fizičkog pomicanja kivete dijagonalno ili upotrebu optičkih vlakana uronjenih direktno u otopinu analita (328,329). Korekcije koje koriste gašenje intenziteta Ramanovih signala vode također mogu biti problematične zbog slabih signala koji lako mogu biti zasjenjeni spektralnim preklapanjima uzrokovanim nevodenim komponentama u otopini. Jasno je i da takve korekcije ne funkcioniraju u slučaju korištenja nevodenih otapala (330,331).

Noviji čitači mikrotitarskih pločica omogućuju jednostavno i brzo podešavanje visine optičkog elementa (koji objedinjuje detektor i izvor zračenja). Opaženo je da varijacije visine optičkog elementa (takozvane *z*-pozicije) imaju vrlo značajan utjecaj na izgled krivulja fluorescencijsko-koncentracijskog odziva. To i ne iznenađuje, s obzirom da iznos IFE ovisi, osim o koncentraciji apsorbera, i o geometrijskim parametrima iluminacije, odnosno o optičkim putevima (273,318,323). Te razlike omogućile su razvoj nove korekcijske metode koja se temelji na mjerenjima fluorescencije na više različitih *z*-pozicija, uz *post hoc* primjenu korekcijske funkcije koja je izvedena prilagodbom metode dijagonalnog pomaka kivete (engl. *cell shift method*) za čitače mikrotitarskih pločica (273,329). Navedena metoda ne iziskuje mjerenje apsorbancije te je stoga pogodna i za mjerenja vršena u neprozirnim pločicama. Metoda je također primjenjiva za mjerenja visokoapsorptivnih uzoraka (273,310).

Razvoj takve metode čini se prijeko potrebnim za kvalitetno provođenje IFE korekcija u titracijskim eksperimentima fluorimetrijskih određivanja konstanti ravnoteže korištenjem mikrotitarskih pločica, s obzirom na generalnu neprilagođenost postojećih metoda za čitače mikrotitarskih pločica.

U kontekstu titracija kompleksiranja glikoformi ljudskog transferina s željezom(III), lokalni apsorpcijski maksimum pri oko 280 nm također predstavlja optimalnu (ili blizu optimalne) fluorescencijsku pobudu (28,332–334). Prema tome, čak i razmjerno razrijeđene otopine transferina ispoljavaju značajan pIFE. Dodatak željeza(III) u obliku nitrilotrioctenog kompleksa također nezanemarivo povećava apsorbanciju u području pobude. U takvim sustavima, sIFE je razmjerno manji od pIFE, ali također nije potpuno zanemariv (28).

Vršenje eksperimenata u vrlo niskim koncentracijama, pri kojima bi se IFE-povezani problemi mogli zanemariti, donosi niz izazova. Smanjeni fluorescencijski signal rezultira lošijim omjerom signala i šuma, što otežava analizu. Također, precizno određivanje koncentracija reaktanata postaje problematično jer dodatno razrjeđivanje otopina, čije su koncentracije prethodno određene spektrofotometrijski, može unijeti dodatne pogreške. Osim toga, sporije postizanje kemijske ravnoteže može predstavljati kinetički izazov. Također, prisutnost čak i manjih količina nečistoća, poput željeza ili drugih metala u radnim puferima, može značajno utjecati na rezultate. S obzirom na visok afinitet transferina za željezo(III) (i neke druge metalne ione), čak i uz upotrebu vrlo čistih reagensa, može doći do nezanemarivog zasićenja apoproteina željezom ako koncentracija transferina nije znatno viša od koncentracije nečistoća metalnih iona. Željezo i drugi metali koje transferin može vezati, a koji su prisutni kao nečistoće u radnim otopinama, mogu u nezanemarivom postotku zasititi apotransferin kada je njegova koncentracija niska. U okviru seta eksperimenata s početnim otopinama istog ili sličnog sastava, koncentracije tih nečistoća mogu se smatrati približno konstantnima, ali njihov omjer u odnosu na transferin ovisi naravno o koncentraciji transferina. Zbog toga korištenje nižih koncentracija transferina može biti problematično.

Jedan od načina djelomičnog anuliranja IFE bez primjene korekcija može se postići pažljivim dizajnom eksperimenta. Konkretno, u titraciji se koncentracija transferina može održavati konstantnom, dok se varira koncentracija kompleksa željeza(III). Ovaj pristup smanjuje relativne razlike u apsorbanciji među uzorcima, jer glavni doprinos apsorbanciji na λ = 280 nm potječe od transferina. Time se osigurava da je IFE relativno ujednačen, što znači da je prigušenje signala zbog IFE podjednako u svim točkama, bez velikog utjecaja na oblik titracijske krivulje. Iako će apsolutne vrijednosti fluorescencije biti niže, nego u slučaju bez IFE, relativni intenziteti fluorescencije ostat će konzistentni, što omogućuje pouzdano praćenje

promjena u sustavu. Sukladno tome, bolje je varirati reaktant koji ima niži apsorbancijski doprinos, dok se onaj s višim doprinosom održava konstantnim.

Zanimljivo je napomenuti da je razvijena metoda korekcije IFE u mikrotitarskim pločicama koja intenziviranjem IFE omogućuje izravnu korekciju bez potrebe za dodatnom matematičkom obradom podataka odnosno primjenom korekcijskih formula (310). Dodatkom fiksnih količina vrlo koncentriranog apsorbera u sve uzorke fluorofora, relativna varijacija u IFE među uzorcima postaje zanemariva, jer je ukupna atenuacija fluorescencije dominantno uvjetovana snažnim apsorberom.

2. RAD 1: OPTIMIZATION OF ENZYMATIC DESIALYLATION OF HUMAN SERUM TRANSFERRIN

Macedonian pharmaceutical bulletin, 68 (Suppl 1) 415 - 416 (2022)
Online ISSN 1857 - 8969
DOI:10.33320/maced.pharm.bull.2022.68.03.200
Short communication

Optimization of enzymatic desialylation of human serum transferrin

Tomislav Friganović*, Valentina Borko, Tin Weitner

Faculty of Pharmacy and Biochemistry, University of Zagreb, Ante Kovačića 1, 10000 Zagreb, Croatia

Introduction

Transferrin (Tf) is one of the major iron transport proteins in the human organism. It is a highly glycosylated bilobal protein that can bind up to two iron(III) ions thus forming a distorted octahedral ternary complex with both the amino acids of the protein and the synergistic carbonate anion. (MacGillivray et al., 1998) Proper glycosylation of transferrin is critical for its proper function in the body; various pathological conditions are closely associated with unusual sialylation patterns. The presence of different transferrin glycoforms is the result of variability in the glycosylation of N-linked oligosaccharide chains. These glycan chains are bi- or trinatenary and bind to residues Asn-413 and Asn-611. (Fu and van Halbeek, 1992) Sialic acid is usually located at the outmost ends of these oligosaccharide chains. Deviations from the usual sialylation patterns are associated with various genetic disorders and chronic diseases. Currently, sialic acid-deficient transferrin levels are commonly used as biomarkers of chronic alcohol abuse. (Del Castillo Busto et al., 2005) To better understand the properties of asialotransferrin, the production and subsequent purification of the protein is required because the percentage of asialotransferrin in native human apotransferrin is low. Asialotransferrin is produced by the action of commercially available sialidase enzymes, which can be quite expensive. Therefore, optimization of the processes to produce asialotransferrin at a low cost is required. After enzymatic desialylation, additional chromatographic purification of asialotransferrin can be performed using the pH gradient method. (Friganović et al., 2021)

Materials and methods

Chemicals and instrumentation

The GlycoCleave® Immobilized Enzymes (GALAB Technologies) and immobilized SialEXO® Microspin columns (Genovis) were used for enzymatic desialylation of human apotransferrin (Biorbyt Ltd, cat. no. orb80927 or Sigma, cat. no. T3309). Tris (Amresco), sodium acetate trihydrate (Kemika), calcium chloride dehydrated (Fluka) were used.

Optimisation of enzymatic desialylation

Desialylation procedures were performed using two different immobilized sialidase enzymes; Glycocleave® and SialEXO®. Both products contain enzymes immobilised on agarose beads. Glycocleave® is sold as a slurry containing the beads, while the immobilized SialEXO® beads are contained in a plastic column. For desialylation using the Glycocleave® kit, the manufacturer recommends using 400 µL of slurry (containing 200 µL beads). The beads must be washed thoroughly several times with the working buffer (0.05 M NaOAc, 0.001 M $CaCl_2$, pH = 5.5). The protein is dissolved in the working buffer (recommended up to 2.5 mg/mL, adjusting the pH to 5.5 if necessary) and added to the beads. Desialylation is performed in 2 mL microcentrifuge tubes containing the protein solution and enzyme beads, which were rotated using a tube revolver (10 rpm) at t = 37° C for at least 6 hours. In our optimization experiments, we varied the acetate buffer concentration, protein concentration, and incubation time. For desialylation using the SialEXO® columns, the protein should be dissolved in 0.02 M Tris working buffer (recommended range 0.1-5 mg/mL, pH = 6.8) and added

*tin.weitner@pharma.unizg.hr

to the column, which was prewashed three times with 300 µL working buffer (centrifugation for 1 min at 200 RCF each time). The column should be incubated at room temperature with end-over-end mixing for 30 min. The desialylated protein is recovered by centrifuging for 1 min at 1000 RCF. The manufacturer states that a single SialEXO® column can be used for desialylation of up to 0.5 mg of protein in a 30 min period, indicating that the SialEXO® column is intended for single use. In our optimization procedure, we reused the SialEXO® columns multiple times and varied both the protein concentration and the time of desialylation.

Validation of the desialylation procedure

To confirm the satisfactory extent of desialylation, the collected protein samples were analyzed by FPLC. Isoelectric focusing was performed using the pIsep buffers (CryoBioPhysica). A single-step linear pH gradient was used. Isoelectric focusing was performed mainly in the range of pH = 7-5.75. For the experiments on the ÄKTA Purifier 10 instrument, the SOURCE™ 15Q 4.6/100 PE anion exchange column was used, while for the experiments on the ÄKTA Start instrument, two or four HiTrap Q HP anion exchange columns connected in series were used. Samples that gave satisfactory results were sent for glycan analysis. The N-glycans were first cleaved by adding 1.2 U PNGase F (Promega, USA) and incubated overnight at 37 °C. Subsequent purification was performed via HILIC-SPE and the fluorescently labeled N-glycans were analyzed by H-Class UPLC (Waters, USA) using a BEH glycan chromatography column (Waters, USA). For some samples, the above UPLC characterization was also coupled with MS/MS analysis using the Synapt G2-Si ESI-QTOF-MS system (Waters, USA).

Results and discussion

For the desialylation performed with the GlycoCleave® kit, we increased the protein concentration from the recommended 2.5 mg/mL to 6.25 mg/mL. With the 800 µL volume used, this corresponds to 5 mg of transferrin per single desialylation cycle. Due to the increased concentration, a greater pH change (acidification) was observed at the end of the incubation period. Therefore, the amount of acetate was increased to 0.2 M, compared with the 0.05 M indicated in the manufacturer's instructions. The desialylation time was either 24 or 48 h. This is a significantly longer time frame than the 6 h indicated by the manufacturer. Glycan analysis results showed that this procedure removed >90% of the sialic acid content from the native protein. In the case of SialEXO® columns, we significantly increased the desialylation time from the recommended 30 min to 24 h. The protein concentration was also increased from the recommended 0.625 mg/mL to 2.5 mg/mL. Further increase in protein concentration gave unsatisfactory results. Glycan analysis results showed that the desialylated protein contained only ≈1% of the original sialic acid content (≈99% removed sialic acid content). This result was obtained by pooling the desialylated samples for the 19 consecutive 24-hour desialylation procedures using 2 SialEXO® columns in parallel. This means that the theoretical mass of transferrin that can be desialylated with a single SialEXO® column is ≥47.5 mg.

Conclusions

Optimization of desialylation processes was performed for 2 different commercially available sialidase enzymes. Increasing the protein mass per single cycle together with a drastic increase in reaction time gave the best results. The fact that we were able to produce nearly 50 mg of desialylated transferrin using a single SialEXO® column designed to produce only 0.5 mg of said protein is particularly intriguing.

References

Del Castillo Busto, M.E., Montes-Bayón, M., Blanco-González, E., Meija, J., Sanz-Medel, A., 2005. Strategies to Study Human Serum Transferrin Isoforms Using Integrated Liquid Chromatography ICPMS, MALDI-Tof, and ESI-Q-TOF Detection: Application to Chronic Alcohol Abuse. Anal. Chem. 77(17), 5615–5621. https://doi.org/10.1021/ac050574s

Friganović, T., Tomašić, A., Šeba, T., Biruš, I., Kerep, R., Borko, V., Šakić, D., Gabričević, M. and Weitner, T., 2021. Low-pressure chromatographic separation and UV/Vis spectrophotometric characterization of the native and desialylated human apo-transferrin. Heliyon 7(9), p.e08030. https://doi.org/10.1016/j.heliyon.2021.e08030

Fu, D., van Halbeek, H., 1992. N-glycosylation site mapping of human serotransferrin by serial lectin affinity chromatography, fast atom bombardment-mass spectrometry, and 1H nuclear magnetic resonance spectroscopy. Anal. Biochem. 206, 53–63. https://doi.org/10.1016/S0003-2697(05)80010

MacGillivray, R.T., Moore, S.A., Chen, J., Anderson, B.F., Baker, H., Luo, Y., Bewley, M., Smith, C.A., Murphy, M.E., Wang, Y., Mason, A.B., Woodworth, R.C., Brayer, G.D., Baker, E.N., 1998. Two high-resolution crystal structures of the recombinant N-lobe of human transferrin reveal a structural change implicated in iron release. Biochemistry 2; 37(22). https://doi.org/10.1021/bi980355j

3. RAD 2: LOW-PRESSURE CHROMATOGRAPHIC SEPARATION AND UV/VIS SPECTROPHOTOMETRIC CHARACTERIZATION OF THE NATIVE AND DESIALYLATED HUMAN APO-TRANSFERRIN

Heliyon 7 (2021) e08030

Contents lists available at ScienceDirect

Heliyon

journal homepage: www.cell.com/heliyon

Research article

Low-pressure chromatographic separation and UV/Vis spectrophotometric characterization of the native and desialylated human apo-transferrin

Tomislav Friganović, Antonela Tomašić, Tino Šeba, Ivan Biruš, Robert Kerep, Valentina Borko, Davor Šakić, Mario Gabričević, Tin Weitner *

Faculty of Pharmacy and Biochemistry, University of Zagreb, Ante Kovačića 1, 10000 Zagreb, Croatia

ARTICLE INFO

Keywords:
Transferrin
Glycoforms
Sialic acid
Chromatography
UV-Vis spectroscopy
Molar absorbance

ABSTRACT

Low-pressure pH gradient ion exchange separation provides a fast, simple and cost-effective method for preparative purification of native and desialylated apo-transferrin. The method enables easy monitoring of the extent of the desialylation reaction and also the efficient separation and purification of protein fractions after desialylation. The *N*-glycan analysis shows that the modified desialylation protocol successfully reduces the content of the sialylated fractions relative to the native apo-transferrin. In the optimized protocol, the desialylation capacity is increased by 150 %, compared to the original protocol provided by the manufacturer. The molar absorption coefficients in the near-UV region for the native and desialylated apo-transferrin differ by several percent, suggesting a subtle dependence of the glycoprotein absorbance on the variable sialic acid content. The method can easily be modified for other glycoproteins and is particularly appropriate for quick testing of sialic acid content in the protein glycosylation patterns prior to further verification by mass spectrometry.

1. Introduction

Glycosylation is one of the most common posttranslational modifications of proteins. Nearly all membrane and secreted proteins, as well as numerous intracellular proteins, are modified with complex glycan structures to enable communication, binding, recognition and/or modification of the protein activity. Such modified proteins play a role in almost every biological process and are involved in numerous major diseases [1]. Glycan moieties of glycoproteins are not synthesized using a direct genetic template. Instead, they result from the interplay of several hundred enzymes organized in complex pathways. Increase of interest for glycosylation and other associated processes resulted in the opening of a new field in biology named glycobiology [2, 3]. Changes in the glycosylation pattern can have an important role in cellular recognition and the regulation of gene expression, in addition to the influence on function of proteins. Furthermore, a change of the glycosylation pattern has been associated with numerous pathological conditions [4].

Transferrin is a heavily glycosylated serum protein that binds to and consequently mediates the cellular transport of iron. Reference range of the human serum levels is 1940–3420 mg/L, but this may be increased during pregnancy, therapy with oral contraceptives and/or due to increased synthesis caused by iron deficiency. Lower values are characteristic for increased catabolism, liver problems, chronic infections, malnutrition, trauma etc. Half-life of transferrin in the serum is about 16 hours. [5]. Transferrin structure consists of 679 amino acids with two glycan structures covalently linked to asparagine residues 413 and 611. Glycan structures can be bi- or tri-antennary and each of them terminates with sialic acid. In normal serum, 85 % is tetra-sialotransferrin and the rest (15 %) is penta- or tri-sialotransferrin [6]. The scheme of human transferrin glycoforms microheterogeneity is shown in Figure 1. Gene mutations can cause defects in glycosylation resulting in inborn errors of metabolism, characterized by deficient or reduced glycosylation and known as congenital disorders of glycosylation (CDGs) [7]. Change of sialylation has also been linked to alcoholism and many pathological states [8, 9]. Nowadays, the analysis of glycosylation change is used as a diagnostic tool for alcoholism and congenital disorders of glycosylation [10, 11]. Importantly, the sialylation of transferrin may alter its fundamental function as iron carrier and may also affect the transfer of iron into liver [12, 13].

Ferroptosis, a newly identified form of non-apoptotic regulated cell death characterized by iron-dependent accumulation of lipid peroxides plays a vital role in the treatment of tumours, renal failure or ischemia reperfusion injury [14]. Both transferrin and transferrin receptor 1 (TFR1) are required for ferroptosis induction [15], and this might

* Corresponding author.
E-mail address: tin.weitner@pharma.unizg.hr (T. Weitner).

https://doi.org/10.1016/j.heliyon.2021.e08030
Received 1 March 2021; Received in revised form 4 May 2021; Accepted 15 September 2021

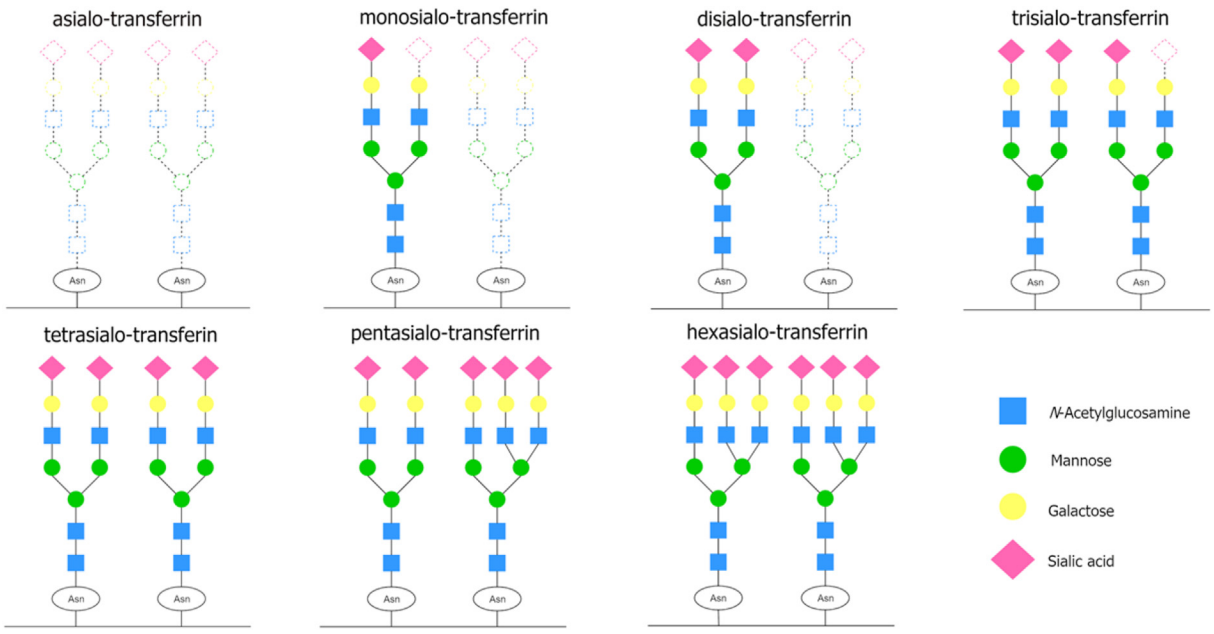

Figure 1. Schematic representation of the microheterogeneity of human transferrin glycoforms.

provide new implications for the function of transferrin sialylation patterns. Recently, it has been hypothesized that ferroptosis may be an important cause of multiple organ involvement in severe coronavirus disease 2019 (COVID-19) for a substantial proportion of patients who have lymphopenia, low serum iron levels, and multiple organ involvement [16]. Severe COVID-19 disease, caused by severe acute respiratory syndrome coronavirus 2 (SARS-CoV-2) has also been associated with disseminated intravascular coagulation and thrombosis, accompanied by an upregulated expression of transferrin in SARS-CoV-2-infected cells [17]. Notably, transferrin has been identified an important clotting regulator and an adjuster in the maintenance of blood coagulation balance [18]. Another recent report indicates that transferrin receptor is possible entry point for SARS-CoV-2 and a promising anti-COVID-19 target [19].

For further mechanistic studies, it is crucial to develop robust methods of preparation and characterization of transferrin sialoforms. The purpose of this study is to define the optimal transferrin desialylation procedure and then separate the desialylated apo-transferrin (Tf-S) from the native apo-transferrin (Tf+S) using low-pressure pH gradient ion exchange chromatography. Detailed *N*-glycan analysis and UV/Vis spectrophotometric characterization of the obtained Tf-S and Tf+S fractions is provided as a first step towards detailed iron binding and/or release studies.

2. Material and methods

2.1. Reagents

Native human apo-transferrin (Biorbyt, UK, cat. no. orb80927), sodium acetate trihydrate (Kemika, Croatia), calcium chloride (Lach-Ner, Croatia), sodium chloride (Kemika, Croatia), neuraminidase (GlycoCleave® Neuraminidase Kit, GALAB Technologies, Germany, cat. no. 132011), pISep Buffer Kit (CryoBioPhysica, USA, cat. no. 20055), hydrogen chloride (Carlo Erba Reagents, Italy, 37 % solution), sodium hydroxide (Kemika, Croatia, pellets 2–5 mm), sodium phosphate (Kemika, Croatia), guanidine hydrochloride (PanReac AppliChem, USA), MES (2-(*N*-morpholino)ethanesulfonic acid, Sigma Aldrich, USA) and potassium chloride (Alkaloid, North Macedonia) were used without further purification. Water used for experiments was double distilled in an all-glass apparatus. All experiments except the enzymatic desialylation were performed at room temperature.

2.2. Methods

2.2.1. Preparation of the desialylated protein

Desialylated apo-transferrin is prepared by incubation of immobilized neuraminidase enzyme beads suspension (Glycocleave) in the native apo-transferrin buffered stock solution (pH = 5.5, t = 38 °C). After the incubation period of 48 hours, the desialylated sample is collected, washed out and concentrated by centrifugal filtration. The complete protocol has been described elsewhere [20].

2.2.2. Separation and purification of desialylated protein

Sialoform separation is performed by using specialized pH gradient ion exchange chromatography buffers (pIsep). The mixture of fully desialylated apo-transferrin and native apo-transferrin is dissolved in the start buffer pIsep A (pH = 8) and injected onto HiTrap Q HP anion exchange chromatography columns (Cytiva, USA). Two 1 mL columns were serially connected for improved separation. Elution is done by single step linear gradient (0–100 % pIsep B, pH = 4) procedure using ÄKTA Start

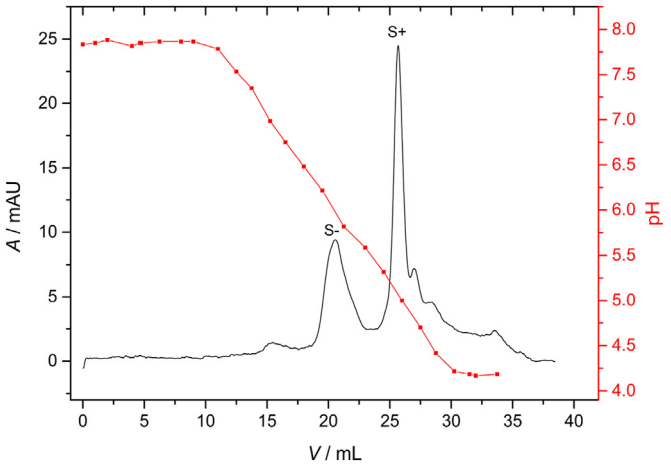

Figure 2. Low-pressure pH gradient ion exchange separation of native (S+) and desialylated (S-) human transferrin with two distinct signals matching different sialoforms, corresponding to 90 μg of Tf-S and 150 μg of Tf+S (black trace). The pH gradient obtained using pISep buffers is displayed as the red trace.

Table 1. Structure and content of *N*-glycans in the native and desialylated apo-transferrin, Tf+S and Tf-S, respectively, as determined by UPLC-MS. The *N*-glycan composition was determined by MS and the percent content of individual structures was calculated from the integrals of corresponding UPLC fluorescence signals [24]. The dominant fractions with a content ≥5% are printed in bold and make up approximately 90% of the total protein. The *IS* value corresponds to the proposed index of sialylation defined in Eq. (1).

Native apo-transferrin (Tf+S): pI = 5.3; *IS* = 158.87					**Desialylated apo-transferrin (Tf-S): pI = 6.5; *IS* = 9.76**		
N*-glycan composition		**Content / %**	**Schematic *N*-glycan structure****	***N*-glycan mass / $[M+2H]^{2+}$ *Theoretical (Measured)***	***N*-glycan composition***		**Content / %**
1	FA2	0.36		792.314 (792.318)	1	FA2	0.35
2	FA2G1	0.31		873.340 (873.345)	2	FA2G1	0.35
3	A2G2	3.43		881.338 (881.343)	**3**	**A2G2**	**77.66**
4	FA2G2	0.52		954.367 (954.371)	**4**	**FA2G2**	**5.23**
				1055.906 (1055.910)	5	FA3G2	0.46
				954.367 (954.371)	6	A2F1G2	1.74
5	**A2G2S1**	**1.62**		1026.885 (1026.891)	7	**A2G2S1**	**8.39**
6	**A2G2S1**	**27.21**		1026.885 (1026.891)			
7	A3G3	0.54		1063.904 (1063.911)	8	A3G3	3.56
8	FA2G2S1	1.98		1099.914 (1099.920) 1136.933 (1136.939)	9	FA2G2S1 A3F1G3	0.56
9* **	**A2G2S2**	**6.49**		1172.433 (1172.438)			
10* **	**A2G2S2**	**53.70**		1172.433 (1172.441)			
11	FA2G2S2	3.84		1245.462 (1245.469)			
				1136.933 (1136.937)	10	A3F1G3	0.89
				1209.452 (1209.456)	11	A3G3S1	0.81

* Structure abbreviations: all *N*-glycans have two core *N*-acetylglucosamines (GlcNAc); Ax, number of antennae (GlcNAc) on trimannosyl core; A2, biantennary with both GlcNAcs as β1,2-linked; A3, triantennary with a GlcNAc linked β1,2 to both mannose and the third GlcNAc linked β1,4 to the α1,3 linked mannose; A4, GlcNAcs linked as A3 with additional GlcNAc β1,6 linked to α1,6 mannose; Gx, number (x) of β1,4 linked galactose on antenna; F(x), number (x) of fucose linked α1,3 to antenna GlcNAc; Sx, number (x) of sialic acids linked to galactose. [24,32]

** Schematic *N*-glycan structures: *N*-acetylglucosamine (■), mannose (●), galactose (●), fucose (▼), sialic acid (◆).

*** Structure A2G2S2 corresponds to a biantennary *N*-glycan with two terminal sialic acids that can be either α2,3 or α2,6 linked to galactose. These *N*-glycans have identical mass but can be separated by UPLC due to the different linkage and are therefore shown as separate fractions.

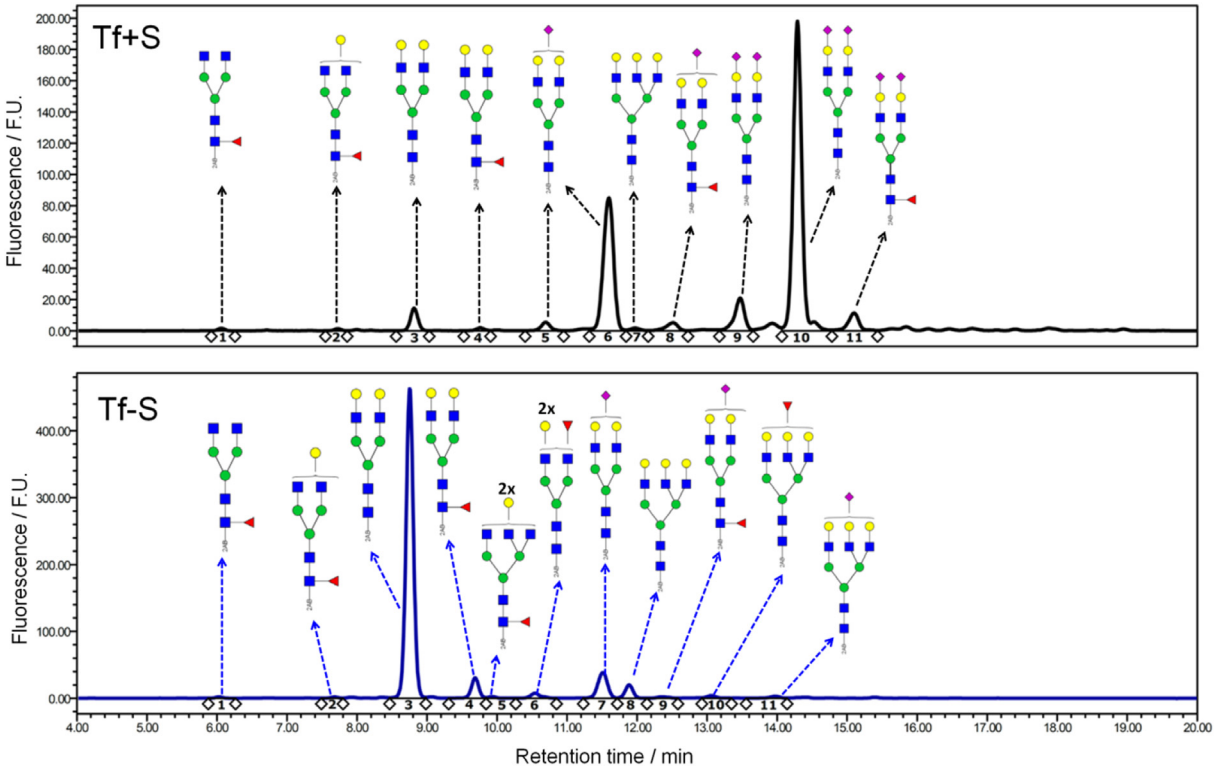

Figure 3. Structures of various *N*-glycan residues in the native apo-transferrin, Tf+S (black trace), and desialylated apo-transferrin, Tf-S (blue trace), as determined by UPLC-MS [24]. Schematic *N*-glycan structures and the corresponding fluorescence signals are indicated by arrows: *N*-acetylglucosamine (blue), mannose (green), galactose (yellow), fucose (red), sialic acid (pink).

Table 2. Structure and content of *N*-glycans in the desialylated apo-transferrin, Tf-S, for two separate batches run at different times from the same original batch of the native protein, as determined by UPLC-MS. The *N*-glycan composition was determined as described in Table 1. The *IS* value corresponds to the proposed index of sialylation defined in Eq. (1).

Desialylated apo-transferrin (Tf-S): pI = 6.5				
Structure		Content/%		
		Fresh Enzyme	Recycled Enzyme*	Difference
1	FA2	0.35	0.46	-0.11
2	FA2G1	0.35	0.39	-0.04
3	A2G2	77.66	78.25	-0.59
4	FA2G2	5.23	5.95	-0.72
5	FA3G2	0.46	0.50	-0.04
6	A2F1G2	1.74	1.71	0.03
7	A2G2S1	8.39	7.80	0.59
8	A3G3	3.56	3.03	0.53
9	FA2G2S1 A3F1G3	0.56	0.61	-0.05
10	A3F1G3	0.89	0.53	0.36
11	A3G3S1	0.81	0.77	0.04
IS		**9.76**	**9.18**	**-0.58**

* Due to the decreased activity of the recycled enzyme, the incubation time was increased from 2 days (for the fresh enzyme) to 9 days (for the recycled enzyme).

protein purification system (Cytiva, USA). Protein concentration in the eluate is monitored by measuring absorbance at $\lambda = 280$ nm and protein fraction recovery can be calculated by integration over surface area (mL × mAU). After separation, the pH value of each fraction containing eluted protein was measured, corresponding to the approximate protein isoelectric point, pI. Full details of the pH-gradient chromatography have been described elsewhere [21].

2.2.3. Protein characterization by UPLC-MS

In order to verify the results of the enzymatic desialylation of the native protein and pH-gradient separation of different sialoforms, the complete *N*-glycan profiling of Tf+S and Tf-S was performed. Briefly, the protein *N*-glycans were released with the addition of 1.2 U of PNGase F (Promega, USA) and overnight incubation at 37° C. The released *N*-glycans were labeled with 2-aminobenzamide (Sigma Aldrich, USA) and purified using hydrophilic interaction liquid chromatography solid-phase extraction (HILIC-SPE). Fluorescently labeled *N*-glycans were separated by Acquity UPLC H-Class instrument (Waters, USA) using BEH Glycan chromatography column (Waters, USA). All glycan structures were annotated with MS/MS analysis using Synapt G2-Si ESI-QTOF-MS system (Waters, USA). Glycan compositions and structural features were assigned using software tools GlycoWorkbench and Glycomode, according to obtained MS and MS/MS spectra [22, 23]. Full details of the protein characterization by UPLC-MS have been described elsewhere [24].

2.2.4. Protein characterization by UV/Vis spectroscopy

In order to facilitate the determination of protein quantities in mechanistic studies, the molar absorption coefficients of both the native and desialylated protein were determined according to the modified Edelhoch method, as described elsewhere [25]. Briefly, the folded protein absorbance at 280 nm (A_{280}) was measured in 25 mM sodium phosphate buffer (pH = 7.4). The unfolded (denatured) protein absorbance at 280 nm ($A_{u\ 280}$) was measured in the same buffer in the presence of 6 M guanidine HCl. The molar absorption coefficient of a folded protein at 280 nm (ε_{280}) is then equal to the product of a reference molar absorption coefficient for the unfolded protein, $\varepsilon_{u\ 280}$, and the ratio of folded and unfolded protein absorbance, i.e. $\varepsilon_{280} = \varepsilon_{u\ 280} \times A_{280}/A_{u\ 280}$. The reference value of $\varepsilon_{u\ 280} = 81080$ has been calculated from the contributions of 8 tryptophan, 26 tyrosine and 19 cystine residues in apo-transferrin structure [26, 27, 28]. The UV/Vis measurements were

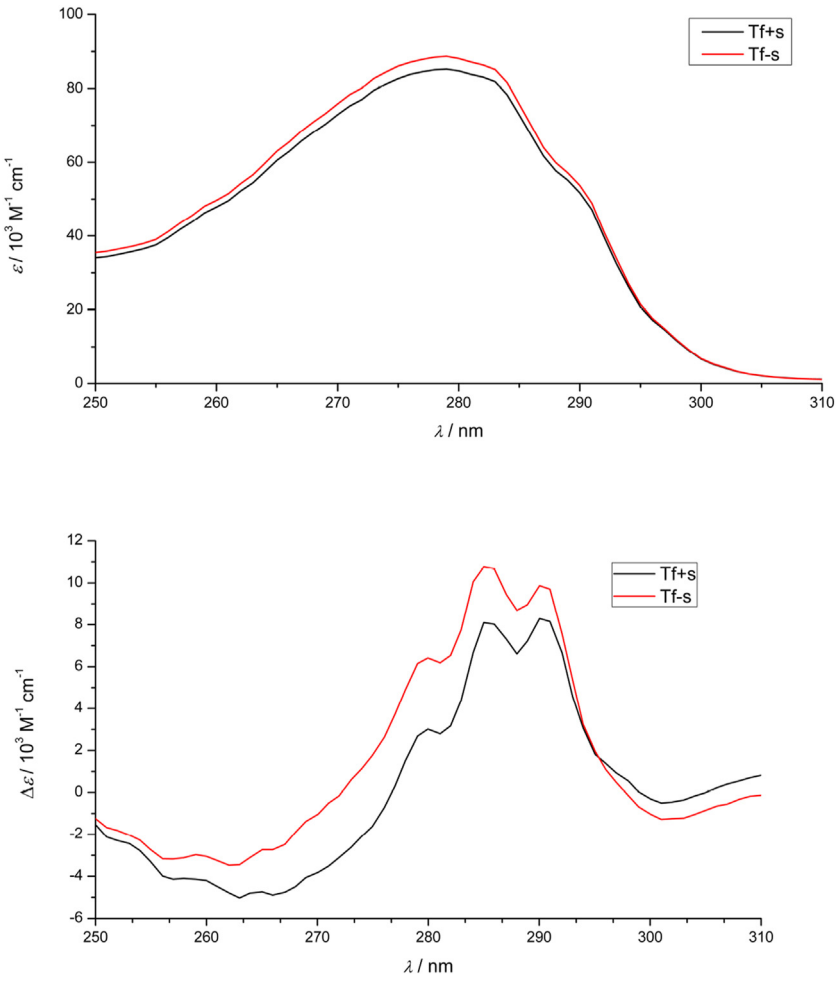

Figure 4. Top: The molar absorption coefficient, ε, of the Tf+S (black) and Tf-S (red) fractions in the near-UV range: ε_{280} (Tf+S) = (84.8 ± 0.2) × 10^3 M^{-1} cm^{-1} and ε_{280} (Tf-S) = (88.2 ± 0.2) × 10^3 M^{-1} cm^{-1}; Bottom: The difference in molar absorption coefficients, $\Delta\varepsilon$, for the intact and denatured proteins: Tf+S (black trace) and Tf-S (red trace). The values were calculated as $\Delta\varepsilon = \varepsilon_f - \varepsilon_u$, where ε_f is the molar absorption coefficient of the intact (folded) protein, and ε_u is the molar absorption coefficient of the denatured (folded) protein in 6 M guanidine [25].

performed on a Varian Cary 50 spectrophotometer (Varian, Australia) using a quartz cell with pathlength $l = 1$ cm (Hellma, Germany).

The dependence of native apo-transferrin absorbance (A_{280}) on salt concentration and pH was also measured in the range 0 M < [KCl] < 1.0 M and 4.9 < pH < 7.6. For salt concentration dependence, a stock solution of Tf+S was prepared in 25 mM sodium phosphate buffer (Buffer 1, pH = 7.4). Another buffer solution containing 25 mM sodium phosphate and 2 M KCl was also prepared (Buffer 2, pH = 7.4). To obtain samples with different total KCl concentrations, 100 μL of the stock transferrin solution was mixed with 100 μL of Buffer 1 and Buffer 2 mixtures in varying ratios to prepare working solutions with the final volume of 200 μL (final Tf+S concentration of 0.4 mg/mL). For measuring pH dependence, a stock solution of Tf+S was prepared in purified water. A buffer solution containing 50 mM MES, 50 mM sodium phosphate, and 0.4 M KCl (Buffer 3) was prepared separately and adjusted to pH values of 5.0, 5.5, 6.0, 6.5, 7.0, and 7.5 by adding an appropriate amount of 5 M NaOH. To obtain samples with different final pH, 100 μL of the stock transferrin solution was mixed with 100 μL of Buffer 3 to prepare working solutions with the final volume of 200 μL (final Tf+S concentration of 0.3 mg/mL). The final pH of the working solutions was measured using Mettler-Toledo MP 220 pH-meter (Mettler-Toledo, Switzerland) calibrated with standard buffer solutions (pH = 4.00 and pH = 7.00).

All samples were prepared in triplicate and A_{280} was measured for each sample in a quartz cell ($l = 1$ cm) using Varian Cary 50 spectrophotometer (Varian, Australia). The data were analyzed using a single factor ANOVA routine in Microsoft Excel Data Analysis Toolpak. If the calculated *P*-value is more than the chosen confidence level ($\alpha = 0.05$), and the obtained *F*-value is less than the critical *F*-value, the null-hypothesis that there is no significant difference between the means of the samples should not be rejected [29].

3. Results and discussion

3.1. Enzymatic desialylation

Compared to the original protocol [30], the concentration of working buffer was increased from 0.05 M to 0.2 M, thus increasing the desialylation capacity from 2 mg of protein to 5 mg of protein per reaction cycle, corresponding to 150 % increase in the reaction throughput. The final ratio is 1 mL of the immobilized enzyme suspension per 25 mg of protein. The desialylation enzyme is stable and can be used multiple times if an appropriate rinsing and preserving procedure is applied. However, the immobilized enzyme activity decreases after repeated use and increased incubation time is necessary to obtain comparable degree of protein desialylation. For successful desialylation, it is crucial to closely monitor the pH of the solution before and during the reaction (optimal pH = 5.5) and adjust accordingly by the addition of alkali. The reaction releases terminal sialic acids and unchecked acidification of the reaction mixture can inactivate the enzyme.

3.2. The pH chromatofocusing of native and desialylated transferrin

Initial attempts to form of externally controlled pH gradient in the range from pH = 8 to pH = 4 using either Servalyt (SERVA Electrophoresis, Germany) or Pharmalyte (Cytiva, USA) buffers were unsuccessful,

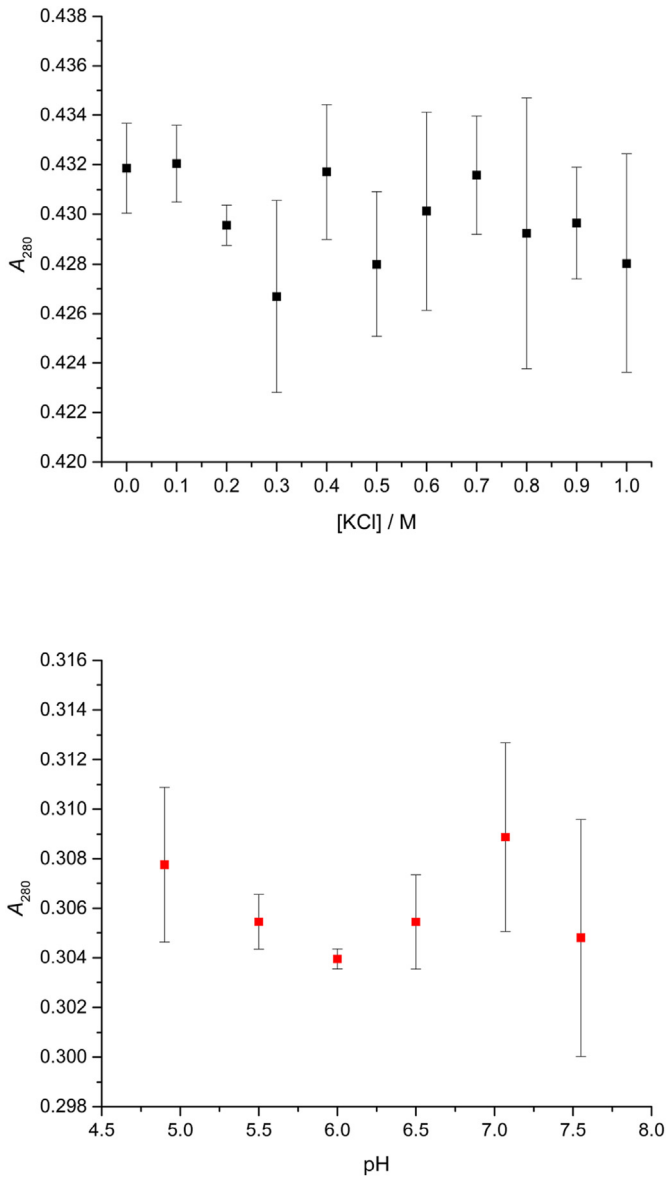

Figure 5. Top: The dependence of Tf+S solution absorbance (A_{280}) on salt concentration: average values (black) and standard deviations (error bars) for triplicate samples, 0 M < [KCl] < 1.0 M, pH = 7.4; Bottom: The dependence of Tf+S solution absorbance (A_{280}) on pH: average values (red) and standard deviations (error bars) for triplicate samples, 4.9 < pH < 7.6, [KCl] = 0.2 M.

presumably due to insufficient buffering capacity at specific pH values (data not shown). However, a very linear pH gradient over the required pH range was achieved using pISep buffers that are specifically designed for chromatofocusing [31]. The pH gradient shown in Figure 2 (red trace) is linear in the range of 11–30 mL, corresponding to the range 7.78 > pH > 4.22 (R2 = 0.999). An additional improvement achieved using pISep buffer was in a significantly reduced absorbance baseline at 280 nm, making it easier to monitor protein elution from the column and more accurately calculate the amount of eluted protein by integrating chromatograms. However, the precise preparation of chromatofocusing buffers requires the special pISep pH gradient maker software.

Further improvement in transferrin sialoform separation was achieved by connecting two 1 mL HiTrap Q HP columns in a series, as compared to using only one 1 mL column. The two-column series backpressure of 0.15 MPa was well within the operational range of the ÄKTA Start system. The observed pI values for the native (pI ≈ 5) and desialylated (pI ≈ 6) apo-transferrin differ significantly and hence can be fully separated (Figure 2).

Table 3. Results of the single factor ANOVA routine in Microsoft Excel for the dependence of native transferrin (Tf+S) absorbance (A_{280}) on salt concentration. The average values and standard deviations of individual measurements are given in Figure 5, Top. The default confidence level for analysis is $\alpha = 0.05$.

Anova: Single Factor ($\alpha = 0.05$)

Summary		A_{280}			
[KCl]/M	Count	Sum	Average	Standard deviation	Variance/10^6
0	3	1.2955	0.4318	0.0018	3.30
0.1	3	1.2961	0.4320	0.0016	2.42
0.2	3	1.2887	0.4296	0.0008	0.65
0.3	3	1.2801	0.4267	0.0039	14.9
0.4	3	1.2951	0.4317	0.0027	7.40
0.5	3	1.2840	0.4280	0.0029	8.51
0.6	3	1.2904	0.4301	0.0040	15.9
0.7	3	1.2947	0.4316	0.0024	5.67
0.8	3	1.2877	0.4292	0.0055	29.9
0.9	3	1.2889	0.4296	0.0023	5.06
1	3	1.2841	0.4280	0.0044	19.4

ANOVA*

Source of Variation	SS/10^4	df	MS/10^5	F	P-value	F crit.
Between Groups	0.977	10	0.977	0.950	**0.510**	2.297
Within Groups	2.262	22	1.028			

* Definitions of parameters: *SS* represents the sum of squared deviations from the mean; *df* represents degrees of freedom; *MS* represents the mean square value; *F* represents the *F*-ratio; *F crit.* represents the critical *F*-value based on the *F*-distribution [29].

3.3. The N-glycan analysis of the native and desialylated transferrin

In order to confirm the results of the pH chromatofocusing, both elution fractions, Tf+S and Tf-S, were analyzed by mass spectroscopy [24, 32]. The detailed *N*-glycan structure and quantification of transferrin sialoforms determined by UPLC-MS (Table 1 and Figure 3) shows that the native apo-transferrin (Tf+S) is dominated by glycan structures with 1 or 2 terminal sialic acid (A2G2S1 and A2G2S2) which together make up approximately 90 % of the total glycan content. Conversely, the *N*-glycan structures without the terminal sialic acids (A2G2, FA2G2) are dominant in desialylated apo-transferrin (Tf-S) and together make up approximately 90 % of the total glycan content. The applied protocol requires 100 μg of protein and should be repeated each time a new commercial sample is purchased and also after each desialylation cycle.

The reproducibility of the *N*-glycan content was tested for two separate batches run at different times from the same original batch of the native protein. The first batch of Tf-S was prepared with the fresh enzyme, whereas the second batch of Tf-S was prepared with the enzyme that has been recycled a number of times. Due to the decreased activity of the recycled enzyme, the incubation time was increased from 2 days (for the fresh enzyme) to 9 days (for the recycled enzyme). However, the content differences are within 1 % for every *N*-glycan fraction, as shown in Table 2.

According to the manufacturer's specifications, the used enzyme preferentially hydrolyzes α2,3 linkages of sialic acid, but will also cleave α2,6 and α2,8 linkages, with the preference for α2,3 linkages estimated at 260-fold [30]. This preference for α2,3 linked sialic acids might account for the observed incomplete desialylation of the native protein (approximately 10 % remaining sialylated *N*-glycan fractions).

For the purpose of simple comparison of the overall protein sialic acid content for different samples we propose a simple measure, *index of sialylation*, defined in Eq. (1):

Table 4. Results of the single factor ANOVA routine in Microsoft Excel for the dependence of native transferrin (Tf+S) UV/Vis spectrum on pH. The average values and standard deviations of individual measurements are given in Figure 5, Bottom. The default confidence level for analysis is $\alpha = 0.05$.

Anova: Single Factor ($\alpha = 0.05$)

Summary		A_{280}			
pH	Count	Sum	Average	Standard deviation	Variance/10^6
4.9	3	0.9233	0.3078	0.0031	9.80
5.5	3	0.9163	0.3054	0.0011	1.22
6.0	3	0.9118	0.3039	0.0004	0.17
6.5	3	0.9163	0.3054	0.0019	3.66
7.1	3	0.9266	0.3089	0.0038	14.6
7.6	3	0.9144	0.3048	0.0048	22.9

ANOVA*

Source of Variation	SS/10^4	df	MS/10^5	F	P-value	F crit.
Between Groups	0.528	5	1.056	1.210	**0.362**	3.106
Within Groups	1.047	12	0.872			

* Definitions of parameters are the same as in Table 3.

$$IS = \sum_{i=1}^{n} f_i \times s_i, \quad (1)$$

where *IS* is the index of sialylation, *n* is the number of the *N*-glycan fraction, f_i is the % content of the particular *N*-glycan fraction and s_i is the number of sialic acids in the structure of the same *N*-glycan fraction. The composition of the native protein sample in Table 1 yields the value *IS* (Tf+S) = 158.87. For comparison, the desialylated protein sample in Table 1 yields the value *IS* (Tf-S) = 9.76, signifying 93.9 % reduction in the protein sialic acid content. Similar comparison of the desialylated protein samples in Table 2 yields only 0.58 % difference in the overall sialic acid content between Tf-S batches.

3.4. The molar absorption coefficients of the native and desialylated transferrin

The determined molar absorption coefficients in the near-UV range for of the Tf+S and Tf-S fractions, ε_{280} (Tf+S) = (84.8 ± 0.2) × 10^3 M^{-1} cm^{-1} and ε_{280} (Tf-S) = (88.2 ± 0.2) × 10^3 M^{-1} cm^{-1} (Figure 4, Top), will allow precise determination of concentrations in protein samples, which is important due to the variable water and salt content in commercial samples (up to 15 % w/w). The observed values of ε_{280} for the native and desialylated protein differ by approximately 4 %, probably due to the change in dielectric microenvironment. This effect can be attributed to interplay of the negatively charged sialic acid groups on the protein surface with aromatic amino acid residues in the protein structure. Alternatively, this effect can also arise from small conformational change in the protein due to different solvation of Tf+S and Tf-S caused by different surface charge. Such a small conformational change might indeed be the reason for the subtle variations in the Tf+S and Tf-S difference spectra obtained by denaturation in 6 M guanidine (Figure 4, Bottom) [25, 33, 34].

The measured absorbance of Tf+S at 280 nm shows no significant dependence on salt concentration up to 1 M KCl or pH in the range 4.9 < pH < 7.6 (Figure 5). The resulting *P*-value calculated using a single factor ANOVA routine in Microsoft Excel was greater than the default confidence level ($P > 0.05$), resulting in the acceptance of the null-hypothesis of equal means (Tables 3 and 4) [29].

These results will allow the precise determination of the molar absorption coefficients of iron-saturated transferrin species, as well as the determination of the fluorescence properties of the proteins. The applied protocol requires 1 mg of protein, of which 60 % can be reused for other measurements. Similarly to the *N*-glycan analysis, the molar absorption coefficients determination should also be repeated for each new native protein batch and each desialylation cycle due to possible variable sialic acid content.

4. Conclusions

Low-pressure pH gradient ion exchange separation provides a fast, simple and cost-effective method for preparative purification of native and desialylated apo-transferrin. The method enables easy monitoring of the extent of the desialylation reaction and also the efficient separation and purification of protein fractions after the desialylation reaction is terminated. Furthermore, the method can easily be modified for other glycoproteins and is particularly appropriate for quick testing of protein sialic acid content prior to verification by mass spectrometry. The *N*-glycan analysis shows that the modified desialylation protocol successfully reduces the content of the sialylated fractions relative to the native apo-transferrin. In the optimized protocol, the desialylation capacity is increased by 150 %, compared to the original protocol provided by the manufacturer.

In order to ensure the reproducibility of any further mechanistic studies, the complete *N*-glycan assignation and molar coefficients determination should be performed for each new native protein batch, as well as after every desialylation cycle. This is important because different native protein batches might have different *N*-glycan profiles, depending on the protein source. Additionally, the decreased enzyme activity after repeated use requires extended incubation time for sufficient desialylation. Importantly, the molar absorption coefficients of the native and desialylated apo-transferrin differ by several percent, suggesting that the literature data on glycoprotein molar absorption coefficients should be taken with caution because the measurement depends on the *N*-glycan composition of the protein, which is variable.

Declarations

Author contribution statement

Tomislav Friganović: Conceived and designed the experiments; Performed the experiments; Analyzed and interpreted the data; Wrote the paper.

Antonela Tomašić; Tino Šeba; Ivan Biruš; Robert Kerep; Valentina Borko: Performed the experiments; Analyzed and interpreted the data.

Davor Šakić: Analyzed and interpreted the data; Wrote the paper.

Mario Gabričević: Contributed reagents, materials, analysis tools or data; Analyzed and interpreted the data.

Tin Weitner: Conceived and designed the experiments; Analyzed and interpreted the data; Contributed reagents, materials, analysis tools or data; Wrote the paper.

Funding statement

This work was supported by Hrvatska Zaklada za Znanost (UIP-2017-05-9537 and IP-2016-06-3672) and European structural and investment funds (KK.01.1.1.01.0010 and KK.01.2.2.03.0006).

Data availability statement

Data will be made available on request.

Declaration of interests statement

The authors declare no conflict of interest.

Additional information

No additional information is available for this paper.

Acknowledgements

The *N*-glycan profiling by UPLC-MS was provided by the Department of Biochemistry and Molecular Biology, Faculty of Pharmacy and Biochemistry, Ante Kovačića 1, 10000 Zagreb, Croatia.

References

[1] K.W. Moremen, M. Tiemeyer, A.V. Nairn, Vertebrate protein glycosylation: diversity, synthesis and function, Nat. Rev. Mol. Cell Biol. 13 (2012) 448–462.
[2] A. Varki, R.D. Cummings, J.D. Esko, H.H. Freeze, P. Stanley, C.R. Bertozzi, G.W. Hart, M.E. Etzler (Eds.), Essentials of Glycobiology, second ed., Cold Spring Harbor Laboratory Press, Cold Spring Harbor (NY), 2009. http://www.ncbi.nlm.nih.gov/books/NBK1908/. (Accessed 12 February 2021).
[3] J. Alper, Searching for medicine's sweet spot, Science 291 (2001) 2338–2343.
[4] A. Kobata, A retrospective and prospective view of glycopathology, Glycoconj. J. 15 (1998) 323–331.
[5] H. Stibler, Carbohydrate-deficient transferrin in serum: a new marker of potentially harmful alcohol consumption reviewed, Clin. Chem. 37 (1991) 2029–2037.
[6] G. de Jong, H.G. van Eijk, Microheterogeneity of human serum transferrin: a biological phenomenon studied by isoelectric focusing in immobilized pH gradients, Electrophoresis 9 (1988) 589–598.
[7] S. Supraha Goreta, S. Dabelic, J. Dumic, Insights into complexity of congenital disorders of glycosylation, Biochem. Med. (2012) 156–170.
[8] P. König, H. Niederhofer, H. Steurer, R. Haller, R. Wölfle, H. Fritzsche, P. Weiss, Changes of carbohydrate-deficient transferrin in chronic, Alcoholism, Neuropsychobiology. 32 (1995) 192–196.
[9] T. Arndt, Carbohydrate-deficient transferrin as a marker of chronic alcohol abuse: a critical review of preanalysis, analysis, and interpretation, Clin. Chem. 47 (2001) 13–27.
[10] M. Grønbaek, J.H. Henriksen, U. Becker, Carbohydrate-deficient transferrin–a valid marker of alcoholism in population studies? Results from the Copenhagen City Heart Study, Alcohol Clin. Exp. Res. 19 (1995) 457–461.
[11] M. Edwards, F. McKenzie, S. O'callaghan, D. Somerset, P. Woodford, J. Spilsbury, M. Fietz, J. Fletcher, Prenatal diagnosis of congenital disorder of glycosylation type Ia (CDG-Ia) by cordocentesis and transferrin isoelectric focussing of serum of a 27-week fetus with non-immune hydrops, Prenat. Diagn. 26 (2006) 985–988.
[12] M. Piagnerelli, K.Z. Boudjeltia, V. Nuyens, D. De Backer, F. Su, Z. Wang, J.-L. Vincent, M. Vanhaeverbeek, Rapid alterations in transferrin sialylation during sepsis, Shock Augusta Ga 24 (2005) 48–52.
[13] Y. Beguin, G. Bergamaschi, H.A. Huebers, C.A. Finch, The behavior of asialotransferrin-iron in the rat, Am. J. Hematol. 29 (1988) 204–210.
[14] P. Lei, T. Bai, Y. Sun, Mechanisms of ferroptosis and relations with regulated cell death: a review, Front. Physiol. 10 (2019).
[15] T. Xu, W. Ding, X. Ji, X. Ao, Y. Liu, W. Yu, J. Wang, Molecular mechanisms of ferroptosis and its role in cancer therapy, J. Cell Mol. Med. 23 (2019) 4900–4912.
[16] M. Yang, C.L. Lai, SARS-CoV-2 infection: can ferroptosis be a potential treatment target for multiple organ involvement? Cell Death Dis. 6 (2020) 130.
[17] K.-M. McLaughlin, M. Bechtel, D. Bojkova, C. Münch, S. Ciesek, M.N. Wass, M. Michaelis, J. Cinatl, COVID-19-Related coagulopathy—is transferrin a missing link? Diagnostics 10 (2020) 539.
[18] X. Tang, Z. Zhang, M. Fang, Y. Han, G. Wang, S. Wang, M. Xue, Y. Li, L. Zhang, J. Wu, B. Yang, J. Mwangi, Q. Lu, X. Du, R. Lai, Transferrin plays a central role in coagulation balance by interacting with clotting factors, Cell Res. 30 (2020) 119–132.
[19] X. Tang, M. Yang, Z. Duan, Z. Liao, L. Liu, R. Cheng, M. Fang, G. Wang, H. Liu, J. Xu, P.M. Kamau, Z. Zhang, L. Yang, X. Zhao, X. Peng, R. Lai, Transferrin receptor is another receptor for SARS-CoV-2 entry, BioRxiv (2020).
[20] T. Friganović, V. Borko, T. Šeba, R. Kerep, I. Biruš, T. Weitner, Protocol for Enzymatic Desialylation of Native Apo-Transferrin, Zenodo, 2020.
[21] T. Friganović, V. Borko, T. Šeba, R. Kerep, T. Weitner, Protocol for pH-Gradient Chromatofocusing of the Native and Desialylated Human Apo-Transferrin, Zenodo, 2020.
[22] A. Ceroni, K. Maass, H. Geyer, R. Geyer, A. Dell, S.M. Haslam, GlycoWorkbench: a tool for the computer-assisted annotation of mass spectra of glycans, J. Proteome Res. 7 (2008) 1650–1659.
[23] C.A. Cooper, E. Gasteiger, N.H. Packer, GlycoMod–a software tool for determining glycosylation compositions from mass spectrometric data, Proteomics 1 (2001) 340–349.
[24] T. Štambuk, A. Cvetko, T. Weitner, Protocol for Ultra Performance Liquid Chromatography-Mass Spectrometry N-Glycan Analysis of the Native and Desialylated Human Apo-Transferrin, Zenodo, 2020.
[25] T. Šeba, T. Friganović, T. Weitner, Protocol for Spectrophotometric Determination of Native and Desialylated Apo-Transferrin Molar Absorption Coefficients, Zenodo, 2020.
[26] G.R. Grimsley, C.N. Pace, Spectrophotometric determination of protein concentration, Curr. Protein Pept. Sci. 33 (2003) 3.1.1–3.1.9.
[27] N.G. James, A.B. Mason, Protocol to determine accurate absorption coefficients for iron-containing transferrins, Anal. Biochem. 378 (2008) 202–207.
[28] S.C. Gill, P.H. von Hippel, Calculation of protein extinction coefficients from amino acid sequence data, Anal. Biochem. 182 (1989) 319–326.
[29] D.M. Bourg, Excel Scientific and Engineering Cookbook, first ed., O'Reilly, Sebastopol, CA, 2006.
[30] Product Description for GlycoCleave® Neuraminidase Kit, 2009.
[31] L.I. Tsonev, A.G. Hirsh, Theory and applications of a novel ion exchange chromatographic technology using controlled pH gradients for separating proteins on anionic and cationic stationary phases, J. Chromatogr. A 1200 (2008) 166–182.
[32] R. Saldova, A. Asadi Shehni, V.D. Haakensen, I. Steinfeld, M. Hilliard, I. Kifer, A. Helland, Z. Yakhini, A.-L. Børresen-Dale, P.M. Rudd, Association of N-glycosylation with breast carcinoma and systemic features using high-resolution quantitative UPLC, J. Proteome Res. 13 (2014) 2314–2327.
[33] A.P. Demchenko, Ultraviolet Spectroscopy of Proteins, Springer Berlin / Heidelberg, Berlin, Heidelberg, 2013.
[34] F.-X. Schmid, Biological macromolecules: UV-visible spectrophotometry, in: John Wiley & Sons, Ltd (Ed.), Encycl. Life Sci., John Wiley & Sons, Ltd, Chichester, UK, 2001.

4. RAD 3: INNER FILTER EFFECT CORRECTION FOR FLUORESCENCE MEASUREMENTS IN MICROPLATES USING VARIABLE VERTICAL AXIS FOCUS

analytical chemistry

pubs.acs.org/ac

Article

Inner Filter Effect Correction for Fluorescence Measurements in Microplates Using Variable Vertical Axis Focus

Tin Weitner,* Tomislav Friganović, and Davor Šakić

Cite This: *Anal. Chem.* 2022, 94, 7107−7114

Read Online

ACCESS | Metrics & More | Article Recommendations | Supporting Information

ABSTRACT: The inner filter effect (IFE) hinders fluorescence measurements, limiting linear dependence of fluorescence signals to low sample concentrations. Modern microplate readers allow movement of the optical element in the vertical axis, changing the relative position of the focus and thus the sample geometry. The proposed *Z*-position IFE correction method requires only two fluorescence measurements at different known vertical axis positions (*z*-positions) of the optical element for the same sample. Samples of quinine sulfate, both pure and in mixtures with potassium dichromate, showed a linear dependence of corrected fluorescence on fluorophore concentration ($R^2 > 0.999$), up to $A_{ex} \approx 2$ and $A_{em} \approx 0.5$. The correction extended linear fluorescence response over ≈98% of the concentration range with ≈1% deviation of the calibration slope, effectively eliminating the need for sample dilution or separate absorbance measurements to account for IFE. The companion numerical IFE correction method further eliminates the need for any geometric parameters with similar results. Both methods are available online at https://ninfe.science.

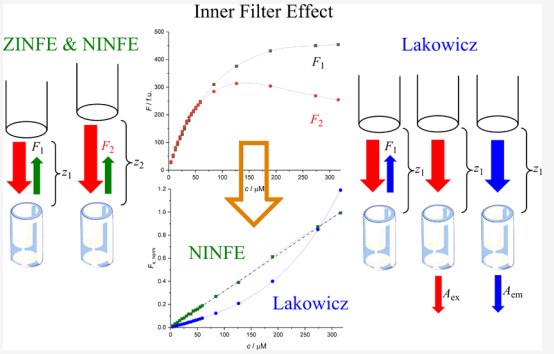

INTRODUCTION

Inner Filter Effect in Fluorescence Spectroscopy. Fluorescence has proven to be an outstanding tool for investigating the structure and dynamics of matter or living systems, with applications in the physical, chemical, material, biological, and medical sciences.[1] Advances in fluorescence technology have resulted in reduction of the cost and complexity of measurement instruments, and fluorescence spectroscopy will continue to contribute to rapid advances in biology, biotechnology, and nanotechnology.[2] Currently, fluorescence experiments for binding studies, quenching, and cell-based assays are being designed using microplate readers that allow the acquisition of spectra, anisotropies, and lifetimes.[2] The optics used in microplate readers is different from those of an instrument designed for use with a cuvette. Typically, the microplate is moved using an $x-y$ scanning stage to position each well in the observation path.[2]

As has been noted by many authors, the apparent fluorescence intensity and spectral distribution can depend on the optical density of the sample and the precise geometry of the sample illumination.[2−4] These effects can (i) reduce the intensity of the excitation at the observation point or (ii) reduce the observed fluorescence by absorbing the emitted fluorescence.[2] The resulting influences of (i) and (ii) on the detected signal are known as primary inner filter effect (IFE) and secondary IFE, or pIFE and sIFE, respectively.[3] The relative importance of each process depends on the optical densities of the sample at the excitation and emission wavelengths.[2] Therefore, fluorescence intensities are proportional to concentration only in a limited range of optical densities, and the nonlinear dependence of fluorescence intensity on the concentration of the fluorescent substance greatly complicates the determination of parameters derived from fluorescence data.[2,5] In addition, sIFE can occur for some substances with small Stokes shift if the overlap of the absorption spectrum and fluorescence emission spectrum results in the emitted fluorescence being reabsorbed by the sample.[6]

Conventional Methods for IFE Correction. Extensive research has addressed the minimization or correction of IFE using mathematical or instrumental procedures, as indicated by a number of recent reviews.[7,8] In general, the use of dilute solutions is considered the best practice,[2,5] but it has been shown that IFE correction should also be performed for low fluorophore concentrations.[5] For example, at an absorbance of $A = 0.06$, the relative error in recorded fluorescence intensity is approximately 8%, and this difference increases further to 12% at $A = 0.1$ and 38% at $A = 0.3$.[5,9] As previously noted by Wang, sample dilution may introduce additional errors and/or alter the chemical properties of the samples.[8]

Received: March 4, 2022
Accepted: April 21, 2022
Published: May 3, 2022

https://doi.org/10.1021/acs.analchem.2c01031
Anal. Chem. 2022, 94, 7107−7114

A simple and approximate method for IFE correction of observed fluorescence proposed by Lakowicz is shown in eq 1

$$F_A = F_1 \cdot 10^{(A_{ex}+A_{em})/2} \quad (1)$$

where F_A is the absorbance IFE-corrected fluorescence intensity, F_1 is the measured (uncorrected) fluorescence intensity, A_{ex} is the absorbance at the fluorescence excitation wavelength, and A_{em} is the absorbance at the selected fluorescence emission wavelength.[2]

The main assumption of this method is that the fluorescence light is collected from the center of the cell, which may not be true depending on the geometry of the sample compartment.[5,7] An additional drawback is that the absorbance of the sample at both λ_{ex} and λ_{em} must be measured independently. For a detailed overview of the properties of this correction method, the article by Panigrahi and Mishra can be referred.[4] Briefly, the authors described a geometry-dependent maximum of the achievable fluorescence intensity corresponding to a maximum concentration of the analyte, beyond which the observed fluorescence intensity decreases and the emission curve exhibits a downward curvature. They have also shown that the Lakowicz model for the IFE correction is valid only up to $A = 0.7$. For larger values of A, this model overestimates the loss of observed fluorescence due to IFE, resulting in an upward curvature of the corrected fluorescence. Notwithstanding its limitations, the Lakowicz model is currently extensively used for correcting IFE-related artifacts in the observed fluorescence intensity.[4,8] Therefore, this method was chosen as the benchmark for IFE correction.

Another relatively simple option for IFE correction is the cell shift method, in which the fluorescence intensity of the sample is measured at different positions with different effective light path lengths.[8] This method does not require direct measurements of the sample absorbance at the excitation and emission wavelengths and allows correction for both pIFE and sIFE by measuring the fluorescence intensity at two points in the sample, according to eq 2

$$F_0 = F_1\left(\frac{F_1}{F_2}\right)^{l_1/(l_2-l_1)} \quad (2)$$

where F_0 is the corrected fluorescence intensity and F_1 and F_2 are the measured fluorescence values for different light path lengths, l_1 and l_2. When using the cell shift method proposed by Lutz and Luisi, the values of l_1 and l_2 are measured along the diagonal in a standard 1 cm rectangular cell.[10] However, this method has limited applicability because it requires special instrumentation that is not commonly available, as noted in the literature.[8,11]

IFE Correction in Microplates. Unlike a standard cuvette with a fixed light path length, the light path length in a microplate well is unknown and depends on the filling volume of the wells. Modern microplate readers allow the optical element used for excitation and emission to be moved in the z-axis (perpendicular to the sample well), allowing the sample geometry to be easily changed with the primary goal of optimizing measurement sensitivity. This movement changes the effective light path lengths, with the geometric parameter p corresponding to the distance between the focal point of the measurement and the surface of the liquid in the microplate well. The parameter p can be calculated from the known adjustable z-position of the optical element and other fixed geometrical parameters of the microplate reader (Figure 1) using eq 3

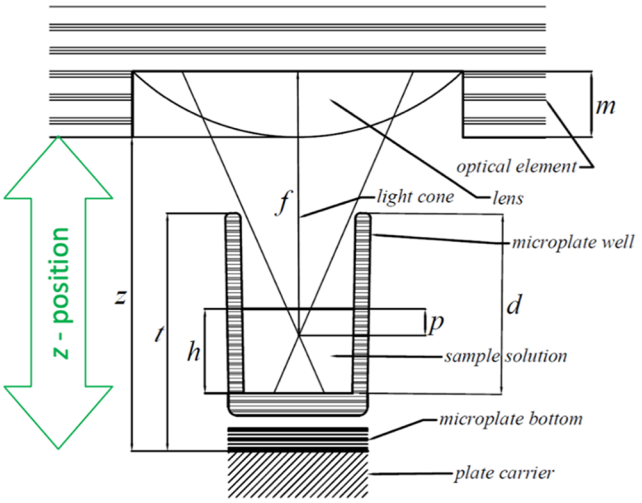

Figure 1. Geometric parameters of the microplate reader used for the ZINFE, eqs 3−5. The values of the parameters used for the calculations can be found in Table S2, Supporting Information.

$$p = (h + t - d) + (f - m) - z \quad (3)$$

where p is the distance between the focal point of the measurement and the surface of the liquid in the microplate well (corresponding to the parameter l in eq 2), d is the microplate well depth, h is the distance from the bottom of the microplate well to the surface of the liquid, t is the total height of the microplate, f is the distance from the optical element to the focal point of the lens, m is the depth of the lens slot of the optical element, and z is the distance from the lens to the bottom of the microplate well (z-position).

The parameters d, h, and t are distinctive for different microplate types, whereas the parameter h also depends on the sample volume in the well. The parameters f and m are distinctive for a particular optical system of the microplate reader instrument. A single overall geometric parameter k for a particular sample volume, microplate, and microplate reader type can be calculated using eq 4

$$k = (h + t - d) + (f - m) \quad (4)$$

The combination of eqs 2 and 4 yields the proposed Z-position inner filter effect (ZINFE) correction using eq 5

$$F_Z = F_1\left(\frac{F_2}{F_1}\right)^{(k-z_2)/(z_2-z_1)} \quad (5)$$

where F_Z is the ZINFE-corrected fluorescence intensity, F_1 and F_2 are the measured fluorescence values at different z-positions, z_1 and z_2, and k is defined in eq 4.

As previously proposed by Lutz and Luisi, eq 5 can be simplified to include a simple exponential term corresponding to a particular combination of k, z_1, and z_2. In addition to calculations from geometry-dependent parameters, this exponential term can also be obtained by least-squares fitting from experimental values of F_1 and F_2, thus obtaining the proposed numerical inner filter effect (NINFE) correction using eq 6

https://doi.org/10.1021/acs.analchem.2c01031
Anal. Chem. 2022, 94, 7107−7114

$$F_N = F_1\left(\frac{F_2}{F_1}\right)^N \quad (6)$$

where F_N is the NINFE-corrected fluorescence intensity based on fluorescence measurements at different z-positions (F_1 and F_2), and the exponential term N is obtained by brute-force optimization. This allows a wider range of applicable z-positions and also helps to account for possible reflection effects or errors in the estimation of geometric parameters. For such NINFE correction, only two sets of fluorescence data, F_1 and F_2, measured at z-positions z_1 and z_2 are needed. The actual values of z_1 and z_2, or indeed any other geometric parameters, are not necessary to obtain the corrected fluorescence, F_N. This correction can also be applied to data generated by the cell shift method mentioned earlier.

Objective and Limitations. Several recent reports have addressed the IFE correction. Panigrahi and Mishra calculated the geometric parameters from the dependence of measured fluorescence on sample absorbance.[4] Kasparek and Smyk used horizontal slits in the light path of the spectrofluorometer to numerically optimize the geometric parameters separately for pIFE and sIFE.[12] Similar to Lutz and Luisi, Kimball *et al.* used a custom stage for lateral cuvette movement in order to determine the geometric sensitivity factor of the spectrofluorometer.[3] Gu and Kenny also used a custom stage for cell shift experiments with additional numerical optimization of the geometric parameters, also separately for pIFE and sIFE.[13] However, all these methods are only applicable to conventional spectrofluorometers with detection at a 90° angle in rectangular cuvettes. Moreover, all these methods require separate measurements of sample absorbance and some kind of numerical procedure to account for sample geometry.

The aim of this work is to validate the proposed principle of IFE correction in microplates by comparing uncorrected fluorescence data, F_1, with the values of F_Z, F_N, and F_A obtained using eqs 5, 6, and 1, respectively. For the first set of experiments, fluorescence and absorbance were measured for the same samples in the same UV-transparent microplates to minimize sample handling. However, the microplates suitable for measuring both UV−vis absorbance and fluorescence and thus a very simple application of eq 1 for the IFE correction are considerably more expensive than non-transparent microplates. To estimate the general applicability of the ZINFE method, which does not require absorbance measurements, all measurements were duplicated using another type of non-transparent microplate as a potentially cost-saving solution.

The proposed approach can be readily applied to virtually any analyte, provided that the appropriate movement of the optical element (or microplate) in the z-axis can be achieved in order to obtain at least two measurements with different z-positions. As far as we know, this is the first attempt at IFE correction specifically intended for measurements in microplates.

EXPERIMENTAL SECTION

IFE correction was first evaluated using a concentration series of a known fluorophore, quinine sulfate (QS), which was chosen as the reference analyte due to its frequent use in similar studies (concentration series Q).[8] In order to test for both pIFe and sIFE, additional experiments were performed for different concentration series of QS in the presence of potassium dichromate (PD), which is known to absorb light at both the excitation and emission wavelengths of QS without exhibiting fluorescence itself.[14] Specifically, PD was added to the QS concentration series: (i) at a fixed ratio of total concentrations of PD and QS in order to observe the behavior of the proposed IFE correction in the presence of an additional proportional background absorbance at the excitation wavelength (i.e., variable total concentrations of QS and PD; concentration series Q-v) or (ii) at a fixed total concentration of PD in order to observe the behavior of the proposed IFE correction in the presence of an additional constant background absorbance (i.e., variable ratio of total concentrations of QS and PD; concentration series Q-f).[13] This was done because the samples may contain either a fixed or a proportional amount of additional absorber(s) in the working solutions (e.g., reaction buffer and storage buffer, respectively).

All experiments were performed at room temperature. The concentration range for the measurement was chosen to correspond to a maximum total absorbance at the excitation wavelength of $A_{ex} \approx 2$, which is acceptable for most spectrophotometers and should be common in most experimental setups. In the experiments with added PD, the concentrations were chosen so that the maximum concentration of PD corresponds to $A_{ex} \approx 1$. Full details on reagents and sample preparation can be found in Section 2 of the Supporting Information.

All measurements were performed in triplicate. The IFE corrections were performed using the averaged values of the background-corrected triplicate fluorescence and absorbance measurements (Section 4, Figures S8 and S11, Supporting Information). Separate calculations were also performed for data without background correction. All experiments were performed in parallel with two different types of microplates. The UV-transparent microplates (black, 96-well, μ-clear, flat bottom, chimney well, cat. no. 655097, Greiner, USA) allowed measurements of both absorbance and fluorescence intensity. The non-transparent microplates (black, 96-well, flat bottom, cat. no. 30122298, Tecan, Austria) allowed measurements of fluorescence intensity only.

For absorbance IFE corrections, a total of 9 corrections (eq 1) were obtained for each concentration series, corresponding to a separate IFE-corrected data set for each different z-position. For the z-position IFE corrections (ZINFE, eq 5), the measured fluorescence intensity values (F_1) obtained for each z-position were corrected using the fluorescence intensity values (F_2) obtained for the remaining z-positions. A total of $n(n-1) = 72$ corrections were obtained. As a measure of linearity, the R^2 statistic was calculated for each data set. The z-position correction whose R^2 value was closest to 1 was selected as optimal and used to compare the results.[12,13]

For the NINFE correction (eq 6), the exponential term N corresponding to the optimal combination of positions z_1 and z_2 found by the procedure described above was chosen as the starting point (seed) for numerical optimization. This starting point is then varied in a series of 20 steps with a step size of 1 in both the positive and negative directions to produce a series of R^2 values. An exponent corresponding to the maximum R^2 value is then used as the seeding point in the next optimization cycle with the same number of steps in both directions, while the step size is decreased by a factor of 10. This procedure continues for 10 cycles or when the difference between the exponents from successive cycles is $\Delta N < 1 \times 10^{-6}$, whichever comes first.

https://doi.org/10.1021/acs.analchem.2c01031
Anal. Chem. 2022, 94, 7107−7114

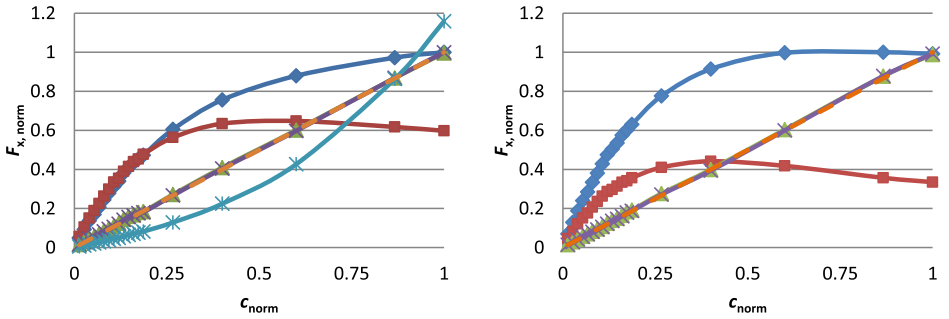

Figure 2. Results of the ZINFE correction: left: Q concentration series in UV-transparent microplates (data set 1); right: Q-v concentration series in non-transparent microplates (data set 4); F_1 (blue diamond solid), F_2 (brown box solid), F_Z (green triangle up solid), F_N (purple multiplication), F_A (blue asterisk), and IFS (orange hyphen). Ordinate values were calculated as $F_{x,norm}$, and abscissa values were calculated as c_{norm}. All results can be found in Figure S9, Supporting Information.

Table 1. Overview of the Least-Squares Linear Fit Results for Normalized, Background-corrected Fluorescence and Absorbance Data

sample[a]	plate type[b]	correction type[c]	R^2	b %[d]	LOD %[e]	z_1/mm	Δz[f]/mm	c_{max}[g]/μM	A_{max}[h] (λ_{ex}, λ_{em})
Q	T (data set 1)	F_1	0.87449	17.5	36.4	19.0	2.0	679.3	1.984, 0.158
		F_Z	0.99980	0.54	1.39				
		F_N	0.99984	0.24	1.20				
		F_A	0.95074	−7.87	21.9				
	NT (data set 2)	F_1	0.81861	21.7	45.2	18.0	2.5		
		F_Z	0.99971	0.12	1.64				
		F_N	0.99973	−0.08	1.59				
Q-v	T (data set 3)	F_1	0.81967	21.3	45.1	19.0	2.0	316.0	1.873, 0.443
		F_Z	0.99951	0.95	2.13				
		F_N	0.99964	0.43	1.83				
		F_A	0.93753	−8.15	24.8				
	NT (data set 4)	F_1	0.73752	25.9	57.3	18.0	2.0		
		F_Z	0.99974	0.47	1.55				
		F_N	0.99979	0.14	1.38				
Q-f	T (data set 5)	F_1	0.98744	5.39	10.8	18.0	1.0	312.9	1.921, 0.464
		F_Z	0.99959	−0.12	1.94				
		F_N	0.99965	0.22	1.80				
		F_A	0.98111	−4.85	13.3				
	NT (data set 6)	F_1	0.98918	4.93	10.0	18.0	3.0		
		F_Z	0.99964	1.24	1.83				
		F_N	0.99972	0.89	1.61				

[a]Q corresponds to the pure QS concentration series; Q-v corresponds to the variable concentration of the absorber PD; Q-f corresponds to the fixed total concentration of PD. [b]T corresponds to the UV-transparent microplates; NT corresponds to the non-transparent microplates. Data set numbers correspond to the averaged triplicate data preformatted for automated processing.[16] [c]F_1 corresponds to uncorrected fluorescence; F_Z corresponds to ZINFE-corrected fluorescence intensity (eq 5); F_A corresponds to absorbance IFE-corrected fluorescence intensity (eq 1); F_N corresponds to NINFE-corrected fluorescence intensity. [d]Percent error of the normalized data slope with respect to the IFS. The values of slope and intercept used for data normalization for each concentration series are given in Table S12, Supporting Information. [e]LOD ($\alpha = \beta = 0.05$); the values were normalized as percentage of c_{max}. [f]Defined as $\Delta z = z_2 - z_1$, where z_1 and z_2 are the different z-positions used for measurements of F_1 and F_2 (eq 5). [g]Maximum concentration of QS in the concentration series. [h]Maximum absorbance at the excitation and emission wavelengths, λ_{ex} = 345 nm and λ_{em} = 390 nm, respectively.

For all comparisons shown in Figure 2 and Table 1, the original and absorbance-corrected data correspond to the z-position (z_1) used for the best z-position correction. Therefore, for each concentration series in a given microplate, all values are derived from the same value of F_1 (corresponding to the uncorrected data) used in eqs 1, 5, and 6. For data processing, a dedicated script was written in the Javascript programming language.[15] Full details on background correction and other data processing, including statistical considerations, can be found in the Supporting Information, Section 3.

For further evaluation of the method and for immediate availability, an online service was set up to run the full correction algorithm at https://ninfe.science.[15] All averaged triplicate data preformatted for automatic online processing and the results obtained have been archived.[16]

RESULTS AND DISCUSSION

The results of the ZINFE correction for the Q concentration series in UV-transparent microplates are shown in Figure 2. The values of F_1 and F_2 deviate from linearity due to IFE caused by increasing sample concentration. Although both F_1 and F_2 are recorded for the same samples in the same microplate, they are measured at different z-positions, resulting in different sample geometries and different dependences of the measured fluorescence on sample concentration. However, the values of F_1 and F_2 obtained in this way can be used to

https://doi.org/10.1021/acs.analchem.2c01031
Anal. Chem. 2022, 94, 7107−7114

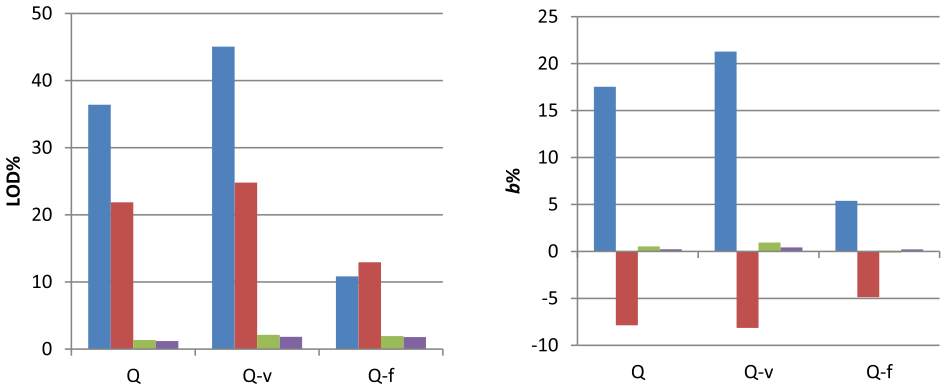

Figure 3. Comparison of uncorrected fluorescence (F_1) and IFE-corrected fluorescence (F_A, F_Z, and F_N) in UV-transparent microplates: left: LOD % from Table 1: F_1 (blue box solid), F_A (red box solid), F_Z (green box solid), and F_N (violet box solid); right: b % from Table 1: F_1 (blue box solid), F_A (red box solid) F_Z (green box solid), and F_N (violet box solid). Data are shown only for UV-transparent microplates and the data for non-transparent microplates are shown in Figures S19 and S20, Supporting Information.

calculate the corrected F with improved linearity according to eqs 5 or 6. The corresponding results for all concentration series can be found in Figure S9, Supporting Information.

For convenient comparison of all results, the data were normalized as follows: (i) abscissa values were calculated as $F_{x,norm} = A_{ex}/A_{max}$, where A_{ex} is the baseline-corrected absorbance at the excitation wavelength and A_{max} is the maximum value of A_{ex} for the given concentration range; (ii) ordinate values were calculated as $c_{norm} = F_x/(a \times c_{max} + b)$, where F_x corresponds to either the uncorrected or corrected fluorescence (F_1, F_Z, F_N or F_A) and a and b are the slope and intercept, respectively, of the linear regression line for the corresponding data (Table S12, Supporting Information). The normalized values are $0 < c_{norm} < 1$ and $0 < F_{x,norm} < \approx 1$, with maximum $F_{x,norm}$ values depending on the deviation of the normalized value of F_A, F_Z, or F_N compared with the slope of the ideal fluorescence signal (IFS).

The IFS corresponds to the linear relationship between F and A in the absence of IFE.[17,18] The slope of this linear relationship depends on the structural characteristics of the fluorophore, and the intercept should be equal to 0 after accounting for background fluorescence and absorbance *via* blank subtraction.[19] Therefore, the value of IFS for the normalized data (i.e., plots of $F_{x,norm}$ vs c_{norm}) is a line with slope $a = 1$ and intercept $b = 0$, which allows very easy comparison of the uncorrected or corrected data with the ideal measurement response. A better match of the normalized data with the IFS requires a smaller deviation of the slope and the intercept of the linear regression from the values $a = 1$ and $b = 0$, respectively.

Considering the fact that $a + b = 1$ is valid for all normalized data, the value of b was given as a suitable measure of linearity and accuracy for comparing the different correction methods (Table 1). The values of b can be either positive or negative, corresponding to the downward or upward curvature of the fluorescence signal, respectively. In addition, the value of b obtained by the described normalization is numerically equal but opposite in sign to the percent error of the slope of the line of corrected fluorescence (*mErr* %, eq S7, Supporting Information), which was used by Gu and Kenny to compare IFE corrections.[13] Therefore, the values of b were also expressed as b %, which means the percent error of the slope of the normalized data from IFS.

Another more conventional measure of linearity and accuracy of calibration curves is the limit of detection (LOD, eq S5, Supporting Information). The LOD value is defined as the concentration corresponding to an instrument signal for which the probability of false positive error (α) or false negative error (β) is a selected threshold percentage (in this study, $\alpha = \beta = 0.05$).[20,21] The LOD value appears to be particularly convenient because it contains both the measure of calibration sensitivity (i.e., the slope of the linear regression) and accuracy (i.e., the standard error of the estimate, s_y, defined in eq S2, Supporting Information). For convenient comparison of the results, the LOD values obtained for the raw data (Table S12, Supporting Information) were normalized as a percentage of the highest concentration of the analyte in the corresponding series (c_{max}), resulting in LOD % values (Table 1).

Uncorrected Fluorescence (F_1). The uncorrected data (F_1) for the QS concentration series show a clear deviation from linearity, except for the Q-f concentration series, that is, for a fixed total concentration of PD (Figure S8, Supporting Information). The linearity of the uncorrected data depends on the z-position at which the fluorescence intensity was measured for all QS concentration series and increases with z-position (Figure S14, Supporting Information). The best R^2 values are observed at $z = 21$ mm for all concentration series, which is consistent with increasing linearity of the fluorescence signal as the light path length decreases (higher z-values correspond to shorter light path lengths), that is, lower effective absorbance and thus smaller IFE. All deviations from the ideal signal were positive (i.e., $b > 0$, Figure 3, right), corresponding to a downward curvature for all concentration series due to IFE.

Linear regression of the uncorrected data at the z-position corresponding to the z_1 value for the best ZINFE correction yield values of $R^2 < 0.875$ and large values of LOD % > 36% of c_{max} and b % > 17%, consistent with the observed downward curvature of the fluorescence signal (Table 1, Q and Q-v concentration series). The Q-f concentration series gave slightly better results ($R^2 > 0.98$, LOD % ≈ 10% of c_{max} and b % ≈ 5%), consistent with the observed lower curvature of the fluorescence signal compared with the Q and Q-v concentration series. The Q-f concentration series also showed the lowest dependence of R^2 values on z-position ($0.971 < R^2 < 0.995$, Figure S14, Supporting Information). Similar results for

https://doi.org/10.1021/acs.analchem.2c01031
Anal. Chem. 2022, 94, 7107−7114

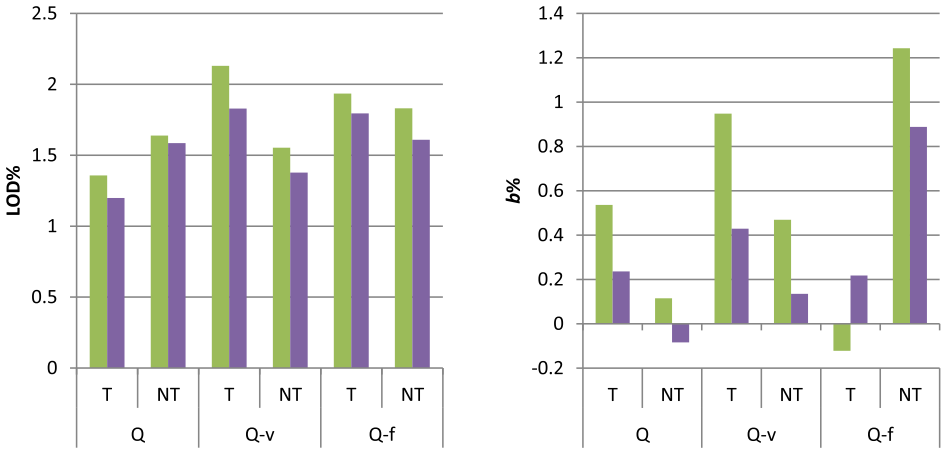

Figure 4. Comparison of ZINFE and NINFE corrections (F_Z and F_N) in UV-transparent (T) and non-transparent (NT) microplates. Left: LOD % from Table 1: F_Z (green box solid) and F_N (violet box solid); right: b % from Table 1: F_Z (green box solid) and F_N (violet box solid).

uncorrected data were also obtained for non-transparent microplates (all results can be found in Tables 1 and S12, Supporting Information). This observation can most likely be attributed to lower variability in total absorbance at the excitation wavelength for this concentration series compared to others (Figure S11 and Table S22, Supporting Information).

Absorbance IFE-corrected Fluorescence (F_A). A total of 9 data sets per concentration series corresponding to different z-positions were obtained for UV-transparent microplates only (measured absorbance data can be seen in Figure S11, Supporting Information). Each absorbance IFE correction (F_A, eq 1) gave better linearity than the uncorrected data, except for the Q-f concentration series (Table 1).

The linearity of the absorbance-corrected data also depends on the z-position at which fluorescence intensity was measured for all concentration series and decreases with z-position (Figure S15, Supporting Information). The variation in R^2 values is smaller and also inverse to the dependence observed for uncorrected data (Figure S14, Supporting Information). This observation is consistent with increasing linearity of the absorbance-corrected fluorescence signal with increasing light path length (lower z-values correspond to longer light path lengths); that is, the effective absorbance approaches the value used for the correction. Notably, the correction factor in eq 2, $(A_{ex} + A_{em})/2$, is independent of z-position.

The best absorbance IFE corrections gave values $R^2 \approx 0.99$ and LOD % $\approx$ 10%, giving a linear response over approximately 90% of the concentration range with less than 3.5% deviation of the calibration slope from the ideal signal. All deviations from the ideal signal were negative (i.e., $b < 0$, Figure 3, right), corresponding to an upward curvature for all concentration series due to overcorrection (i.e., overestimated fluorescence loss) associated with the Lakowicz model, especially at higher absorbance.[4] The Q-f concentration series again showed the least dependence of R^2 values on z-position ($0.975 < R^2 < 0.989$, Figure S15, Supporting Information). The absorbance IFE correction decreases the LOD % values by approximately 40%, compared to the uncorrected data for the Q and Q-v concentration series. Surprisingly, the LOD % value was increased by 20% compared to the uncorrected data for the Q-f concentration series, indicating that this type of correction is not appropriate in the presence of a background absorber.

ZINFE-corrected Fluorescence (F_Z). A total of 72 data sets per concentration series were obtained, corresponding to different combinations of z-positions. The optimal z-position IFE correction (F_Z, eq 5) significantly improves the linearity of the fluorescence signal for all QS concentration series, yielding values of $R^2 > 0.999$ and deviation from the ideal signal response in the range of $-0.122 < b\ \% < 1.243$. The LOD % values for all concentration series were in the range of 1.358–2.130% of the c_{max}. Therefore, a linear response was obtained for all concentration series over approximately 98% of the concentration range with a maximum deviation of the calibration slope from the ideal signal of approximately 1% (Figure 3). For comparison, the uncorrected data at the same z-position for the entire concentration range gave values of $R^2 < 0.9$, except for the Q-f series, which gave values of $R^2 < 0.99$. The deviations from the ideal signal were much worse for the uncorrected data ($b\ \% \approx 20\%$ for the Q and Q-v concentration series, and $b\ \% \approx 5\%$ for the Q-f concentration series) and also for the absorbance-corrected values ($b\ \% \approx -5\%$).

The quality of the z-position correction depends largely on the choice of F_1 and F_2 (i.e., the measured fluorescence values at different z-positions) used in eq 5. However, each ZINFE correction gave better linearity than the uncorrected data, and the best overall R^2 value is obtained with the z-position correction. The three-dimensional plots for the dependence of the linear regression model error, calculated as $\Delta R = -1/(1 - R^2)$, on the values of z_1 and z_2 showed a complex surface with multiple minima for all concentration series (Figure S13, Supporting Information). Such a shape of the error surface seems to justify the attempt of further numerical optimization according to eq 6.

NINFE-corrected Fluorescence (F_N). The results obtained by numerical optimization of the exponent in eq 6 for a particular combination of k, z_1, and z_2, which yielded the highest R^2 value, show a slight improvement compared with the calculation using geometry-dependent parameters (Table S16, Supporting Information). The exponents obtained from the geometric parameters and numerical optimization are in good agreement for Q and Q-v concentration series, with relatively small differences between the exponents (approximately 0.05), whereas slightly larger differences were obtained for the Q-f concentration series (approximately 0.2) (Table S16, Supporting Information). In general, the exponent optimization curves (Figure S17, Supporting Information)

https://doi.org/10.1021/acs.analchem.2c01031
Anal. Chem. 2022, 94, 7107−7114

show remarkable similarity between the calculated and numerically optimized exponent values.

Regardless of the values of the differences in the exponents, similar improvements in the IFE correction were obtained for all concentration series: the R^2 values were increased in the fourth or fifth decimal range, while the LOD % and b % were improved by approximately 0.5%, except for a single data set (b % was larger for Q-f concentration series in UV-transparent microplates).

Transparent Versus Non-transparent Microplates and the Effect of Background Correction. The ZINFE and NINFE corrections performed in the two different types of 96-well plates gave very similar results. As can be seen in Figure 4, the LOD % and b % values for all F_Z corrections were comparable for all concentration series, with slightly better values obtained by numerical optimization (F_N). A particularly interesting feature of the ZINFE correction or the NINFE correction is the ability to use fluorescence data without background correction. The results obtained for such data gave only slightly worse results, again with values of $R^2 > 0.999$ for all concentration series with approximately 0.5% higher values of LOD and 0.4% higher absolute values of b %, compared with the data with background correction (Table S18 and Figures S19 and S20, Supporting Information). However, data without background correction should be used with caution because different behaviors of the background signal can be expected for samples other than those described here.

IFE Correction for Low-Concentration Samples. Although the IFE correction may be considered unnecessary for low sample concentrations, we tested the use of this method for a lower range of sample concentrations. The uncorrected fluorescence (F_1) is very linear ($R^2 > 0.994$) for the first seven points in each concentration series. However, even for this concentration range, slightly increased R^2 values and lower b % values were observed for the ZINFE- and NINFE-corrected data for the Q and Q-v concentration series in both UV-transparent and non-transparent microplates (Table S21, Supporting Information). Slightly decreased R^2 values and higher b % values were observed for the Q-f concentration series for all IFE corrections, which may be attributed to increased noise due to the use of two measured values instead of only one. This is an indication that the regression residuals at low sample concentrations are mainly due to measurement errors rather than IFE.

CONCLUSIONS

The described method of ZINFE correction is successful in extending the concentration range of the linear fluorescence signal for all concentration series, increasing the maximum applicable sample absorbance and eliminating the need for sample dilutions. The method is suitable for simultaneous correction of both pIFE and sIFE with an applicable maximum sample absorbance of at least $A_{ex} \approx 2$ and $A_{em} \approx 0.5$, with possible applicability at higher absorbance values. A simple heuristic for performing the measurements is to select a set of available z-positions depending on the characteristics of the microplate reader and find the optimal combination of z_1 and z_2 based on the quality of the linearization. In general, for this particular experimental setup, the best combinations of z-positions yielding the highest R^2 values were obtained with F_1 values measured at $z_1 = 18$ or $z_1 = 19$, while the F_2 values are measured at 1−3 mm lower values of z_2 (lower z-values correspond to a longer light path length).

Overall, the best corrections were obtained by numerical optimization of the exponent in eq 6. Thus, it was shown that the described method for NINFE correction provides an efficient IFE correction in microplates. The method does not require direct measurements of sample absorbance at the excitation and emission wavelengths or any additional parameters other than two fluorescence measurements at two different distances from the optical element of the microplate reader to obtain an IFE correction with a very linear response. The improvements obtained with NINFE could most likely be due to possible reflections from the walls of the microplate wells, which cannot be easily accounted for by geometric parameters alone. A major advantage of such numerical optimization is that no geometric parameters are needed, including the actual z-positions for the measurements. Moreover, NINFE can be used not only for measurements in microplate readers but also for any measurements obtained by the cell shift method. However, this method can be considered as a black-box system that may not be suitable for all users, who may then prefer to use the ZINFE method with known geometric parameters.

Both the ZINFE and NINFE methods give similar results compared to IFE corrections obtained with conventional spectrofluorometers. Lutz and Luisi, in their original work on the cell shift method, reported an accuracy of 3% for experiments with QS.[10] Gu and Kenny have reported an accuracy of about 1.5% for their experiments with QS, while additional numerical optimization yielded an accuracy of about 0.2%.[13] More recently, Panigrahi and Mishra reported an accuracy of about 0.5% for their experiments with QS (calculated from the values in the Supporting Information provided with the article).[4] The results reported here are in good agreement with these values ($|b$ %$| < 1.3$% for all concentration series, Figure 4). In addition, we have shown that both ZINFE and NINFE are comparably effective for samples with an additional absorber in varying proportions. Similarly, we have shown that both methods are comparably effective in both UV-transparent and non-transparent microplates. The extended linear response of the fluorescence signal provided by ZINFE or NINFE allows simplified fluorescence measurements without sample dilution, thus eliminating the often complex and time- and resource-consuming liquid handling associated with microplates.

ASSOCIATED CONTENT

Supporting Information

The Supporting Information is available free of charge at https://pubs.acs.org/doi/10.1021/acs.analchem.2c01031.

Additional experimental details including instrumental parameters, sample preparation, statistical considerations, and results for all data sets (PDF)

AUTHOR INFORMATION

Corresponding Author

Tin Weitner − *Faculty of Pharmacy and Biochemistry, University of Zagreb, Zagreb 10000, Croatia;* orcid.org/0000-0003-4132-2295; Email: tin.weitner@pharma.unizg.hr

Authors

Tomislav Friganović − *Faculty of Pharmacy and Biochemistry, University of Zagreb, Zagreb 10000, Croatia*

https://doi.org/10.1021/acs.analchem.2c01031
Anal. Chem. 2022, 94, 7107−7114

Davor Šakić − *Faculty of Pharmacy and Biochemistry, University of Zagreb, Zagreb 10000, Croatia*

Complete contact information is available at: https://pubs.acs.org/10.1021/acs.analchem.2c01031

Author Contributions

The manuscript was written through contributions of all authors. All authors have given approval to the final version of the manuscript.

Notes

The authors declare no competing financial interest.

■ ACKNOWLEDGMENTS

This work was supported by funding from the Croatian Science Foundation grant UIP-2017-05-9537—Glycosylation as a factor in the iron transport mechanism of human serum transferrin (GlyMech). Additional support was provided by the European Structural and Investment Funds for the "Croatian National Centre of Research Excellence in Personalized Healthcare" (contract #KK.01.1.1.01.0010), "Centre of Competences in Molecular Diagnostics" (contract #KK.01.2.2.03.0006), and the European Regional Development Fund grant for "Strengthening of Scientific Research and Innovation Capacities of the Faculty of Pharmacy and Biochemistry at the University of Zagreb" (FarmInova, contract #KK.01.1.1.02.0021).

■ REFERENCES

(1) Valeur, B.; Berberan-Santos, M. N. *Molecular Fluorescence: Principles and Applications*, 2nd; Wiley-VCH Verlag GmbH & Co. KGaA: Weinheim, Germany, 2013.
(2) Lakowicz, J. R. Instrumentation for Fluorescence Spectroscopy. *Principles of Fluorescence Spectroscopy*; Springer US: Boston, MA, 2006; pp 27−61.
(3) Kimball, J.; Chavez, J.; Ceresa, L.; Kitchner, E.; Nurekeyev, Z.; Doan, H.; Szabelski, M.; Borejdo, J.; Gryczynski, I.; Gryczynski, Z. *Methods Appl. Fluoresc.* **2020**, *8*, 033002.
(4) Panigrahi, S. K.; Mishra, A. K. *Photochem. Photobiol. Sci.* **2019**, *18*, 583−591.
(5) Fonin, A. V.; Sulatskaya, A. I.; Kuznetsova, I. M.; Turoverov, K. K. *PLoS One* **2014**, *9*, No. e103878.
(6) Ma, C.; Li, L.; Gu, J.; Zhu, C.; Chen, G. *Spectrosc. Lett.* **2018**, *51*, 319−323.
(7) Panigrahi, S. K.; Mishra, A. K. *J. Photochem. Photobiol., C* **2019**, *41*, 100318.
(8) Wang, T.; Zeng, L.-H.; Li, D.-L. *Appl. Spectrosc. Rev.* **2017**, *52*, 883−908.
(9) Kubista, M.; Sjöback, R.; Eriksson, S.; Albinsson, B. *Analyst* **1994**, *119*, 417−419.
(10) Lutz, H.-P.; Luisi, P. L. *Helv. Chim. Acta* **1983**, *66*, 1929−1935.
(11) Puchalski, M. M.; Morra, M. J.; von Wandruszka, R. *Fresenius. J. Anal. Chem.* **1991**, *340*, 341−344.
(12) Kasparek, A.; Smyk, B. *Spectrochim. Acta, Part A* **2018**, *198*, 297−303.
(13) Gu, Q.; Kenny, J. E. *Anal. Chem.* **2009**, *81*, 420−426.
(14) Tucker, S. A.; Amszi, V. L.; Acree, W. E. *J. Chem. Educ.* **1992**, *69*, A8.
(15) Šakić, D.; Weitner, T.; Friganović, T. NINFE. https://ninfe.science/.
(16) Weitner, T.; Friganović, T.; Šakić, D. *Inner Filter Effect Correction for Fluorescence Measurements in Microplates*, 2022, DOI: 10.5281/zenodo.5849302.
(17) Holland, J. F.; Teets, R. E.; Kelly, P. M.; Timnick, A. *Anal. Chem.* **1977**, *49*, 706−710.
(18) Miller, J. N. Inner Filter Effects, Sample Cells and Their Geometry in Fluorescence Spectrometry. In *Standards in Fluorescence Spectrometry: Ultraviolet Spectrometry Group*; Miller, J. N., Ed.; Techniques in Visible and Ultraviolet Spectometry; Springer Netherlands: Dordrecht, 1981; pp 27−43.
(19) Kothawala, D. N.; Murphy, K. R.; Stedmon, C. A.; Weyhenmeyer, G. A.; Tranvik, L. J. *Limnol. Oceanogr.: Methods* **2013**, *11*, 616−630.
(20) Miller, J. N.; Miller, J. C. *Statistics and Chemometrics for Analytical Chemistry*, 6th ed.; Prentice Hall: Harlow, 2010.
(21) Brunetti B, D. E. *Pharm. Anal. Acta* **2015**, *6*, 355.

4.1. RAD 3 - DODATAK

Supplementary information

Inner filter effect correction for fluorescence measurements in microplates using variable vertical axis focus

Tin Weitner*, Tomislav Friganović, Davor Šakić

Faculty of Pharmacy and Biochemistry, University of Zagreb, Ante Kovačića 1, 10000 Zagreb, Croatia

Corresponding author:

Tin Weitner, PhD

e-mail: tin.weitner@pharma.unizg.hr

tel.: +385 1 6394 452

Contents

1. Instrumental parameters

Fluorescence and absorbance measurements were performed using the Tecan Spark M10 multimode microplate reader (Tecan, Austria). Fluorescence intensity was measured for λ_{ex} = 345 nm and λ_{em} = 390 nm using *z*-position values in the range of 14.6 - 21.0 mm (Table S1). The absorbance values for both wavelengths were measured to obtain the values A_{ex} and A_{em} (Eq. 1), respectively in UV-transparent microplates (Figure S11). Instrument settings of the microplate reader can be found in Table S3, SI. The solution volume in each microplate well was 200 µL. The distance from the bottom of the microplate well to the surface of the liquid, *h*, (Figure 1) was estimated for Greiner microplates by measuring the absorbance of pure water. The values of *h* for Tecan plates were measured using transparent microplates of the same geometry (transparent, 96-well, flat bottom, cat. no. 30122304, Tecan, Austria), allowing a correct calculation of *k* = 20.593 mm, which was used in calculations. Full details of the measurement of parameter *h* and specific values of geometric parameters in Figure 1 and Eq. 3, can be found in Table S2. Required geometric parameters of the microplate reader sample compartment and optical element were kindly provided by the manufacturer.

Table S1. Values of *z*-positions used for fluorescence intensity measurements and subsequent IFE corrections. The values are given in mm for clarity, and the actual instrumental parameter is adjustable to the nearest µm.

***z*-position number**	***z* / mm**
1	14.6
2	15.0
3	15.5
4	16.0
5	17.0
6	18.0
7	19.0
8	20.0
9	21.0

Table S2. Values of geometric parameters shown in Figure 1 used for the *z*-position IFE corrections.

parameter	**value / mm**	**significance**
d	10.9	microplate well depth; value according to manufacturer's specifications
h	5.093 ± 0.042	distance from the bottom of the microplate well to the surface of the liquid; measurement described in the SI, Section 3.2
t	14.4	height of the microplate; value according to manufacturer's specifications
f	16	distance from the optical element to the focal point of the lens; value obtained from manufacturer specifications
m	4	depth of the optical element lens slot; value according to manufacturer's specifications
k	20.593	overall geometric parameter *k* for a particular experimental setup (i.e., sample volume, microplate, and microplate reader type), calculated using Eq. 4 (see Manuscript)

Table S3. Printout of the device settings for the Tecan Spark M10 multimode microplate reader.

Device:	Tecan Spark M10	
Application:	SparkControl V2.3	
Shaking (Linear) Duration	5	s
Shaking (Linear) Position	Current	
Shaking (Linear) Amplitude	1	mm
Shaking (Linear) Frequency	1440	rpm
Mode	**Fluorescence Top Reading**	
Excitation	Monochromator	
Excitation wavelength	345	nm
Excitation bandwidth	20	nm
Emission	Monochromator	
Emission wavelength	390	nm
Emission bandwidth	20	nm
Gain	40	Manual
Mirror	Automatic (50% Mirror)	
Number of flashes	30	
Integration time	40	µs
Lag time	0	µs
Settle time	0	ms
Z-Position mode	Manual	
Mode	**Absorbance**	
Wavelength start	200	nm
Wavelength end	700	nm
Wavelength step size	1	nm
Number of flashes	1	
Settle time	50	ms

Measurements were performed at ambient temperature (range 22.0 – 28.4 ºC, measured in the sample compartment of the microplate reader). The maximum temperature deviation for any concentration series was 0.18 ºC.

2. Sample preparation

2.1. Reagents

Water used for sample preparation was double distilled in an all-glass apparatus. Quinine sulfate (QS, 99.0-101.0 %, cat. no. 22640, Sigma-Aldrich, USA), potassium dichromate (PD, 99 %, cat. no. 1112907, Kemika, Croatia) and concentrated sulfuric acid (96 %, cat. no. 410261, Carlo Erba Reagents, France) were used without further purification. All experiments were performed in 0.05 M H_2SO_4 prepared from concentrated solution. All working solutions were prepared using Opentrons OT-2 liquid handling robot (Opentrons, USA).

2.2. General remarks

All titrations in all experiments were performed by pipetting into 0.65 mL centrifuge tubes. Liquid handling robot Opentrons OT-2 (Opentrons, USA) was used to prepare all samples from stock solutions. Volumes of less than or equal to 30 µL were dispensed into a larger volume of solution and then 30 µL of the solution was aspirated and dispensed again to rinse the tip. After pipetting, all tubes were capped and thoroughly mixed on a vortex mixer. After mixing, aliquots of 200 µL were transferred to microplates for measurement, again using the robot. Prior to measurement, microplates were centrifuged for 2 min at 2550 rpm using a microplate centrifuge (Benchmark Scientific, USA) with additional shaking in the microplate reader sample compartment for 5 s at 1440 rpm and amplitude of 1 mm.

2.3. Solutions

a) 0.05 M sulfuric acid

For all solutions containing QS and PD, 0.05 M sulfuric acid was used as solvent (details of chemicals are given in the manuscript). A solution of 0.05 M sulfuric acid was obtained by diluting concentrated sulfuric acid in an appropriate volume of redistilled water. The required volume of concentrated acid was calculated using the density and percent content indicated by the manufacturer on the original bottle.

b) Quinine sulfate (QS) in 0.05 M sulfuric acid (concentration series Q)

The QS stock solution was prepared by first dissolving an arbitrary amount of QS in 0.05 M sulfuric acid. The resulting solution has a very high absorbance, so aliquots of this solution were added to 0.05 M sulfuric acid to obtain the maximum absorbance $A_{ex} \sim 2$ in the concentration series. The actual concentration of QS for each point was calculated in triplicate from the absorbance measurements.

c) Quinine sulfate (QS) in 0.05 M sulfuric acid (concentration series Q-f and Q-v).

The procedure was the same as for the Q concentration series, except that the maximum absorbance of the QS was $A_{ex} \sim 1$ in the concentration series Q-f and Q-v.

d) Potassium dichromate (PD) in 0.05 M sulfuric acid (concentration series Q-f and Q-v)

The PD stock solution was prepared by first dissolving an arbitrary amount of PD in 0.05 M sulfuric acid and diluting it so that the maximum absorbance of the stock solution was A_{ex} ~ 5. For experiments with fixed total concentration of PD, aliquots of this stock solution were added to obtain the constant absorbance A_{ex} ~ 1 for PD in all samples in the Q-f concentration series. For experiments with variable total concentration of PD, different aliquots of this stock solution and 0.05 M sulfuric acid were added to obtain increasing absorbance to the maximum of A_{ex} ~ 1 for PD in the Q-v concentration series.

e) Spectral measurements

UV/Vis spectra were measured using Varian Cary 50 spectrophotometer (Varian, Australia) in a quartz cuvette (l = 1 cm) at room temperature. Values for QS were normalized to the reference value of ε_{345} = 5700 M^{-1} cm^{-1} in 0.05 M sulfuric acid and are given in Table S4.[1] Values for PD were normalized to the reference value of ε_{350} = 3150 M^{-1} cm^{-1} in 0.01 M sulfuric acid.[2] Briefly, the spectrum of PD was measured in 0.05 M H_2SO_4, the solution was diluted 5 times with water to give 0.01 M H_2SO_4 and the spectrum was measured again. For each solution, the corresponding background (solution of 0.05 M H_2SO_4 and the same solution diluted 5 times with water) was measured and subtracted from the spectrum of PD. The value of ε_{350} in 0.05 M H_2SO_4 was calculated as (A_{350} (0.05 M H_2SO_4) / (A_{350} (0.01 M H_2SO_4) × 5)) × 3150 M^{-1} cm^{-1} = 2965 M^{-1} cm^{-1}. The values of ε_{345} and ε_{390} were then calculated from the ratio of the measured absorbance relative to A_{350} and are given in Table S4.

The fluorescence spectrum of QS was measured at room temperature using Olis RSM 1000F spectrofluorometer (Olis, USA). The excitation wavelength was 345 nm ($A_{345} \approx 1$) and the excitation bandwidth was 13 nm. The fluorescence units (f.u.) correspond to the ratio of signals obtained from sample and reference PMTs. The fluorescence spectrum was normalized to the maximum value obtained at 452 nm.

Table S4. Molar absorbance coefficients, ε, for quinine sulfate and potassium dichromate at excitation and emission wavelengths, λ_{ex} = 345 nm and λ_{em} = 390 nm, respectively.

Sample	ε_{345} / M^{-1} cm^{-1}	ε_{390} / M^{-1} cm^{-1}
Quinine sulfate	5700	348
Potassium dichromate	2939	1049

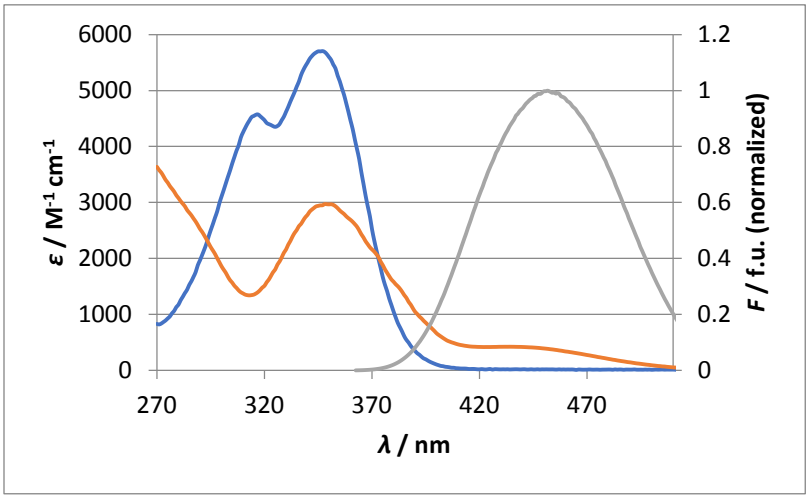

Figure S5. Molar absorbance spectra for quinine sulfate (—) and potassium dichromate (—) in 0.05 M H_2SO_4 at room temperature. The secondary *y*-axis is used for the normalized fluorescence spectrum of quinine sulfate (—).

f) Sample concentrations

A total of 3 concentration series were prepared in triplicate and each concentration series was measured in 2 types of microplates (transparent or non-transparent), corresponding to a total of 6 datasets:

Dataset 1: concentration series Q in UV-transparent microplates
Dataset 2: concentration series Q in non-transparent microplates
Dataset 3: concentration series Q-v in UV-transparent microplates
Dataset 4: concentration series Q-v in non-transparent microplates
Dataset 5: concentration series Q-f in UV-transparent microplates
Dataset 6: concentration series Q-f in non-transparent microplates

Separate calculations were performed with and without background correction (see manuscript).

Table S6. Sample concentrations of quinine sulfate and potassium dichromate for all concentration series; Q, Q-v and Q-f.

Sample number	*c* / µM					ratio [QS]/[PD]	
	Quinine Sulfate (QS)			Potassium dichromate (PD)			
	Q [1]	Q-v [1]	Q-f [1]	Q-v [1]	Q-f [1]	Q-v [1]	Q-f [1]
1	9.057	4.214	4.172	8.173			0.006
2	18.11	8.428	8.344	16.35			0.013
3	27.17	12.64	12.52	24.52			0.019
4	36.23	16.86	16.69	32.69			0.025
5	45.28	21.07	20.86	40.86			0.032
6	54.34	25.28	25.03	49.04			0.038
7	63.40	29.50	29.20	57.21			0.044
8	72.45	33.71	33.38	65.38			0.051
9	81.51	37.92	37.55	73.55			0.057
10	90.57	42.14	41.72	81.73	658.7	0.516	0.063
11	99.62	46.35	45.89	89.90			0.070
12	108.7	50.57	50.06	98.07			0.076
13	117.7	54.78	54.24	106.2			0.082
14	126.8	58.99	58.41	114.4			0.089
15	181.1	84.28	83.44	163.5			0.127
16	271.7	126.4	125.2	245.2			0.190
17	407.6	189.6	187.7	367.8			0.285
18	588.7	273.9	271.2	531.2			0.412
19	679.3	316.0	312.9	613.0			0.475

[1]Q corresponds to the pure QS concentration series; Q-v corresponds to the variable concentration of the absorber PD (fixed ratio of the total concentrations of PD and QS); Q-f corresponds to the fixed total concentration of PD (variable ratio of the total concentrations of PD and QS), see manuscript for details.

3. Statistical considerations

3.1. Quality of fit and linearity measures

a) Coefficient of determination, R^2

This represents the proportion of the variance of the dependent variable that is explained by the independent variable(s) in a regression model, and is defined as:[3]

$$R^2 = \frac{(\mathrm{cov}(x,y))^2}{\mathrm{var}(x)\mathrm{var}(y)} = \frac{(\mathrm{SS}_{xy})^2}{\mathrm{SS}_{xx}\mathrm{SS}_{yy}}. \qquad \text{Eq S1}$$

Values closer to 1 indicate a better fit.

b) Standard error of the estimate, s_y

This represents the measure of variation used to check the accuracy of the predictions made with the regression line, and is defined as:[4]

$$s_y = \sqrt{\frac{1}{(n-2)}\left[\sum_{i=1}^{n}(y_i - \bar{y})^2 - \frac{\left[\sum_{i=1}^{n}(x_i-\bar{x})(y_i-\bar{y})\right]^2}{\sum_{i=1}^{n}(x_i-\bar{x})^2}\right]}, \qquad \text{Eq. S2}$$

where n is the number of data points for linear interpolation. Values closer to 0 indicate a better fit.

c) Limit of detection, LOD

This is defined as the least amount of a substance that can be distinguished from the blank (i.e. absence of the substance) at a given confidence level, i.e. probability of false positive error (α) or false negative error (β).

The background-corrected signal, $y_{\mathrm{SAMPLE}} - y_{\mathrm{BLANK}}$, is proportional to the sample concentration c:

$$y_{\mathrm{SAMPLE}} - y_{\mathrm{BLANK}} = m \cdot c, \qquad \text{Eq. S3}$$

where y_{BLANK} is the signal from the blank sample and m is the slope of the calibration line.

Limit of detection is then defined as:[5]

$$\mathrm{LOD} = \frac{ns_y}{m}, \qquad \text{Eq. S4}$$

where s_y is the standard error of the estimate (eq. S2) and n is chosen depending on the confidence level required.

For a chosen confidence level of 5 % (i.e., $\alpha = \beta = 0.05$), the eq. S5 amounts to:[3,6]

$$\mathrm{LOD} = \frac{3.3s}{m}. \qquad \text{Eq. S5}$$

d) Percent error of the slope, *mErr%*

Originally calculated from the slope *m* of the line of corrected fluorescence (LCF), compared to the slope of the line of dilute solutions (LDS), defined as:[7]

$$\mathrm{mErr}\ \% = (m_{\mathrm{LCF}} - m_{\mathrm{LDS}})/m_{\mathrm{LDS}} \cdot 100\ \%. \qquad \text{Eq. S6}$$

Considering that the ideal fluorescence signal, IFS, which corresponds to the linear relationship between *F* and *A* in the absence of IFE, is a line with slope $a = 1$ and intercept $b = 0$ for normalized data, the eq. S3 simplifies to:[3,8,9]

$$\mathrm{mErr}\ \% = (a - 1)/1 \cdot 100\ \%. \qquad \text{Eq. S7}$$

where *a* is the slope of the linear regression line for normalized data (Table 1 in the manuscript). Values closer to 0 indicate a better fit.

3.2. Error estimation

a) Error estimation for absorbance (*A*), uncorrected fluorescence intensity (F_1 and F_2) and light path length (*h*)

The sample standard deviations, *s*, were estimated for all absorbance and fluorescence intensity measurements (denoted as x_i) as shown in equation:

$$s = \sqrt{\frac{1}{n-1}\sum_{i=1}^{n}(x_i - \bar{x})^2}. \qquad \text{Eq. S8}$$

The sample variances were calculated using the equation:

$$\mathrm{var}(x) = s^2 = \frac{1}{n-1}\sum_{i=1}^{n}(x_i - \bar{x})^2. \qquad \text{Eq. S9}$$

Background corrections were performed for all absorbance and fluorescence intensity measurements. Values measured at zero concentrations of the fluorophore were subtracted from each data point in the fluorophore concentration series. The variance of each background-corrected data point (x_{BC}) was calculated as the sum of the data point (x) variance and the background (x_{B}) variance:

$$\mathrm{var}(x_{\mathrm{BC}}) = \mathrm{var}(x) + \mathrm{var}(x_{\mathrm{B}}). \qquad \text{Eq. S10}$$

We have assumed that there is no correlation between the background and the errors of the titration data points. The main source of variability is likely due to the pipetting errors, which are expected to be random and uncorrelated.

Standard deviations were calculated for the background-corrected data as follows:

$$s = \sqrt{\mathrm{var}(x_{\mathrm{BC}})} = \sqrt{\mathrm{var}(x) + \mathrm{var}(x_{\mathrm{B}})}. \qquad \text{Eq. S11}$$

For aqueous solutions, the path length can be calculated from the absorbance values for water in the near-infrared wavelength range (900 nm to 1000 nm) using a cuvette and the corresponding microplate. The estimation of h was made by measuring the path length of pure water with parameters: test wavelength λ = 977 nm, reference wavelength λ = 900 nm and correction factor value of 0.186. The correction factor is defined as the absorbance value of water at the test wavelength corrected by the absorbance value of water at the reference wavelength for a path length of 1 cm.[10] The path length of pure water was measured in decaplicate and the average value of the path length obtained for a sample volume of 200 µL was used as the h-estimator.

b) Error estimation for the exponential term (N)

The exponential coefficient in eqs. 5 and 6 in the manuscript can be written as:

$$N = \frac{l_1}{l_1 - l_2} = \frac{d-(h-t)+f-z_2}{d-(h-t)+f-z_1-(d-(h-t)+f-z_2)} = \frac{d-(h-t)+f-z_2}{z_2-z_1}. \qquad \text{Eq. S12}$$

The uncertainties in the geometric parameters f and z were not considered in the error estimation calculations. We did not have numerical values for these uncertainties, which result from the tolerances in the manufacture of microplates. The Tecan Spark M10 multimode microplate reader software displays the parameter z in 5 significant figures. The parameter f is a spatial dimension that should be easily measured with high precision.

It is reasonable to assume that the variations of these parameters are statistically insignificant compared to the variation of the parameter h caused by pipetting errors. Therefore, the standard deviation of the term N is calculated to be equal to the standard deviation of the parameter h, assuming that the standard deviations of the parameters f, z_1, and z_2 are statistically insignificant:

$$s(N) \approx s(h). \qquad \text{Eq. S13}$$

The values of $s(N)$ were calculated only for combinations of z-positions that gave the best results in the correction procedure and were used for comparison with uncorrected (F_1) and absorbance-corrected fluorescence (F_{A}).

c) Error propagation for the absorbance IFE correction (F_A)

The correction function given in eq. 1 is a function of three variables and can be written as follows:

$$f(F_1, A_{ex}, A_{em}) = F_1 \cdot 10^{[(A_{ex}+ A_{em})/2]}. \quad \text{Eq. S14}$$

The partial derivatives of the above function were calculated with respect to all three variables as:

$$\frac{\partial f(F_1, A_{ex}, A_{em})}{\partial F_1} = 10^{[(A_{ex}+ A_{em})/2]}, \quad \text{Eq. S15}$$

$$\frac{\partial f(F_1, A_{ex}, A_{em})}{\partial A_{ex}} = F_1 \cdot \ln(10) \cdot 2^{\left[\frac{1}{2}(A_{ex}+ A_{em}-2)\right]} \cdot 5^{\left[\frac{1}{2}(A_{ex}+ A_{em})\right]}, \quad \text{Eq. S16}$$

$$\frac{\partial f(F_1, A_{ex}, A_{em})}{\partial A_{em}} = \frac{\partial f(F_1, A_{ex}, A_{em})}{\partial A_{ex}}. \quad \text{Eq. S17}$$

The error propagation was estimated using the following expressions:[4]

$$s_f = \left(\frac{\partial f}{\partial F_1} \cdot s_{F_1}\right)^2 + \left(\frac{\partial f}{\partial A_{ex}} \cdot s_{A_{ex}}\right)^2 + \left(\frac{\partial f}{\partial A_{em}} \cdot s_{A_{em}}\right)^2, \quad \text{Eq. S18}$$

$$s_f{}' = \left(\frac{\partial f}{\partial F_1} \cdot s_{F_1}\right)^2 + \left(\frac{\partial f}{\partial A_{ex}} \cdot s_{A_{ex}}\right)^2 + \left(\frac{\partial f}{\partial A_{em}} \cdot s_{A_{em}}\right)^2$$
$$+ 2 \cdot \left(\frac{\partial f}{\partial F_1} \cdot \frac{\partial f}{\partial A_{ex}}\right) \cdot \mathrm{cov}(F_1, A_{ex}) + 2 \cdot \left(\frac{\partial f}{\partial F_1} \cdot \frac{\partial f}{\partial A_{em}}\right) \cdot \mathrm{cov}(F_1, A_{em})$$
$$+ 2 \cdot \left(\frac{\partial f}{\partial A_{ex}} \cdot \frac{\partial f}{\partial A_{em}}\right) \cdot \mathrm{cov}(A_{ex}, A_{em}). \quad \text{Eq. S19}$$

The first expression (eq. S18) is used to calculate the standard deviation for the F_A values without considering the covariance factors. The second expression (eq. S19) considers the covariance terms calculated for all the pairs of variables (F_1, A_{em}, A_{ex}). The covariance terms seem to be significant in the total sum, considering that it is reasonable to assume that errors in the three variables are not independent of each other, since they are probably the result of pipetting errors and/or geometric imperfections and/or contamination of the microplate. Therefore, eq. S19 was used to calculate the standard deviation for the F_A values.

d) Error propagation for the *z*-position IFE correction (ZINFE, F_Z)

The correction function given in eqs. 5 and S12 is a function of three variables, and can be written as follows:

$$g(F_1, F_2, N) = F_1 \left(\frac{F_1}{F_2}\right)^N. \qquad \text{Eq. S20}$$

The exponential term *N* is a constant for each IFE correction procedure, since it is a function of the pairs of *z*-position values (z_1 and z_2) used for the particular correction. The term *N* varies from one correction to another as the combinations of *z*-position pairs also vary in this respect.

The partial derivatives of the above function were calculated with respect to all three variables as:

$$\frac{\partial g(F_1,\ F_2,\ N)}{\partial F_1} = (N+1) \cdot \left(\frac{F_1}{F_2}\right)^N, \qquad \text{Eq. S21}$$

$$\frac{\partial g(F_1,\ F_2,\ N)}{\partial F_2} = -N \cdot \left(\frac{F_1}{F_2}\right)^{(1+N)}, \qquad \text{Eq. S22}$$

$$\frac{\partial g(F_1,\ F_2,\ N)}{\partial N} = F_1 \cdot \left(\frac{F_1}{F_2}\right)^N \cdot \ln\left(\frac{F_1}{F_2}\right). \qquad \text{Eq. S23}$$

The error propagation was estimated using the following expressions:

$$s_g = \left(\frac{\partial g}{\partial F_1} \cdot s_{F_1}\right)^2 + \left(\frac{\partial g}{\partial F_2} \cdot s_{F_2}\right)^2 + \left(\frac{\partial g}{\partial N} \cdot s_N\right)^2, \qquad \text{Eq. S24}$$

$$s_g^{'} = \left(\frac{\partial g}{\partial F_1} \cdot s_{F_1}\right)^2 + \left(\frac{\partial g}{\partial F_2} \cdot s_{F_2}\right)^2 + \left(\frac{\partial g}{\partial N} \cdot s_N\right)^2 + \mathrm{cov}(F_1, F_2). \qquad \text{Eq. S25}$$

Similar to eqs. S18 and S19, the eq. S24 was used to calculate the standard deviation for the F_Z values without considering the covariance factors. The eq. S25 considers the covariance terms calculated for the F_1 and F_2 values (*N* is constant for each correction). The covariance term may also be significant in the overall sum, since it depends on the combination of *z*-positions used for a particular correction. Therefore, eq. S25 was used to calculate the standard deviation for the F_Z values.

In general, it can be observed that for the closest pairs of *z*-positions (in terms of numerical values) there is often a very significant correlation. This can be easily verified by plotting the F_1 vs. F_2 values (Figure S7). This shows a very good positive correlation between the measured *F* values over the entire concentration range for the combination of adjacent *z*-position measurements (z = 14.6 mm and z = 15 mm, red symbols). However, for the pair of the most distant *z*-positions (z = 14.6 mm and z = 21 mm, blue symbols), there is significantly worse correlation measured *F* values, especially at the highest concentrations of the fluorophore.

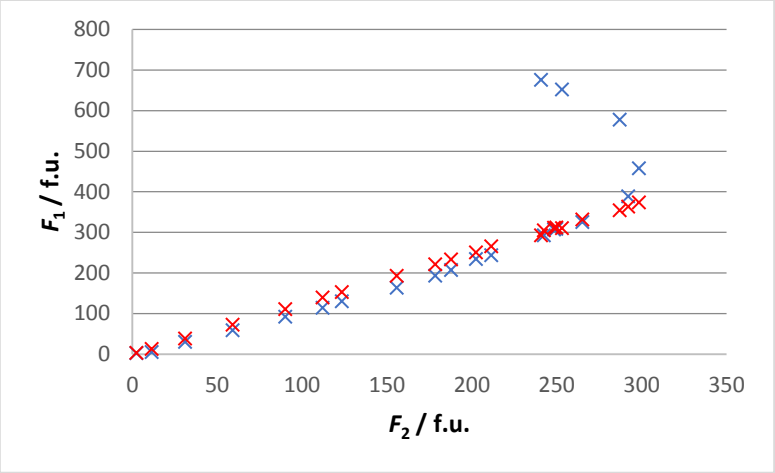

Figure S7. Plot of F_1 (z = 15 mm, ×, and z = 21 mm, ×) *vs.* F_2 (z = 14.6 mm) for the Q concentration series.

4. Experimental data

All averaged triplicate data preformatted for automatic online processing and the results obtained have been permanently archived.[11]

In total, there are 6 different datasets for 3 different concentration series (Q, Q-v and Q-f) in 2 different types of microplates (T and NT). For each concentration series, a total of 9 fluorescence measurements were performed using the selected available *z*-positions (n = 9, Table S1).

4.1. Fluorescence data

The measured data and the results of the ZINFE correction (F_Z) and the NINFE correction (F_N) are summarized in Figures S8, S9 and S10.

All plots in these figures were created using the JavaScript open-source graphing library Plotly[12] in the online calculator available at https://ninfe.science.[13]

Due to incompatible algorithms, two separate online calculators were created: (i) for the proposed ZINFE and NINFE correction, and (ii) for the absorbance IFE correction. The online service requires the properly formatted fluorescence measurements and *z*-position data (both for NINFE and ZINFE), as well as known geometric parameters for the specific microplate and microplate reader (for ZINFE only).

a) Q – transparent microplates (Dataset 1)

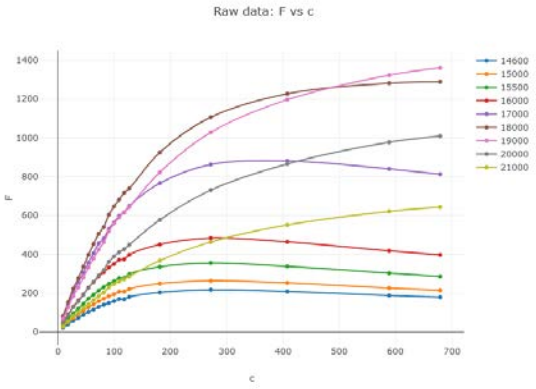

b) Q – non-transparent microplates (Dataset 2)

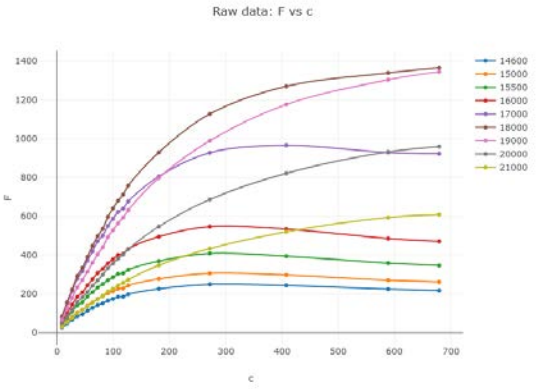

c) Q-v – transparent microplates (Dataset 3)

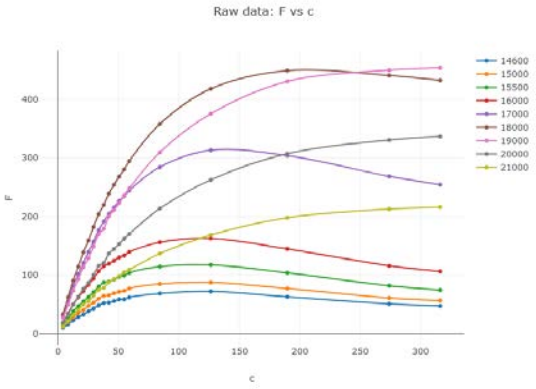

d) Q-v – non-transparent microplates (Dataset 4)

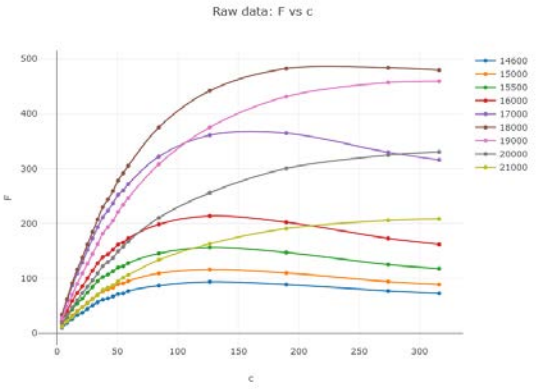

e) Q-f – transparent microplates (Dataset 5)

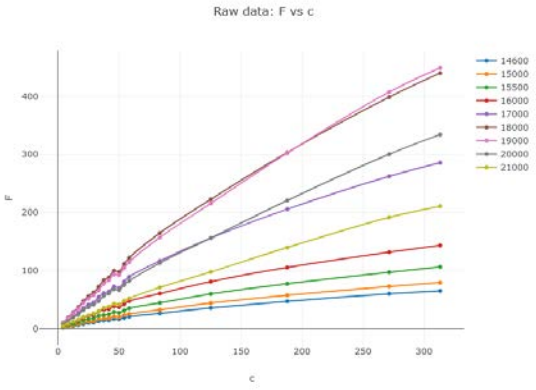

f) Q-f – non-transparent microplates (Dataset 6)

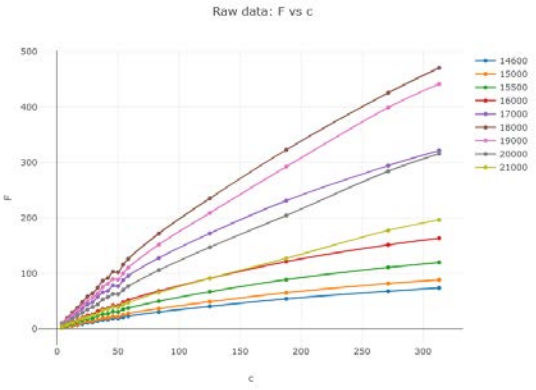

Figure S8. Dependence of background-corrected fluorescence measured at different *z*-positions on QS concentration (values of *z*-positions are given in the legend of each plot).

a) Q – transparent microplates (Dataset 1)

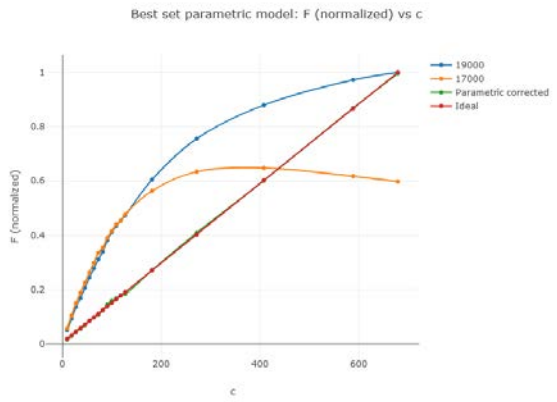

b) Q – non-transparent microplates (Dataset 2)

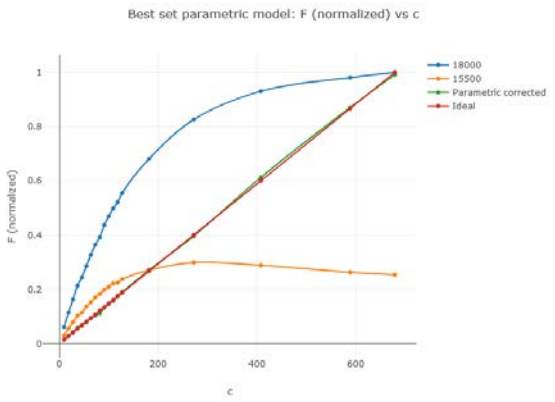

c) Q-v – transparent microplates (Dataset 3)

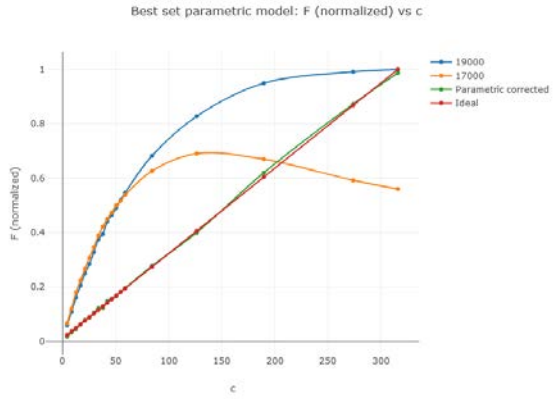

d) Q-v – non-transparent microplates (Dataset 4)

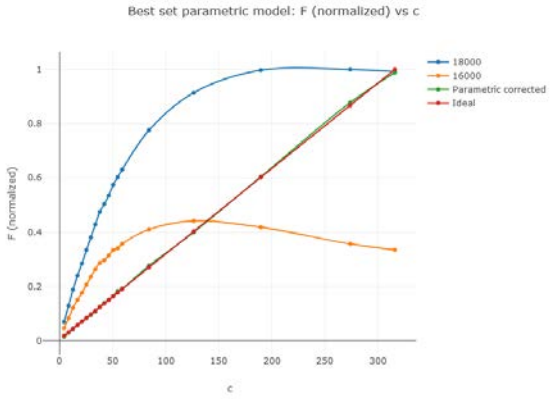

e) Q-f – transparent microplates (Dataset 5)

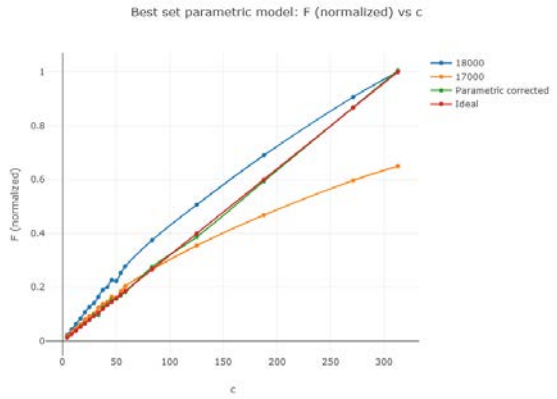

f) Q-f – non-transparent microplates (Dataset 6)

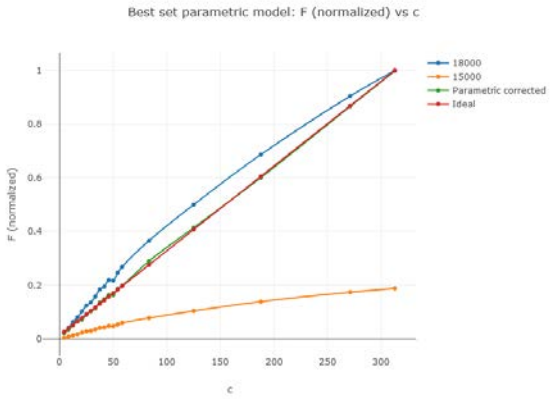

Figure S9. Comparison of the optimal ZINFE corrections (F_Z, —), the uncorrected values of (F_1, —) and (F_2, —) used for the calculation, and the ideal fluorescence signal (IFS, —). All values of F_x were normalized as described in the manuscript.

a) Q – transparent microplates (Dataset 1)

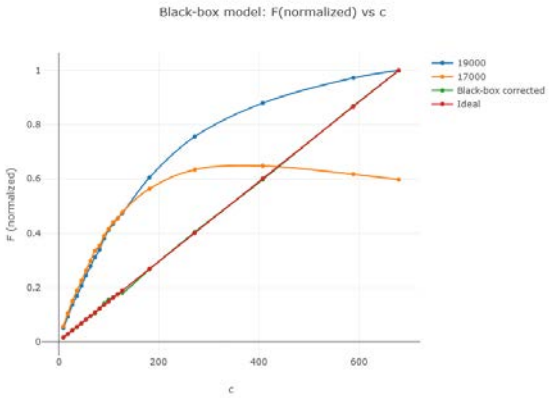

b) Q – non-transparent microplates (Dataset 2)

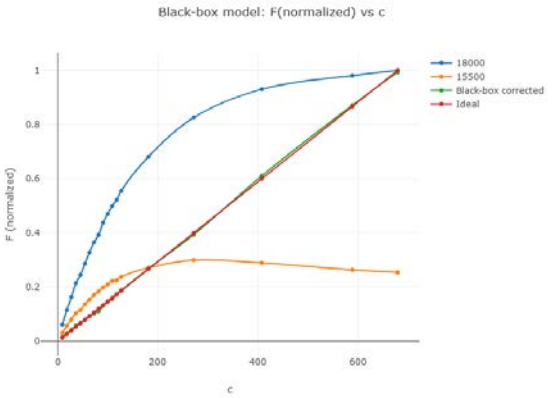

c) Q-v – transparent microplates (Dataset 3)

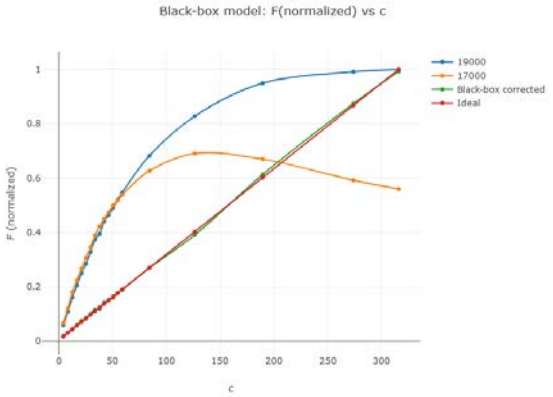

d) Q-v – non-transparent microplates (Dataset 4)

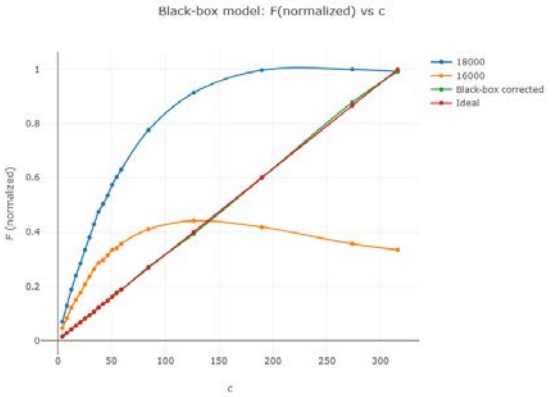

e) Q-f – transparent microplates (Dataset 5)

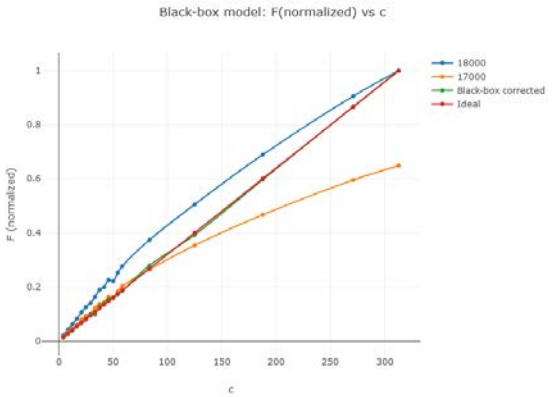

f) Q-f – non-transparent microplates (Dataset 6)

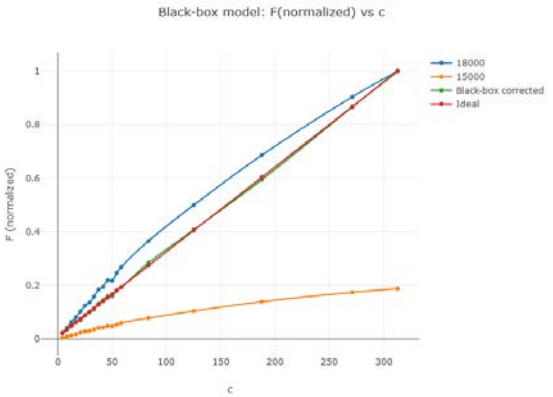

Figure S10. Comparison of the optimal NINFE corrections (F_N, —), the uncorrected values of (F_1, —) and (F_2, —) used for the calculation, and the ideal fluorescence signal (IFS, —). All values of F_x were normalized as described in the manuscript.

4.2. Absorbance data

a) Q concentration series (Dataset 1)

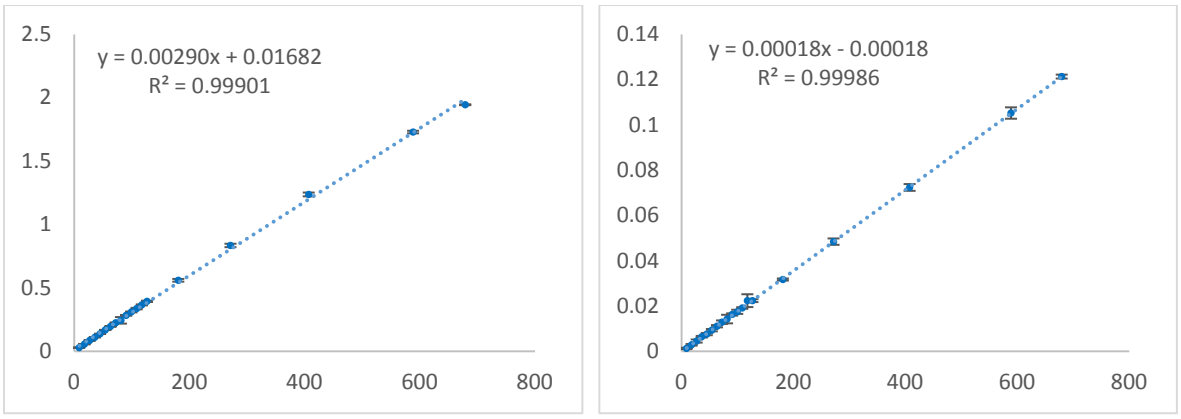

b) Q-v concentration series (Dataset 3)

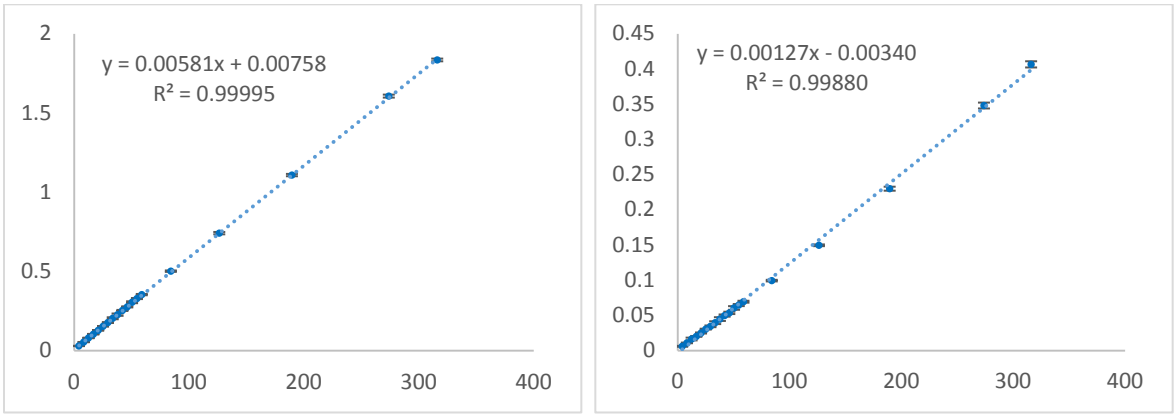

c) Q-f concentration series (Dataset 5)

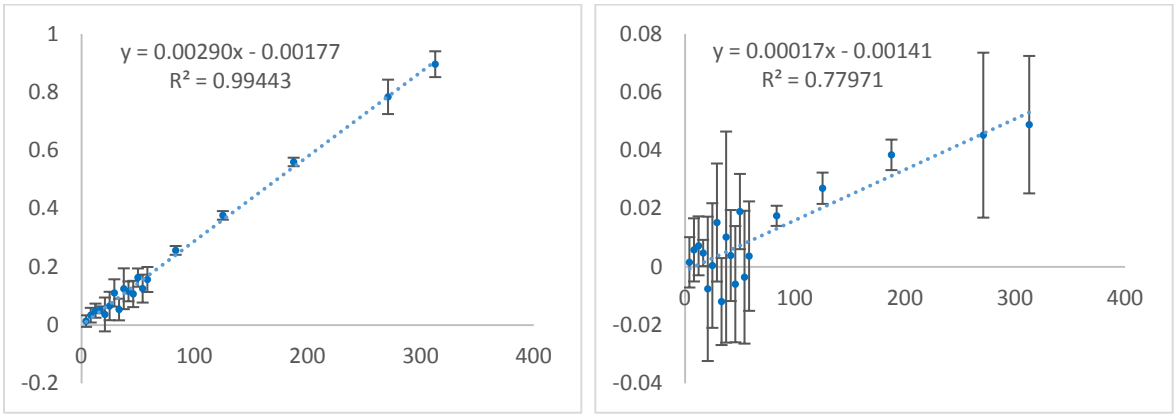

Figure S11. Dependence of the absorbance at excitation and emission wavelengths on QS concentration (UV-transparent microplates only): **left:** A_{ex} values; **right**: A_{em} values. The error bars denote standard deviations of the measurements in triplicate. The results of the linear regression are shown in the insets of individual plots.

4.3. Results of the linear regression for raw (unscaled) data.

Table S12. Overview of least squares linear fit results for unscaled, background-corrected data. Slope and intercept values were used for data normalization (Table 1 in the manuscript; see manuscript for details).

Sample [1]	Plate type [2]	correction type[3]	R^2	Slope (a) / μM^{-1}	Intercept (b)	s_y [5]	LOD [6] / μM
Q	T	F_1	0.87449	1.9	276.6	143.5	247.2
		F_Z	0.99980	5.0	18.5	14.1	9.2
		F_N	0.99984	5.2	8.3	12.8	8.1
		F_A	0.95074	20.1	-997.3	906.2	148.5
	NT	F_1	0.81861	1.9	349.6	173.4	307.2
		F_Z	0.99971	33.0	25.9	111.5	11.1
		F_N	0.99973	34.5	-19.7	112.6	10.8
Q-v	T	F_1	0.81967	1.3	115.2	58.2	142.4
		F_Z	0.99951	4.1	12.4	8.3	6.7
		F_N	0.99964	4.3	5.8	7.5	5.8
		F_A	0.93753	17.2	-409.6	408.5	78.4
	NT	F_1	0.73752	1.4	152.0	75.7	181.1
		F_Z	0.99974	18.5	27.5	27.5	4.9
		F_N	0.99979	19.6	8.4	25.8	4.4
Q-h	T	F_1	0.98744	1.4	25.0	14.4	33.9
		F_Z	0.99959	6.6	-2.5	12.1	6.1
		F_N	0.99965	5.9	4.0	10.1	5.6
		F_A	0.98111	4.0	-57.8	50.5	41.7
	NT	F_1	0.98918	1.5	24.4	14.3	31.4
		F_Z	0.99964	33.4	131.6	58.0	5.7
		F_N	0.99972	46.7	131.0	71.3	5.0

[1] Q corresponds to the pure QS concentration series; Q-v corresponds to the variable concentration of the absorber PD (fixed ratio of the total concentrations of PD and QS); Q-f corresponds to the fixed total concentration of PD (variable ratio of the total concentrations of PD and QS), see manuscript for details.
[2] T corresponds to UV-transparent microplates; NT corresponds to non-transparent microplates.
[3] F_1 corresponds to uncorrected fluorescence; F_Z corresponds to ZINFE-corrected fluorescence intensity (eq. 5); F_A corresponds to absorbance IFE-corrected fluorescence intensity (eq. 1); F_N corresponds to NINFE-corrected fluorescence intensity.
[4] Standard error of the estimate defined by eq. S2.
[5] Limit of detection ($\alpha = \beta = 0.05$); see manuscript for details.
[6] LOD values normalized as percentage of c_{max}, see manuscript for details.

4.4. Error surfaces

a) Q – transparent microplates (Dataset 1)

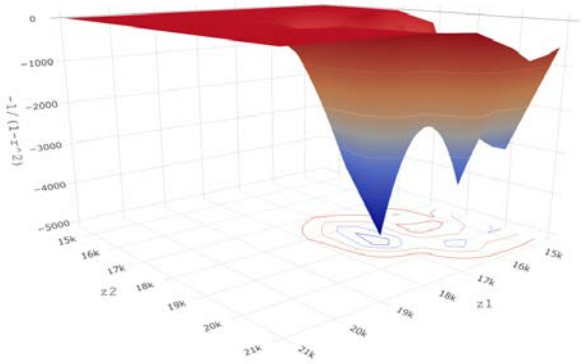

b) Q – non-transparent microplates (Dataset 2)

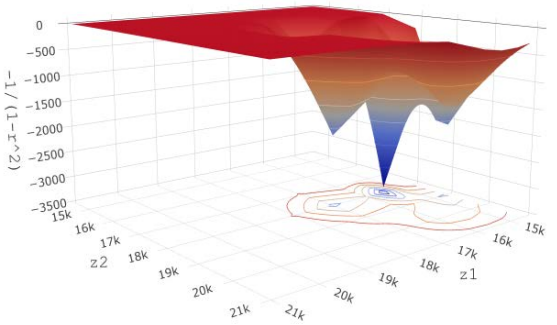

c) Q-v – transparent microplates (Dataset 3)

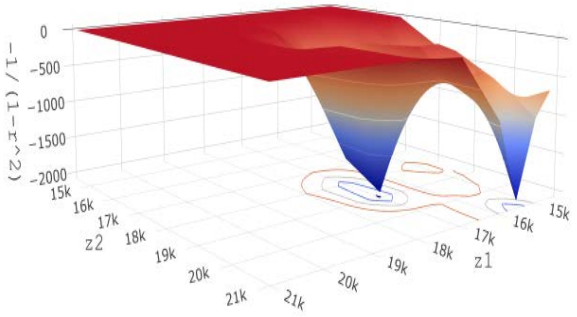

d) Q-v – non-transparent microplates (Dataset 4)

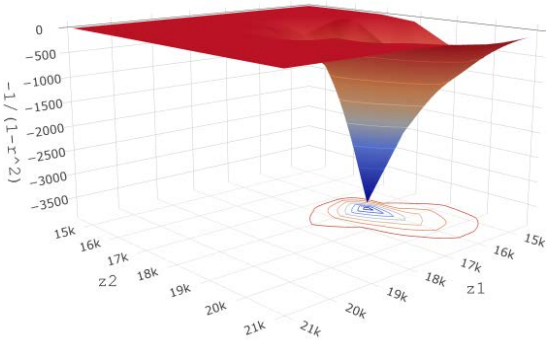

e) Q-f – transparent microplates (Dataset 5)

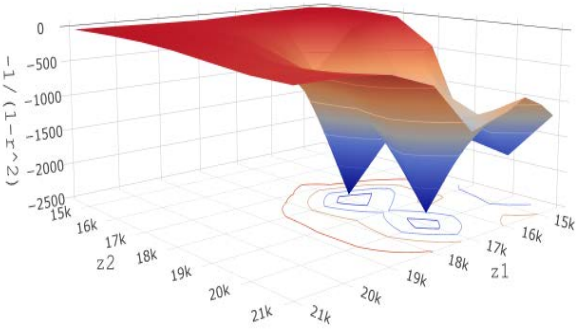

f) Q-f – non-transparent microplates (Dataset 6)

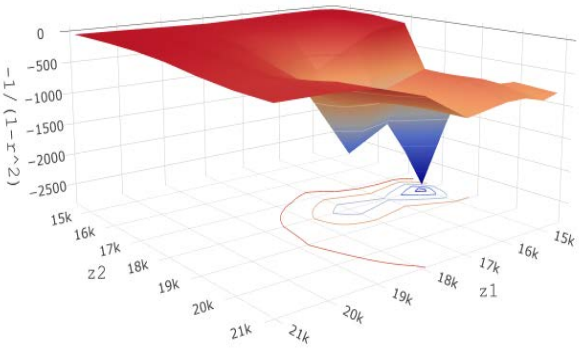

Figure S13. The 3D plot for the dependence of the model error, $\Delta R = -1 / (1 - R^2)$, on the values of z_1 and z_2. All plots were created using the JavaScript open-source graphing library Plotly[12] and the online calculator NINFE.[13]

4.5. Miscellaneous information

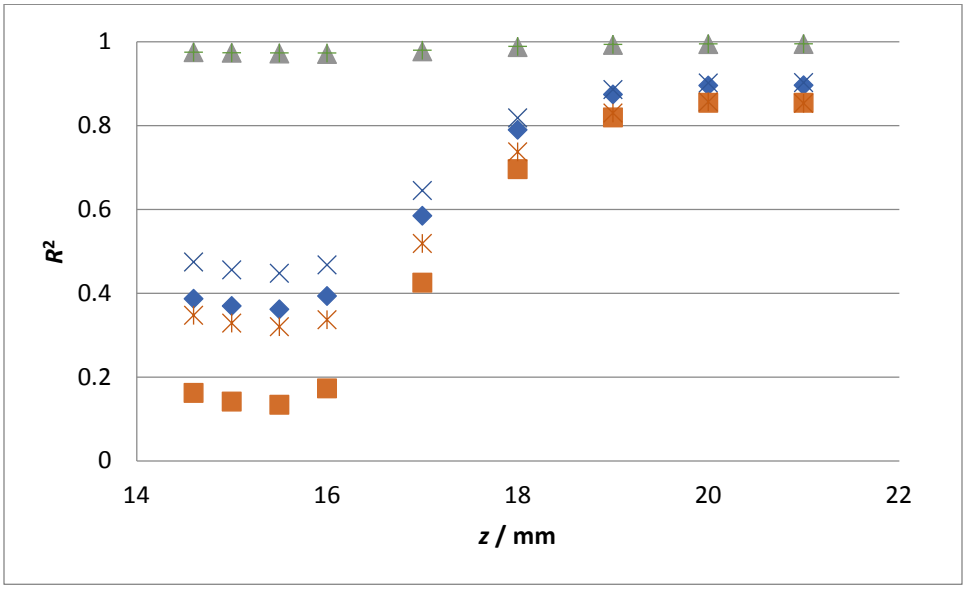

Figure S14. Dependence of calculated R^2 values for uncorrected fluorescence (F_1) on *z*-position: UV-transparent plates, concentration series: Q (◆), Q-v (■) and Q-f (▲); non-transparent plates, concentration series: Q (×), Q-v (✳) and Q-f (+).

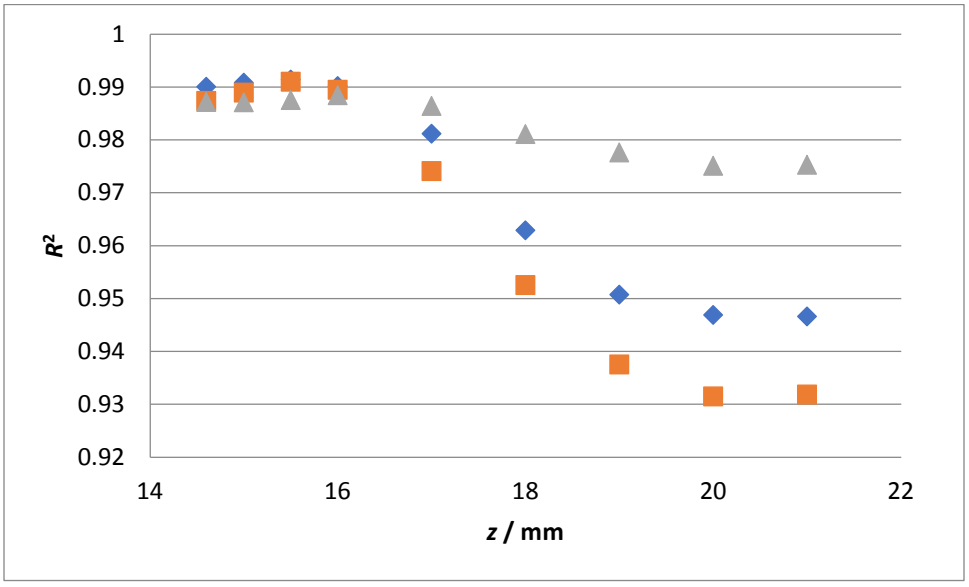

Figure S15. Dependence of calculated R^2 values for absorbance-corrected data (F_A) on *z*-position: concentration series Q (◆), Q-v (■) and Q-f (▲). Data are shown only for UV-transparent plates.

Table S16. Comparison of exponents resulting from geometric parameters (eq. 5) and numerical optimization (eq. 6).

Sample [1]	Plate type [2]	Correction type [3]	Exponent N	$\lvert F_Z - F_N \rvert$
Q	T	F_Z	-1.7965	*0.0480*
		F_N	*-1.8445*	
	NT	F_Z	-2.0372	*0.0312*
		F_N	*-2.0684*	
Q-v	T	F_Z	-1.7965	*0.0730*
		F_N	*-1.8695*	
	NT	F_Z	-2.2965	*0.0522*
		F_N	*-2.3487*	
Q-f	T	F_Z	-3.593	*0.2600*
		F_N	*-3.333*	
	NT	F_Z	-1.8643	*0.2017*
		F_N	*-2.066*	

[1,2,3] See Table S12 and manuscript for details.

a) Q – transparent microplates (Dataset 1)

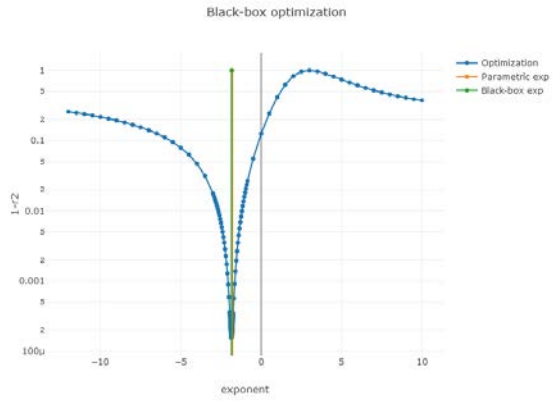

b) Q – non-transparent microplates (Dataset 2)

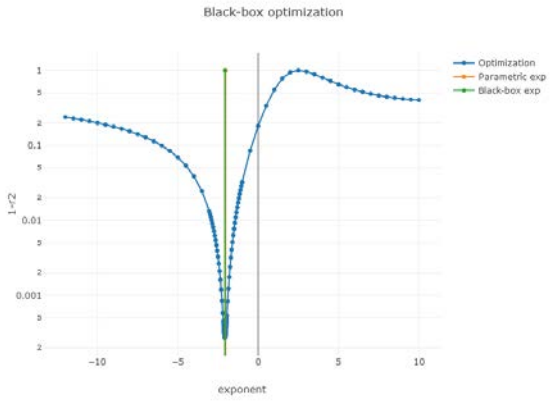

c) Q-v – transparent microplates (Dataset 3)

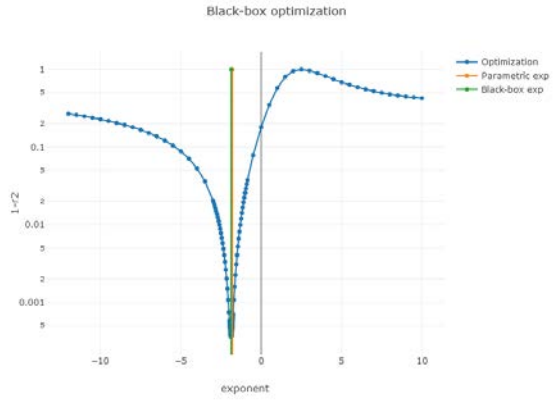

d) Q-v – non-transparent microplates (Dataset 4)

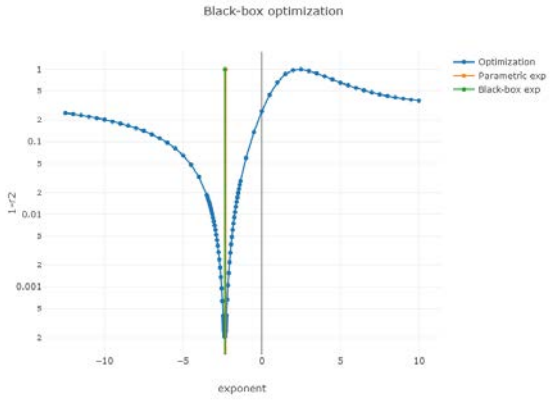

e) Q-f – transparent microplates (Dataset 5)

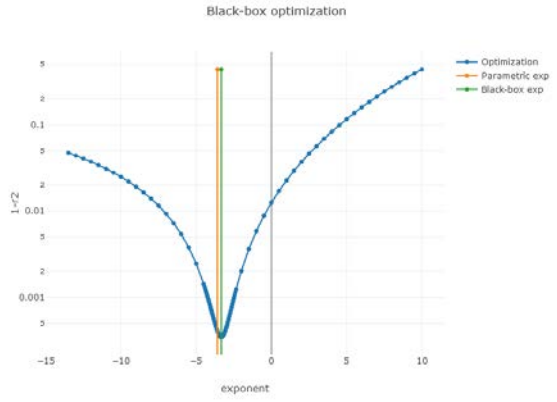

f) Q-f – non-transparent microplates (Dataset 6)

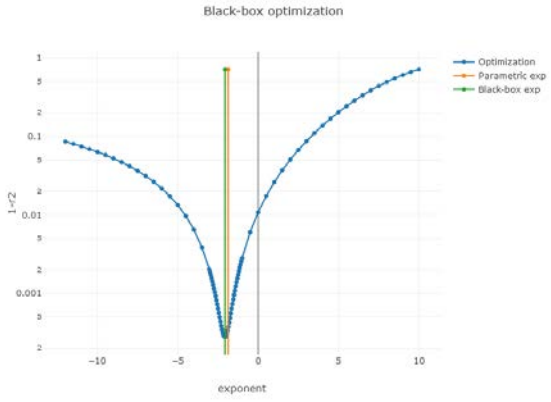

Figure S17. Exponent optimization error curves: exponent value used for ZINFE correction (F_Z, —), exponent value used for NINFE correction (F_N, —). All plots were created using JavaScript open-source graphing library Plotly[12] and the online calculator NINFE.[13]

Table S18. Comparison of linear regression of data with and without background correction (F_Z and F_N).

Sample [1]	Plate type [2]	Correction type [3]	WITH background correction [4]			WITHOUT background correction [5]		
			R^2	LOD%	b %	R^2	LOD%	b %
Q	T	F_Z	0.99964	1.82	0.68	0.99980	1.36	0.54
		F_N	0.99985	1.16	-0.01	0.99984	1.20	0.24
	NT	F_Z	0.99968	1.72	0.20	0.99971	1.64	0.12
		F_N	0.99972	1.60	-0.11	0.99973	1.59	-0.08
Q-v	T	F_Z	0.99924	2.65	-1.28	0.99951	2.13	0.95
		F_N	0.99925	2.63	-1.16	0.99964	1.83	0.43
	NT	F_Z	0.99957	1.99	0.76	0.99974	1.55	0.47
		F_N	0.99979	1.40	0.09	0.99979	1.38	0.14
Q-f	T	F_Z	0.99961	1.90	-0.16	0.99959	1.93	-0.12
		F_N	0.99967	1.74	0.22	0.99965	1.79	0.22
	NT	F_Z	0.99962	1.86	1.02	0.99964	1.83	1.24
		F_N	0.99972	1.59	0.57	0.99972	1.61	0.89

[1, 2, 3] See Table S12 and manuscript for details.
[4] Background-corrected data, copied from Table 1 in the manuscript for clarity.
[5] No background correction, i.e. only raw sample fluorescence data was used for IFE correction.

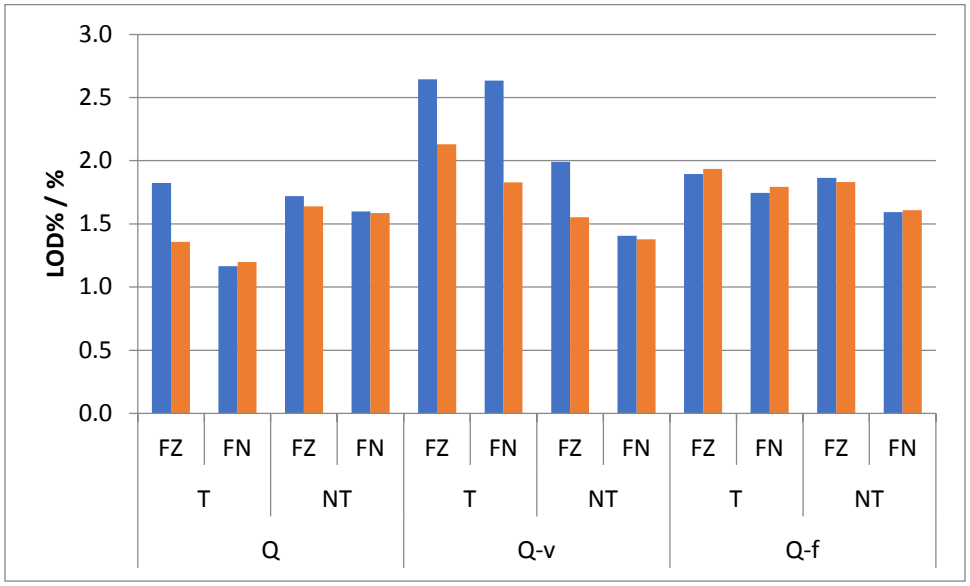

Figure S19. Comparison of LOD% values (F_Z and F_N): with background correction (■), without background correction (■). All values are LOD% < 2.7 % for ZINFE correction and LOD% < 2.2 % for NINFE correction.

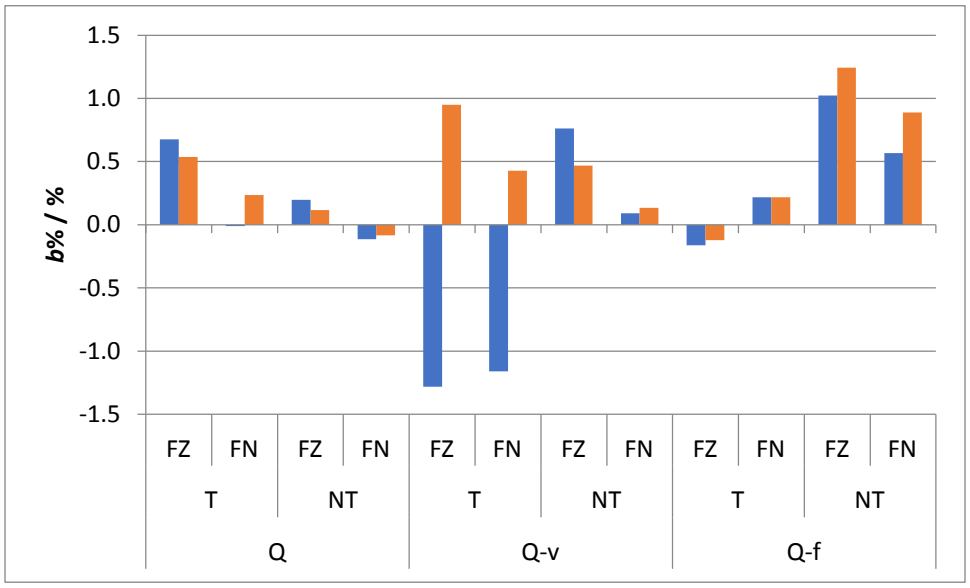

Figure S20. Comparison of b % values (F_Z and F_N): with background correction (■), without background correction (■). The absolute values of all b % values, corresponding to the direction-insensitive deviation from the ideal fluorescence signal, are $|b\ \%| < 1.3$ % for either the ZINFE correction or the NINFE correction.

Table S21. Overview of the least-squares linear fit results for normalized, background-corrected fluorescence and absorbance data in the low concentration range (the first 7 points of each dataset).

Sample [1]	Plate type [2]	Correction type [3]	R^2	b %	LOD%
Q	T	F_1	0.9983	5.92	4.67
		F_Z	0.9986	2.31	4.11
		F_N	0.9986	2.22	4.15
		F_A	0.9988	-0.33	3.93
	NT	F_1	0.9944	7.95	8.37
		F_Z	0.9964	3.89	6.70
		F_N	0.9964	3.83	6.70
Q-v	T	F_1	0.9964	6.37	6.68
		F_Z	0.9968	2.96	6.32
		F_N	0.9967	2.83	6.41
		F_A	0.9996	0.17	2.25
	NT	F_1	0.9972	6.82	5.96
		F_Z	0.9988	2.69	3.91
		F_N	0.9988	2.60	3.88
Q-f	T	F_1	0.9973	2.25	5.78
		F_Z	0.9968	-2.68	6.37
		F_N	0.9975	-2.34	5.57
		F_A	0.9957	-1.09	7.31
	NT	F_1	0.9967	2.24	6.41
		F_Z	0.9946	7.76	8.25
		F_N	0.9931	8.42	9.28

[1, 2, 3] See Table S12 and manuscript for details.

Table S22. Overview of the total change of absorbance, ΔA, for all concentration series, calculated from the data shown in Figure S11.

Sample [1]	ΔA	
	excitation	emission
Q	1.92	0.12
Q-v	1.80	0.40
Q-f	0.88	0.04

[1,] See Table S12 for details.

Conflicts of interest

There are no conflicts of interest to declare.

Acknowledgements

This work was supported by funding from the Croatian Science Foundation grant UIP-2017-05-9537 – *Glycosylation as a factor in the iron transport mechanism of human serum transferrin* (GlyMech). Additional support was provided by the European Structural and Investment Funds for the 'Croatian National Centre of Research Excellence in Personalized Healthcare' (contract #KK.01.1.1.01.0010), 'Centre of Competences in Molecular Diagnostics' (contract #KK.01.2.2.03.0006), and the European Regional Development Fund grant for 'Strengthening of Scientific Research and Innovation Capacities of the Faculty of Pharmacy and Biochemistry at the University of Zagreb' (FarmInova, contract #KK.01.1.1.02.0021).

References

(1) Taniguchi, M.; Lindsey, J. S. Database of Absorption and Fluorescence Spectra of >300 Common Compounds for Use in PhotochemCAD. *Photochemistry and Photobiology* **2018**, *94* (2), 290–327. https://doi.org/10.1111/php.12860.

(2) Spijkerman, J. J.; Travis, J. C.; Pella, P. A.; DeVoe, J. R. Preliminary Study on the Characteristics and Design Parameters for Mossbauer Resonant Detector, 1971.

(3) Miller, J. N.; Miller, J. C. *Statistics and Chemometrics for Analytical Chemistry*, 6. ed.; Prentice Hall: Harlow, 2010.

(4) Taylor, J. R. *An Introduction to Error Analysis: The Study of Uncertainties in Physical Measurements*, 2nd ed.; University Science Books: Sausalito, Calif, 1997.

(5) ICH Harmonised Tripartite Guideline: Validation of Analytical Procedures: Text and Methodology Q2 (R1); Geneva, Switzerland, 2005; Vol. 11. https://doi.org/10.1163/ej.9789004163300.i-1081.897.

(6) Brunetti B, D. E. About Estimating the Limit of Detection by the Signal to Noise Approach. *Pharm Anal Acta* **2015**, *06* (04). https://doi.org/10.4172/2153-2435.1000355.

(7) Gu, Q.; Kenny, J. E. Improvement of Inner Filter Effect Correction Based on Determination of Effective Geometric Parameters Using a Conventional Fluorimeter. *Anal. Chem.* **2009**, *81* (1), 420–426. https://doi.org/10.1021/ac801676j.

(8) Holland, J. F.; Teets, R. E.; Kelly, P. M.; Timnick, Andrew. Correction of Right-Angle Fluorescence Measurements for the Absorption of Excitation Radiation. *Anal. Chem.* **1977**, *49* (6), 706–710. https://doi.org/10.1021/ac50014a011.

(9) Kothawala, D. N.; Murphy, K. R.; Stedmon, C. A.; Weyhenmeyer, G. A.; Tranvik, L. J. Inner Filter Correction of Dissolved Organic Matter Fluorescence. *Limnology and Oceanography: Methods* **2013**, *11* (12), 616–630. https://doi.org/10.4319/lom.2013.11.616.

(10) Tecan Spark Instructions for Use – Reference Guide V1.2, 2017.

(11) Weitner, T.; Friganović, T.; Šakić, D. Inner Filter Effect Correction for Fluorescence Measurements in Microplates, 2022. https://doi.org/10.5281/zenodo.5849302.

(12) Plotly Technologies Inc., C. Plotly JavaScript Graphing Library https://plotly.com/javascript/.

(13) Šakić, D.; Weitner, T.; Friganović, T. NINFE https://ninfe.science/.

5. RAD 4: PROTEIN SIALYLATION AFFECTS THE pH-DEPENDENT BINDING OF FERRIC ION TO HUMAN SERUM TRANSFERRIN

Dalton Transactions

ROYAL SOCIETY OF CHEMISTRY

PAPER

View Article Online
View Journal | View Issue

Check for updates

Cite this: *Dalton Trans.*, 2024, **53**, 10462

Protein sialylation affects the pH-dependent binding of ferric ion to human serum transferrin†

Tomislav Friganović, Valentina Borko and Tin Weitner *

Received 3rd May 2024,
Accepted 1st June 2024

DOI: 10.1039/d4dt01311e

rsc.li/dalton

Physiological or pathophysiological changes lead to posttranslational changes in the sialic acid content of human serum transferrin (hTf), an essential mediator of iron transport in the human body, resulting in a significantly increased concentration of desialylated hTf. The intrinsic fluorescence quenching upon binding of iron to hTf was successfully modeled using the binding polynomial for two iron-binding sites, allowing measurements in a high-throughput format. Removal of sialic acid residues resulted in a 3-fold increase in iron binding affinity for both sites of hTf at pH 7.4. The pH-dependence of iron binding showed significant differences in equilibrium constants, resulting in a 10-fold increase in binding affinity for desialylated hTf at pH 5.9. The changes in hTf sialylation apparently result in tuning of the stability of the conformational state, which in turn contributes to the stability of the diferric hTf. The observed differences in the conditional thermodynamic equilibrium constants suggest that the desialylated protein has a higher preference for diferric hTf over monoferric hTf species down to pH 6.5, which may also influence the interaction with transferrin receptors that preferentially bind to diferric hTf. The results suggest a link between changes in hTf glycan structure and alterations in iron binding equilibrium associated with tissue acidosis.

Introduction

Human serum transferrin (hTf), the primary iron transport protein in the human body, is a globular glycoprotein with an approximate molecular weight of 79 kDa that is predominantly produced in the liver.[1,2] This highly glycosylated protein is bilobal, with each lobe—the N-lobe containing 336 amino acids and the C-lobe containing 343—harbouring a thermodynamically distinct binding site for iron(III) ions.[3] The lobes are interconnected by a short peptide and stabilized by 19 intra-chain disulfide bonds.[4] Structurally, the N-lobe consists of 14 helices and 13 strands, while the C-lobe is composed of 17 helices and 13 strands.[5]

Transferrin binds iron(III), forming a stable ternary chelate-protein complex with a distorted octahedral coordination. In this complex, iron(III) is bound bidentately to the synergistic carbonate anion and monodentately to two tyrosine, one aspartic acid, and one histidine amino acid.[6] The presence of the synergistic anion, like carbonate or oxalate, is critical for the formation of stable iron-transferrin complexes.[7] Transferrin also forms complexes with Fe(II), though these are less stable.[8] Four isoforms of hTf can be distinguished based on iron content: apo-hTf (no iron bound), Fe_N-hTf or Fe_C-hTf (one iron bound per hTf, in either lobe), and Fe_2hTf (both binding sites occupied).

The proper binding of iron to transferrin, in terms of both thermodynamic and kinetic aspects, is essential for the normal functioning of the human organism. Unbound iron cations are hazardous as they can produce reactive and toxic oxygen species through the Fenton reaction, leading to significant cellular damage.[9] The body maintains a tight regulation of iron, with only about 1% of total iron bound to transferrin, undergoing a considerable daily turnover of around 25 mg, 80% of which is used for haemoglobin synthesis in the bone marrow.[10,11] In addition to iron, various cations can form more or less stable complexes with transferrin, some of which might be of physiological importance.[12]

The extent of transferrin-iron complexation, which is reflected in the values of the equilibrium constants, is pH-dependent. This is attributed to the release of protons during the iron binding process.[13] The affinity of transferrin for iron decreases with decreasing pH, a property that is effectively utilized in iron release in endosomes at pH 5.6.[14] The process of iron release is further facilitated by binding to the human transferrin receptors $hTfR_1$ and $hTfR_2$.[15,16] Despite the notable difference in binding affinities between $hTfR_1$ and $hTfR_2$ for transferrin, the lower affinity of $hTfR_2$ does not diminish its ability to facilitate iron endocytosis.[16]

Another important factor that can influence the iron binding affinity of transferrin is the extent of glycosylation.[17] Transferrin exhibits microheterogeneity due to the varying

Faculty of Pharmacy and Biochemistry, University of Zagreb, Ante Kovačića 1, 10000 Zagreb, Croatia. E-mail: tin.weitner@pharma.unizg.hr

† Electronic supplementary information (ESI) available. See DOI: https://doi.org/10.1039/d4dt01311e

degree of sialylation of its N-linked oligosaccharide chains, which can be bi- or triantennary and typically terminate with sialic acid residues.[18] Different sialoforms can be distinguished by isoelectric focussing or chromatography, highlighting the importance of sialic acid content in determining the physicochemical properties and possibly biological functions of transferrin.[19] In healthy individuals, approximately 80% of hTf is present as a tetrasialoform shown in Fig. 1.[20] Deviations from normal sialylation patterns may indicate various pathological conditions or genetic diseases.[21]

For example, during pregnancy, there is a progressive and gradual shift towards highly sialylated hTf, which is quickly reversed postpartum.[22] In addition, the reduction in transferrin sialylation is observed as part of the acute phase response in septic patients, and a reduction in transferrin sialylation may be a predictor of severe sepsis and septic shock.[23,24] In normal serum, glycosylated transferrin exhibits a half-life of 7 to 10 days.[25] The half-life of desialylated hTf is significantly shorter, resulting in increased iron turnover and faster delivery of iron to hepatic stores.[24] The degree of transferrin sialylation can also serve as a marker for chronic alcohol abuse by identifying elevated levels of carbohydrate-deficient transferrin isoforms.[26]

Over the past 45 years, the accurate determination of the equilibrium constants of transferrin-iron complexes has been the subject of numerous studies, which have been complicated by exceptionally high equilibrium constants and the potential hydrolysis of the hexaaquairon(III) cation. Under these circumstances, methods for iron exchange between transferrin and suitable iron chelators are required. This is due to the fact that direct application of solutions containing free Fe(III) ions has proven ineffective.[12] Typically, either an iron chelator complex is added to unsaturated transferrin or, *vice versa*, saturated transferrin is treated with the chelator to remove the iron.

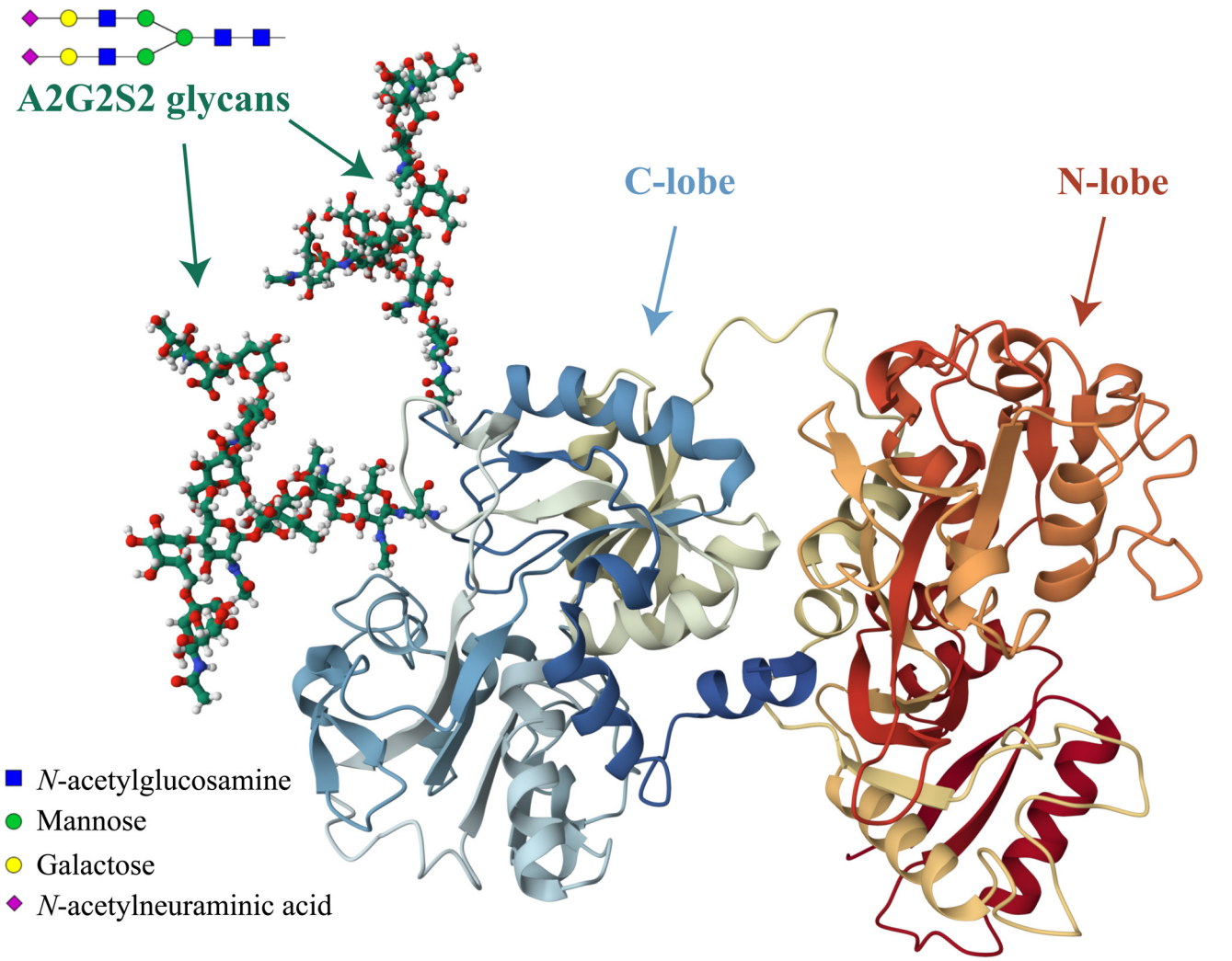

Fig. 1 Visual representation of the predominant glycosylated variant of human serum transferrin based on the glycan-free structure identified by Yang *et al.*[5] The structure was modified by adding two A2G2S2 glycans and by performing Molecular Dynamics (MD) optimization using the GLYCAM glycoprotein builder tool.[40] The A2G2S2 glycans were determined to be the most abundant fraction of Tf+S by UHPLC *N*-glycan analyses reported in previous studies.[17,39] Further details on the *N*-glycan analysis can be found in the ESI,† subsection 2.3.

Suitable chelators include nitrilotriacetic acid (NTA), ethylenediaminetetraacetic acid (EDTA), citrate, and others.[27] In addition, kinetic considerations are crucial for iron exchange, as the time required to reach equilibrium varies greatly, depending on the experimental conditions.[28]

The formation of transferrin-iron complexes can be effectively monitored by UV-Vis spectroscopy, with a broad spectral peak around $\lambda \approx 460$ nm indicating iron-saturated transferrin.[29–31] However, this method requires relatively high protein concentrations due to the low molar absorption coefficients in this spectral range.[31,32] Alternatively, fluorescence spectroscopy can be used to study transferrin-iron binding, which allows lower protein concentrations by monitoring the partial quenching of the intrinsic fluorescence of transferrin upon iron binding.[33]

In addition to spectroscopic techniques, isothermal titration calorimetry (ITC) and differential scanning calorimetry (DSC) have been successfully used to determine the equilibrium constants of transferrin-iron complexes.[34,35] Our recent calorimetric study on the effect of sialylation and synergistic anion on the binding of iron to hTf suggests that desialylated hTf has a higher capacity for iron sequestration, suggesting possible effects on iron metabolism.[17] Furthermore, we observed that decreasing the sialic acid content in hTf leads to more exothermic apparent binding enthalpies and increased apparent binding constants in the presence of carbonate for both iron binding sites.[17] This emphasises the potentially important role of sialylation in modulating the iron-binding properties of transferrin.

Considering that the uptake and release of iron by hTf is pH-dependent (pH ≈ 7.4 in serum *vs.* pH ≈ 5.6 in the endosome),[36] the aim of this study was to further investigate the pH dependence of the binding of ferric ions to native sialylated hTf (Tf+S) and enzymatically desialylated hTf (Tf−S) using a high-throughput method. First, we established a spectrofluorometric method to determine the thermodynamic equilibrium constants at serum pH by independently repeating the measurements on Tf+S performed 45 years ago by Aisen *et al.*[37] The spectrofluorometric method was chosen because of its high sensitivity[38] and suitability for high-throughput analysis using a microplate reader. After successfully benchmarking the iron binding process with Tf+S, we enzymatically removed the terminal sialic acids from Tf+S and performed detailed glycan characterisation of both Tf+S and Tf−S, as reported previously.[17,39] We then examined the iron binding of Tf+S and Tf−S at five different pH values ranging from serum to endosome conditions (7.4, 6.9, 6.5, 6.2 and 5.9) to better understand the potential effects of different physiological pH values.

The emerging research on sialic acids underscores their role in cancer initiation, progression, and immune evasion, highlighting the broader biological significance of sialylation.[41,42] The phenomenon of hypersialylation in cancer cells, resulting from increased metabolic flux of sialic acids and dysregulated enzyme expression, seems to align well with the investigation into transferrin sialylation reported herein. This relationship is particularly relevant, considering that alterations in sialic acid content on transferrin impact its primary function as an iron carrier with potential consequences in cellular management of oxidative stress associated with cancer or ferroptosis.[43]

As far as we know, prior to this and our other recent work,[17,39] there was only one study addressing the possible effects of hTf sialic acid content on metal binding.[44] This study showed a preference of iron for the N-site in hTf, with similar binding affinities observed for both native and asialo forms. The lack of significant differences was attributed to the inherently high affinity of iron for hTf and the relatively low sensitivity of the HPLC/ICP-MS method.

Experimental

Chemicals and instrumentation

The following chemicals were used in this study without further purification: hydrochloric acid, HCl (37%, CAS 7647-01-0, Carlo Erba, cat. no. 403871, lot no. V3A465153A), nitrilotriacetic acid trisodium salt, Na_3NTA (≥98%, CAS 5064-31-3, Sigma, cat. no. N-0253, lot. no. 023K0126), sodium hydroxide, NaOH (≥98%, CAS 1310-73-2, Kemika, cat. no. 1452506), iron (III) chloride, $FeCl_3$ (≥98%, CAS 7705-08-0, Riedel-de Haën, cat. no. 231-729-4, lot no. 50250), piperazine-*N*,*N*′-bis(2-ethanesulfonic acid) dipotassium salt, PIPES (≥97%, CAS 108321-27-3, AMRESCO, cat. no. E912-500G, lot no. 0795C478), 2-(*N*-morpholino) ethanesulfonic acid hydrate, MES (≥99.5%, CAS 1266615-59-1, Sigma-Aldrich, cat. no M8250-1006, lot no. 021M5406), potassium chloride, KCl (≥99.5%, CAS 7447-40-7, Sigma-Aldrich, cat. no. 60128-2506-F, lot no. BCCF7782), 10 000 ppm iron ICP standard in 5% HNO_3(aq) (9992 ± 30 μg mL^{-1}, Inorganic Ventures, cat. no. CGFE10, lot no. P2-FE676240), and pISep Buffer Kit (CryoBioPhysica, cat. no. 20055). Human serum transferrin was purchased from Sigma-Aldrich, cat. no. T2036, lot no. SLCF3538. Water used for the experiments was double distilled in an all-glass apparatus.

The following instrumentation and consumables were used in this study: UV-Vis spectrophotometer (Varian Cary 50 Bio with UV Scan application software, version: 3.00), ICP-MS instrument (Agilent 7900), titrator T70 (Mettler Toledo with LabX™ Titration Software, version 2.62), multimode microplate reader (Tecan Spark M10), pipetting robot (Opentrons OT-2), ÄKTA Purifier 10 FPLC system (GE Healthcare), SOURCE™ 15Q 4.6/100 PE anion exchange chromatographic column (Cytiva, cat. no. 17-5181-01), immobilized SialEXO® microspin columns (Genovis, cat. no. G1-SM6-050), Amicon® Ultra centrifugal filters (0.5 mL, MWCO 30 K, Merck Millipore, cat. no. UFC503096), and 96-well microplates (black, flat bottom, Greiner, cat. no. 655097).

Desialylated apo-transferrin (Tf−S) was prepared according to the modified SialEXO protocol,[45] starting from a solution of native hTf (Tf+S) in 20 mM TRIS buffer, pH 6.8, γ = 2.5 mg mL^{-1}. For desialylation, 800 μL of this solution was added to SialEXO® columns containing the enzyme and the mixture

was incubated at 25 °C for 48 hours. The protein was then recovered by centrifugation, leaving the enzyme beads in the column, so that the process could be repeated with a new transferrin solution. The initial evaluation of the desialylation process was performed by FPLC.[39,46] Detailed glycan profiling was carried out using UHPLC *N*-glycan analysis. Further details on the preparation of Tf–S and the subsequent analyses can be found in the ESI (section 2).†

Titration experiments

For the titration experiments, buffer solutions (25 mM PIPES, 0.2 M KCl, 0.01 M K_2CO_3) were prepared by dissolving exact amounts of solid substances in volumetric flasks, followed by a short ultrasonic treatment and careful pH adjustment. The transferrin solutions were then prepared by dissolving transferrin in these buffers, readjusting the pH as necessary. The protein concentration was determined spectrophotometrically at λ = 280 nm. The molar absorption coefficient for Tf+S solutions was redetermined using the modified Edelhoch method.[47] The obtained value of $\varepsilon_{280\ nm}$ = 84.4 ± 0.8 × 10^3 M^{-1} cm^{-1} agrees with our previous results ($\varepsilon_{280\ nm}$ = 84.8 ± 0.2 × 10^3 M^{-1} cm^{-1})[39] as well as literature values ($\varepsilon_{280\ nm}$ = 84.0 ± 0.2 × 10^3 M^{-1} cm^{-1}).[48] The molar absorption coefficient for Tf–S solutions was $\varepsilon_{280\ nm}$ = 88.2 ± 0.2 × 10^3 M^{-1} cm^{-1}, as reported in our previous study.[39]

Buffer solutions containing NTA chelator were prepared by the addition of a standardized NTA stock solution (c = 0.4703 M) to the buffer stock solutions.[31] Excess NTA was present in all working solutions to ensure iron solubility and maintain the appropriate titration regime (see later). The FeNTA solutions used for iron loading were prepared by diluting a concentrated FeNTA stock solution (c_{NTA} = 0.3043 M, $c_{Fe(III)}$ = 0.1505 M, pH = 2.23) in a suitable buffer and then carefully adjusting the pH. The final FeNTA concentration was determined spectrophotometrically at λ = 260 nm ($\varepsilon_{260\ nm}$ = 5.93 × 10^3 M^{-1} cm^{-1}), as reported in our previous study.[31] For the titration experiments, all samples were prepared using the OT-2 liquid handling robot. The final working solutions were first transferred to microcentrifuge tubes for incubation and then to 96-well microplates for fluorescence measurements, with samples randomly placed in the wells to minimize position effects and ensure unbiased analysis. A detailed description of all experimental procedures can be found in the ESI.†

Fluorescence and absorbance measurements

Single-wavelength fluorescence intensity and absorbance spectra were measured in UV-Vis-transparent 96-well microplates (Greiner, cat. no. 655097) using a Tecan Spark M10 multimode microplate reader. Absorbance spectra was collected from 200 to 1000 nm with 1 nm increments, and fluorescence was measured at an excitation wavelength of 280 nm and an emission wavelength of 335 nm, utilizing a custom optical filter for excitation (bandwidth 15 nm, Tecan cat. no. 30092080). The position of the optical element along the vertical axis (z-position) was optimized for each microplate to ensure consistent fluorescence intensity readings across different z-positions. Full details on the instrumental measurements are given in the ESI (sections 4 and 5).†

The experimental design maintained a constant protein concentration in all measured samples to minimize the variability of the fluorescence signal due to the Inner Filter Effect (IFE), which can mainly be attributed to protein absorbance at λ = 280 nm. Despite the constant transferrin concentration, variations in IFE may result in measurement errors due to differences in the molar absorbance coefficients of iron-containing transferrin forms and due to the spectral contribution of FeNTA.[31,48] Therefore, special care was taken to account for IFE artifacts, considering that the relative error in recorded fluorescence intensity is about 8% at an absorbance of A = 0.06, increasing further to 12% at A = 0.1 and 38% at A = 0.3.[49,50] In our experiments, the maximum absorbance values were ≈0.33 at 280 nm (excitation) and ≈0.12 at 335 nm (emission).

IFE corrections were performed using the recently developed ZINFE method that takes advantage of the variable z-position of the optical element. The ZINFE correction is specifically suited for measurements in microplates since it requires no absorbance measurements.[51] To evaluate the performance of the ZINFE method under the experimental conditions of this study, fluorescence measurements were adjusted using the established technique described by Lakowicz as a reference standard.[52] Both correction procedures are detailed in the ESI (subsection 5.1).†

Binding model and data fitting

The dependence of the measured fluorescence on the concentration of added FeNTA was modelled according to the binding polynomial for two iron binding sites of hTf. The binding polynomial theory provides a general statistical thermodynamic framework for studying ligand binding to macromolecules. The modelling procedure consisted of the following steps: (i) define the binding polynomial for two binding sites; (ii) calculate the total concentration of the protein and iron(III) for each experimental point; (iii) solve analytically the mass conservation equation for iron(III) for each experimental point, assuming certain values of the macroscopic association constants; (iv) calculate the concentration of the different complexes for each experimental point, assuming certain values for the association constants; (v) calculate the expected signal, assuming certain values for the molar fluorescence of the contributing species, which can be floating parameters in the nonlinear least squares analysis; and (vi) obtain the optimal set of macroscopic association constants that reproduce the experimental data using an iterative method.[53]

The interaction between free iron and transferrin, characterized by the equilibrium constants K_{1m} and K_{2m}, can be expressed as follows (charges were omitted for simplicity):

$$\mathrm{Fe} + \mathrm{apoTf} \rightleftarrows \mathrm{FeTf} \quad (1)$$

$$\mathrm{Fe} + \mathrm{FeTf} \rightleftarrows \mathrm{Fe_2Tf} \quad (2)$$

The thermodynamic equilibrium constants K_{1m} and K_{2m} are then defined as:

$$K_{1m} = \frac{[FeTf]}{[Fe][apoTf]} \quad (3)$$

$$K_{2m} = \frac{[Fe_2Tf]}{[Fe][FeTf]} \quad (4)$$

It follows that the value of [X] can be determined from the cubic equation:

$$p[X]^3 + q[X]^3 + r[X] - X_t = 0 \quad (5)$$

where [X] is the equilibrium free iron concentration, and the coefficients p, q and r are given as:

$$p = K_{1m}K_{2m} \quad (6)$$

$$q = K_{1m}(2K_{2m}nP_t - K_{2m}X_t + 1) \quad (7)$$

$$r = K_{1m}(nP_t - X_t) + 1 \quad (8)$$

The values of P_t and X_t are the bulk concentrations of the protein and iron, respectively, and n is the average number of binding sites per protein molecule.

The relative concentrations of the apoTf, FeTf and Fe_2Tf species for each data point were calculated[53,54] as:

$$f(apoTf) = \frac{n}{1 + K_{1m}[X] + K_{1m}K_{2m}[X]^2} \quad (9)$$

$$f(FeTf) = \frac{nK_{1m}[X]}{1 + K_{1m}[X] + K_{1m}K_{2m}[X]^2} \quad (10)$$

$$f(Fe_2Tf) = \frac{nK_{1m}K_{2m}[X]^2}{1 + K_{1m}[X] + K_{1m}K_{2m}[X]^2} \quad (11)$$

where the sum of all fractions is equal to n, corresponding to a 100% of bulk active protein concentration.

The measured fluorescence values were normalized as $F_{norm} = F_x/F_{apo}$, where F_{norm} is the normalized fluorescence, F_x is the measured fluorescence for the point x in the data set and F_{apo} is the measured fluorescence of the apo-transferrin without added iron. This allowed the use of relative molar fluorescence values for the calculation of total normalized relative fluorescence using relative concentrations of the apoTf, FeTf and Fe_2Tf species. The total normalized relative fluorescence for each data point F_{calc} corresponding to the model parameters was calculated as:

$$F_{calc} = f(apoTf) + (s + (1 - s)t)f(FeTf) + sf(Fe_2Tf) \quad (12)$$

where s corresponds to the relative fluorescence of Fe_2Tf *vs.* apoTf and t corresponds to relative contribution of individual binding site to the total fluorescence quenching. The values of $s \approx 0.2$ and $t = 0.5$ were used for all data sets, corresponding to the relative fluorescence of apoTf : FeTf : Fe_2Tf = 1.0 : 0.6 : 0.2.[55]

According to Jarmoskaite *et al.*, two steps are required for equilibrium binding measurements: (i) varying the incubation time to test for equilibration, and (ii) controlling for titration artifacts that can arise when the concentration of the constant limiting component is too high relative to the dissociation constant (K_D).[56] In our experiments, all working solutions were equilibrated at 25 °C for a period of ≥1 day before measurement. No further change in the fluorescence signal was observed with longer incubation times, which indicates that the proportion of the formed complex does not change further over time, thus ensuring that equilibrium has been reached. It is known that the kinetics of iron(III) uptake is strongly dependent on the type of chelator used. In the presence of the bicarbonate anion, the reaction with the FeNTA chelator shows a biphasic character and very fast kinetics, with the slower phase being completed in about 10 seconds (for c(hTf) ≈ 10^{-5} M, c(FeNTA) ≈ 10^{-4} M).[28] This expected reaction time is significantly shorter than the incubation time we used. In all titrations, an excess of the competing ligand (NTA) was present in the solution to quench the apparent binding constants and ensure an appropriate concentration regime.

The value of s corresponding to the relative fluorescence of Fe_2Tf was determined in a separate experiment without excess NTA, corresponding to the titration regime where essentially all added Fe is depleted from solution due to binding to hTf, until there is no free hTf left and a break in the titration curve can be observed.[56] Consequently, the values of the relative fluorescence of Fe_2Tf obtained in the titration regime (s = 0.174 for Tf+S and s = 0.183 for Tf–S) were used for fitting the titration data.

The obtained macroscopic binding constants K_{1m} and K_{2m} are apparent constants that correspond to the exchange of iron from the FeNTA complex to transferrin. For the calculation of the conditional thermodynamic binding constants from the apparent binding constants, the equilibria for the FeNTA complex must be considered.[57] The pH-specific conditional thermodynamic binding constants K'_{1m} and K'_{2m} were calculated from the obtained values of K_{1m} and K_{2m} alongside the pH-dependent conditional constant K'_{110} which characterizes the interaction between iron(III) and NTA:

$$\log(K'_{1m}) = \log(K_{1m}) + \log(K'_{110}) \quad (13)$$

$$\log(K'_{2m}) = \log(K_{2m}) + \log(K'_{110}) \quad (14)$$

For additional details on the calculation of the binding constants and data fitting, see ESI, section 7.†

Statistical considerations

All results are expressed as means of at least 3 replicate measurements, with standard deviations in parentheses. The statistical significance of the differences between the native and desialylated protein for each pH value was evaluated using the Satterthwaite's approximate t-test, a method in the Behrens-Welch family based on the more robust t-statistic with approximate degrees of freedom.[58] All values of $p \leq 0.05$ were considered statistically significant. Further details on the statistical analyses can be found in the ESI, section 8.†

Uncertainties in fitting parameters were obtained using the "jackknife" procedure by omitting a data point one by one from the calculation of the RSS and fitting all remaining points to obtain a new set of parameters.[59] The standard devi-

ations of the parameters were calculated as described in the ESI, subsection 7.3.† A custom VBA routine was written for automatic application of this procedure to all data sets.

Results and discussion

Iron binding at normal serum pH

The addition of FeNTA to the solution of apoTf leads to a decrease in the observed fluorescence due to the quenching of the intrinsic protein fluorescence upon binding of the paramagnetic Fe(III) ion.[55] The decrease in fluorescence is proportional to the amount of iron-containing transferrin and thus allows the calculation of the apparent binding constants K_{1m} and K_{2m} according to the binding model (eqn (1)–(11)). A typical titration experiment and the calculated fluorescence, F_{calc}, obtained by fitting the observed normalized fluorescence, F_{norm}, using the Solver tool in Microsoft Excel are shown in Fig. 2. Table 1 shows the calculated binding constants for Tf+S and Tf–S at different pH levels. Additionally, data for all titrations can be found in the ESI, Fig. S7–S40.†

The conditional thermodynamic constants for the binding of the first and second iron(III) ion determined at pH = 7.4 agree reasonably well with the earlier studies by Aisen *et al.* and Martin *et al.*[37,60] This indicates the validity of the model and provides a basis for comparison with literature data and further comparison of Tf+S and Tf–S. To compare the results obtained at different solution HCO_3^- concentrations, the literature values were corrected by adding $\log(10\ M/[HCO_3^-])$ to the values of $\log(K'_{1m})$ and $\log(K'_{2m})$, where $[HCO_3^-] = 10$ mM (in all experiments).[60,61] As noted by Harris and Pecoraro, this correction only applies at pH = 7.4, because all equilibria involved are pH-dependent.[61]

Protein sialic acid content appears to influence iron binding at normal human serum pH, with $\log(K'_{1m})$ and $\log(K'_{2m})$ values for desialylated transferrin, Tf–S, being approximately 0.5 log units higher, corresponding to an approximately 3-fold increase in iron binding affinity for both sites. This corresponds to a change in free energy of about $\Delta\Delta_r G^\circ_1$+S/ − S ≈ $\Delta\Delta_r G^\circ_2$+S/ − S ≈ −3 kJ mol^{-1} for binding of the first and second iron ion, respectively. Furthermore, at normal human serum pH, the two binding sites appear to have low positive cooperativity, *i.e.* $K_{1m} < K_{2m}$, for both Tf+S and Tf–S.

Based on the considerations of Thordarson[54] the extent of cooperativity in binding can be quantified using the interaction parameter α, which is calculated as follows:

$$\alpha = \frac{4K_{2m}}{K_{1m}} \quad (15)$$

Positive cooperativity is indicated by $\alpha > 1$, negative cooperativity by $\alpha < 1$ and non-cooperative binding by $\alpha = 1$. This corresponds to the parameter ρ_2 in the work of Freire *et al.*,[53] who equate the value of $\alpha = \rho_2$ with a cooperativity association constant κ, which reflects the energy loss or gain due to simultaneous binding of the ligand to both binding sites.

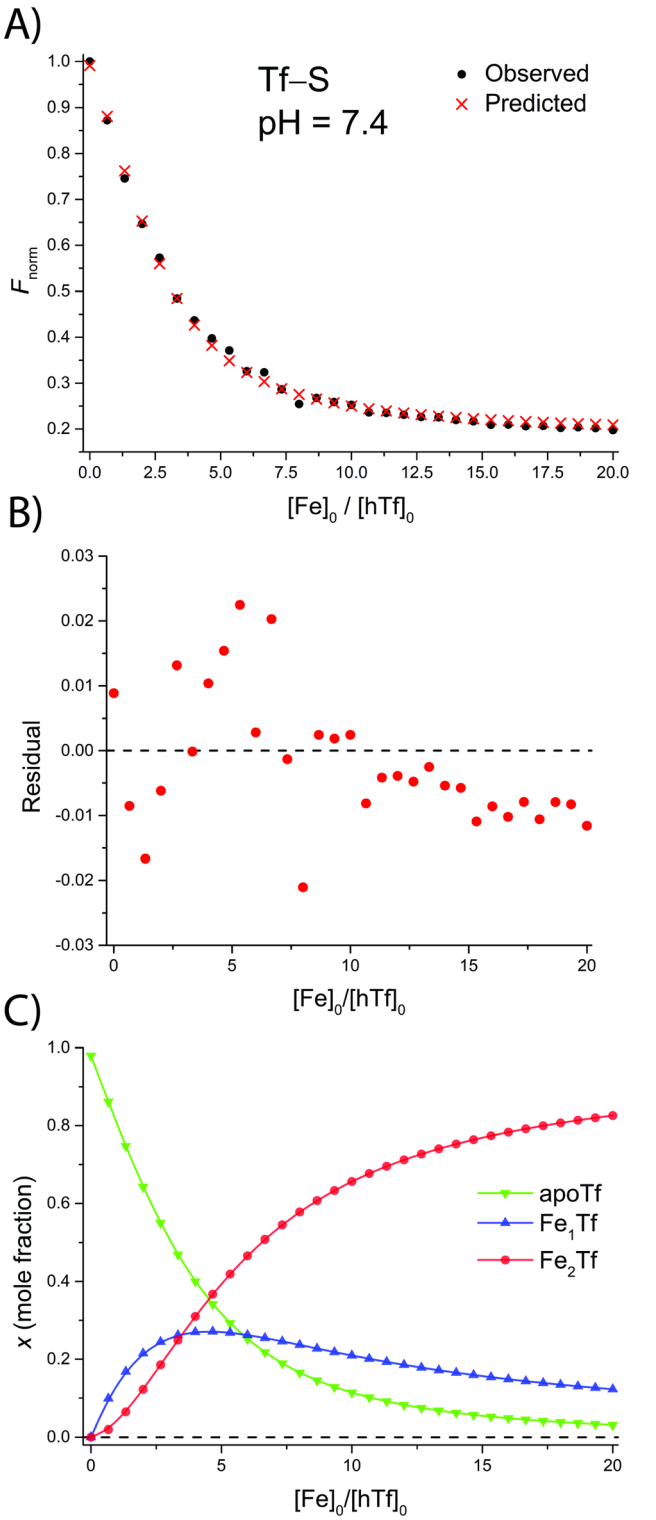

Fig. 2 A typical spectrofluorometric titration of human serum transferrin with FeNTA: $[Tf]_0$ = 3.84 μM, [PIPES] = 25 mM, [KCl] = 0.2 M, pH = 6.5, 25 °C. The parameters determined with the Solver tool in Microsoft Excel to calculate F_{calc} defined in eqn (12) are: $\log(K_{1m})$ = 5.886 ± 0.026, $\log(R)$ = 1.175 ± 0.019, R^2 = 0.9934. (A): Measured normalized fluorescence (F_{obs}) and calculated normalized fluorescence (F_{calc}); (B): residuals of fit calculated as $F_{calc} - F_{obs}$; (C): transferrin speciation according to eqn (9)–(11).

Table 1 Conditional macroscopic thermodynamic equilibrium constants for the binding of iron to human serum transferrin, determined under the following conditions: T = 25 °C, [PIPES] = 25 mM, [HCO^{3-}] = 10 mM, and [KCl] = 0.2 M. The values are expressed as means obtained from 3 replicate measurements (except the literature values at pH = 7.4), with standard deviations in parentheses. A full overview of the results obtained by fitting the fluorescence titration data is given in the ESI, section 5.† The literature values at pH = 7.4 were corrected by adding log(10 M/c) to the reported values of log(K'_{1m}) and log(K'_{2m}), where c = [HCO^{3-}] reported in the respective study. It is important to note that the literature values presented here were determined under different conditions and are given for reference purposes only

	Native apo-transferrin (Tf+S), IS = 127.79,[a] pI = 5.4				Desialylated apo-transferrin (Tf–S), IS = 1.51, pI = 6.8			
pH	log(K'_{1m})		log(K'_{2m})		log(K'_{1m})		log(K'_{2m})	
7.4	21.510	(0.019)	21.743	(0.013)	22.011	(0.027)	22.271	(0.013)
	22.5	(0.1)[b]	21.3	(0.1)[b]				
	22.3	(0.1)[c]	21.7	(0.1)[c]				
	23.22	(0.15)[d]	21.06	(0.12)[d]	24.06	(0.23)[d]	22.31	(0.15)[d]
6.8[e]	15.302	(0.010)	24.833	(0.017)	15.407	(0.043)	24.863	(0.046)
6.5	20.589	(0.033)	19.414	(0.015)	20.791	(0.033)	20.657	(0.014)
6.2	19.915	(0.065)	18.395	(0.027)	20.233	(0.161)[f]	18.841	(0.056)[f]
5.9	18.937	(0.016)	17.396	(0.012)	19.933	(0.050)	18.369	(0.015)

[a] IS is the index of sialylation defined as: $IS = \sum_{i=1}^{n} f_i \cdot s_i$. n represents the N-glycan fraction number, f_i denotes the percentage content of the specific N-glycan fraction, and s_i indicates the count of sialic acids within the structure of the corresponding N-glycan fraction.[39] [b] Obtained by Aisen *et al.* for native hTf (Tf+S) by equilibrium dialysis at ambient $p(CO_2) = 3.6 \times 10^4$ atm, corresponding to the concentration of [HCO^{3-}] = 0.14 mM.[37] The original values of the conditional thermodynamic constants were subsequently recalculated and corrected by Martin *et al.*[60] [c] Obtained by Martin *et al.* for native hTf (Tf+S) by UV/Vis spectroscopy and [HCO^{3-}] = 5 mM.[60] [d] Values obtained from ITC data for the reaction of FeNTA with apoTf at 25 °C in 0.1 M HEPES, pH 7.4, and [HCO^{3-}] = 25 mM. Data were analysed using a model for two non-identical binding sites.[17] [e] At pH = 6.8 we observed significant cooperative binding (*i.e.*, $K'_{1m} \ll K'_{2m}$) that can complicate the accurate determination of equilibrium constants.[63] For clarity, these results were omitted from Fig. 2–5 and discussed separately (see text). [f] Omitting a significant single-point outlier, the adjusted values become log(K'_{1m}) = 20.216 (0.017), log(K'_{2m}) = 18.837 (0.014).

Consequently, $\alpha > 1$ in a 2 : 1 binding system corresponding to two iron binding sites of hTf indicates a preference for the formation of a 2 : 1 complex over a 1 : 1 complex, *i.e.* for equivalent degrees of saturation, the concentration of single liganded species is lower than in the case of independent binding.

The observed low positive cooperativity at pH 7.4 is consistent with the earlier recalculation of binding constants by Freire *et al.* using digitally extracted ITC titration data for hTf published by Lin *et al.*[34] They also found a cooperative effect of α = 2.2 (expressed as the equivalent parameter ρ_2), corresponding to a cooperative Gibbs energy of $\Delta_r G^\circ_{coop.} \approx -2\,kJ\,mol^{-1}$.[53] Our results show slightly higher values for α, corresponding to Gibbs energies of $\Delta_r G^\circ_{coop.} \approx -4.8\,kJ\,mol^{-1}$ for Tf+S and $\Delta_r G^\circ_{coop.} \approx -4.9\,kJ\,mol^{-1}$ for Tf–S. Very similar values for Tf+S and Tf–S indicate that sialylation does not appear to affect the binding cooperativity at pH = 7.4 (p = 0.126, Table S6, ESI†).

On the other hand, Aisen *et al.*[37] and subsequently Martin *et al.*[60] reported non-cooperative binding with values corresponding to log(K'_{1m}) and log(K'_{2m}), listed in Table 1 for reference. These values differ by more than 0.6 units, which is the expected statistical factor for binding to a two-sited protein with equal and independent binding sites (*i.e.*, α = 1 and $K'_{1m}/K'_{2m} = 4 \approx 10^{0.6}$).[37] Methodological differences, such as buffer compositions and ionic strengths, between our study and those of Aisen *et al.* and Martin *et al.*, may account for these discrepancies, highlighting the need for careful consideration of experimental conditions.

The results obtained by spectrofluorometric titrations in this study are also in some contrast to our results for the reaction of hTf with FeNTA obtained by ITC.[17] These showed a difference of about two orders of magnitude in the values corresponding to the conditional thermodynamic constants log(K'_{1m}) and log(K'_{2m}), indicating sequential binding. In addition, desialylation was found to increase the binding of the first iron(III) ion by about 10-fold, while the effect on the binding of the second iron(III) ion was about 20-fold, which is much higher than observed in this study.

The differences in the binding constants observed between the fluorometric and ITC methods can be attributed, at least in part, to differences in the ionic strength and buffer composition of the samples. The fluorometric experiments reported here used solutions containing 0.2 M KCl and PIPES buffer, as opposed to the HEPES buffer used in the previous ITC study. This observation is consistent with the findings of Abdizadeh *et al.*,[62] who showed that variations in salt concentration significantly affect the dynamics and conformation of transferrin, which in turn can affect its iron-binding affinity.

Importantly, our two studies both confirm the increased iron binding affinity for desialylated hTf. It seems reasonable to attribute the observed differences to the different experimental techniques and conditions. The results presented in this work were obtained under conditions with an excess of competing ligand (NTA) and long incubation time. On the other hand, the ITC experiments were performed by incremental addition of reactant aliquots and measuring the resulting heat change immediately after addition, which emphasizes the kinetic aspects of the interaction.

Therefore, under the conditions of the spectrofluorimetric titrations reported here, additional site-exchange reactions mediated by the competing ligand that occur at longer incubation times may be reflected in the results. Such observations

are consistent with previous studies that have shown that iron binding site preference is determined by kinetic as well as thermodynamic factors.[13,34,37]

The pH-dependence of iron binding

A significant effect of sialylation can be observed on the pH-dependence of iron binding, as can be seen from the decreasing macroscopic binding constants K'_{1m} and K'_{2m} with decreasing pH for both Tf+S and Tf–S (Fig. 3). The shift in pH from 7.4 to 5.9 results in a change in free energy of approximately $\Delta\Delta_r G_1^\circ \mathrm{pH} = 14.7\ \mathrm{kJ\ mol^{-1}}$ for the binding of the first iron cation to Tf+S and $\Delta\Delta_r G_2^\circ \mathrm{pH} = 24.8\ \mathrm{kJ\ mol^{-1}}$ for the second, while for Tf–S the corresponding changes are $\Delta\Delta_r G_1^\circ \mathrm{pH} = 11.9\ \mathrm{kJ\ mol^{-1}}$ and $\Delta\Delta_r G_2^\circ \mathrm{pH} = 22.3\ \mathrm{kJ\ mol^{-1}}$. This means that the binding affinity for Tf–S is increased about 10-fold compared to Tf+S at pH 5.9, while the binding affinity for Tf–S is only increased 3-fold compared to Tf+S at pH 7.4.

A mathematical model that can account for the observed pH-dependence of the binding constants was presented by Chasteen and Williams.[13] Briefly, the metal-binding sites are affected by the apparent ionization of the functional groups of the protein according to the following model:

$$f_{sp} = \frac{f_{sp,min}}{1 + \frac{K'_a{}^{n'}}{[H^+]^{n'}}} + \frac{f_{sp,max}}{1 + \frac{[H^+]^{n'}}{K'_a{}^{n'}}} \quad (16)$$

where f_{sp} is the site preference factor defined as $K_{1m}/K_{2m} = K'_{1m}/K'_{2m}$, $f_{sp,\ min}$ is the lower asymptote (at higher pH values), $f_{sp,\ max}$ is the upper asymptote (at lower pH values), K'_a is the apparent acid dissociation constant and n' is the apparent number of protons in the apparent acid–base equilibrium.

In their work, Chasteen and Williams found that the site preference factor of native transferrin is pH-dependent and is

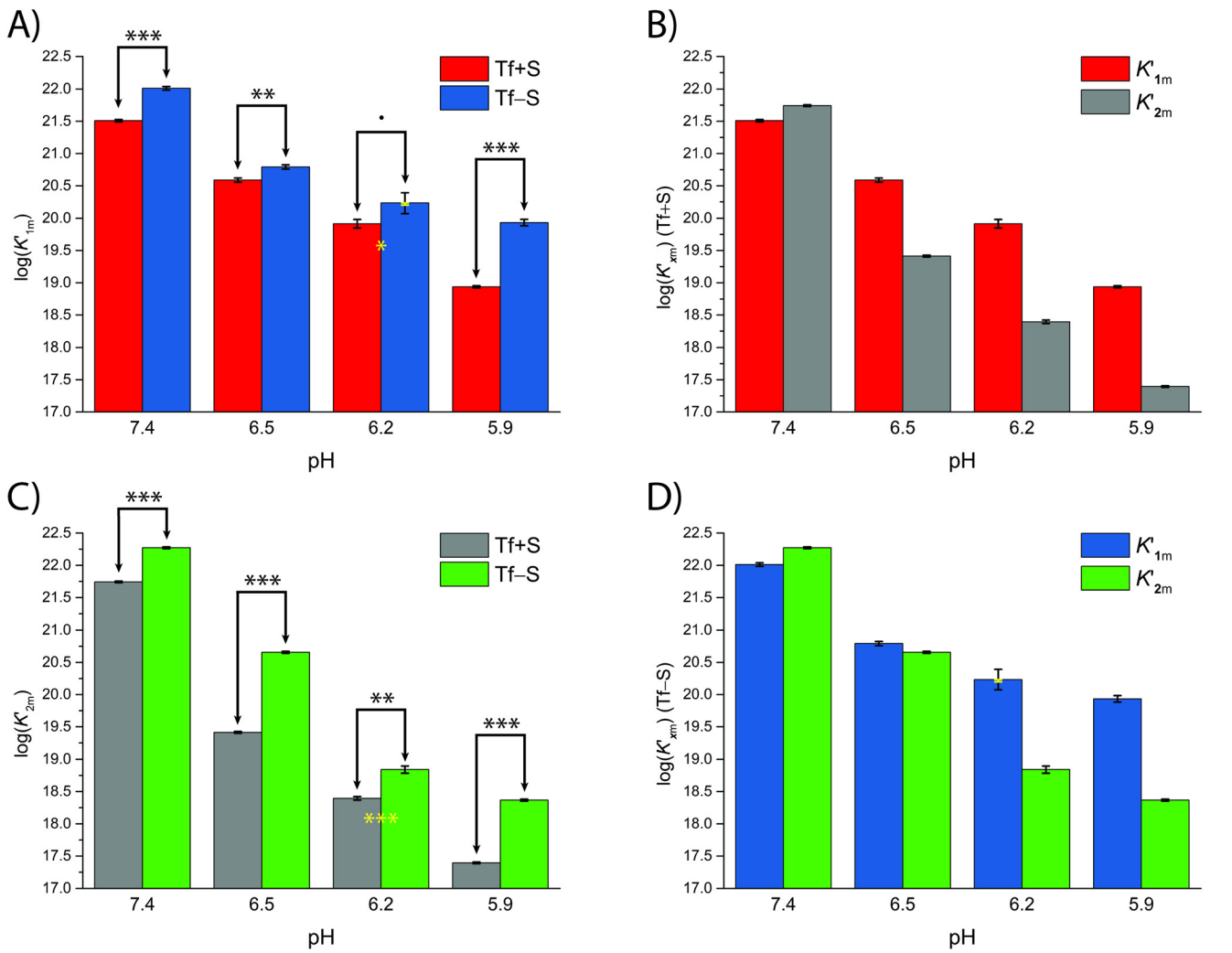

Fig. 3 The pH dependence of the apparent macroscopic binding constants K'_{1m} and K'_{2m} for different pH values at 25 °C (values are listed in Table 1): (A): log(K'_{1m}) values for Tf+S and Tf–S; (B): log(K'_{1m}) and log(K'_{2m}) values for Tf+S; (C): log(K'_{2m}) values for Tf+S and Tf–S; (D): log (K'_{1m}) and log(K'_{2m}) values for Tf–S. The statistical significance of the observed differences in panels (A) and (C) is coded as $p < 0.001$ (***), $p < 0.01$ (**), $p < 0.025$ (*), see Table S5, ESI.† The error bar and the estimated K'_{1m} value, pH = 6.2, Tf–S, highlighted in yellow, were derived by omitting the outlier at the 21st titration point from the analysis.

significantly affected by the presence of 0.5 M NaCl. Below a certain pH, referred to as the transition zone, iron binding shows a preference for the C-terminal site, independent of the presence of NaCl. Above this transition zone, the binding affinities for iron at both sites become similar in the absence of NaCl. However, in the presence of NaCl, the N-terminal site becomes more favourable, with a preference of almost 2 : 1. Interestingly, the pH profiles between pH 6.0 and 6.5 are similar under both conditions.[13]

The f_{sp} values for Tf+S and Tf–S were calculated from log (K'_{1m}) and log(K'_{2m}), which are listed in Table 1. The results of fitting of these f_{sp} values to the model described in eqn (16) using the Solver tool in Microsoft Excel are shown in Fig. 4 and in Table S8, ESI.† The results in Fig. 4 show that native hTf has a slightly higher pK'_a value by about 0.2 units, implying that the site preference shifts to the first site at a less acidic pH compared to Tf–S. In other words, binding to the second site of the desialylated protein appears to be more resistant to an increase in acidity. This altered sensitivity of the second site to changes in solution pH seems to be mediated by the terminal sialic acids of the protein glycan chains.

Considering that hTf undergoes significant conformational changes during the processes of iron uptake and release,[3,64,65] the effect of the relatively large glycan structures (about 6% of hTf mass, see Fig. 1 for illustration) could have a significant impact on these processes. Moreover, the apparent number of protons increases from $n' \approx 4.7$ for Tf+S to $n' \approx 6.4$ for Tf–S, indicating a reduced pH-buffering capacity due to the sialic acid residues in Tf+S. The increase in proton exchange in desialylated transferrin suggests that the removal of sialic acids affects the protein conformation. This conformational change likely exposes more sites that can interact with protons, thus increasing the n' value. The possible effect of the hTf sialylation pattern could therefore be in tuning the stability of the conformational state, which in turn contributes to the stability of the second site and decreases the value of the site-preference factor for Tf–S at pH 6.5 (Fig. 5).

A recent study has highlighted a conformational stabilizing influence of sialic acids on hTf, suggesting a possible link to interactions between anionic sialic acid residues and cationic lysine residues within the N-lobe (*e.g.* Lys206 and Lys296).[66] These lysine residues are involved in a pH-sensitive dilysine interaction that contributes to the stability of the N-site. Notably, the disruption of this dilysine pair has been found to trigger the release of Fe from the N-site.[44,67]

Furthermore, it has recently been shown that changes in the glycan composition of the human insulin receptor can alter long-range allosteric communication between protein residues. Specifically, removal of sialic acid residues resulted in increased flexibility of insulin-binding residues, accompanied by perturbations in glycan–protein interactions. Importantly, the same study has shown that even in the absence of significant changes in protein dynamics at the global level, changes in glycan composition induce perturbations at the local level.[68] Our results seem to confirm a similar effect of sialic acid content on the iron binding dynamics of hTf.

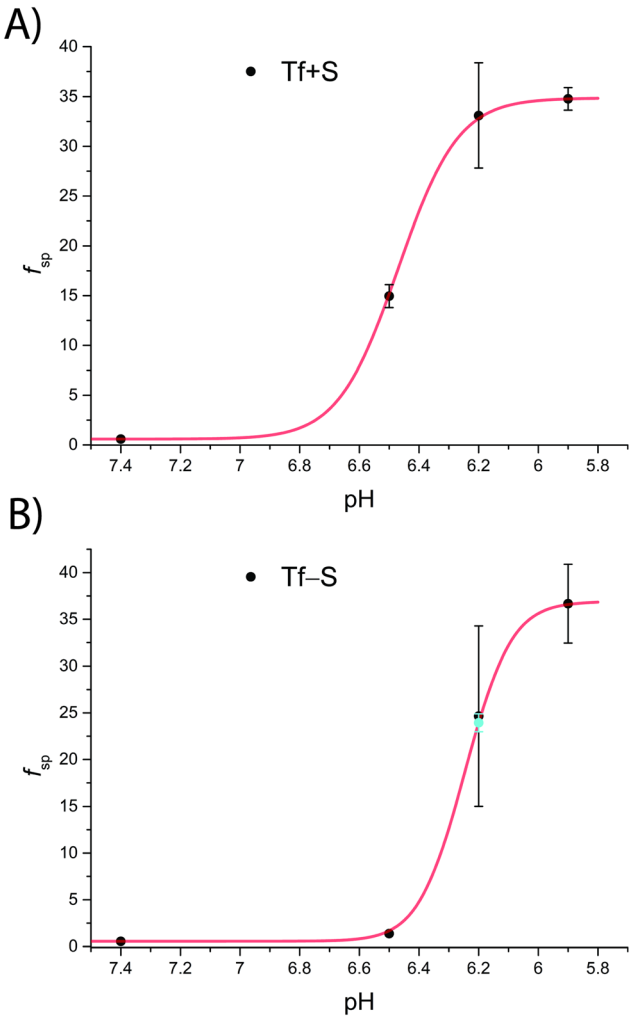

Fig. 4 The pH-dependence of the site preference factor (K_{1m}/K_{2m}) defined by eqn (16) for different pH values at 25 °C. (A): Native hTf (Tf+S): pK'_a = 6.47, $f_{sp,\ min}$ = 0.58, $f_{sp,\ max}$ = 34.8, n' = 4.73, R^2 > 0.999, (B): desialylated hTf (Tf–S): pK'_a = 6.25, $f_{sp,\ min}$ = 0.55, $f_{sp,\ max}$ = 36.9, n' = 6.45, R^2 > 0.999. The values of f_{sp} were calculated from the values of log (K'_{1m}) and log(K'_{2m}) obtained by fitting the titration data (Table 1). The numerical data are shown in Table S7, ESI.† The error bar and the estimated f_{sp} value for Tf–S at pH = 6.2 (highlighted in cyan) result from omitting the outlier at the 21st titration point from the analysis.

Not surprisingly, the observed pH-dependence of the site preference factor translates directly into the fractional population of the intermediate complex at half saturation, F(FeTf), defined[53] as:

$$F(\mathrm{FeTf}) = \frac{K_{1m}}{2\sqrt{K_{1m}K_{2m}} + K_{1m}} \quad (19)$$

A reference value of F(FeTf) < 0.3 is observed for pH values close to 7.4 (Fig. 5), which corresponds to positive cooperativity, *i.e.* at equivalent saturation levels, the concentration of each liganded species is lower than for independent binding

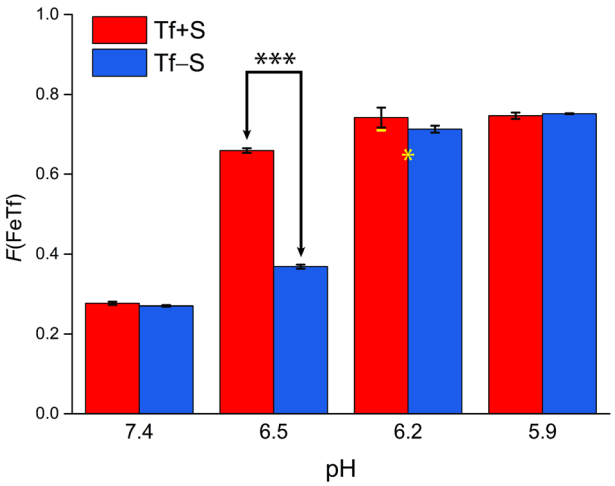

Fig. 5 The pH-dependence of the fractional population of the intermediate complex at half saturation, F(FeTf), for experiments at 25 °C, at different pH values (values are shown in Tables S2 and S3, ESI†). Statistical significance of observed differences is coded as $p < 0.001$ (***), $p < 0.01$ (**), $p < 0.025$ (*), $p < 0.1$ (') (Table S7, ESI†). The error bar and the estimated f_{sp} value for Tf–S at pH = 6.2 (highlighted in yellow) result from omitting the outlier at the 21st titration point from the analysis.

with a corresponding value of F(FeTf) = 0.5. Increasing the pH values led to an increase in the maximum value of F(FeTf) to higher values (above 0.7), corresponding to the values of the apparent acid dissociation constant pK'_a. This means that for both Tf+S and Tf–S there is a much higher preference for FeTf over Fe_2Tf at pH values closer to 5.9, which corresponds to conditions in the endosome, facilitating iron release.

However, the increased affinity of the second site of desialylated hTf maintains the value of F(FeTf) ≈ 0.37 at pH 6.5, followed by a sharp increase to above 0.7 at pH 6.2 and further to about 0.75 at pH 5.9. Fig. 5 shows very similar values of F(FeTf) for Tf+S and Tf–S at endosomal pH, which corresponds to the similar values of the site preference factor as shown in Fig. 4 ($f_{sp} \approx 35$ for Tf+S and $f_{sp} \approx 37$ for Tf–S). These overall differences in f_{sp} values translate to differences in the free energy of $\Delta\Delta_r G^\circ_{sp} \approx 10\,\mathrm{kJ\,mol^{-1}}$ for both Tf+S and Tf–S, which is consistent with the results of Chasteen and Williams, who determined corresponding values of 7–9 kJ mol^{-1} for native hTf (Tf+S) under different experimental conditions (1 mM $NaHCO_3$, pH range 7–9).[13] Adding further context to these values, the absolute magnitude of the average change in free energy due to protein unfolding in water is $\left|\Delta\Delta_r G^\circ_{H_2O}\right| \approx 8.4\,\mathrm{kJ\,mol^{-1}}$ for a single amino acid mutation.[69] This value is comparable to the $\Delta\Delta_r G^\circ_{sp}$ values determined for hTf, suggesting that sialylation as a post-translational modification can have a comparable impact on the stability and function of the protein without altering its primary structure.

Again, these results contrast with our results for the same reaction obtained with ITC, due to the different values of K_{1m} and K_{2m} and the associated different values of f_{sp} and F(FeTf). In particular, the values corresponding to the site preference factor in the ITC study can be calculated as $f_{sp} \approx 170$ for Tf+S and $f_{sp} \approx 60$ for Tf–S. This also resulted in a lower value of F(FeTf) for desialylated protein (F(FeTf) = 0.87 for Tf+S and F(FeTf) = 0.79 for Tf–S), indicating an increased proportion of Fe_2Tf species due to the increased value of K'_{2m}.[17] Regardless of these differences, the general effect of desialylation, namely the increased stability of the second site to changes in pH, appears to be confirmed by both sets of experiments and may be reflected in the increased proportion of Fe_2Tf species for Tf–S observable from the physiological pH of 7.4 to at least pH 6.5.

Physiological significance and other considerations

The observed influence of Tf sialylation may be related to the *in vivo* preference for iron binding to the N-lobe of the protein. In human serum, the average distribution of Tf iron variants was determined as follows: apoTf, 39.2%; Fe_CTf, 11.2%; Fe_NTf, 22.9%; and holoTf (Fe_2Tf), 26.7%.[67] The stabilization of the second binding site and the observed positive cooperativity at normal serum pH seem to be consistent with this distribution. The observed effect of transferrin desialylation could also influence the interaction with its receptors, hTfR_1 and/or hTfR_2. At pH 7.4, hTfR_1 preferentially binds Fe_2Tf, with about 5-fold lower affinity for FeTf species and about 30-fold lower affinity for apoTf.[67] Therefore, the increased preference for Fe_2Tf over FeTf for Tf–S at pH 6.5 may facilitate its binding to hTfR_1. In the presence of the receptor, the rate of iron release from the C-lobe is increased, while the rate of release from the N-lobe is decreased. Furthermore, the interaction with the receptor favours the initial release of iron from the C-lobe at pH 5.6, which is reversed in the absence of hTfR_1.[67]

Molecular dynamics simulations performed at pH 5.6 and 7.4 showed that at the lower, endosomal pH, the cooperative interaction between the two domains of holo-transferrin decreases, facilitating iron release. The authors concluded that the pH-dependent change in hTf dynamics is due to the altered electrostatic potential distribution on the protein surface.[70] This is consistent with our experimental results, where we found a lack of cooperativity at lower pH values. In addition, the ionic strength of the solution could play an important role in altering the electrostatic potential distribution around the protein surface. This in turn could contribute to the energetic pathways required for the protonation of tyrosine residues, a necessary precursor for iron release.[62]

The physiological significance of our results could also lie in understanding the behaviour of hTf in an acidic environment. Tissue acidosis is common in various pathological conditions such as cancer, inflammation, arthritis, stroke, ischemia, and others. Decreased tissue pH is the result of changes in cellular metabolism, often associated with hypoxia and impaired blood supply, leading to increased acid production through glycolysis.[71] For example, in the tumour microenvironment, factors such as deregulated energy metabolism, insufficient perfusion, and uncontrolled proliferation collectively contribute to tissue acidity. Local pH values as low as 5.6 have been recorded in human tumours, with typical values

between 6.4 to 7, which corresponds well to the experimental conditions in this study.[72] As mentioned in the introduction, alterations in transferrin sialylation are also closely associated with various acute and chronic disease states. For example, acute pancreatitis has been shown to be associated with a rapid decrease in hTf sialylation from the first to the second day of illness, which has been shown to be a good prognostic marker.[73]

By demonstrating that Tf–S binds iron much more effectively under acidic conditions, our study suggests a possible mechanism by which iron availability and toxicity could be modulated in ischemic tissues. This modulation could influence the dynamics of the labile iron pool (LIP) and potentially impact the pathophysiological consequences of ischemic events. For example, transferrin-mediated iron transport has recently been shown to play an important role in increasing LIP during ischemia and to contribute to Fenton reaction-mediated lipid peroxidation in the early reperfusion phase of cardiac ischemia/reperfusion injury.[74]

Unexpectedly, we observed a pronounced positive cooperativity for both Tf+S and Tf–S at pH = 6.8, which was not observed at other pH values (Table 1 and Fig. S20–S22 and S35–S37, ESI†). Apparently, the initial binding of an iron ion to apo-transferrin significantly enhances the binding of the subsequent ion, resulting in a persistent scarcity of the monoferric form, as additional iron tends to further saturate the half-saturated monoferric transferrin. This suggests that the second iron ion binding event may dominate and possibly mask the effects of the first binding event, leading to incorrect values of the equilibrium constant.[63] Our observations indicate that the pronounced cooperativity in the experiments at pH = 6.8 is likely due to a particular interplay between pH and ionic strength.

In the context of the high-throughput fluorescence measurements used in this study, a recently developed *z*-position inner filter effect correction method (ZINFE) was successfully used to correct the measured fluorescence in microplates[51] and compared with the commonly used method proposed by Lakowicz.[52] The two IFE correction methods are highly correlated, as can be observed by plotting the results of one correction against the other (Fig. S5 and S6, ESI†). This indicates that both methods are suitable for the range of absorbance values observed in this study. However, the ZINFE method does not require direct measurements of sample absorbance at the excitation and emission wavelengths. As previously reported, it is important to clarify that the high and constant IFE itself does not cause nonlinearity with respect to the fluorescence concentration response; rather, this is caused by the variation of IFE in the samples.[75] To minimize the variation of the primary IFE, the experiments were designed to keep the transferrin concentration constant for all samples in each titration.

Conclusions

The intrinsic fluorescence quenching upon binding of iron to hTf was successfully modelled according to the binding polynomial for two independent iron binding sites. This provided a general solution to obtain both the apparent and conditional thermodynamic equilibrium constants by using only 2 parameters to fit the experimental data. The results obtained at pH = 7.4 for Tf+S were in good agreement with previous benchmark studies, confirming the validity of the model and allowing further measurements in a high-throughput format. Removal of the sialic acid residues resulted in an approximately 3-fold increase in iron binding affinity for both sites of desialylated hTf at pH 7.4. In general, this appears to be consistent with our previous ITC study, but the results reported here seem to emphasize the effects of excess competing ligand and a long incubation time on the obtained results.

A significant effect is also observed in the pH-dependence of iron binding, with differences in the conditional thermodynamic equilibrium constants indicating a higher stability of the second binding site for the desialylated hTf down to pH = 6.5. Such an effect can possibly be attributed to the effects of sialic acid residues on the conformational state of hTf, leading to a tuning of the stability of the second site. This suggests that variations in the sialic acid content of the protein influence the iron binding dynamics of hTf through allosteric interactions. This could explain the distribution of hTf binding sites *in vivo* and also influence binding to the hTf receptor. Beyond the scope of this work, the obtained results could help to establish a correlation between the changes in hTf glycan structure associated with different conditions and the observed changes in iron binding equilibrium. This study demonstrates that desialylated hTf binds iron more efficiently under acidic conditions, highlighting the potential role of hTf in regulating iron availability and toxicity in ischemic tissues.

Furthermore, in this study we have developed an efficient template for the numerical calculation of chemical equilibrium problems using Microsoft Excel. This approach, which is based on the binding polynomial, serves as a basis for a comprehensive and model-independent investigation of binding experiments.[53] The presented spreadsheet-based approach may be a practical addition to the tools available to researchers and educators alike. In our previous work,[31] the distribution of FeNTA species obtained using the Jenkins–Traub algorithm in Excel showed excellent agreement with the species distribution from the HySS software, which uses the Newton–Raphson algorithm to solve mass balance equations with known equilibrium constants.[76] These results outperform those of the original treatment of FeNTA equilibria by Hegenauer *et al.*, which requires an iterative procedure that is difficult to implement in spreadsheet software and is only applicable to solutions with an excess of total NTA over total Fe.[77] However, future studies applied to systems with well-characterized binding constants should further validate the accuracy of the approach.

Author contributions

Tomislav Friganović and Valentina Borko carried out the experiments under the supervision of Tin Weitner. Tin

Weitner created the Excel template that was used for the equilibrium constants. Tomislav Friganović created the Python software utilized for the glycan analysis. All authors contributed to the writing of the manuscript.

Data availability

Data for this paper, including all measurements, fitting results and statistical analyses are available at Zenodo at **https://doi.org/10.5281/zenodo.10881688**.

Conflicts of interest

There are no conflicts to declare.

Acknowledgements

This work was supported by funding from the Croatian Science Foundation grant UIP-2017-05-9537 – Glycosylation as a factor in the iron transport mechanism of human serum transferrin (GlyMech). Valentina Borko was additionally financed by the Croatian Science Foundation grant DOK-2018-09-1042. Additional support was provided by the European Regional Development Fund grants for 'Strengthening of Scientific Research and Innovation Capacities of the Faculty of Pharmacy and Biochemistry at the University of Zagreb' (KK.01.1.1.02.0021), 'Development of methods for production and labelling of glycan standards for molecular diagnostics' (KK.01.1.1.07.0055) and 'Scientific center of excellence for personalized health care' (KK.01.1.1.01.0010).

References

1 J. Parkkinen, L. Von Bonsdorff, F. Ebeling and L. Sahlstedt, *Vox Sang.*, 2002, **83**, 321–326.
2 Y. Yu, L. Jiang, H. Wang, Z. Shen, Q. Cheng, P. Zhang, J. Wang, Q. Wu, X. Fang, L. Duan, S. Wang, K. Wang, P. An, T. Shao, R. T. Chung, S. Zheng, J. Min and F. Wang, *Blood*, 2020, **136**, 726–739.
3 R. Pakdaman and J.-M. E. H. Chahine, *Eur. J. Biochem.*, 1996, **236**, 922–931.
4 P. T. Gomme, K. B. McCann and J. Bertolini, *Drug Discovery Today*, 2005, **10**, 267–273.
5 N. Yang, H. Zhang, M. Wang, Q. Hao and H. Sun, *Sci. Rep.*, 2012, **2**, 999.
6 R. T. A. MacGillivray, S. A. Moore, J. Chen, B. F. Anderson, H. Baker, Y. Luo, M. Bewley, C. A. Smith, M. E. P. Murphy, Y. Wang, A. B. Mason, R. C. Woodworth, G. D. Brayer and E. N. Baker, *Biochemistry*, 1998, **37**, 7919–7928.
7 M. R. Schlabach and G. W. Bates, *J. Biol. Chem.*, 1975, **250**, 2182–2188.
8 N. Kojima and G. W. Bates, *J. Biol. Chem.*, 1981, **256**, 12034–12039.
9 M. Wessling-Resnick, *Crit. Rev. Biochem. Mol. Biol.*, 1999, **34**, 285–314.
10 M. E. Conrad, J. N. Umbreit and E. G. Moore, *Am. J. Med. Sci.*, 1999, **318**, 213.
11 A. H. Schmaier, *Cell Res.*, 2020, **30**, 101–102.
12 J. B. Vincent and S. Love, *Biochim. Biophys. Acta, Gen. Subj.*, 2012, **1820**, 362–378.
13 N. D. Chasteen and J. Williams, *Biochem. J.*, 1981, **193**, 717–727.
14 D. A. Lee and J. M. Goodfellow, *Biophys. J.*, 1998, **74**, 2747–2759.
15 P. Aisen, *Ann. Neurol.*, 1992, **32 Suppl**, S62–S68.
16 C. A. Worthen and C. A. Enns, *Front. Pharmacol.*, 2014, **5**, DOI: **10.3389/fphar.2014.00034**.
17 V. Borko, T. Friganović and T. Weitner, *J. Inorg. Biochem.*, 2023, **244**, 112207.
18 J. Caslavska and W. Thormann, *J. Sep. Sci.*, 2018, **41**, 303–322.
19 G. De Jong and H. G. Van Eijk, *Electrophoresis*, 1988, **9**, 589–598.
20 V. Sanz-Nebot, E. Balaguer, F. Benavente, C. Neusüß and J. Barbosa, *Electrophoresis*, 2007, **28**, 1949–1957.
21 M. Edwards, F. McKenzie, S. O'Callaghan, D. Somerset, P. Woodford, J. Spilsbury, M. Fietz and J. Fletcher, *Prenatal Diagn.*, 2006, **26**, 985–988.
22 G. De Jong, R. Feelders, W. L. Van Noort and H. G. Van Eijk, *Glycoconjugate J.*, 1995, **12**, 219–226.
23 M. Piagnerelli, K. Z. Boudjeltia, V. Nuyens, D. De Backer, F. Su, Z. Wang, J.-L. Vincent and M. Vanhaeverbeek, *Shock*, 2005, **24**, 48–52.
24 O. Gornik, I. Gornik, I. Z. Kolednjak and G. Lauc, *Intern. Med.*, 2011, **50**, 861–869.
25 B.-J. Kim, J. Zhou, B. Martin, O. D. Carlson, S. Maudsley, N. H. Greig, M. P. Mattson, E. E. Ladenheim, J. Wustner, A. Turner, H. Sadeghi and J. M. Egan, *J. Pharmacol. Exp. Ther.*, 2010, **334**, 682–692.
26 M. E. del Castillo Busto, M. Montes-Bayón, E. Blanco-González, J. Meija and A. Sanz-Medel, *Anal. Chem.*, 2005, **77**, 5615–5621.
27 R. Aasa, B. G. Malmström, P. Saltman and T. Vänngaard, *Biochim. Biophys. Acta*, 1963, **75**, 203–222.
28 G. W. Bates and J. Wernicke, *J. Biol. Chem.*, 1971, **246**, 3679–3685.
29 J. O. Jeppsson, H. Kristensson and C. Fimiani, *Clin. Chem.*, 1993, **39**, 2115–2120.
30 A. Levina, A. R. M. Chetcuti and P. A. Lay, *Biomolecules*, 2022, **12**, 1319.
31 V. Borko, T. Friganović and T. Weitner, *Anal. Methods*, 2023, **15**, 6499–6513.
32 D. C. Harris, A. L. Rinehart, D. Hereld, R. W. Schwartz, F. P. Burke and A. P. Salvador, *Biochim. Biophys. Acta, Gen. Subj.*, 1985, **838**, 295–301.
33 N. G. James, C. L. Berger, S. L. Byrne, V. C. Smith, R. T. A. MacGillivray and A. B. Mason, *Biochemistry*, 2007, **46**, 10603–10611.
34 L. N. Lin, A. B. Mason, R. C. Woodworth and J. F. Brandts, *Biochemistry*, 1993, **32**, 9398–9406.

35 L. N. Lin, A. B. Mason, R. C. Woodworth and J. F. Brandts, *Biochemistry*, 1994, **33**, 1881–1888.
36 N. G. James, S. L. Byrne and A. B. Mason, *Biochim. Biophys. Acta, Proteins Proteomics*, 2009, **1794**, 532–540.
37 P. Aisen, A. Leibman and J. Zweier, *J. Biol. Chem.*, 1978, **253**, 1930–1937.
38 T. J. Egan, O. Zak and P. Aisen, *Biochemistry*, 1993, **32**, 8162–8167.
39 T. Friganović, A. Tomašić, T. Šeba, I. Biruš, R. Kerep, V. Borko, D. Šakić, M. Gabričević and T. Weitner, *Heliyon*, 2021, **7**, e08030.
40 Woods Group. (2005–2024) GLYCAM Web. Complex Carbohydrate Research Center, University of Georgia, Athens, GA. (**https://glycam.org**).
41 R. Wen, H. Zhao, D. Zhang, C.-L. Chiu and J. D. Brooks, *Carbohydr. Res.*, 2022, **519**, 108598.
42 G. Murugesan, B. Weigle and P. R. Crocker, *Curr. Opin. Chem. Biol.*, 2021, **62**, 34–42.
43 H. Yan, T. Zou, Q. Tuo, S. Xu, H. Li, A. A. Belaidi and P. Lei, *Signal Transduction Targeted Ther.*, 2021, **6**, 49.
44 M. Hamano Nagaoka and T. Maitani, *Biochim. Biophys. Acta, Gen. Subj.*, 2001, **1526**, 175–182.
45 T. Friganović, V. Borko and T. Weitner, *Maced. Pharm. Bull.*, 2022, **68**, 415–416.
46 T. Friganović, V. Borko, T. Šeba, R. Kerep and T. Weitner, Protocol for pH-gradient chromatofocusing of the native and desialylated human apo-transferrin, *Zenodo*, 2020, DOI: **10.5281/zenodo.4006002**.
47 T. Šeba, T. Friganović and T. Weitner, Protocol for spectrophotometric determination of native and desialylated apo-transferrin molar absorption coefficients, *Zenodo*, 2020, DOI: **10.5281/zenodo.4001959**.
48 N. G. James and A. B. Mason, *Anal. Biochem.*, 2008, **378**, 202–207.
49 A. V. Fonin, A. I. Sulatskaya, I. M. Kuznetsova and K. K. Turoverov, *PLoS One*, 2014, **9**, e103878.
50 M. Kubista, R. Sjöback, S. Eriksson and B. Albinsson, *Analyst*, 1994, **119**, 417–419.
51 T. Weitner, T. Friganović and D. Šakić, *Anal. Chem.*, 2022, **94**, 7107–7114.
52 *Principles of Fluorescence Spectroscopy*, ed. J. R. Lakowicz, Springer, US, Boston, MA, 2006, pp. 27–61.
53 E. Freire, A. Schön and A. Velazquez-Campoy, in *Methods in Enzymology*, Elsevier, 2009, vol. 455, pp. 127–155.
54 P. Thordarson, *Chem. Soc. Rev.*, 2011, **40**, 1305–1323.
55 S. L. Byrne and A. B. Mason, *JBIC, J. Biol. Inorg. Chem.*, 2009, **14**, 771–781.
56 I. Jarmoskaite, I. AlSadhan, P. P. Vaidyanathan and D. Herschlag, *eLife*, 2020, **9**, e57264.
57 R. J. Motekaitis and A. E. Martell, *J. Coord. Chem.*, 1994, **31**, 67–78.
58 P. Armitage, G. Berry and J. N. S. Matthews, *Statistical Methods in Medical Research*, Wiley, 1st edn, 2002.
59 D. C. Harris, *J. Chem. Educ.*, 1998, **75**, 119.
60 R. B. Martin, J. Savory, S. Brown, R. L. Bertholf and M. R. Wills, *Clin. Chem.*, 1987, **33**, 405–407.
61 W. R. Harris and V. L. Pecoraro, *Biochemistry*, 1983, **22**, 292–299.
62 H. Abdizadeh, A. R. Atilgan and C. Atilgan, *J. Phys. Chem. B*, 2017, **121**, 4778–4789.
63 J. Peacock and J. B. Jaynes, *Biochim. Biophys. Acta, Gen. Subj.*, 2017, **1861**, 2789–2801.
64 S. L. Byrne, A. N. Steere, N. D. Chasteen and A. B. Mason, *Biochemistry*, 2010, **49**, 4200–4207.
65 M. Hirose, *Biosci., Biotechnol., Biochem.*, 2000, **64**, 1328–1336.
66 G. Li, A. Phetsanthad, M. Ma, Q. Yu, A. Nair, Z. Zheng, F. Ma, K. DeLaney, S. Hong and L. Li, *Anal. Chem.*, 2022, **94**, 2142–2153.
67 A. M. N. Silva, T. Moniz, B. De Castro and M. Rangel, *Coord. Chem. Rev.*, 2021, **449**, 214186.
68 R. M. Rao, H. Wong, M. Dauchez and S. Baud, *Glycobiology*, 2021, cwab049.
69 R. Nikam, A. Kulandaisamy, K. Harini, D. Sharma and M. M. Gromiha, *Nucleic Acids Res.*, 2021, **49**, D420–D424.
70 H. Abdizadeh and C. Atilgan, *Phys. Chem. Chem. Phys.*, 2016, **18**, 7916–7926.
71 Y. K. Reshetnyak, A. Moshnikova, O. A. Andreev and D. M. Engelman, *Front. Bioeng. Biotechnol.*, 2020, **8**, 335.
72 E. Boedtkjer and S. F. Pedersen, *Annu. Rev. Physiol.*, 2020, **82**, 103–126.
73 O. Gornik, I. Gornik, V. Gašparović and G. Lauc, *Clin. Biochem.*, 2008, **41**, 504–510.
74 D. Lee, E. Son and Y.-H. Kim, *Free Radical Res.*, 2022, **56**, 713–729.
75 T. Friganović and T. Weitner, *Anal. Chem.*, 2023, **95**, 13036–13045.
76 L. Alderighi, P. Gans, A. Ienco, D. Peters, A. Sabatini and A. Vacca, *Coord. Chem. Rev.*, 1999, **184**, 311–318.
77 J. Hegenauer, P. Saltman and G. Nace, *Biochemistry*, 1979, **18**, 3865–3879.

5.1. RAD 4 - DODATAK

Electronic Supplementary Material (ESI) for Dalton Transactions.

Supplementary information

Protein sialylation affects the pH-dependent binding of ferric ion to human serum transferrin

Tomislav Friganović, Valentina Borko, and Tin Weitner*

Faculty of Pharmacy and Biochemistry, University of Zagreb, Ante Kovačića 1, 10000 Zagreb, Croatia

Corresponding author:
Tin Weitner, PhD
e-mail: tin.weitner@pharma.unizg.hr
tel.: +385 1 6394 452

Contents

1. Preparation and standardization of solutions

1.1. Preparation of working buffer solutions

The working buffer solutions were prepared by dissolving the appropriate amounts of solid substances in volumetric flasks. The flasks were filled with double-distilled water to about 80% of the total volume. The mixtures were briefly placed in an ultrasonic bath (a few minutes) to accelerate dissolution. The pH was then finely adjusted with aqueous HCl and/or NaOH. Water was added until the volume mark on the flask was almost reached, followed by a final pH adjustment. Further drops of water were then added to fill the flasks exactly to the marked line. The flasks were shaken vigorously after each addition of liquid and the pH electrode was always recalibrated before the working solutions were prepared. All working buffer solutions contained: 25 mM PIPES (piperazine-N,N′-bis(2-ethanesulfonic acid) dipotassium salt), 0.2 M KCl and 10 mM K_2CO_3. The pH values of the buffer solutions were adjusted to: 7.4, 6.9, 6.5, 6.2 and 5.9 during buffer preparation (in the volumetric flask).

1.2. Preparation and standardization of FeNTA solutions

The FeNTA stock solution was prepared by stepwise addition of ≈ 0.5 M Na_3NTA(aq) (pH ≈ 8.5) to a ≈ 0.5 M $FeCl_3$ solution (dissolved in 0.05 M HCl) in a molar ratio of 2 : 1. The Na_3NTA solution had previously been standardized by potentiometric titration with a NaOH standard solution to determine its exact concentration (c(Na_3NTA) = 0.4703 M). The pH of the resulting FeNTA stock solution was ≈ 2.2. ICP-MS analysis was performed to verify the exact iron concentration in the FeNTA stock solution.

The iron concentration in the FeNTA stock solution was determined using an Agilent 7900 ICP-MS instrument with an ASX-500 series autosampler and a quadrupole detector. In the first step, a calibration standard stock solution was prepared by diluting a commercially available Fe standard solution (9992 ± 30 µg/mL iron ICP standard in 5% HNO_3(aq), Inorganic Ventures, cat. no. CGFE10, lot no. P2-FE676240) by a factor of 100 in 1% v/v HNO_3. A calibration curve was then established by measurements on six different calibration standard solutions. These solutions were prepared by diluting the stock solution of the working calibration standard. An equal volume of an internal standard (1001 ± 4 µg/mL germanium ICP standard, tr. HNO_3 and HF) was added to each solution. The reference blank contained 1% HNO_3 and the internal standard. Six aliquots of the FeNTA sample were diluted 10,000-fold in 1% HNO_3. For this purpose, 10 µL of the sample was taken and diluted to 100 mL, adding 100 µL of the internal standard to each aliquot.

A nickel skimmer cone, a MicroMist nebulizer and a nickel sample cone were used for the measurements. Argon was used as the carrier gas at a flow rate of 1.2 L/min. Acquisition was performed in "He mode" using a collision cell with helium at 5 mL/min. General-purpose plasma mode and the pulse/analog detector mode were used. Data analysis was performed using MassHunter 4.1 ICP-MS Workstation software. The final iron concentration was calculated as the average of five replicate measurements, excluding one of the six aliquots due to experimental error in dilution. Subsequently, the FeNTA stock solution was divided into aliquots and stored at −20°C until further use. The final FeNTA solution contained: c(Fe) = 0.1505 M, c(NTA) = 0.3043 M with an estimated molar ratio of NTA : Fe = 1 : 2.022.

FeNTA working solutions were prepared by diluting the FeNTA stock solution in the titration buffer (25 mM PIPES, 10 mM K_2CO_3, 0.2 M KCl). pH corrections were performed as required. The FeNTA working solutions were always freshly prepared (immediately before performing the titration experiments). The dilution of the titration buffer by the FeNTA addition and the subsequent pH readjustments was less than 1 part per 1000. In our estimation, this source of error is small compared to

other sources of error in this study. The exact concentration of FeNTA in the working solutions was determined spectrophotometrically, as described in more detail in the following subsection.

1.3. Spectrophotometric determination of FeNTA concentration

The expression of the Beer-Lambert law for the FeNTA solutions (λ = 260 nm) can be written as shown in the Eq. S1:

$$\varepsilon_{\mathrm{NTA(260\ nm)}} c_{\mathrm{NTA}} + \varepsilon_{\mathrm{FeNTA(260\ nm)}} c_{\mathrm{FeNTA}} = \frac{A_{260\ \mathrm{nm}}}{l} \qquad \text{Eq. S1}$$

The spectral signal at λ = 260 nm is the result of the combined contributions of FeNTA and NTA species. NTA denotes species without iron (chelates of different protonation), while FeNTA denotes all chelated species containing iron. It is noteworthy that the molar absorption coefficient of the FeNTA species is about 3 orders of magnitude greater than that of the NTA species.[1] The same FeNTA stock solution was used for all experiments in this study. For this solution, the exact concentrations of both iron(III) and NTA species were determined as described in the previous subsection. Therefore, in all prepared FeNTA working solutions, the Fe : NTA ratio should match the 1 : 2.022 ratio used in the experiments to determine the molar absorption ratio.

The molar absorption coefficient for the FeNTA solution in the working buffer was calculated as $\varepsilon_{260\ \mathrm{nm}} = 5.93 \cdot 10^3\ \mathrm{M^{-1}\ cm^{-1}}$.[1] The molar absorption coefficient for the FeNTA stock solution was determined according to the following procedure. The FeNTA stock solution (c(Fe) = 0.1505 M and c(NTA) = 0.3043 M) was diluted 1000-fold in working buffer solution. To ensure precision and minimize possible pipetting errors due to the considerable volume ratios, each 1000-fold dilution was performed in three consecutive 10-fold dilutions. After each dilution step, vigorous shaking with a vortex mixer (Cole-Parmer, USA) was performed. Spectroscopic measurements were performed in a quartz glass cuvette with a light path length of 1 cm (Hellma, Germany). All spectrophotometric measurements were performed with a Varian Cary 50 Bio UV-Vis spectrophotometer (Varian, Australia). The averaged spectrum was calculated for all twelve replicates within each set. The baseline was determined by calculating the average of six replicate measurements. The final expression for FeNTA concentration is given[1] by Eq. S2:

$$c(\mathrm{FeNTA}) = \frac{\frac{A_{260\ \mathrm{nm}}}{l} - c_{\mathrm{NTA(total)}} \varepsilon_{\mathrm{NTA(260\ nm)}}}{\varepsilon_{\mathrm{FeNTA(260\ nm)}} - \varepsilon_{\mathrm{NTA(260\ nm)}}} \qquad \text{Eq. S2}$$

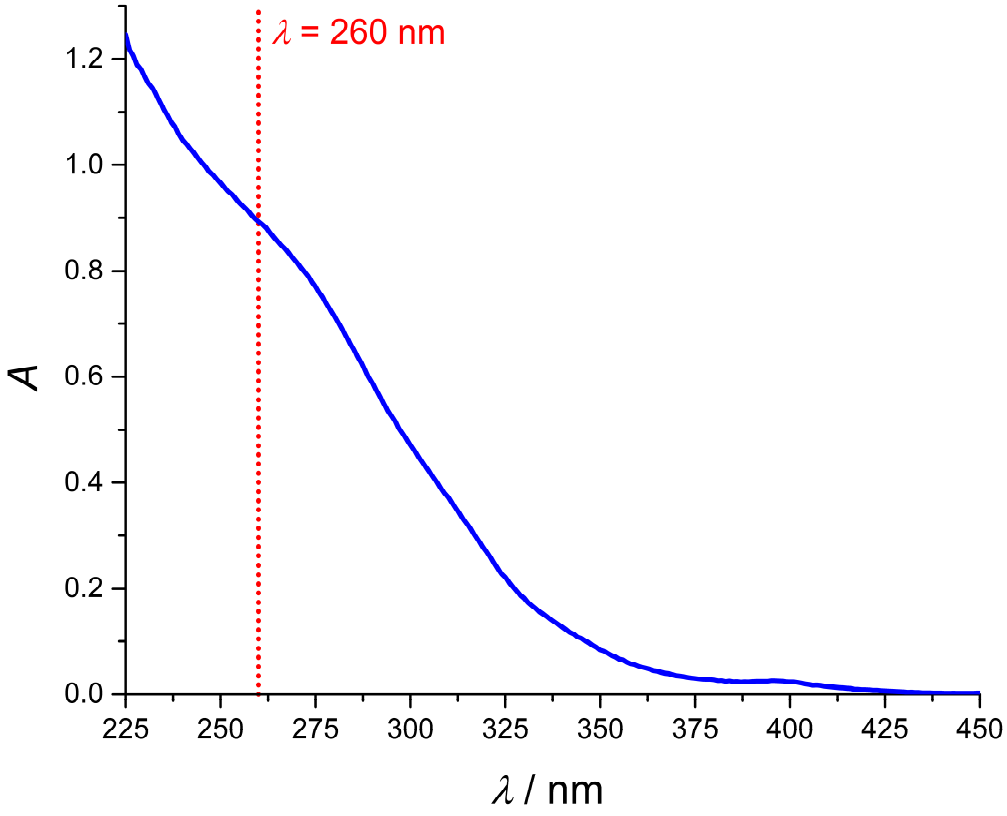

Figure S1. Example of the UV-Vis spectrum of the FeNTA working buffer solution (l = 1 cm, c(FeNTA) = 0.150 mM).

1.4. Preparation of hTf working solutions

The hTf working solutions were prepared by weighing and dissolving the appropriate amounts of hTf in the appropriate working buffers. The samples were briefly treated with the vortex mixer (Cole-Parmer, USA) to ensure proper dissolution. The pH was adjusted to the target values with small volumes of HCl(aq) and/or NaOH(aq). The exact protein concentrations were determined spectrophotometrically using the molar absorbance coefficients: ε_{280nm} = 84.4 x 10^3 M^{-1} cm^{-1} for Tf+S and ε_{280nm} = 84.8 x 10^3 M^{-1} cm^{-1} for Tf−S. The molar absorbance coefficient for Tf−S was determined in a previous study[2], while the coefficient for Tf+S was redetermined as described in the following subsection.

1.5. Redetermination of the molar absorbance coefficient for Tf+S

The molar absorbance coefficient for Tf+S was re-evaluated using the Edelhoch method, with measurements performed in decaplicate. The absorbance at λ = 280 nm of the folded protein was determined in a working buffer (25 mM PIPES, 0.2 M KCl, 10 mM K_2CO_3). Simultaneously, the absorbance at λ = 280 nm of the unfolded (denatured) protein was determined in the same buffer in the presence of 6 M guanidine-HCl. The molar absorbance coefficient ($\varepsilon_{folded,\ 280\ nm}$) for the folded protein was then calculated as the product of a reference molar absorbance coefficient for the unfolded protein ($\varepsilon_{unfolded,\ 280\ nm}$) and the ratio of the absorbance of the folded protein to that of the unfolded protein, as shown in Eq. S3:

$$\varepsilon_{\text{folded, 280 nm}} = \varepsilon_{\text{unfolded, 280 nm}} \cdot \frac{A_{\text{folded, 280 nm}}}{A_{\text{unfolded, 280 nm}}} \qquad \text{Eq. S3}$$

The reference value for $\varepsilon_{\text{unfolded, 280 nm}}$ = 81080 M^{-1} cm^{-1} was calculated based on the contributions of 8 tryptophan, 26 tyrosine, and 19 cystine residues in the apo-transferrin structure.[2] These measurements were also performed in a quartz glass cuvette with a light path length of 1 cm (Hellma, Germany) using the Varian Cary 50 Bio UV-Vis spectrophotometer (Varian, Australia).

2. Enzymatic desialylation

2.1. Preparation of desialylated transferrin (Tf−S)

Desialylated apo-transferrin (Tf−S) was prepared according to the optimized protocol for SialEXO® (Genovis, Sweden).[3] Native transferrin (Tf+S) was first dissolved in a 20 mM TRIS buffer solution with a pH of 6.8. The pH was then adjusted to 6.8 with 1 M HCl and NaOH solutions. The mass concentration of transferrin was approximately 2.5 mg/mL. Specifically, 800 µL of the native transferrin solution was added to each of the four SialEXO® columns containing 2 sialidase enzymes derived from *Akkermansia muciniphila* and expressed in *E. coli*. This corresponds to approximately 8 mg of transferrin for each desialylation cycle. The SialEXO® columns were rotated on the tube revolver at 25 °C and 10 rpm for 48 hours. The protein was recovered by centrifugation (3 min, 1000 RCF). The SialEXO® columns have plastic caps on the bottom, which must be removed before the centrifugation step. After centrifugation, the enzyme beads remain in the SialEXO® columns while the protein solution is collected in 2 mL centrifuge tubes. This setup facilitates repeated desialylation cycles as fresh native transferrin can be added directly to the columns.

2.2. Preliminary FPLC assessment

To confirm sufficient desialylation, equal aliquots were taken from all 2 mL centrifuge tubes (each containing approximately 2 mg asialotransferrin) and pooled. The pooled protein contained 200 µL (≈ 0.5 mg), which we considered to be sufficient for chromatographic analysis. The chromatographic experiment was performed on the ÄKTApurifier 10 FPLC instrument (Cytiva, USA) using the isoelectric focusing method, as the pI values of native and asialotransferrin differ significantly.[2]

pISep pH gradient buffers (CryoBioPhysica, USA, cat. No. 20055) were prepared by mixing the appropriate amounts of pISep starting buffers. Elution buffer 1 with a pH of 7.4 consisted of 50.3% pISep A and 49.7% pISep B. Elution buffer 2 with a pH of 5.5 consisted of 67.56% A and 32.44% B. 600 µL of elution buffer 1 was added to 200 µL of the pooled protein sample. For each sample, the pH was adjusted to 7.4 or a very close value above (up to pH = 7.5) by adding HCl(aq) and/or NaOH(aq). The Source 15Q 4.6/100 PE anion exchange column was used for the experiments. Chromatofocusing was performed with a one-step linear gradient phase supplemented by two short isocratic intervals, starting with 100% buffer 1 and ending with 100% buffer 2. The flow rate was maintained at 0.5 mL/min throughout the experiment, with absorbance measurements recorded at λ = 280 nm and l = 1 cm. Similarly, we subjected native apo-transferrin (Tf+S) to chromatofocusing for comparison. The resulting chromatograms (Figure S2) for Tf+S and Tf−S were in good agreement with previously published results, indicating successful desialylation.[2]

All asialotransferrin samples prepared in the 17 consecutive desialylation cycles were pooled and concentrated by centrifugal filtration using Amicon® Ultra centrifugal filters (0.5 mL, MWCO 30 K, Merck Millipore, USA, cat. no. UFC503096). Each centrifugation step was performed for 5 minutes and at 14000 RCF. The concentrates were thoroughly washed five times with pure water and then centrifuged as described above. These concentrates were then transferred to several 200 µL tubes and stored at −20 °C until further use.

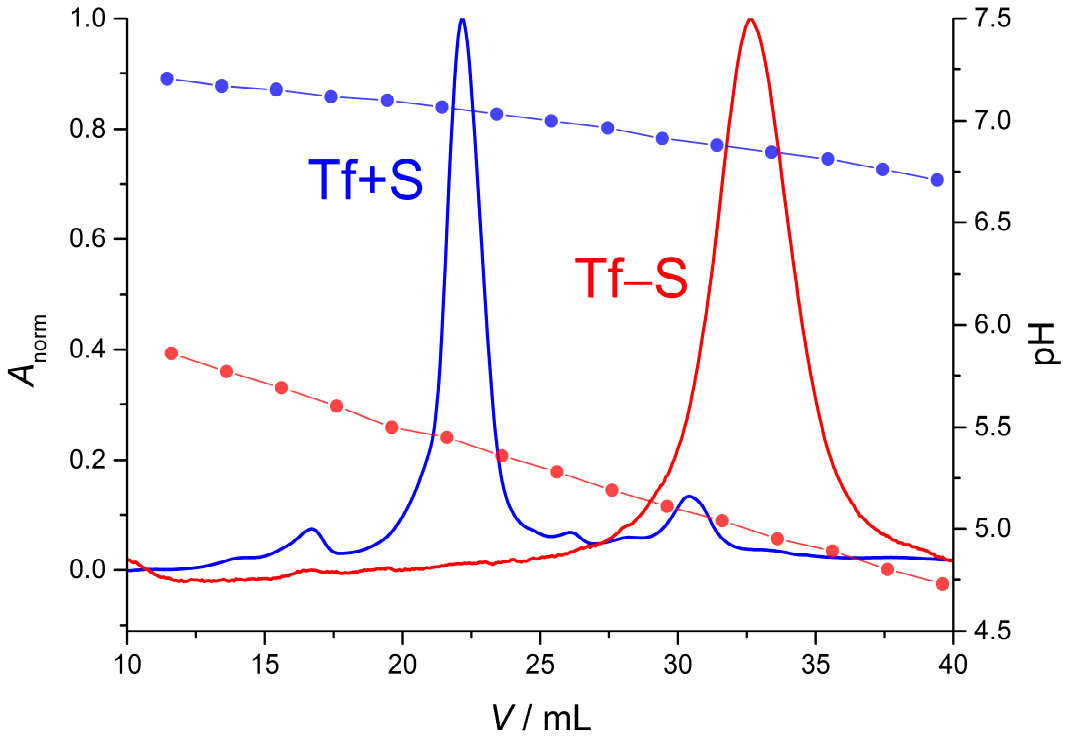

Figure S2. FPLC pH gradient ion-exchange chromatograms of native human apo-transferrin (Tf+S, blue) and desialylated human apo-transferrin (Tf−S, red). For the sake of clarity, the absorbance values for each experiment are normalized as $A_{i,\,norm} = A_{i,\,norm} / A_{max}$. The solid curves depict normalized absorbance values (λ = 280 nm chromatographic signals), while the connected dots on the line represent the measured pH values.

2.3. UHPLC N-glycan analysis

UHPLC analysis of N-glycans was performed according to the procedure described in a previous study.[2] The analysis was performed for both native (Tf+S) and desialylated (Tf−S) human apo-transferrin. Briefly, the required amount of protein concentrate corresponding to 200 µg of native (Tf+S) or desialylated (Tf−S) apo-transferrin was dissolved in 50 µL of freshly distilled water. The samples were then dried in a vacuum centrifuge. The samples were denatured by adding 30 µL of a 1.33% (w/v) SDS solution and incubated at 65 °C for 10 minutes. After denaturation, 10 µL of a 4% (v/v) Igepal-CA630 solution was added to the samples and the mixture was shaken on a plate shaker for 15 minutes. The N-glycans were then released by adding 1.2 U PNGase F and incubated overnight at 37 °C.

The free N-glycans were labeled using the following labeling mixture:

(i) 2-aminobenzamide (2-AB) (19.2 mg/mL; Sigma Aldrich, USA)
(ii) 2-picoline borane (44.8 mg/mL; Sigma Aldrich, USA)
(iii) mixture of dimethyl sulfoxide (Sigma Aldrich, USA) and glacial acetic acid (Merck, Germany) mixture (70:30 v/v).

To each sample, 25 µL of the labeling mixture was added and the samples were then incubated at 65 °C for 2 hours. Free markers and reducing agents were then removed from the samples by hydrophilic

interaction liquid chromatography solid-phase extraction (HILIC-SPE). After the incubation period, 700 µL of acetonitrile (ACN) was added to the samples to achieve a final concentration of 96% ACN by volume. The samples were then applied to individual wells of a 0.2 µm GHP filter plate. The solvent was removed by vacuum application using a vacuum manifold. All wells were first pre-washed with 70% ethanol and water, followed by equilibration with 96 % ACN. The loaded samples were then washed 5 times with 96% ACN. Finally, the N-glycans were eluted with water and stored at −20 °C until further use.

Fluorescently labeled N-glycans were separated by hydrophilic interaction chromatography using an Acquity UPLC H-Class instrument (Waters, USA). This instrument contains a quaternary solvent manager, a sample manager, and a fluorescence detector with an excitation wavelength of λ_{ex} = 250 nm and an emission wavelength of λ_{em} = 428 nm. The device was controlled by Empower 3 software (build 3471, Waters, USA). The labeled N-glycans were separated on a Waters BEH glycan chromatography column, where solvent A was 100 mM ammonium formate at pH = 4.4 and solvent B was ACN. The separation method involved a linear gradient from 70% to 53% acetonitrile with a flow rate of 0.56 mL/min during a 25-minute analytical run. The system was calibrated with an external standard of hydrolyzed and 2-AB-labeled glucose oligomers, which allowed the conversion of retention times for individual glycans to glucose units (GU).

The recorded chromatograms were preprocessed by replacing negative values in the chromatographic signals with 0. This was achieved using the IF() function in Microsoft Excel. Subsequently, the chromatographic peaks corresponding to the signals of the labeled glycans were identified and integrated within the retention time window of 4 to 20 minutes. The very intense peak with a maximum at about 0.7 minutes, corresponding to the free fluorescent labeling molecule, was excluded from the analysis. Based on data from a previous UHPLC-MS analysis, the N-glycan peaks were determined by comparing their retention times and peak shapes with those previously observed. Integration of the signals was performed using the custom Python script. Specifically, the function np.trapz() from the NumPy library was used, which employs the composite trapezoidal rule for integration. The percentages of glycans were determined by multiplying the integrals corresponding to the chromatographic peaks of the specific glycans by 100 and dividing by the difference of the total integral minus the integral of the residual noise.

The extent of transferrin desialylation was estimated using the values of the index of sialylation (*IS*) according to Eq. S4.

$$IS = \sum_{i=1}^{n} f_i \cdot s_i \qquad \text{Eq. S4}$$

n represents the N-glycan fraction number, f_i denotes the percentage content of the specific N-glycan fraction, and s_i indicates the number of sialic acids within the structure of the corresponding N-glycan fraction. The obtained *IS* values for Tf+S = 127.79 and Tf−S = 1.51 confirmed a remarkable ≈ 99% reduction in sialic acid content for the enzymatically desialylated protein (Tf−S). The UHPLC chromatograms (and the corresponding glycan structures) are shown in Figure S3.

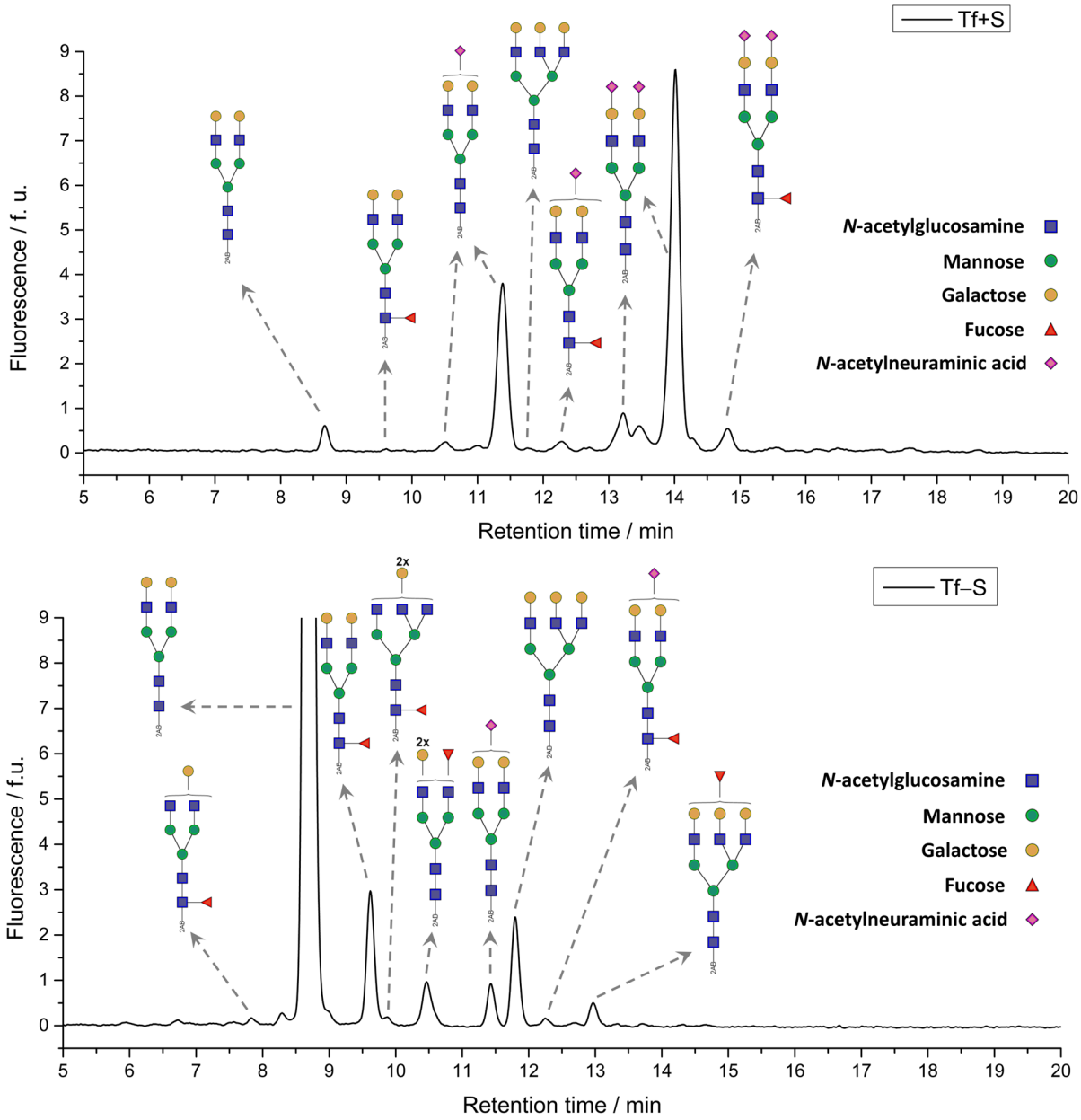

Figure S3. UHPLC chromatograms showing the assigned N-glycan residues in native apo-transferrin (Tf+S, **top**) and desialylated apo-transferrin (Tf−S, **bottom**).

3. Titration methods

3.1. Titrating liquids into microcentrifuge tubes

All liquid samples in the titration experiments were prepared using the Opentrons OT-2 pipetting robot (Opentrons, USA). The first generation (GEN1) P-20 and P-300 pipettes were used together with the corresponding original Opentrons pipette tips. The protocols for these specific experiments were created using custom Python scripts and tab-delimited tables containing the specified volumes for pipetting. Solutions were pipetted from the 5 mL or 50 mL plastic tubes into the 500 µL microcentrifuge tubes. All plastic tubes were secured in their respective customized 3D-printed holders. Pipetting was performed by gradually lowering the relative height of the pipette tip, considering the previously transferred liquid volume (the optimal height was determined for each step based on the geometric parameters of the labware depending on the transferred volume). This was done to ensure uniform immersion of the tip(s) and to avoid possible errors due to unequal hydrostatic pressures and possible deposition of the liquid on the outer layer of the tip (dripping could be observed if the tip is immersed too deeply into the solution).

Each titration experiment consisted of two separate steps: in the first step (i), only the non-protein components were mixed; in the second step (ii), the protein solution was added to the mixture. The addition of the non-protein components (i) was performed by first pipetting all volumes > 30 µL with a single pipette tip per compound. This was done from a relatively high tip position within the 500 µL microtube to avoid possible contamination of the tip by contact with other liquids. Volumes ≤ 30 µL were then added directly to the liquid present (2 mm from the bottom of the 500 µL microtube). After the addition of each volume ≤ 30 µL, the pipette tip was rinsed in place and a blow-out procedure was performed to ensure complete transfer of the liquid.

The protein component (ii) was added to the non-protein mixture (2 mm from the bottom of the 500 µL microtube) and rinsed with blowout. The protein solutions were added directly to the non-protein mixture due to viscosity and adhesion problems (bubble formation and incomplete volume transfer were observed when the protein was added without tip immersion). To avoid cross-contamination, pipette tips were replaced after each volume addition that required tip immersion in the 500 µL microtube. The total volumes in the titrations were either 300 or 500 µL per microtube. The protein-containing substance accounted for only 1/3 or at most 1/2 of the total volume. After completion of the titration, each 500 µL microtube was capped and mixed with the vortex mixer. The samples were then equilibrated for >1 day at 25° C.

3.2. Transferring samples to 96-well microplates

After the equilibration phase, the microtubes were mixed on a vortex mixer, decapped, and placed in a suitable holder in the OT-2 pipetting robot. 200 µL of each sample from the 500 µL microtube was pipetted into the 96-well plate. The pipette tip was changed for each sample to prevent possible cross-contamination. Samples were added to the microtiter plate at (pseudo-)randomized positions. Randomization was performed via a custom Python script and was done to reduce possible systematic errors due to possible irregularities in the microtiter plate, anisotropy of positions (e.g. wells in the middle and at the edge of the microtiter plate) and/or other effects that could strongly apply to the adjacent positions in the microtiter plate.

4. Fluorescence and absorbance

4.1. Fluorescence measurements

Fluorescence was measured with the Tecan Spark M10 (Tecan, Austria) multimode microplate reader using the 96-well UV-Vis transparent microplates (black, μ-clear, flat bottom, chimney well, Greiner, USA, cat. no. 655097). For each set of measurements, the *z*-position (the vertical distance between the optical element and the bottom of the microplate well) was first optimized using the optimization method built into the reader's software.[4] The optimal *z*-position is the height of the optical element which produces the strongest fluorescence response. Optimization of the *z*-position was always performed for the apo-transferrin sample, as this is the sample that produces the strongest fluorescence response within a given titration set (as iron binding to transferrin quenches protein fluorescence). This optimization was performed separately for each titration experiment. The optimal values determined are all very similar and are around 17000 μm, with less than 1 % deviation. In addition to the optimal *z*-positions, several additional fixed *z*-positions were used for data acquisition in all titrations (as indicated in Table S1), mainly for the purpose of subsequent IFE (Inner Filter Effect) correction.

The gain parameter was also optimized separately for each set before the fluorescence measurements. The gain represents the amplification factor applied to the photomultiplier tube (PMT) detector and influences the measurement sensitivity. In general, measuring at higher gain values should improve the sensitivity of fluorescence measurements. On the other hand, over-amplification can saturate the signal and thus overload the detector. For this reason, the gain for the apo-transferrin samples (which give the strongest fluorescence response within a given titration) was optimized using the optimized *z*-position value (as this height of an optical element produces the maximum fluorescence response within a given range of *z*-positions). All measurements at the different *z*-positions for a given titration experiment were always recorded with the same gain value.

The fluorescence measurements were performed with an excitation wavelength λ_{ex} = 280 nm and an emission wavelength λ_{em} = 335 nm. These measurements were performed in top-reading mode, where both the light source and the detector were positioned above the microplate well. Excitation at 280 nm is commonly used for various fluorescent proteins. The emission wavelength of 335 nm was chosen because it produces a strong fluorescence signal near the emission maximum while minimizing the crosstalk effect. Crosstalk is the overlap of the fluorescence excitation radiation and the emitted signal. For the specific microplate reader that we used in our experiments, it is recommended to measure at a spectral difference $\lambda_{em} - \lambda_{ex} \geq 45$ nm. In our measurements, this difference was 55 nm. We also used a suitable optical filter for excitation (280 nm, bandwidth 15 nm, Tecan, Austria, cat. no. 30092080) mounted on a custom-made 3D-printed holder to ensure that the excitation light did not contribute to the fluorescence signal. An empty microplate was examined for possible overlap, as shown in Figure S4.

Table S1. The *z*-position values used for the fluorescence measurements.

z-position / µm
optimized ≈ 17000
14600
15000
15500
16000
17000
18000
19000
20000
21000

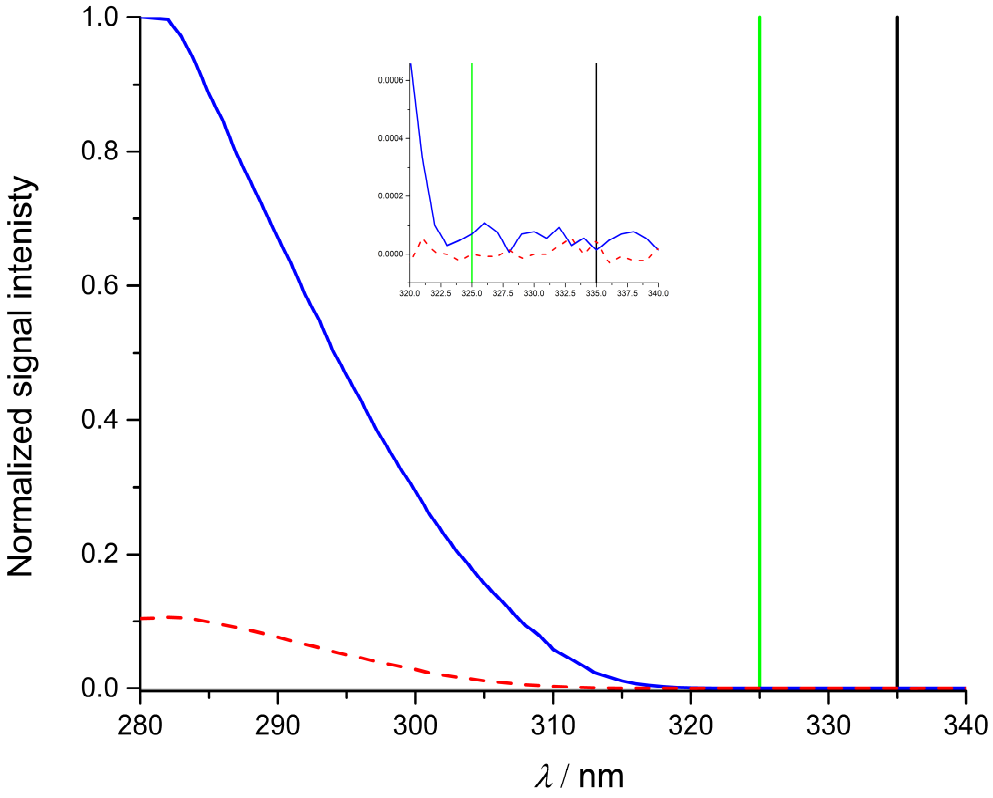

Figure S4. Results of fluorescence measurements (λ_{ex} = 280 nm) of an empty 96-well microplate with (red dashed line) and without (solid blue line) use of an optical filter. The spectra were normalized by setting the point with the highest fluorescence signal as reference. The green vertical line represents the crosstalk threshold $\lambda_{em} - \lambda_{ex} \geq 45$ nm (λ_{em} = 325 nm) recommended by the manufacturer of the microplate reader (Tecan, Austria). The black vertical line represents the value of λ_{em} = 335 nm used in this work. **Inset:** An enlarged section of this plot in the range of λ_{em} 320-340 nm.

4.2. Absorbance measurements

The absorbance values of the protein and FeNTA solutions used for the titrations were measured with the Varian Cary 50 Bio UV-Vis spectrophotometer (Varian, Australia) using a quartz glass cuvette with a path length of l = 1 cm (Hellma, Germany). The absorbances of the titration samples were measured in the range of 200-1000 nm in 1 nm steps in the 96-well microplates (black, μ-clear, flat bottom, chimney well, Greiner, USA, cat. no. 655097) on the Tecan Spark M10 (Tecan, Austria) multimode microplate reader.

5. Fluorescence data

5.1. Inner Filter Effect (IFE) corrections

IFE corrections were performed using the ZINFE (Z-position INner Filter Effect) method, as previously described.[4] ZINFE method utilizes the differences in the measured fluorescence at variable heights (*z*-positions) of light source/detector. The method can be described by Eq. S5.

$$F_Z = F_{0(z_1)} \left(\frac{F_{0(z_2)}}{F_{0(z_1)}}\right)^{\frac{k-z_2}{z_2-z_1}} \quad \text{Eq. S5}$$

F_Z represents the fluorescence intensity corrected with ZINFE. $F_{0(z1)}$ and $F_{0(z2)}$ denote measured fluorescence values at different *z*-positions, z_1 and z_2, while k is a geometric parameter that only applies to a specific combination of sample volume, microplate, and microplate reader. For the volume of 200 µL per microplate well, the geometric parameter k was estimated to be 20593 µm.[4] The ZINFE corrections were performed with $F_{0(z1)}$ measured at the optimized value of $z \approx 17000$ µm, while $F_{0(z2)}$ was measured at $z = 20000$ µm.

This technique was developed specifically for microplate readers and has been shown to be effective for absorbance values up to approximately $A_{ex} \approx 2$, $A_{em} \approx 0.5$.[4] The absorbance values obtained in hereby presented experiments are well below these thresholds, suggesting suitability of ZINFE correction procedure for this study. To further confirm our claim that the ZINFE method is suitable, the measured fluorescence was also processed using the common IFE correction method proposed by Lakowicz in his popular textbook on fluorescence spectroscopy.[5] As mentioned in the literature, the Lakowicz correction loses its effectiveness at absorbance values > 0.7.[4,6,7] This limit is more than twice as high as the absorbance that occurs in the experiments presented here. The Lakowicz correction procedure is shown in Eq. S6.

$$F_A = F_0 \cdot 10^{\left(\frac{A_{ex}+A_{em}}{2}\right)} \quad \text{Eq. S6}$$

F_A is the IFE-corrected fluorescence, F_0 is the uncorrected (measured) fluorescence, A_{ex} and A_{em} are the absorbance at the excitation and emission wavelengths, respectively. As expected, the two methods described above yielded very similar results. This becomes particularly clear when the results of one method are plotted against the results of the other, as shown in Figs. S5 and S6. The coefficients of determination obtained by regressing the results of one correction against the other are $R^2 > 0.99$ in all cases, as can be seen in Table S2.

Table S2. R^2 values obtained from the linear regressions using two different IFE correction methods.

	pH	5.9	6.2	6.5	6.8	7.4
R^2	Tf+S	0.9932	0.9946	0.9990	0.9986	0.9991
	Tf–S	0.9995	0.9981	0.9997	0.9982	0.9996

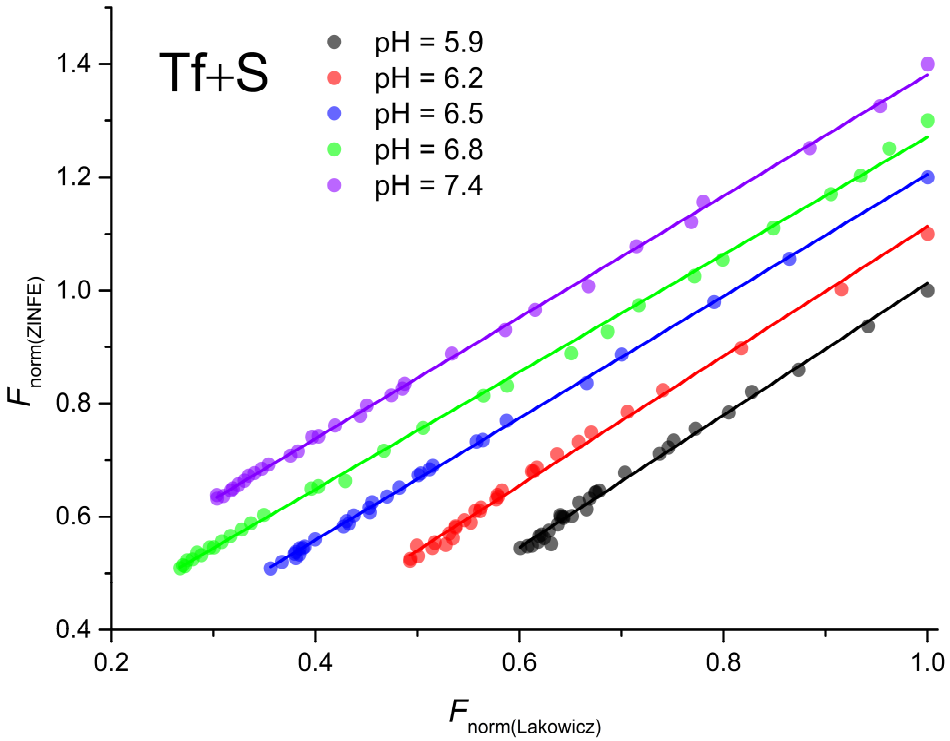

Figure S5. ZINFE IFE correction as a function of Lakowicz IFE correction for Tf+S (native human apo-transferrin) titrations. The values are normalized as $F_{i,\mathrm{norm}} = F_i / F_{\mathrm{max}}$. For visual clarification, the linear interpolations ($y = a + bx$) are shifted by value $a_{\mathrm{shifted}} = a + n \cdot 0.1$ for each increasing pH value, $n = 0, 1, 2, 3, 4$; for pH = 5.9, 6.2, 6.5, 6.8, 7.4, respectively.

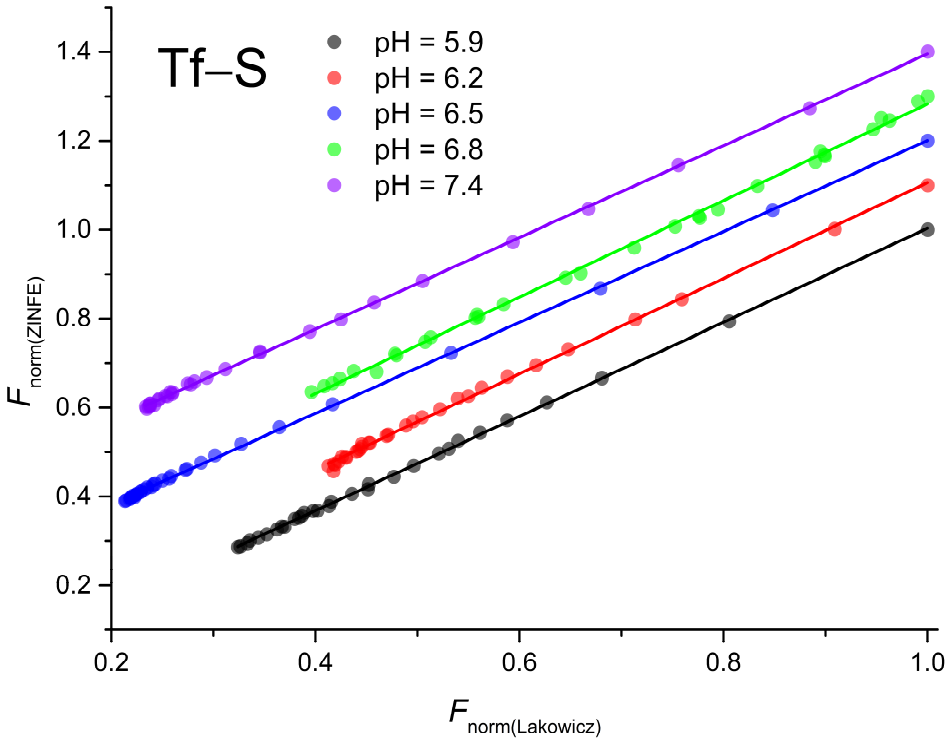

Figure S6. ZINFE IFE correction as a function of Lakowicz IFE correction for Tf–S (desialylated human apo-transferrin) titrations. The values are normalized as $F_{i,\mathrm{norm}} = F_i / F_{\mathrm{max}}$. For visual clarification, the linear interpolations ($y = a + bx$) are shifted by value $a_{\mathrm{shifted}} = a + n \cdot 0.1$ for each increasing pH value, n = 0, 1, 2, 3, 4; for pH = 5.9, 6.2, 6.5, 6.8, 7.4, respectively.

5.2. Fluorometric titrations for determination of the active protein fraction

The values of the relative fluorescence of Fe_2Tf (s = 0.174 for Tf+S and s = 0.183 for Tf−S) were determined in the 'titration regime' defined by Jarmoskaite *et al*. in their considerations on 1:1 binding experiments.[8] Under these conditions, the concentration of the constant component is much higher than the K_D, so that essentially all of the added titrant is depleted from the solution by binding to the titrand until there is no more free titrand to bind. In this case, the concentration of titrant that results in half binding is not equal to the K_D. However, these conditions are suitable for determining the titrand content and the fluorescence signal corresponding to complete saturation of the binding sites.

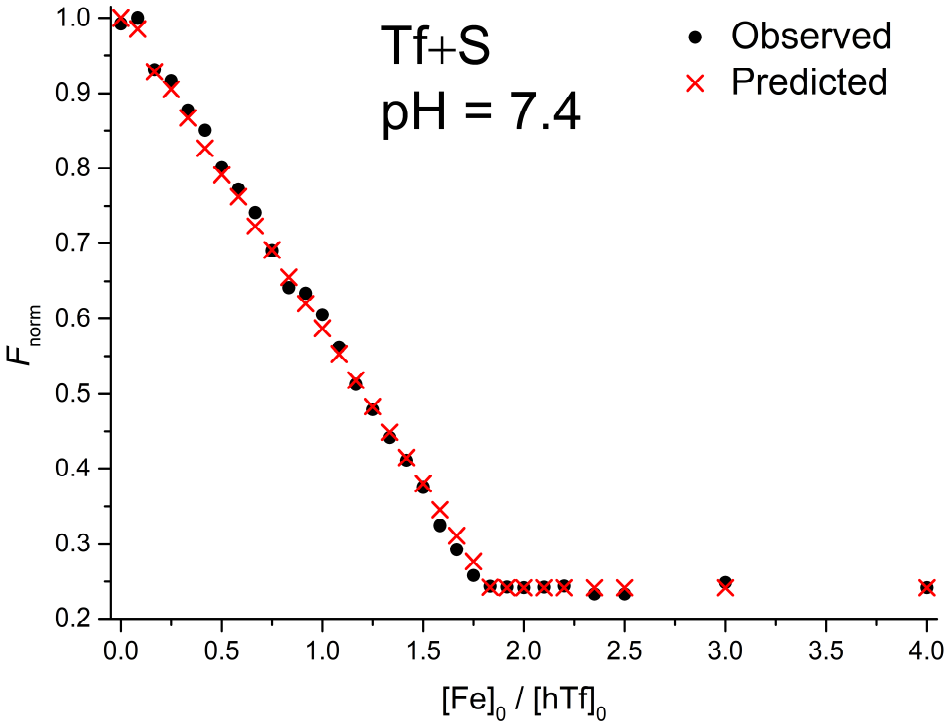

Figure S7. Measured (F_{obs}) and calculated (F_{calc}) normalized fluorescence for fluorometric titration of human serum transferrin (Tf+S) with FeNTA: $[hTf]_0$ = 1.93 µM, [PIPES] = 25 mM, [KCl] = 0.2 M, $[HCO_3^-]$ = 10 mM, $[NTA]_0$ = 0 mM, pH = 7.4, 25 °C.

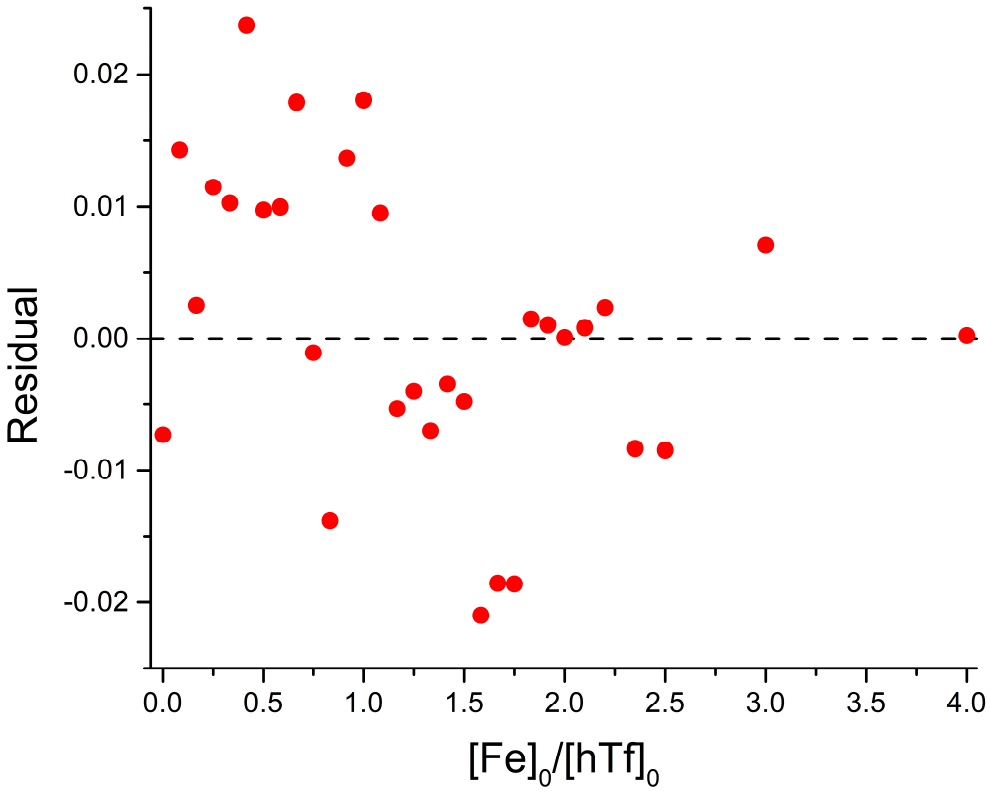

Figure S8. Residuals of the fit related to the experiment shown in Figure S7, calculated as $F_{calc} - F_{obs}$.

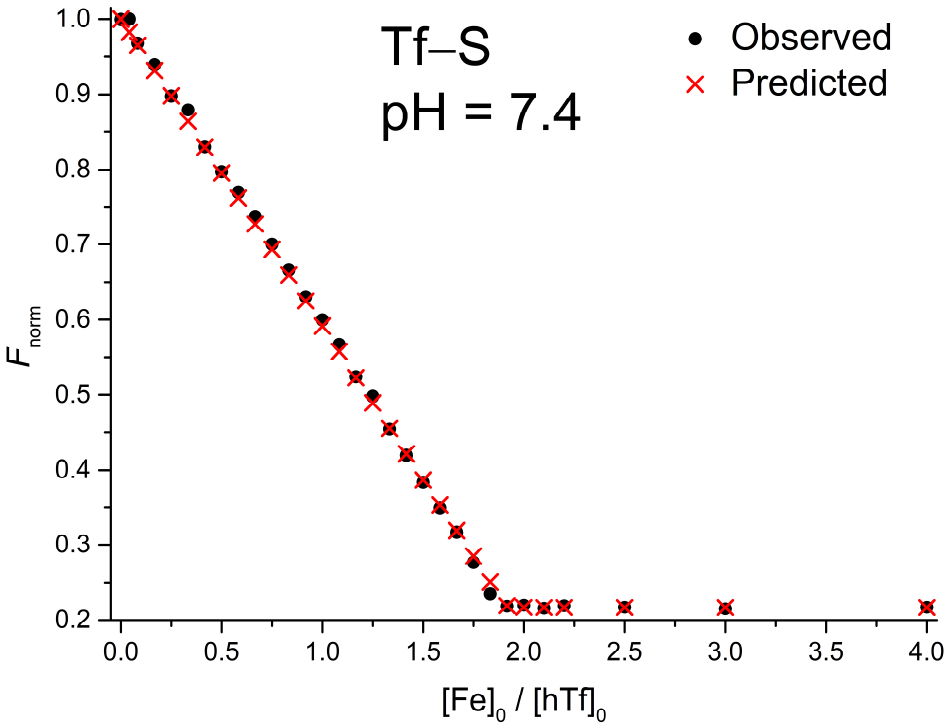

Figure S9. Measured (F_{obs}) and calculated (F_{calc}) normalized fluorescence for fluorometric titration of desialylated human serum transferrin (Tf–S) with FeNTA: $[hTf]_0$ = 2.09 μM, [PIPES] = 25 mM, [KCl] = 0.2 M, $[HCO_3^-]$ = 10 mM, $[NTA]_0$ = 0 mM, pH = 7.4, 25 °C.

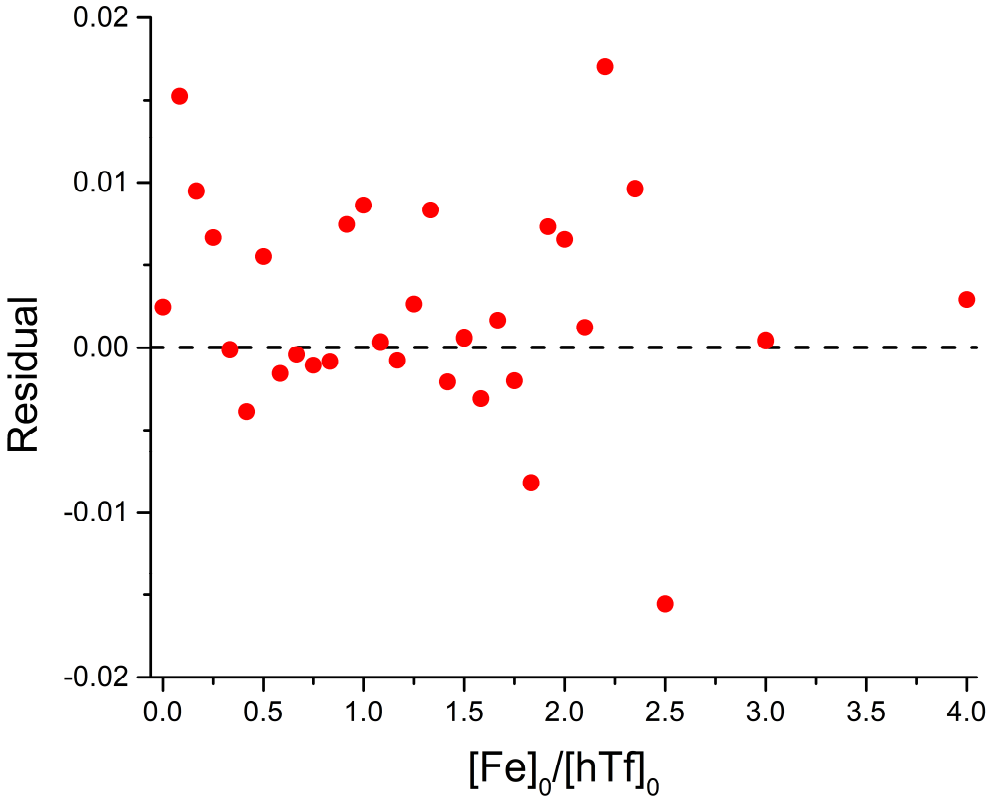

Figure S10. Residuals of the fit related to the experiment shown in Figure S9, calculated as $F_{calc} - F_{obs}$.

5.3. Fluorometric titrations for determination of the apparent binding constants

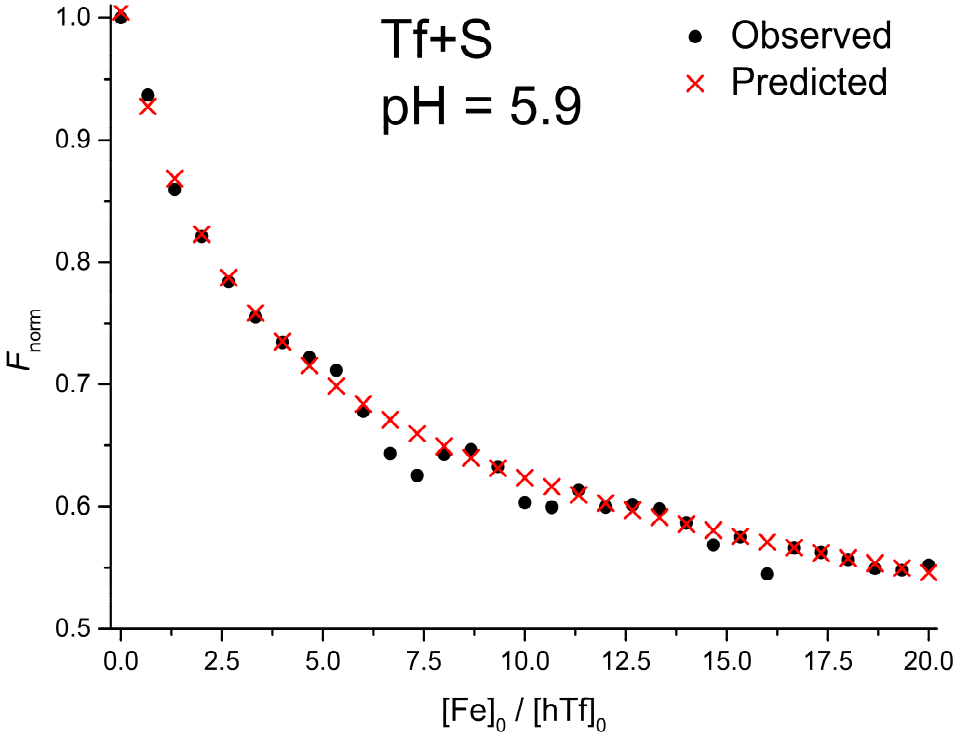

Figure S11. Measured (F_{obs}) and calculated (F_{calc}) normalized fluorescence for the spectrofluorometric titration of human serum transferrin (Tf+S) with FeNTA: $[hTf]_0$ = 1.78 µM, [PIPES] = 25 mM, [KCl] = 0.2 M, $[HCO_3^-]$ = 10 mM, $[NTA]_0$ = 0.1 mM, pH = 5.9, 25 °C. The parameters determined with the Solver tool in Microsoft Excel for the calculation of F_{calc} are: $\log(K_{1m})$ = 5.425 ± 0.012, $\log(R)$ = 1.541, ± 0.008 R^2 = 0.9913.

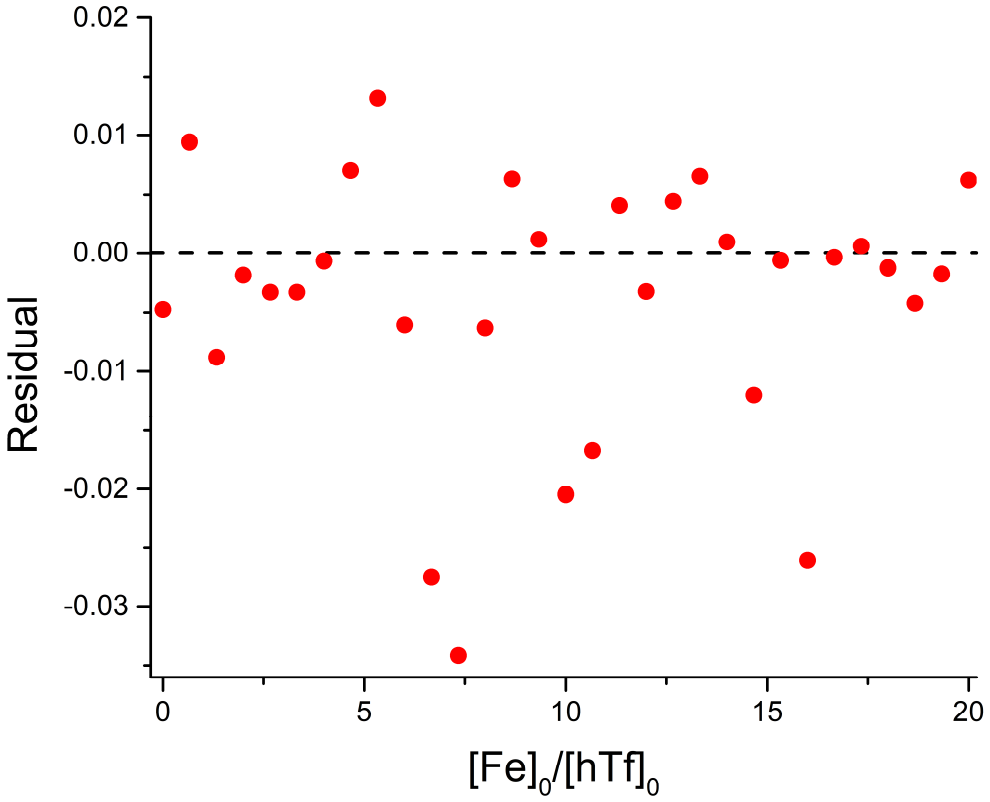

Figure S12. Residuals of fit related to experiment presented in Figure S11 calculated as $F_{calc} - F_{obs}$.

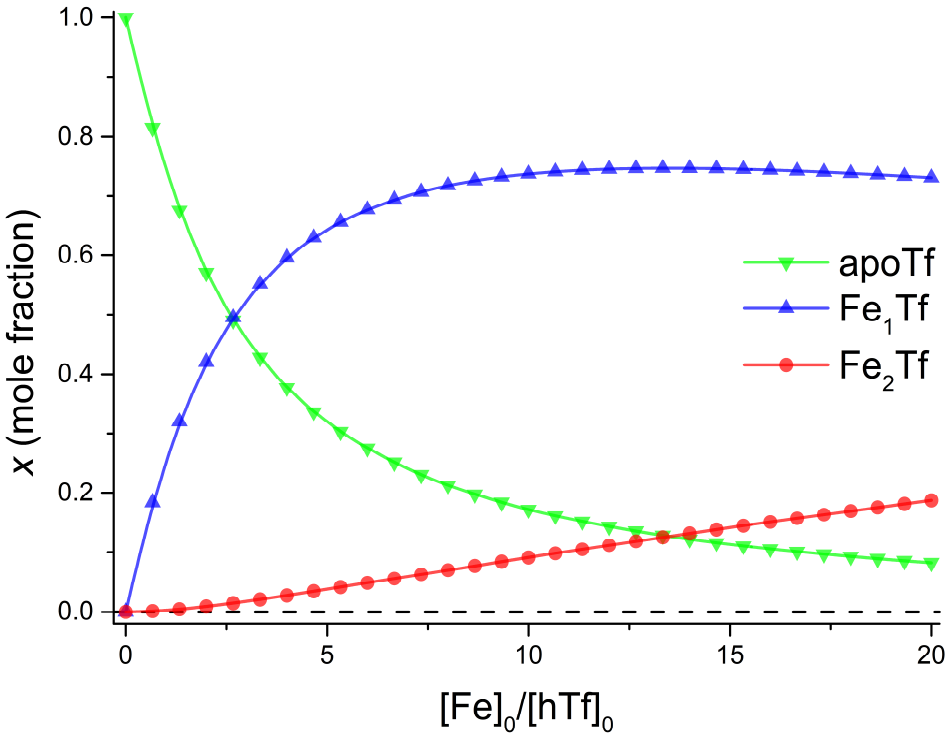

Figure S13. Transferrin speciation related to experiment presented in Figure S11 according to Eqs. 9-11 in the manuscript.

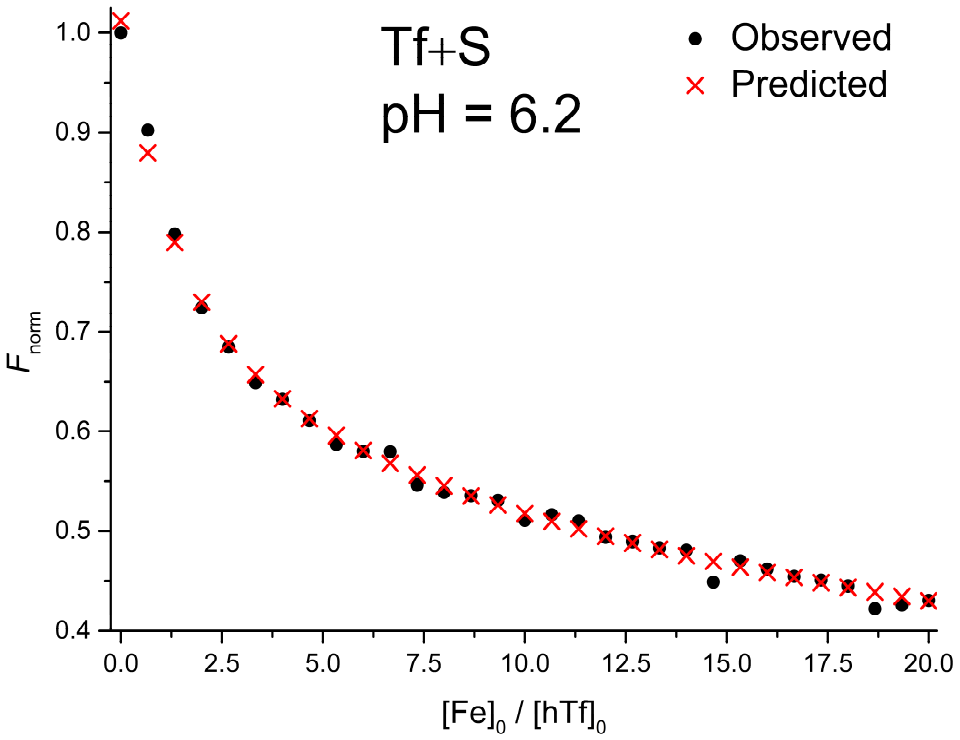

Figure S14. Measured (F_{obs}) and calculated (F_{calc}) normalized fluorescence for the spectrofluorometric titration of human serum transferrin (Tf+S) with FeNTA: $[hTf]_0$ = 2.05 µM, [PIPES] = 25 mM, [KCl] = 0.2 M, $[HCO_3^-]$ = 10 mM, $[NTA]_0$ = 0.5 mM, pH = 6.2, 25 °C. The parameters determined with the Solver tool in Microsoft Excel for the calculation of F_{calc} are: $\log(K_{1m})$ = 5.812 ± 0.065, $\log(R)$ = 1.522 ± 0.041, R^2 = 0.9960.

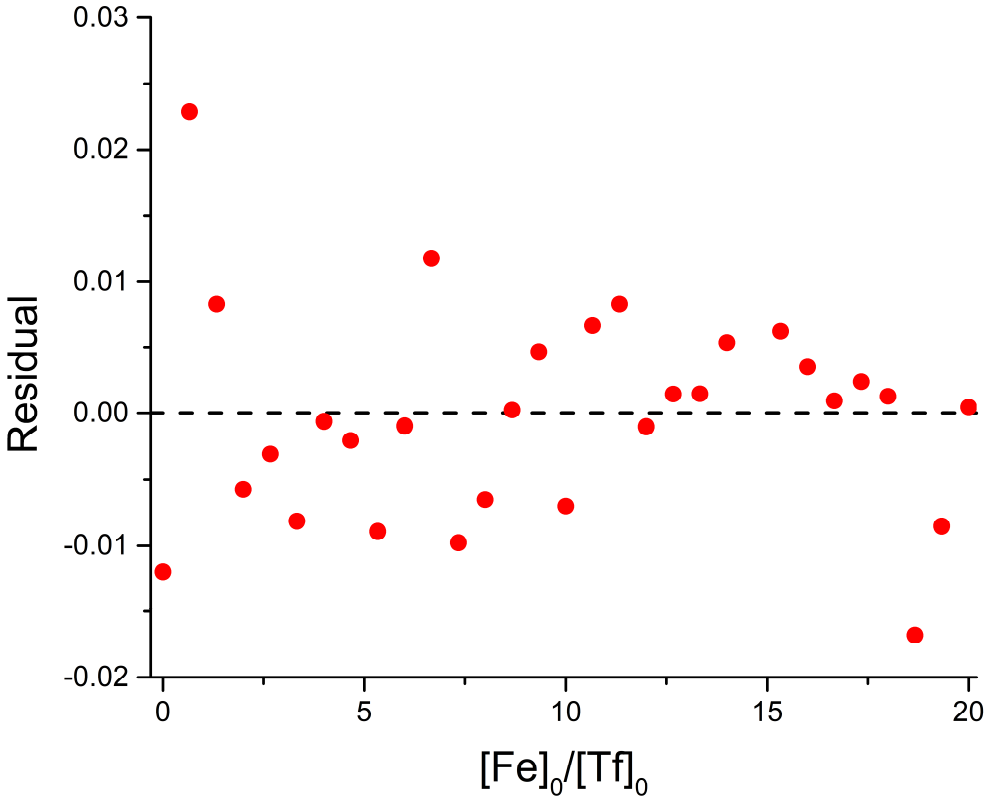

Figure S15. Residuals of fit related to experiment presented in Figure S14 calculated as $F_{calc} - F_{obs}$.

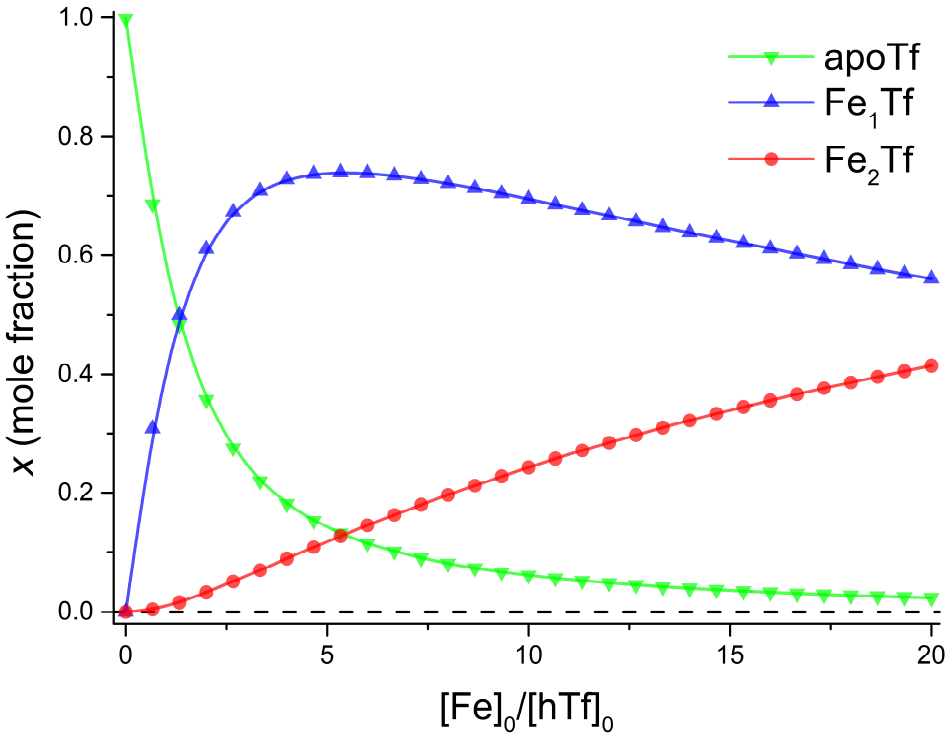

Figure S16. Transferrin speciation related to experiment presented in Figure S14 according to Eqs. 9-11 in the manuscript.

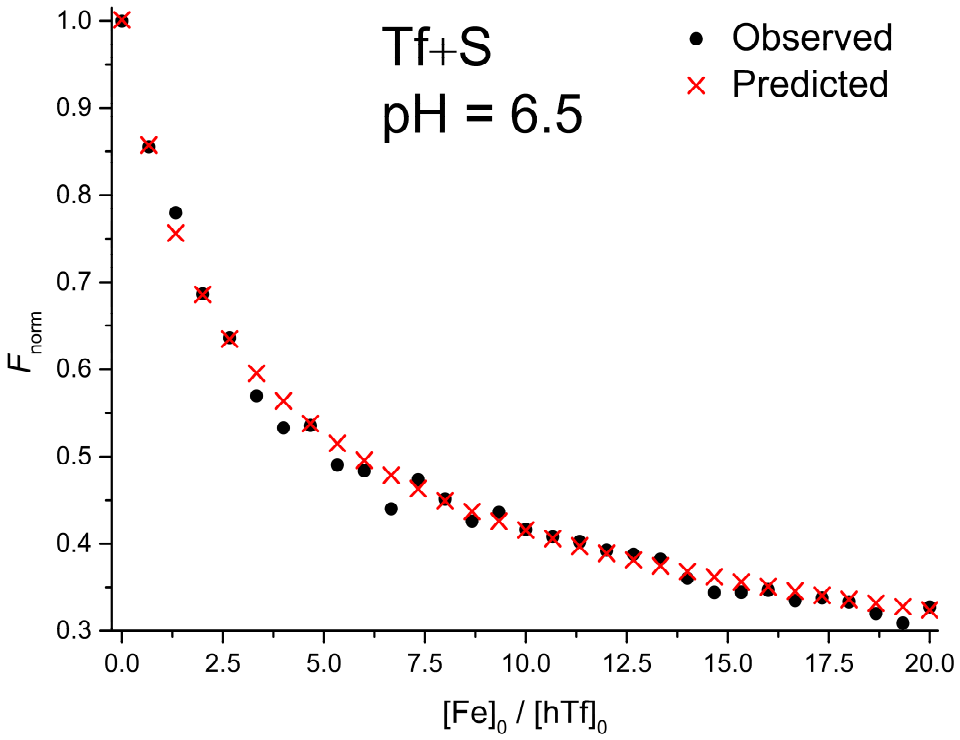

Figure S17. Measured (F_{obs}) and calculated (F_{calc}) normalized fluorescence for the spectrofluorometric titration of human serum transferrin (Tf+S) with FeNTA: $[hTf]_0$ = 2.04 µM, [PIPES] = 25 mM, [KCl] = 0.2 M, $[HCO_3^-]$ = 10 mM, $[NTA]_0$ = 0.5 mM, pH = 6.5, 25 °C. The parameters determined with the Solver tool in Microsoft Excel for the calculation of F_{calc} are: $\log(K_{1m})$ = 5.887 ± 0.032, $\log(R)$ = 1.176 ± 0.022, R^2 = 0.9938.

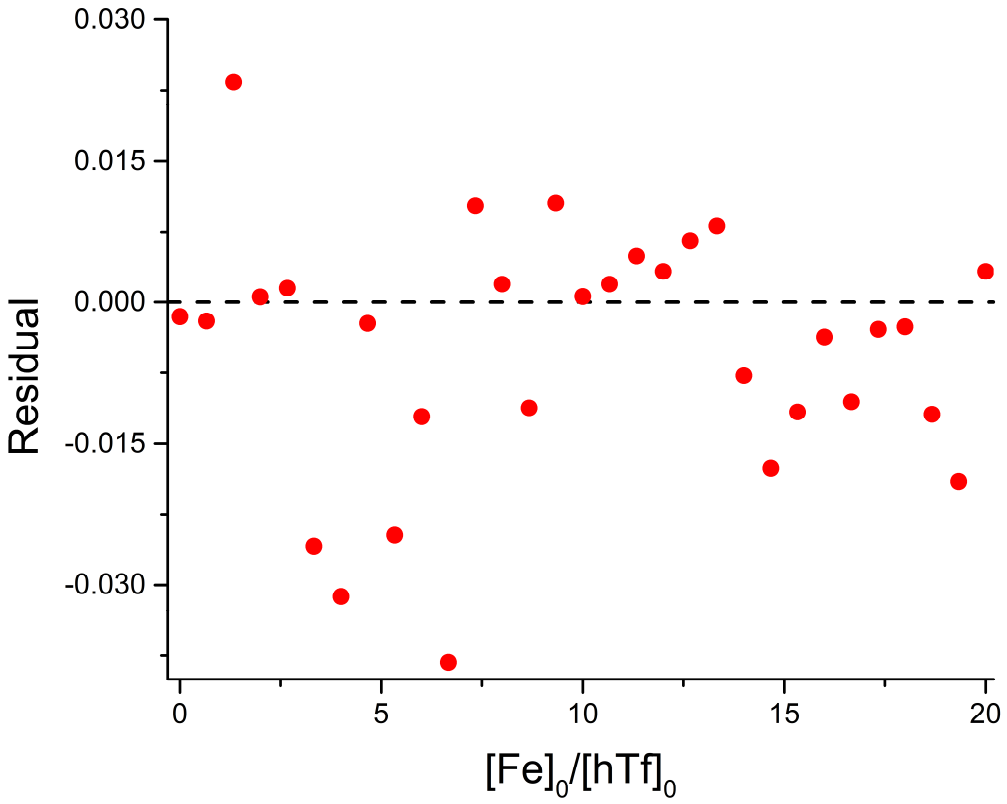

Figure S18. Residuals of fit related to experiment presented in Figure S17 calculated as $F_{calc} - F_{obs}$.

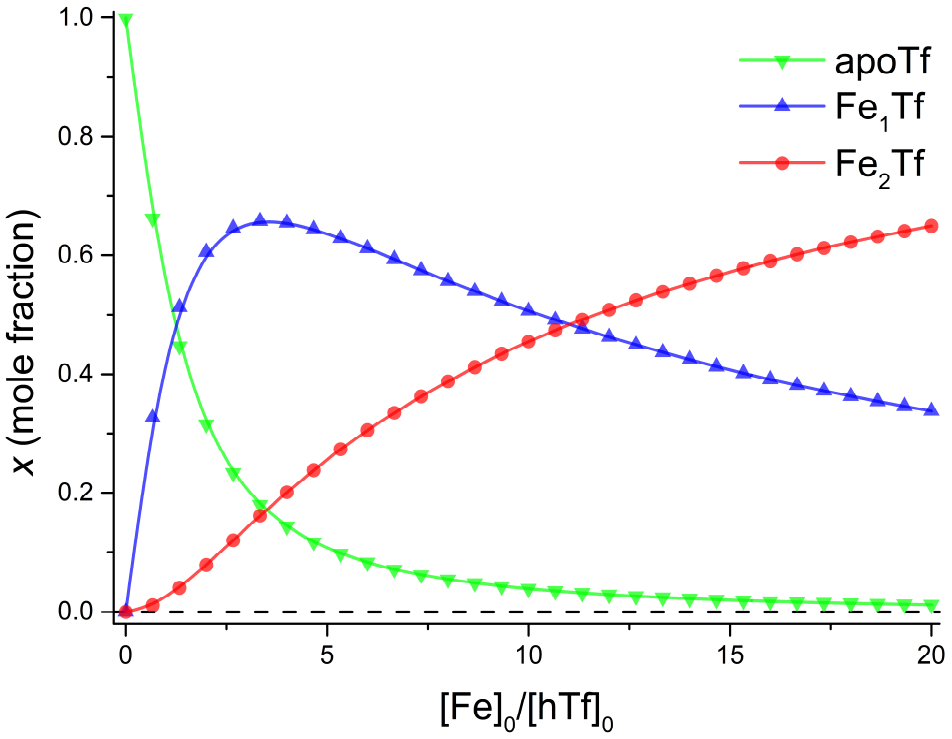

Figure S19. Transferrin speciation related to experiment presented in Figure S17 according to Eqs. 9-11 in the manuscript.

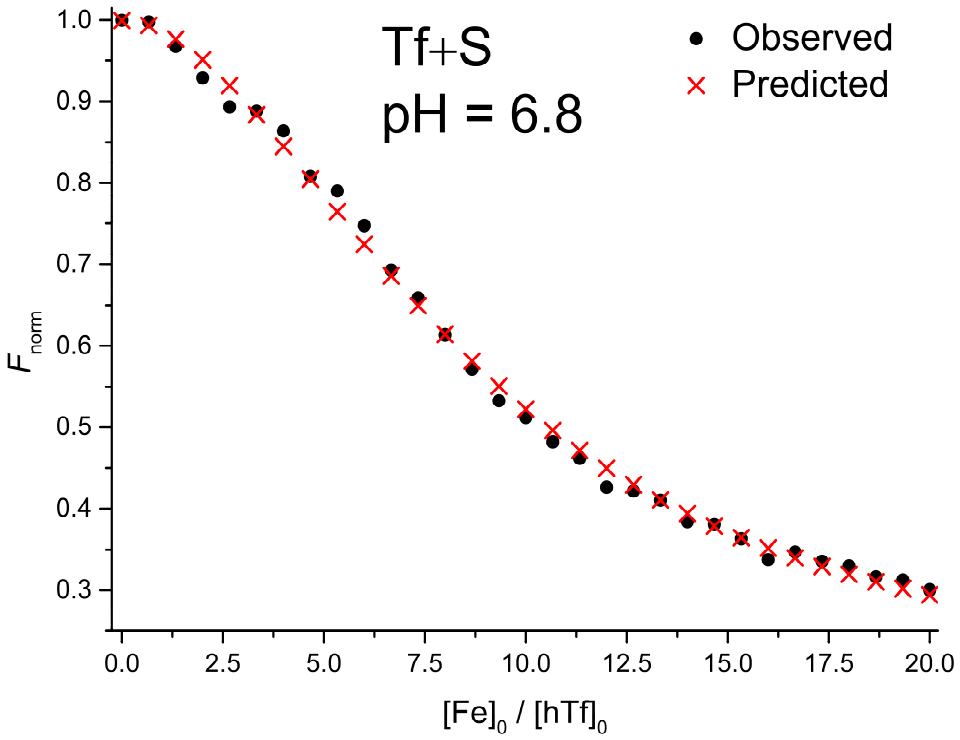

Figure S20. Measured (F_{obs}) and calculated (F_{calc}) normalized fluorescence for the spectrofluorometric titration of human serum transferrin (Tf+S) with FeNTA: $[hTf]_0$ = 2.27 μM, [PIPES] = 25 mM, [KCl] = 0.2 M, $[HCO_3^-]$ = 10 mM, $[NTA]_0$ = 10 mM, pH = 6.8, 25 °C. The parameters determined with the Solver tool in Microsoft Excel for the calculation of F_{calc} are: $\log(K_{1m}) = 0 \pm 0$, $\log(R) = -9.532 \pm 0.014$, $R^2 = 0.9971$. At pH = 6.8, the calculated $\log(K_{1m})$ and $\log(R)$ are not meaningful because the second iron ion binding event may dominate and possibly mask the effects of the first binding event, leading to incorrect values of the equilibrium constant.

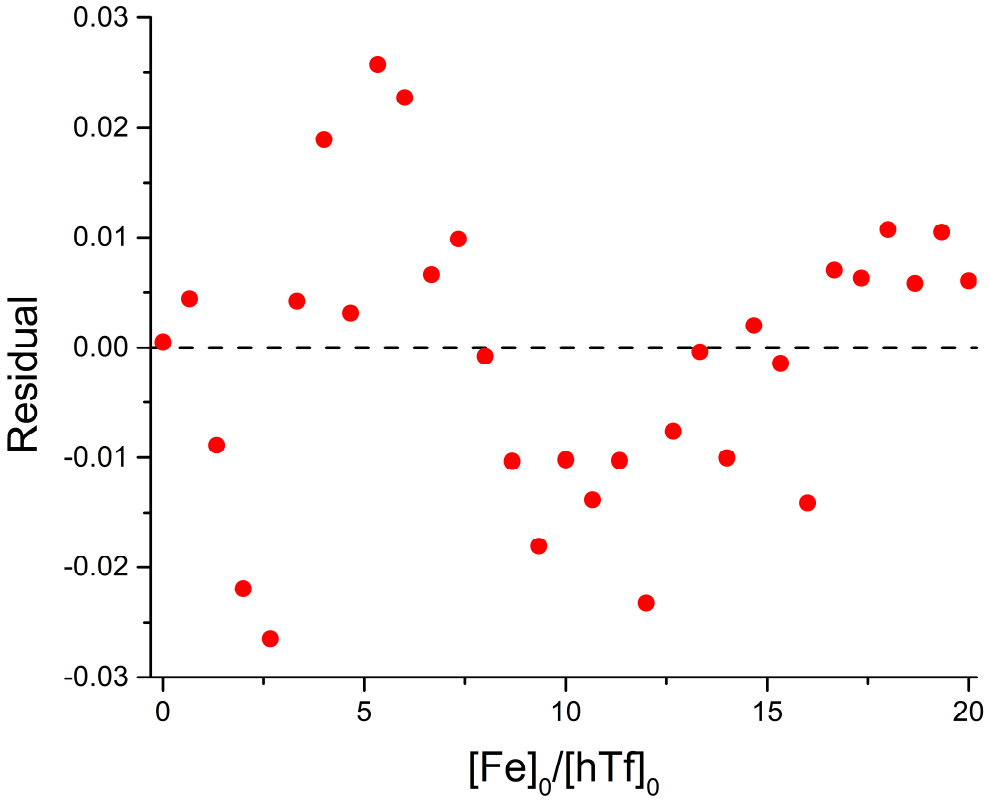

Figure S21. Residuals of fit related to experiment presented in Figure S20 calculated as $F_{calc} - F_{obs}$.

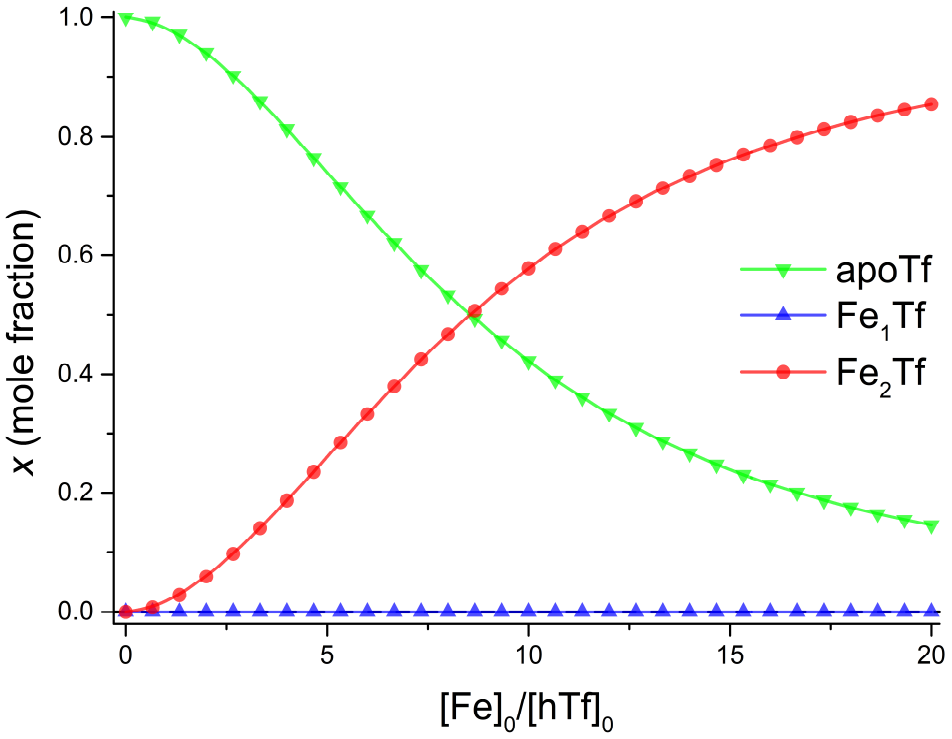

Figure S22. Transferrin speciation related to experiment presented in Figure S20 according to Eqs. 9-11 in the manuscript.

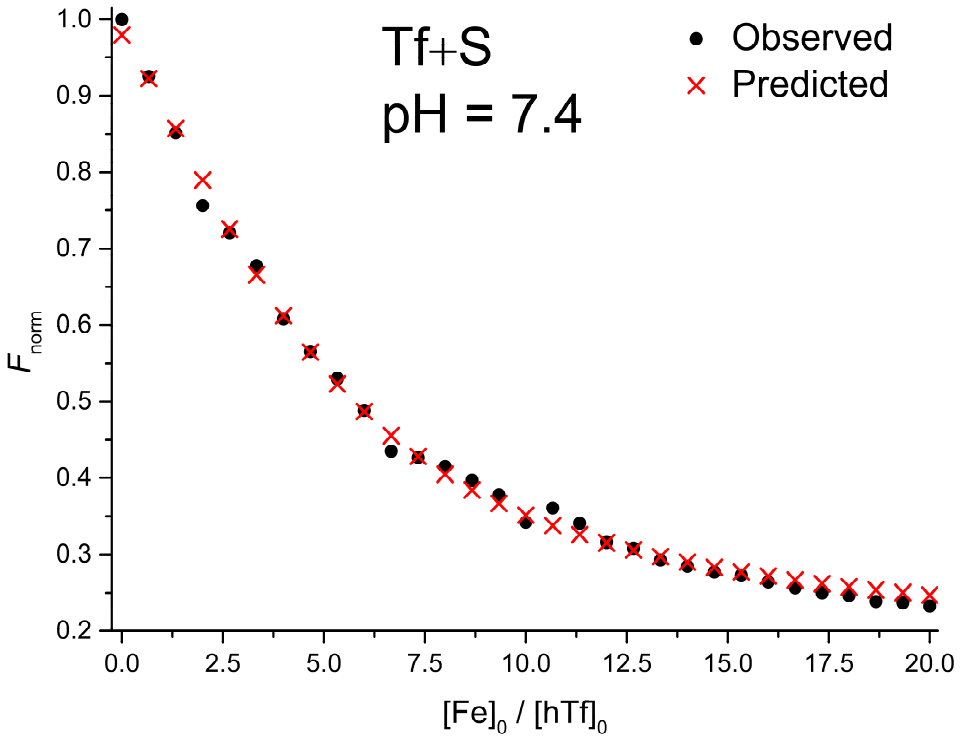

Figure S23. Measured (F_{obs}) and calculated (F_{calc}) normalized fluorescence for the spectrofluorometric titration of human serum transferrin (Tf+S) with FeNTA: $[hTf]_0$ = 2.11 µM, [PIPES] = 25 mM, [KCl] = 0.2 M, $[HCO_3^-]$ = 10 mM, $[NTA]_0$ = 50 mM, pH = 7.4, 25 °C. The parameters determined with the Solver tool in Microsoft Excel for the calculation of F_{calc} are: $\log(K_{1m})$ = 5.011 ± 0.016, $\log(R)$ = −0.233 ± 0.018, R^2 = 0.9970.

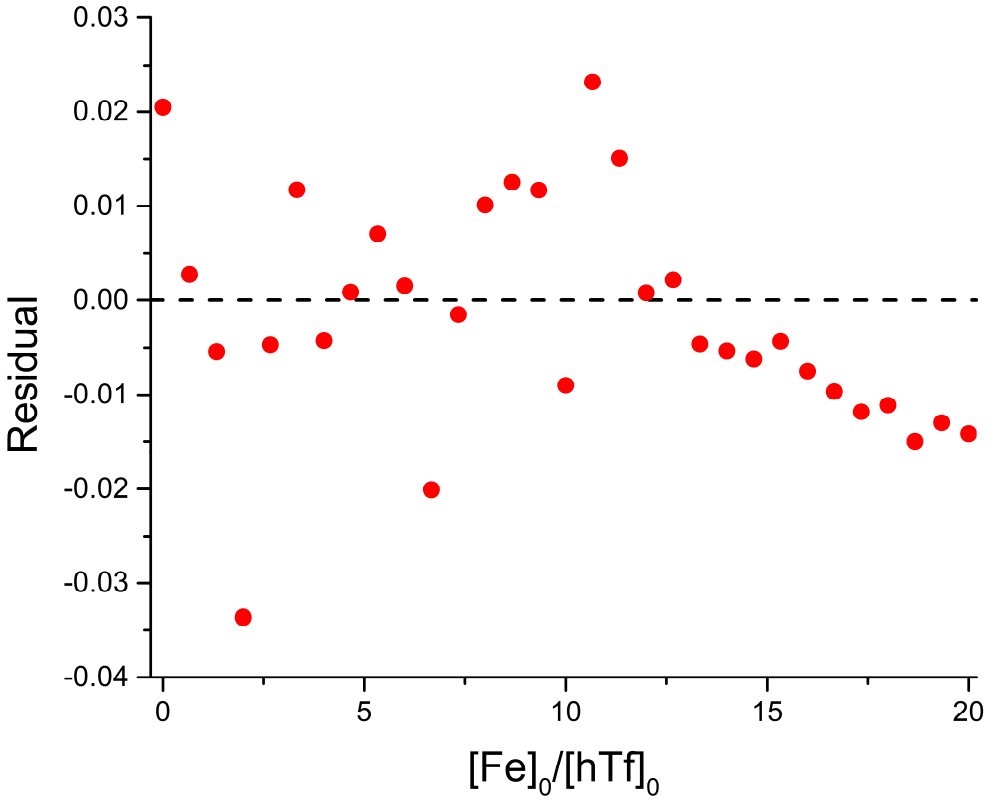

Figure S24. Residuals of fit related to experiment presented in Figure S23 calculated as $F_{calc} - F_{obs}$.

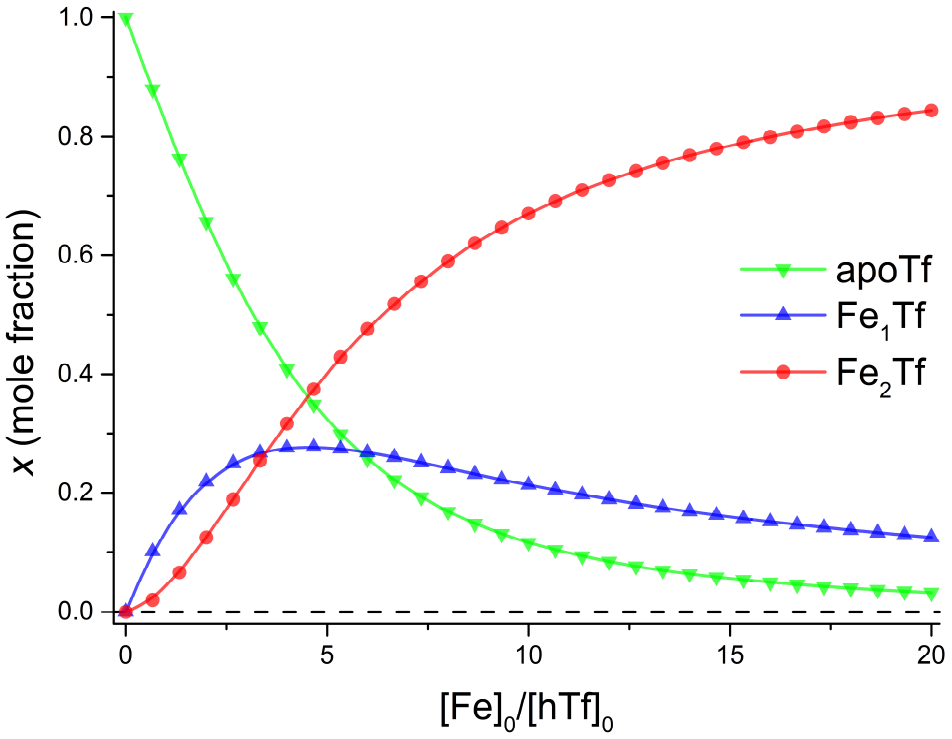

Figure S25. Transferrin speciation related to experiment presented in Figure S23 according to Eqs. 9-11 in the manuscript.

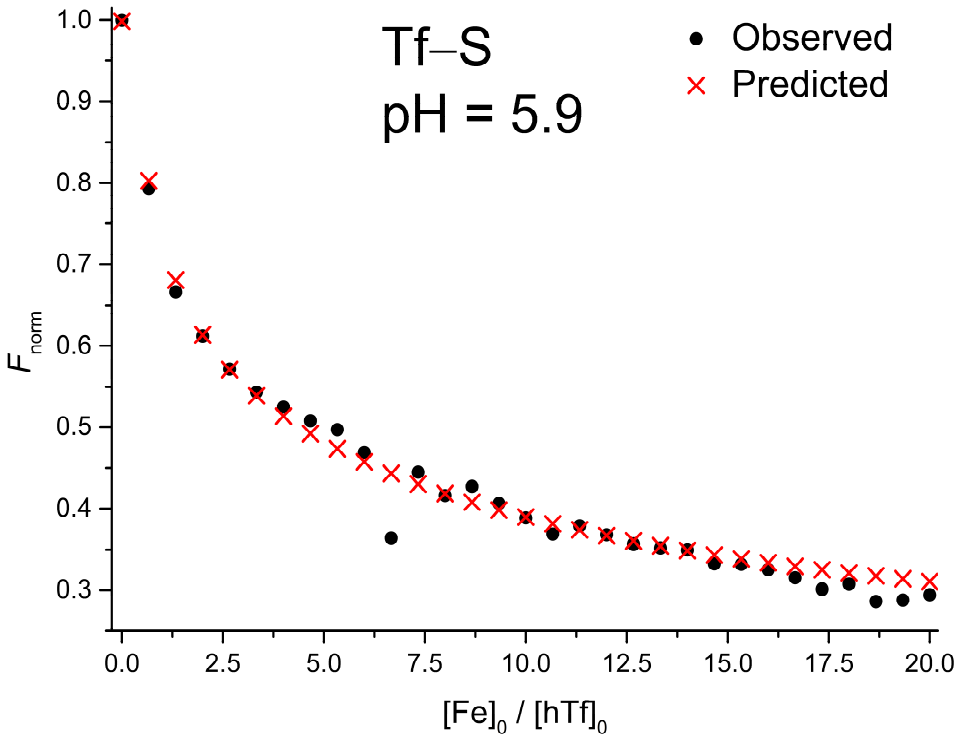

Figure S26. Measured (F_{obs}) and calculated (F_{calc}) normalized fluorescence for the spectrofluorometric titration of desialylated human serum transferrin (Tf–S) with FeNTA: $[hTf]_0$ = 1.70 µM, [PIPES] = 25 mM, [KCl] = 0.2 M, $[HCO_3^-]$ = 10 mM, $[NTA]_0$ = 0.1 mM, pH = 5.9, 25 °C. The parameters determined with the Solver tool in Microsoft Excel for the calculation of F_{calc} are: $\log(K_{1m})$ = 6.425 ± 0.049, $\log(R)$ = 1.569 ± 0.041, R^2 = 0.9863.

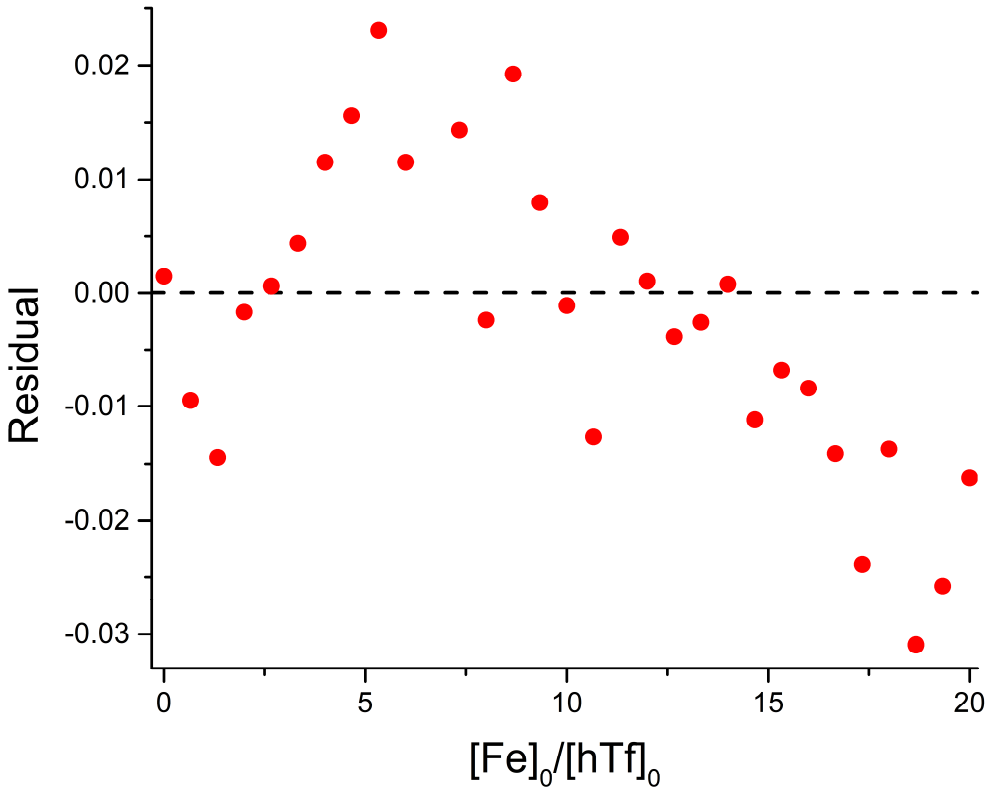

Figure S27. Residuals of fit related to experiment presented in Figure S26 calculated as $F_{calc} - F_{obs}$.

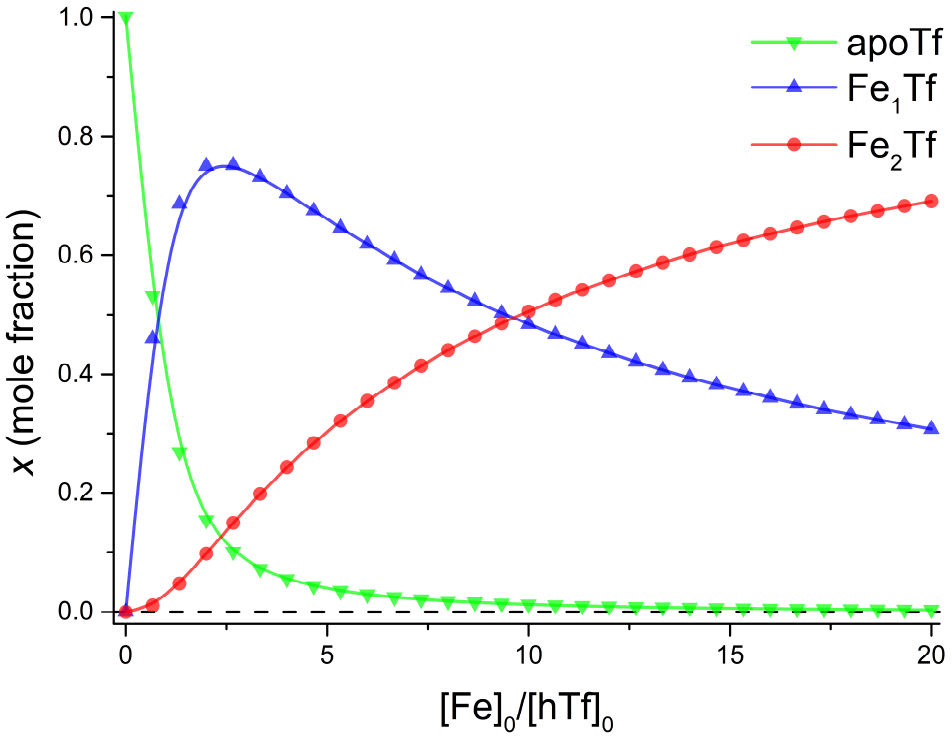

Figure S28. Transferrin speciation related to experiment presented in Figure S26 according to Eqs. 9-11 in the manuscript.

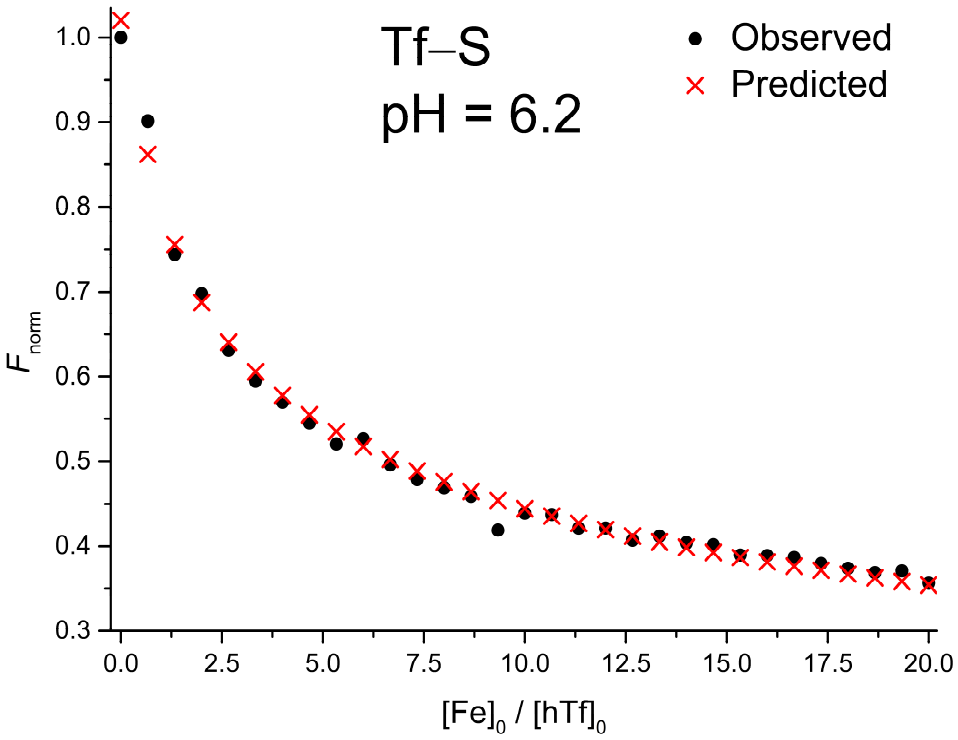

Figure S29. Measured (F_{obs}) and calculated (F_{calc}) normalized fluorescence for the spectrofluorometric titration of desialylated human serum transferrin (Tf–S) with FeNTA: $[hTf]_0$ = 1.60 µM, [PIPES] = 25 mM, [KCl] = 0.2 M, $[HCO_3^-]$ = 10 mM, $[NTA]_0$ = 0.5 mM, pH = 6.2, 25 °C. The parameters determined with the Solver tool in Microsoft Excel for the calculation of F_{calc} are: $\log(K_{1m})$ = 6.141 ± 0.160, $\log(R)$ = 1.406 ± 0.109, R^2 = 0.9930.

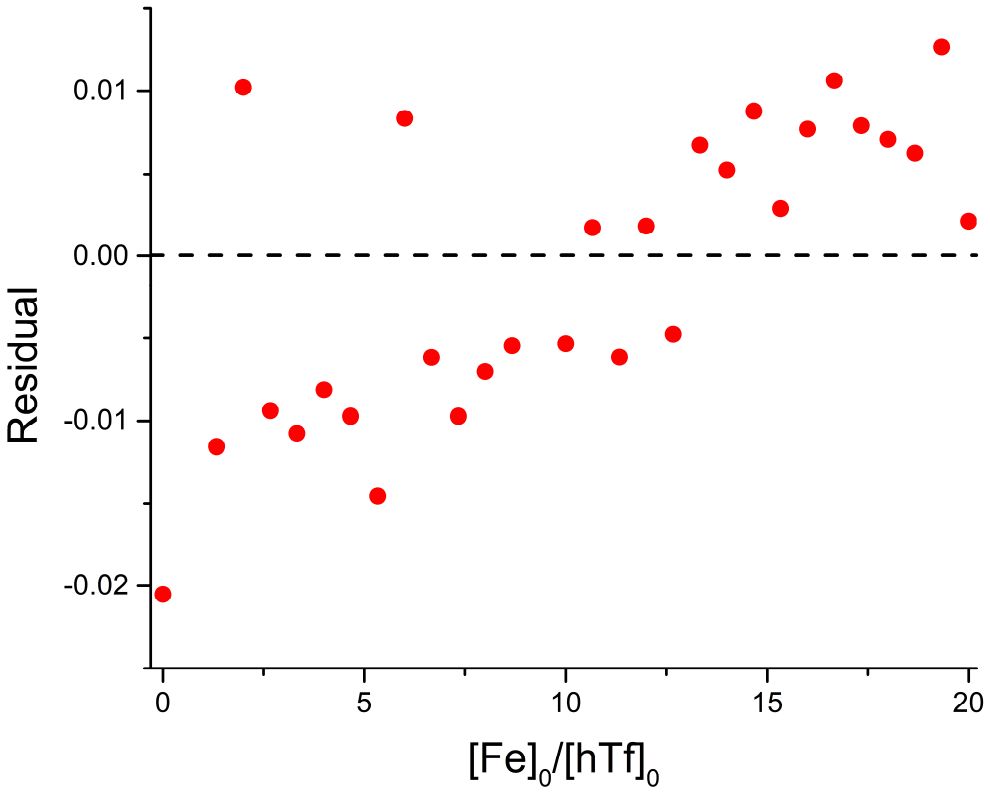

Figure S30. Residuals of fit related to experiment presented in Figure S29 calculated as $F_{calc} - F_{obs}$.

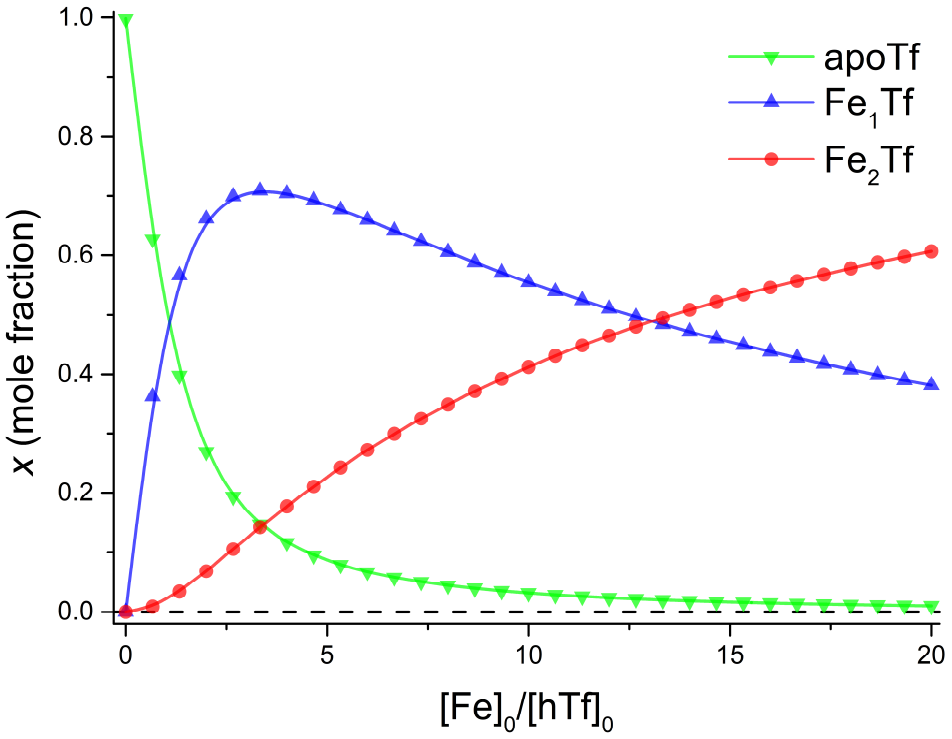

Figure S31. Transferrin speciation related to experiment presented in Figure S29 according to Eqs. 9-11 in the manuscript.

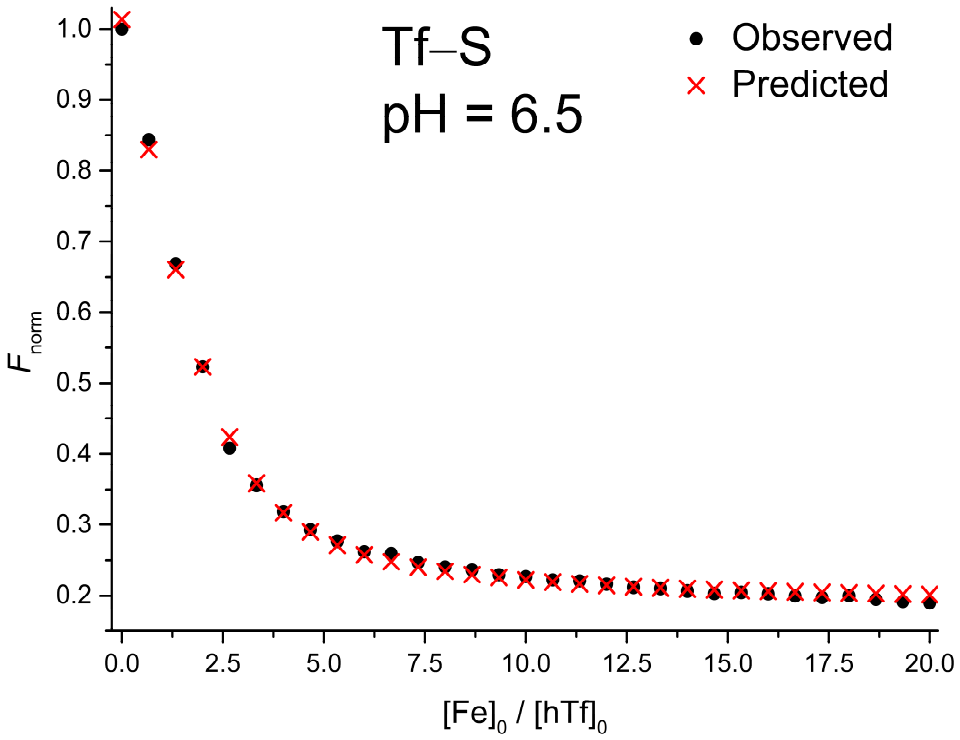

Figure S32. Measured (F_{obs}) and calculated (F_{calc}) normalized fluorescence for the spectrofluorometric titration of desialylated human serum transferrin (Tf–S) with FeNTA: $[hTf]_0$ = 1.61 µM, [PIPES] = 25 mM, [KCl] = 0.2 M, $[HCO_3^-]$ = 10 mM, $[NTA]_0$ = 0.5 mM, pH = 6.5, 25 °C. The parameters determined with the Solver tool in Microsoft Excel for the calculation of F_{calc} are: $\log(K_{1m})$ = 6.090 ± 0.031, $\log(R)$ = 0.136 ± 0.027, R^2 = 0.9987.

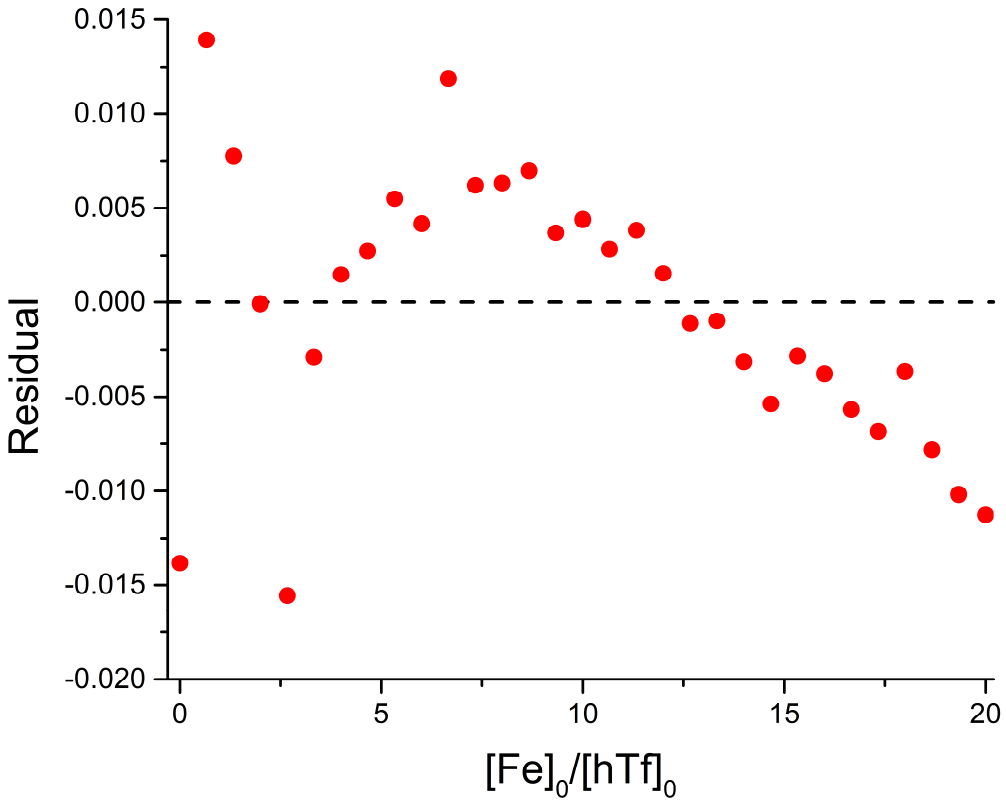

Figure S33. Residuals of fit related to experiment presented in Figure S32 calculated as $F_{calc} - F_{obs}$.

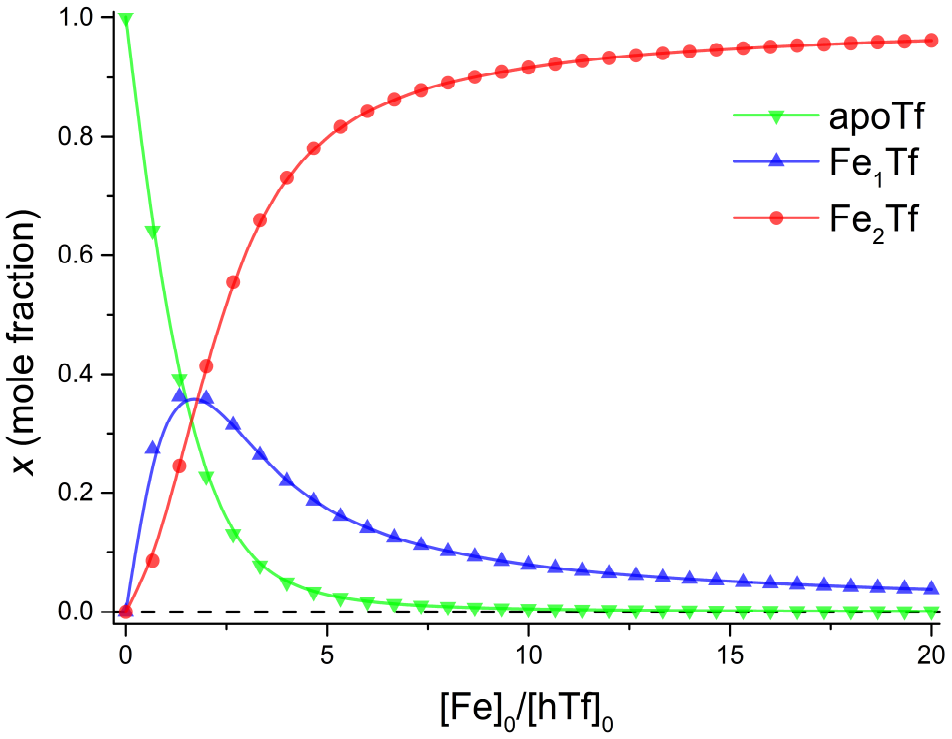

Figure S34. Transferrin speciation related to experiment presented in Figure S32 according to Eqs. 9-11 in the manuscript.

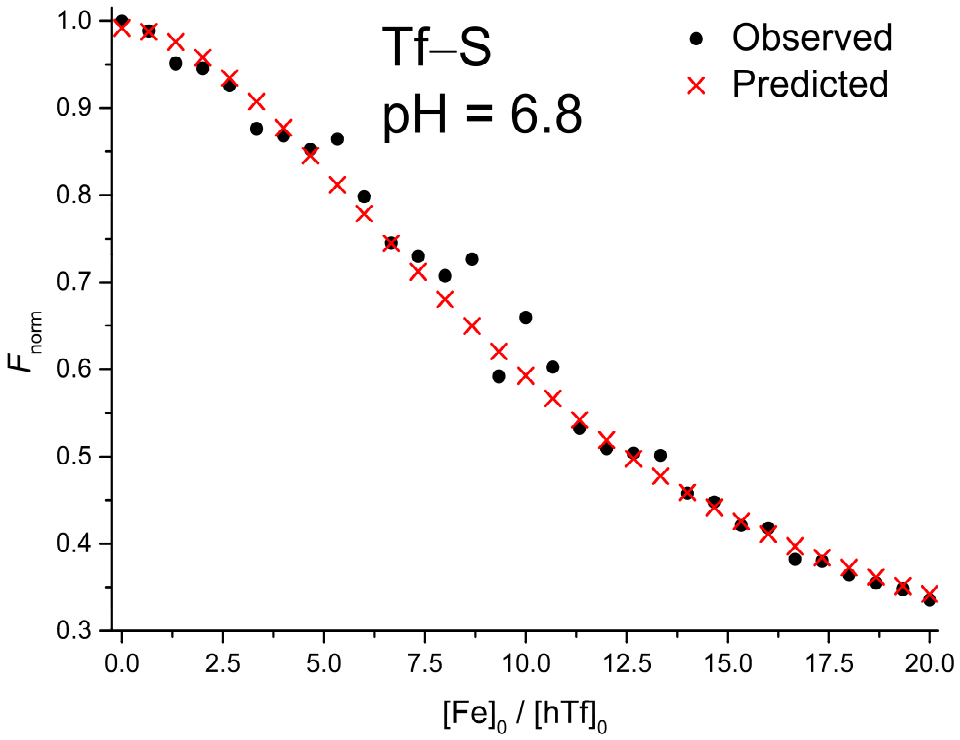

Figure S35. Measured (F_{obs}) and calculated (F_{calc}) normalized fluorescence for the spectrofluorometric titration of desialylated human serum transferrin (Tf–S) with FeNTA: $[hTf]_0$ = 3.84 µM, [PIPES] = 25 mM, [KCl] = 0.2 M, $[HCO_3^-]$ = 10 mM, $[NTA]_0$ = 10 mM, pH = 6.8, 25 °C. The parameters determined with the Solver tool in Microsoft Excel for the calculation of F_{calc} are: $\log(K_{1m})$ = 0.079 ± 0.041, $\log(R)$ = −9.504 ± 0.085, R^2 = 0.9873. At pH = 6.8, the calculated $\log(K_{1m})$ and $\log(R)$ are not meaningful because the second iron ion binding event may dominate and possibly mask the effects of the first binding event, leading to incorrect values of the equilibrium constant.

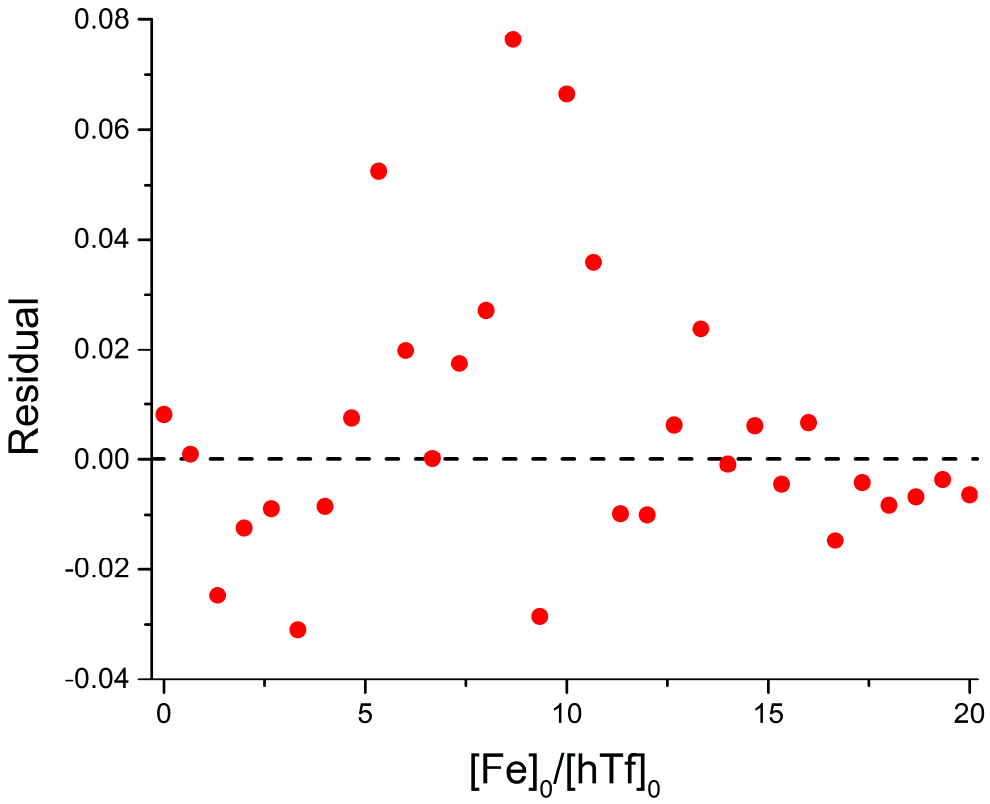

Figure S36. Residuals of fit related to experiment presented in Figure S35 calculated as $F_{calc} - F_{obs}$.

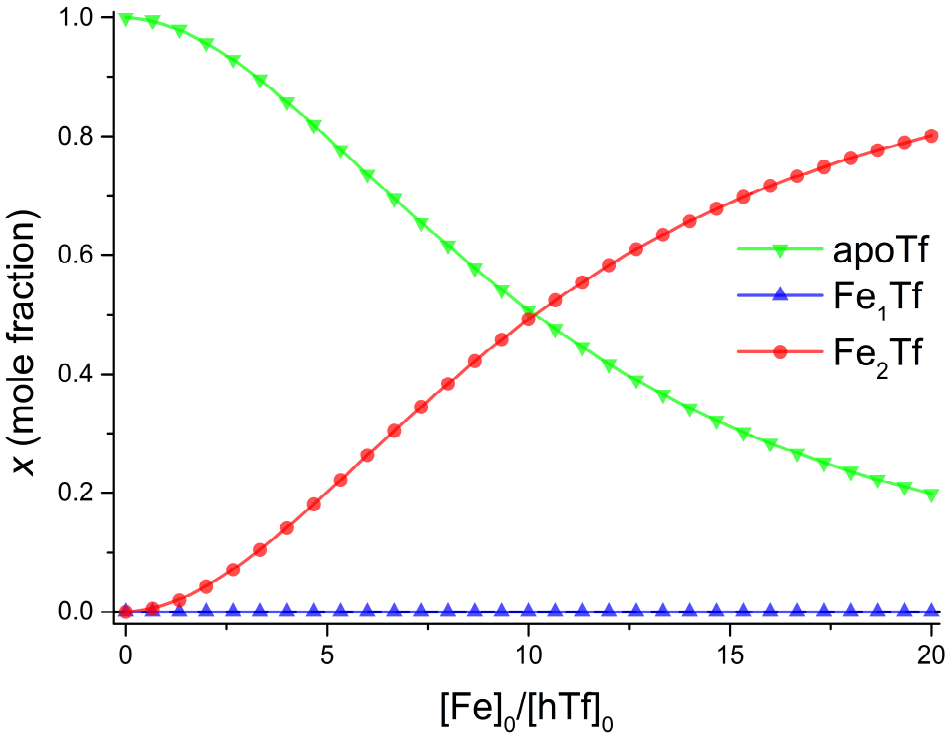

Figure S37. Transferrin speciation related to experiment presented in Figure S35 according to Eqs. 9-11 in the manuscript.

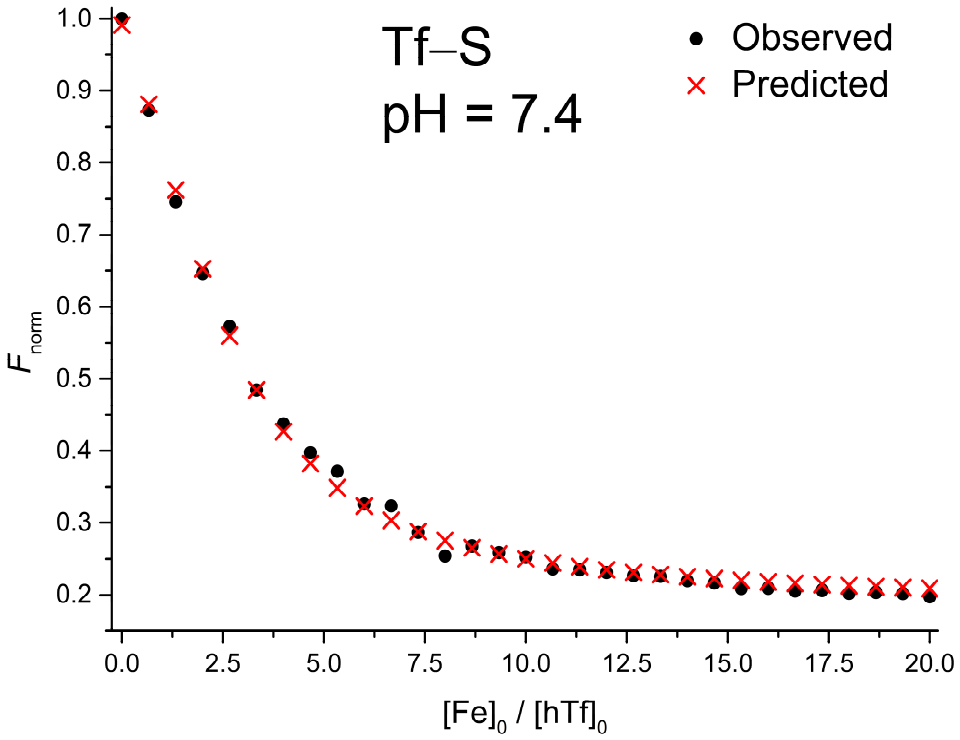

Figure S38. Measured (F_{obs}) and calculated (F_{calc}) normalized fluorescence for the spectrofluorometric titration of desialylated human serum transferrin (Tf–S) with FeNTA: $[hTf]_0$ = 1.54 µM, [PIPES] = 25 mM, [KCl] = 0.2 M, $[HCO_3^-]$ = 10 mM, $[NTA]_0$ = 50 mM, pH = 7.4, 25 °C. The parameters determined with the Solver tool in Microsoft Excel for the calculation of F_{calc} are: $\log(K_{1m})$ = 5.513 ± 0.025, $\log(R)$ = −0.260 ± 0.025, R^2 = 0.9977.

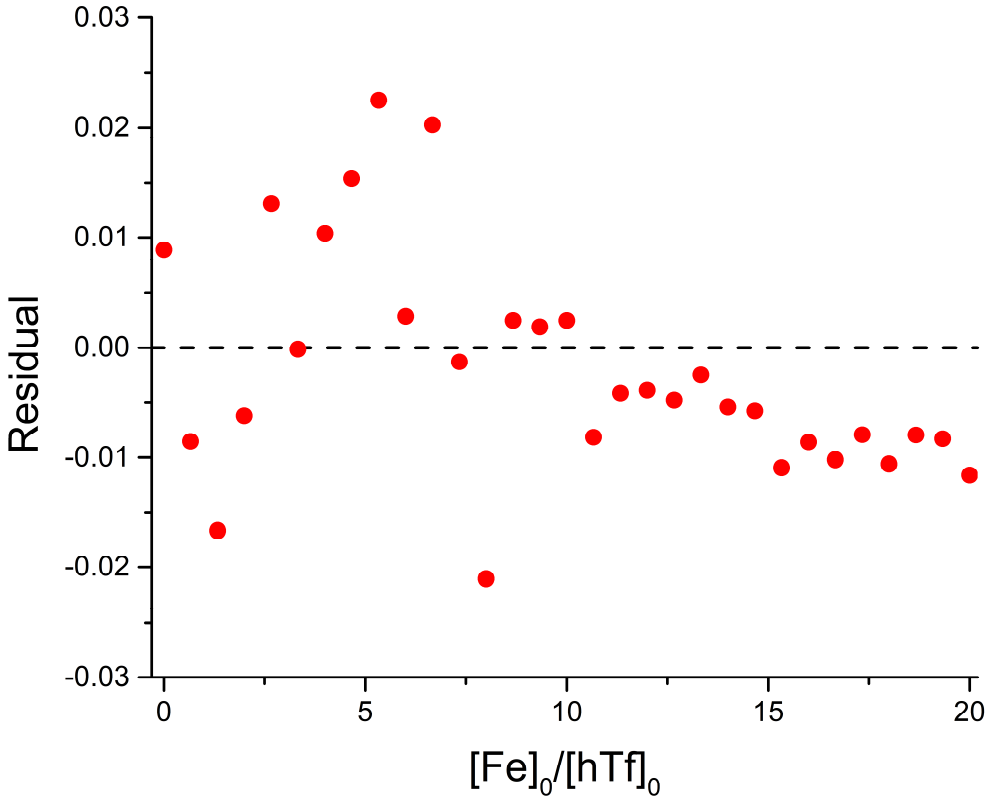

Figure S39. Residuals of fit related to experiment presented in Figure S38 calculated as $F_{calc} - F_{obs}$.

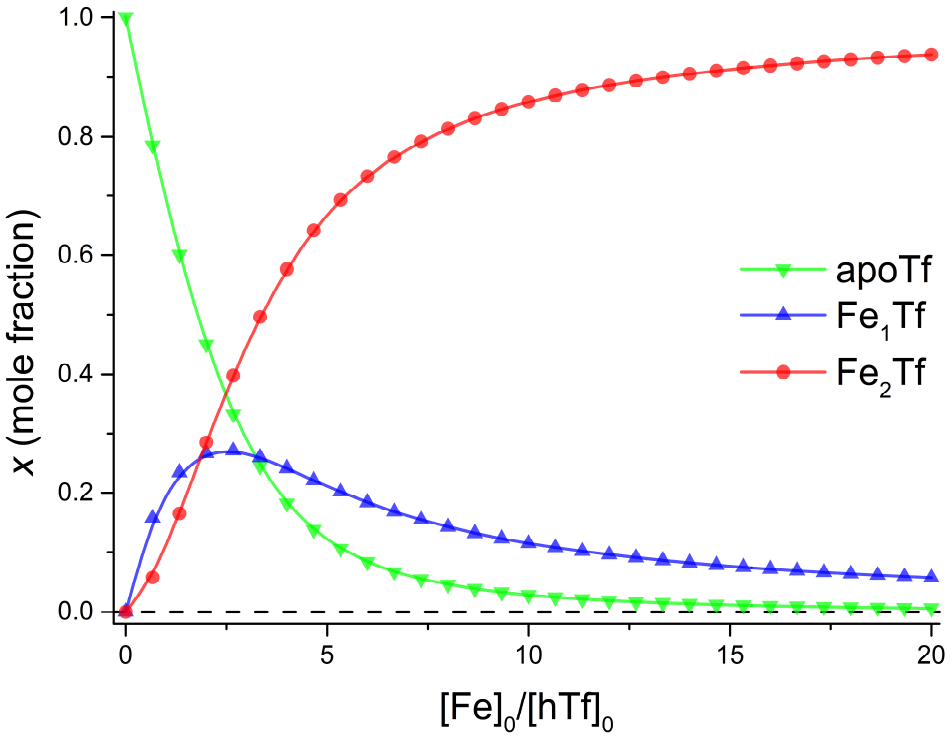

Figure S40. Transferrin speciation related to experiment presented in Figure S38 according to Eqs. 9-11 in the manuscript.

5.4. List of abbreviations

The abbreviations used in this subsection are as follows.

$\log(K_{1m})$ and $\log(K_{2m})$ are logarithmic values of the apparent binding (association) constants K_{1m} and K_{2m} for binding sites 1 and 2, respectively, as defined by Eqs. 3 and 4 in the manuscript (see also Subsection 7.1 in this document).

$\log(R)$ is the logarithmic value of the ratio K_{2m}/K_{1m}. Instead of fitting independent nominal values of the binding constants, the values of $\log(K_{1m})$ and $\log(R)$ were fitted, and the corresponding value of K_{2m} was calculated as $\log(K_{2m}) = \log(K_{1m}) + \log(R)$ (see also Subsection 7.2 of this document).

σ represents the standard deviations of the reported parameters. Details on error propagation can be found in Subsection 7.3 of this document.

R^2 is the coefficient of determination which quantifies the proportion of the variance in the dependent variable that is explained by the independent variable(s) in a regression model.

RSS represents the sum of the squared differences between the observed values (the actual data points) and the predicted values (the values estimated by the regression model).

F(FeTf) is the fractional population of the intermediate complex at half saturation defined by Eq. 19 in the manuscript.

K'_{110} is the pH-dependent conditional constant for the reaction of iron(III) with NTA.

$[NTA]_0$ / M represents fixed concentration of the NTA species within the titration.

Table S3. Output for titrations of native hTf (Tf+S) with FeNTA with carbonate as synergistic anion (25 mM PIPES, 10 mM K_2CO_3, 0.2 M KCl) obtained with the VBA routine for cubic equations with the coefficients given in Eqs. 6-8 in the manuscript using the Jenkins-Traub algorithm in Microsoft Excel 365 (Version 2304, build 16.0.16327.20200, 64-bit).[9–12]

pH	log(K_{1m})	σ	log(R)	σ	log(K_{2m})	σ	R^2	RSS	F(FeTf)	σ	K'_{110}	[NTA]$_0$ / M
7.4	5.011	0.016	−0.233	0.018	5.244	0.008	0.99695	0.00033	0.277	0.002	16.50	0.050
6.8[a]	0.001	<0.001	−9.531	0.013	9.532	0.014	0.99707	0.00053	<0.001	<0.001	15.30	0.010
6.5	5.886	0.032	1.175	0.022	4.711	0.012	0.99375	0.00018	0.659	0.006	14.70	0.0005
6.2	5.809	0.065	1.520	0.041	4.289	0.025	0.99601	0.00021	0.742	0.009	14.11	0.0005
5.9	5.425	0.012	1.541	0.008	3.884	0.007	0.99126	0.00016	0.747	0.001	13.51	0.0001

[a] At pH = 6.8, the calculated log(K_{1m}) and log(R) are not meaningful because the second iron ion binding event may dominate and possibly mask the effects of the first binding event, leading to incorrect values of the equilibrium constant.

Table S4. Output for titrations of desialylated hTf (Tf−S) with FeNTA with carbonate as synergistic anion (25 mM PIPES, 10 mM K_2CO_3, 0.2 M KCl) obtained with the VBA routine for cubic equations with the coefficients given in Eqs. 6-8 in the manuscript using the Jenkins-Traub algorithm in Microsoft Excel 365 (Version 2304, build 16.0.16327.20200, 64-bit).[9–12]

pH	log(K_{1m})	σ	log(R)	σ	log(K_{2m})	σ	R^2	RSS	F(FeTf)	σ	K'_{110}	[NTA]$_0$ / M
7.4	5.512	0.025	−0.261	0.025	5.773	0.008	0.99769	0.00012	0.270	0.004	16.50	0.050
6.8[a]	0.106	0.042	−9.456	0.085	9.561	0.045	0.98731	0.00085	<0.001	<0.001	15.30	0.010
6.5	6.089	0.031	0.135	0.027	5.954	0.009	0.99866	0.00021	0.369	0.006	14.70	0.0005
6.2	6.127	0.160	1.392	0.109	4.735	0.055	0.99301	0.00071	0.713	0.025	14.11	0.0005
6.2[b]	6.110	0.014	1.379	0.012	4.731	0.010	0.99319	0.00073	0.710	0.001	14.11	0.0005
5.9	6.421	0.049	1.564	0.041	4.857	0.011	0.98627	0.00044	0.752	0.008	13.51	0.0001

[a] At pH = 6.8, the calculated log(K_{1m}) and log(R) are not meaningful because the second iron ion binding event may dominate and possibly mask the effects of the first binding event, leading to incorrect values of the equilibrium constant.

[b] Values obtained omitting a single-point outlier from analysis.

6. Equilibria in the FeNTA solutions

The equilibrium reactions[14] related to the dissociation of H_4NTA^+ (in aqueous solutions) are as follows:

$$H^+ + NTA^{3-} \rightleftarrows HNTA^{2-} \qquad \log(K_1) = 9.59 \qquad \text{Eq. S7}$$

$$H^+ + HNTA^{2-} \rightleftarrows H_2NTA^- \qquad \log(K_2) = 2.58 \qquad \text{Eq. S8}$$

$$H^+ + H_2NTA^- \rightleftarrows H_3NTA \qquad \log(K_3) = 1.47 \qquad \text{Eq. S9}$$

$$H^+ + H_3NTA \rightleftarrows H_4NTA^+ \qquad \log(K_4) = 1.00 \qquad \text{Eq. S10}$$

The cumulative concentrations of all NTA species in the solution can be expressed as follows:

$$[NTA]_{total} = [H_4NTA^+] + [H_3NTA] + [H_2NTA^-] + [HNTA^{2-}] + [NTA^{3-}] \qquad \text{Eq. S11}$$

The coefficient[13] α^{-1} for the species NTA^{3-} can be represented as the ratio of $[NTA]_{total}$ to $[NTA^{3-}]$:

$$\alpha^{-1}(NTA^{3-}) = \frac{[NTA]_{total}}{[NTA^{3-}]} \qquad \text{Eq. S12}$$

$$= 1 + [H^+]K_1 + [H^+]^2 K_1 K_2 + [H^+]^3 K_1 K_2 K_3 + [H^+]^4 K_1 K_2 K_3 K_4$$

The following chemical equilibria[14,15] are valid for iron and NTA species in aqueous solutions:

$$Fe^{3+} + NTA^{3-} \rightleftarrows FeNTA \qquad \log(K_{110}) = 15.9 \qquad \text{Eq. S13}$$

$$FeNTA + NTA^{3-} \rightleftarrows Fe(NTA)_2{}^{3-} \qquad \log(K_{120}) = 8.07 \qquad \text{Eq. S14}$$

$$FeNTA \rightleftarrows Fe(OH)NTA^- + H^+ \qquad \log(K_{11-1}) = -4.36 \qquad \text{Eq. S15}$$

$$Fe(OH)NTA^- \rightleftarrows Fe(OH)_2NTA^{2-} + H^+ \qquad \log(K_{11-2}) = -7.58 \qquad \text{Eq. S16}$$

$$Fe(OH)_2NTA^{2-} \rightleftarrows Fe(OH)_3NTA^{3-} + H^+ \qquad \log(K_{11-3}) = -10.72 \qquad \text{Eq. S17}$$

$$2\,FeNTA + 2\,H_2O \rightleftarrows (Fe(OH)NTA)_2{}^{2-} + 2\,H^+ \qquad \log(K_{22-2}) = -6.0 \qquad \text{Eq. S18}$$

The total concentration of iron bound in all complexes with NTA ($[FeNTA]_{total}$) can be expressed as the sum of the individual concentrations of the iron-NTA species:

$$[FeNTA]_{total} = [FeNTA] + [Fe(NTA)_2{}^{3-}] + [Fe(OH)NTA^-] + [Fe(OH)_2NTA^{2-}] \qquad \text{Eq. S19}$$
$$+[Fe(OH)_3NTA^{3-}] + 2\left[(Fe(OH)NTA)_2{}^{2-}\right]$$

The coefficient α^{-1} for the FeNTA species (Eq. S12) can be determined by calculating the ratio of $[FeNTA]_{total}$ to [FeNTA]:

$$\alpha^{-1}(FeNTA) = \frac{[FeNTA]_{total}}{[FeNTA]} = 1 + K_{120}[NTA^{3-}] + \frac{K_{11-1}}{[H^+]} + \frac{K_{11-1}K_{11-2}}{[H^+]^2}$$
$$+ \frac{K_{11-1}K_{11-2}K_{11-3}}{[H^+]^3} + 2\,\frac{K_{22-2}\,K_{110}\,[Fe^{3+}]\,[NTA^{3-}]}{[H^+]^2} \qquad \text{Eq. S20}$$

Since the second and last components of the equation are insignificant under the experimental conditions of this study[1], the above expression simplifies to:

$$\alpha^{-1\prime}(\mathrm{FeNTA}) = \frac{[\mathrm{FeNTA}]_{\mathrm{total}}}{[\mathrm{FeNTA}]} = 1 + \frac{K_{11-1}}{[\mathrm{H}^+]} + \frac{K_{11-1}K_{11-2}}{[\mathrm{H}^+]^2} + \frac{K_{11-1}K_{11-2}K_{11-3}}{[\mathrm{H}^+]^3} \qquad \text{Eq. S21}$$

where $\alpha^{-1\prime}$(FeNTA) is constant at a fixed pH.

The analytical concentration of all NTA-containing species (usually referred to as $[\mathrm{NTA}]_0$) can be written as follows:

$$[\mathrm{NTA}]_0 = [\mathrm{NTA}]_{\mathrm{total}} + [\mathrm{FeNTA}]_{\mathrm{total}} \qquad \text{Eq. S22}$$

For further consideration of transferrin equilibria in Section 7, the reciprocal values of the α^{-1} coefficient can be conveniently written as follows:

$$\alpha(\mathrm{NTA}) = \frac{1}{\alpha^{-1}(\mathrm{NTA}^{3-})} \qquad \text{Eq. S23}$$

$$\alpha'(\mathrm{FeNTA}) = \frac{1}{\alpha^{-1\prime}(\mathrm{FeNTA})} \qquad \text{Eq. S24}$$

7. Equilibrium constants

7.1. Apparent and conditional equilibrium constants

In all the following expressions, charges have been omitted for the sake of clarity. The binding of the iron(III) ion in the form of FeNTA to apoTf can be described as follows:

$$\mathrm{apoTf} + \mathrm{FeNTA} \leftrightarrows \mathrm{FeTf} + \mathrm{NTA} \qquad \text{Eq. S25}$$

This corresponds to an apparent equilibrium constant:

$$K_{1\mathrm{app.}} = \frac{[\mathrm{FeTf}]\,[\mathrm{NTA}]}{[\mathrm{apoTf}]\,[\mathrm{FeNTA}]} \qquad \text{Eq. S26}$$

At fixed pH, a conditional equilibrium constant[13] can be defined:

$$K'_{1\mathrm{app.}} = \frac{[\mathrm{FeTf}]\,[\mathrm{NTA}]_{\mathrm{total}}}{[\mathrm{apoTf}]\,[\mathrm{FeNTA}]_{\mathrm{total}}} \qquad \text{Eq. S27}$$

where $[\mathrm{NTA}]_{\mathrm{total}}$ and $[\mathrm{FeNTA}]_{\mathrm{total}}$ are defined in Eqs. S11 and S19, respectively.

By combining Eq. S13 with S23 and S24, a pH-dependent conditional equilibrium constant for the association of Fe and NTA can also be formulated as follows:

$$K'_{110} = \frac{[\mathrm{FeNTA}]_{\mathrm{total}}}{[\mathrm{Fe}]\,[\mathrm{NTA}]_{\mathrm{total}}} = \frac{[\mathrm{FeNTA}]\,\alpha(\mathrm{NTA})}{[\mathrm{Fe}][\mathrm{NTA}]\,\alpha'(\mathrm{FeNTA})} = \frac{K_{110}\alpha(\mathrm{NTA})}{\alpha'(\mathrm{FeNTA})} \qquad \text{Eq. S28}$$

The Eq. S28 can be rearranged to:

$$\frac{[\mathrm{NTA}]_{\mathrm{total}}}{[\mathrm{FeNTA}]_{\mathrm{total}}} = \frac{\alpha'(\mathrm{FeNTA})}{[\mathrm{Fe}]\,K_{110}\,\alpha(\mathrm{NTA})} \qquad \text{Eq. S29}$$

The interaction between the unbound iron(III) ion and apoTf can be described as:

$$\mathrm{Fe} + \mathrm{apoTf} \leftrightarrows \mathrm{FeTf} \qquad \text{Eq. S30}$$

The corresponding equilibrium constant is defined as follows:

$$K'_{1\mathrm{m}} = \frac{[\mathrm{FeTf}]}{[\mathrm{Fe}]\,[\mathrm{apoTf}]} \qquad \text{Eq. S31}$$

Substituting Eq. S29 into Eq. S27 and combining with Eq. S31 gives:

$$K'_{1\mathrm{app.}} = \frac{K'_{1\mathrm{m}}\,\alpha'(\mathrm{FeNTA})}{K_{110}\,\alpha(\mathrm{NTA})} \qquad \text{Eq. S32}$$

The conditional equilibrium constant for the binding of the first iron(III) ion to apoTf can then be expressed as follows:

$$K'_{1\mathrm{m}} = K'_{1\mathrm{app.}}\, K'_{110} \qquad \text{Eq. S33}$$

The logarithmic representation of Eq. S33 is as follows:

$$\log(K'_{1\mathrm{m}}) = \log\left(K'_{1\mathrm{app.}}\right) + \log(K'_{110}) \qquad \text{Eq. S34}$$

The expression for the binding of the second iron(III) ion in the form of FeNTA to FeTf can be written as follows:

$$\mathrm{FeTf} + \mathrm{FeNTA} \leftrightarrows \mathrm{Fe_2Tf} + \mathrm{NTA} \qquad \text{Eq. S35}$$

The corresponding conditional equilibrium constant (similar to Eq. S27) can be written as follows:

$$K'_{2\mathrm{app.}} = \frac{[\mathrm{Fe_2Tf}]\,[\mathrm{NTA}]_{\mathrm{total}}}{[\mathrm{FeTf}]\,[\mathrm{FeNTA}]_{\mathrm{total}}} \qquad \text{Eq. S36}$$

Similar to Eq. S30, the binding of the unbound iron(III) ion to FeTf can be written as follows:

$$\mathrm{Fe} + \mathrm{FeTf} \leftrightarrows \mathrm{Fe_2Tf} \qquad \text{Eq. S37}$$

This corresponds to an equilibrium constant:

$$K'_{2m} = \frac{[\mathrm{Fe_2Tf}]}{[\mathrm{Fe}]\,[\mathrm{FeTf}]} \qquad \text{Eq. S38}$$

Again, substituting Eq. S29 into Eq. S36 and combining with Eq. S38 gives the following:

$$K'_{2\mathrm{app.}} = \frac{K'_{2\mathrm{m}}\,\alpha(\mathrm{FeNTA})}{K_{110}\,\alpha(\mathrm{NTA})} \qquad \text{Eq. S39}$$

$$K'_{2\mathrm{m}} = K'_{2\mathrm{app.}}\, K'_{110} \qquad \text{Eq. S40}$$

$$\log K'_{2\mathrm{m}} = \log K'_{2\mathrm{app.}} + \log K'_{110} \qquad \text{Eq. S41}$$

As Harris and Pecoraro have noted[16], the values of $K'_{1\mathrm{m}}$ and $K'_{2\mathrm{m}}$ are conditional constants, valid only for a given pH of the solution and a given HCO_3^- concentration.

7.2. Data fitting

The concentration of free iron (Eq. 5 in the manuscript) was calculated for each data point with the initial values of $\log(K_{1m})$ and $\log(R)$ using the VBA cubic equation routine (with the coefficients from Eqs. 6-8 in the manuscript) using the Jenkins-Traub algorithm in Microsoft Excel 365 (version 2304, build 16.0.16327.20200, 64-bit).[17–20] The differences $F_{calc} - F_{norm}$ were squared and summed for all data points to obtain the residual sum of squares (RSS). Inverse-variance weighting ($1/\sigma^2$, where σ^2 is the variance of the fluorescence measurements in triplicate) was used to calculate the RSS value to optimize the accuracy of the fitting process. This approach effectively minimizes the impact of random errors in the dataset and ensures that the fitting algorithm highlights the most reliable and reproducible data points. The RSS value was then minimized through an iterative procedure to obtain the optimal set of binding constants using the solver tool in Microsoft Excel.

Several strategies were used to improve the convergence of the fit: (i) normalized fluorescence values were used instead of raw values, (ii) instead of fitting independent nominal values of the binding constants, the values of $\log(K_{1m})$ and $\log(R)$ were fitted, and the corresponding value of K_{2m} was calculated as $\log(K_{2m}) = \log(K_{1m}) + \log(R)$, and (iii) the data were randomized before fitting. The values of $\log(K_{1m})$ were used to ensure positive non-zero values of K_{1m}. Randomization of data points was performed by calculating (pseudo-)random values using the function RAND() and sorting by the obtained values.

7.3. Error propagation

7.3.1. Fluorescence measurements

The standard deviation of the respective replicated (and baseline-corrected) fluorescence titration point was calculated by considering both the contributions of the standard deviation of the measured sample and the standard deviation of the baseline, as shown in Eqs. S42, S43, and S44.

$$s(F_{\mathrm{BASELINE-CORRECTED}})_i^{\,2} = s(F_{\mathrm{MEASURED}})_i^{\,2} + s(F_{\mathrm{BASELINE}})_i^{\,2} \qquad \text{Eq. S42}$$

$$s(F_{\mathrm{BASELINE-CORRECTED}})_i = \sqrt{s(F_{\mathrm{MEASURED}})_i^{\,2} + s(F_{\mathrm{BASELINE}})_i^{\,2}} \qquad \text{Eq. S43}$$

As mentioned previously, the fluorescence was IFE-corrected using the ZINFE method (F_Z, Eq. S5). The exponential term, which is a function of the geometric parameters, can be denoted as a single term N[4], as shown in Eq. S44:

$$F_Z = F_{0(z1)} \left(\frac{F_{0(z1)}}{F_{0(z2)}}\right)^N \qquad \text{Eq. S44}$$

The procedure for calculating the equilibrium constants requires the determination of weighting coefficients for fluorescence measurements. Since weighting factors with inverse variance are used for the fitting procedure, the variance of the IFE-corrected, baseline-corrected fluorescence must be estimated. To estimate the error of the IFE-corrected fluorescence, the partial derivatives were calculated according to Eqs. S45 and S46:

$$\frac{\partial F_Z(F_{0(z1)},F_{0(z2)},N)}{\partial F_{0(z1)}} = (N+1)\left(\frac{F_{0(z1)}}{F_{0(z2)}}\right)^N \qquad \text{Eq. S45}$$

$$\frac{\partial F_Z(F_{0(z1)},F_{0(z2)},N)}{\partial F_{0(z2)}} = -N\left(\frac{F_{0(z1)}}{F_{0(z2)}}\right)^{(1+N)} \qquad \text{Eq. S46}$$

$$\frac{\partial F_Z(F_{0(z1)},F_{0(z2)},N)}{\partial N} = F_{0(z1)}\left(\frac{F_{0(z1)}}{F_{0(z2)}}\right)^N \ln\left(\frac{F_{0(z1)}}{F_{0(z2)}}\right) \quad \text{Eq. S47}$$

The error of the exponent N results primarily from inaccuracies in the liquid height within the microplate well, since the internal geometrical parameters of the microplate reader, the dimensions of the microplate and the z-positions are precisely defined (*e.g.* the z-positions are specified with an accuracy of up to 1 µm). $F_{0(z1)}$ and $F_{0(z2)}$ represent fluorescence values measured at two different z-positions.

The variance, including the correlation, is determined as described in Eq. S48.

$$s_{F_Z}{}^2 = \left(\frac{\partial F_Z}{\partial F_{0(z1)}} s_{F_{0(z1)}}\right)^2 + \left(\frac{\partial F_Z}{\partial F_{0(z2)}} s_{F_{0(z2)}}\right)^2 + \left(\frac{\partial F_Z}{\partial N} s_N\right)^2$$

$$-2\mathrm{cov}\left(F_{0(z1)}, F_{0(z2)}\right)(N+1)N\left(\frac{F_{0(z1)}}{F_{0(z2)}}\right)^N\left(\frac{F_{0(z1)}}{F_{0(z2)}}\right)^{(1+N)} \quad \text{Eq. S48}$$

The standard deviation of the IFE-corrected fluorescence is calculated as the square root of the variance obtained by Eq. S48.

7.3.2. Equilibrium constants

The values of $\log(K_{1m})$ and $\log(R)$ were determined by iterative fitting while solving the equations for mass conservation, as described in the manuscript. The uncertainties in the fitting parameters $\log(K_{1m})$ and $\log(R)$ were determined using the "jackknife" method by omitting one data point at a time from the RSS calculation and fitting all remaining points to obtain a new set of parameters.[21] For each omitted titration point, $\log(K_{1m})$ and $\log(R)$ were determined, and the average value was calculated.

Standard deviations are first approximated using Eqs. S49 and S50:

$$s(K_{1m}) = \sqrt{\frac{1}{n-1}\sum_{i=1}^{n}(K_{1mi} - \bar{K}_{1m})} \quad \text{Eq. S49}$$

$$s(R) = \sqrt{\frac{1}{n-1}\sum_{i=1}^{n}(R_i - \bar{R})} \quad \text{Eq. S50}$$

Where K_{1mi} and R_i are i-th values of K_{1m} and R, n is the number of titration points used for the calculation.

The above expressions do not take into account the systematic errors resulting from the slight uncertainties in the concentrations of transferrin and FeNTA due to the uncertainties in their respective molar absorbance coefficients. Due to the difficulty in propagating the error through the iterative procedure, we performed a sensitivity analysis to assess the impact of concentration variations on the uncertainties of the calculated equilibrium constants.[22] Concentrations were adjusted to both higher (H) and lower (L) estimates, resulting in four scenarios: LL, LH, HL, HH. These adjustments are based on the addition or subtraction of one standard deviation from the average concentrations. "L" refers to the lower estimate of a concentration calculated by subtracting one standard deviation from the mean, while "H" refers to the higher estimate obtained by adding one standard deviation to the mean. K_{1m} and R were recalculated for each scenario across all titration points, expanding the data set by a factor of four.

Accordingly, the standard deviations were calculated using this (fourfold) extended data set. They were then rescaled to the original data set, assuming that the relative standard deviation remains consistent in both the extended and the original data set. Therefore, the reported K_{1m} and R values are based on the original, unadjusted concentrations, but the associated uncertainties were estimated as described above.

The K_{2m} is calculated as shown in Eq. S51.

$$K_{2m} = K_{1m}R \quad \text{Eq. S51}$$

Therefore, the error propagation for K_{2m} (including the covariance) is described in Eq. S52.

$$s(K_{2m}) = \sqrt{\left(\frac{\partial K_{2m}}{\partial K_{1m}}\right)^2 s(K_{1m})^2 + \left(\frac{\partial K_{2m}}{\partial R}\right)^2 s(R)^2 + 2\frac{\partial K_{2m}}{\partial K_{1m}}\frac{\partial K_{2m}}{\partial R}\mathrm{COV}(K_{1m}, R)} \quad \text{Eq. S52}$$

The partial derivatives are calculated as shown in the following equations:

$$\frac{\partial K_{2m}}{\partial K_{1m}} = R \quad \text{Eq. S53}$$

$$\frac{\partial K_{2m}}{\partial R} = K_{1m} \quad \text{Eq. S54}$$

For logarithmic transformations of: K_{1m}, R, K_{2m}, the uncertainties in their logarithmic expressions can be represented as shown below.

$$s(\log(X)) = \frac{s(X)}{\ln(10)X} \quad \text{Eq. S55}$$

where X represents either: K_{1m}, R, or K_{2m}.

From K_{1m} and K_{2m}, the conditional thermodynamic binding constants K'_{1m} and K'_{2m} are calculated as given in Eq. S56 and Eq. S57.

$$K'_{1m} = K_{1m}K'_{110} \quad \text{Eq. S56}$$

$$K'_{2m} = K_{2m}K'_{110} \quad \text{Eq. S57}$$

The error propagation is estimated as shown below.

$$s(K'_{1m}) = \sqrt{s^2(K_{1m}) + s^2(K'_{110})} \quad \text{Eq. S58}$$

$$s(K'_{2m}) = \sqrt{s^2(K_{2m}) + s^2(K'_{110})} \quad \text{Eq. S59}$$

The standard deviation for the logarithmically transformed pH-dependent conditional constant, $\log(K'_{110})$, is set to 0.01, as previously reported.[14,23]

7.3.3. Other calculations

Error propagation for the fractional population of the intermediate complex at 50% saturation, *F*(FeTf), defined by Eq. 19 in the manuscript, was performed using the following equations:

$$\frac{\partial F(\mathrm{FeTf})}{\partial K_{1\mathrm{m}}} = \frac{\partial\left(\frac{K_{1\mathrm{m}}}{2\sqrt{K_{1\mathrm{m}}K_{2\mathrm{m}}}+K_{1\mathrm{m}}}\right)}{\partial K_{1\mathrm{m}}} = \frac{\sqrt{K_{1\mathrm{m}}K_{2\mathrm{m}}}}{\left(2\sqrt{K_{1\mathrm{m}}K_{2\mathrm{m}}}+K_{1\mathrm{m}}\right)^2} \quad \text{Eq. S60}$$

$$\frac{\partial F(\mathrm{FeTf})}{\partial K_{2\mathrm{m}}} = \frac{\partial\left(\frac{K_{2\mathrm{m}}}{2\sqrt{K_{1\mathrm{m}}K_{2\mathrm{m}}}+K_{1\mathrm{m}}}\right)}{\partial K_{2\mathrm{m}}} = -\frac{{K_{1\mathrm{m}}}^2}{\sqrt{K_{1\mathrm{m}}K_{2\mathrm{m}}}\left(2\sqrt{K_{1\mathrm{m}}K_{2\mathrm{m}}}+K_{1\mathrm{m}}\right)^2} \quad \text{Eq. S61}$$

$$s(F(\mathrm{FeTf})) = \sqrt{\left(s(K_{1\mathrm{m}})\frac{\partial F(\mathrm{FeTf})}{\partial K_{1\mathrm{m}}}\right)^2 + \left(s(K_{2\mathrm{m}})\frac{\partial F(\mathrm{FeTf})}{\partial K_{2\mathrm{m}}}\right)^2 + 2\mathrm{COV}(K_{1\mathrm{m}}, K_{2\mathrm{m}})\frac{\partial F(\mathrm{FeTf})}{\partial K_{1\mathrm{m}}}\frac{\partial F(\mathrm{FeTf})}{\partial K_{2\mathrm{m}}}} \quad \text{Eq. S62}$$

Error propagation for the site preference factor f_{sp}, defined as $K_{1m}/K_{2m} = K'_{1m}/K'_{2m}$, was performed using the following equations:

$$\frac{\partial f_{\mathrm{sp}}}{\partial K_{1\mathrm{m}}} = \frac{1}{K_{2\mathrm{m}}} \quad \text{Eq. S63}$$

$$\frac{\partial f_{\mathrm{sp}}}{\partial K_{2\mathrm{m}}} = -\frac{K_{1\mathrm{m}}}{{K_{2\mathrm{m}}}^2} \quad \text{Eq. S64}$$

$$s(f_{\mathrm{sp}}) = \sqrt{\left(s(K_{1\mathrm{m}})\frac{\partial f_{\mathrm{sp}}}{\partial K_{1\mathrm{m}}}\right)^2 + \left(s(K_{2\mathrm{m}})\frac{\partial f_{\mathrm{sp}}}{\partial K_{2\mathrm{m}}}\right)^2 + 2\mathrm{COV}(K_{1\mathrm{m}}, K_{2\mathrm{m}})\frac{\partial f_{\mathrm{sp}}}{\partial K_{1\mathrm{m}}}\frac{\partial f_{\mathrm{sp}}}{\partial K_{2\mathrm{m}}}} \quad \text{Eq. S65}$$

8. Statistical analysis

For the *t*-test to work well, the data must fulfill the conditions of independence, normality, and homoscedasticity of errors. While it is known that the *t*-test is robust to small deviations from normality, it has been shown that heteroscedasticity, skewness, and outliers affect both the type I error and power. Therefore, a more robust Satterthwaite's approximate *t*-test was used when comparing the means of two independent groups with unequal variances. A conventional *t*-test assumes that the variances in both groups are equal. Satterthwaite's approach provides a more accurate and robust solution by estimating the degrees of freedom based on the sample variances of the two groups. This modification helps to account for the unequal variances and improves the validity of the *t*-test. By adjusting the degrees of freedom, Satterthwaite's approximate *t*-test ensures that the *p*-value and confidence intervals of the test are more accurate, leading to more reliable inferences about the population means.[24]

Specifically, the test statistic *d* is calculated as:

$$d = \frac{\bar{x}_1 - \bar{x}_2}{\sqrt{\frac{{s_1}^2}{n_1} + \frac{{s_2}^2}{n_2}}} \qquad \text{Eq. S66}$$

where $\bar{x}_1$ and $\bar{x}_2$ are the mean values of the parameters obtained from the measurements, $n_1 = n_2 = 3$ is the number of replicate measurements, and s_1^2 and s_2^2 are the variances of the parameters.

The approximate degrees of freedom are then calculated as follows:

$$df = \frac{\left[\frac{{s_1}^2}{n_1} + \frac{{s_2}^2}{n_2}\right]^2}{\frac{\left({s_1}^2/n_1\right)^2}{n_1 - 1} + \frac{\left({s_2}^2/n_1\right)^2}{n_2 - 1}} \qquad \text{Eq. S67}$$

Using the same values for *n* and s^2.

In the context of Satterthwaite's approximate *t*-test, the null hypothesis states that there is no significant difference between the mean values of the two independent groups to be compared. The obtained *p*-values correspond to the probability that the observed differences are due to random error only, and the values of $p \leq \alpha$ were determined to be statistically significant. The chosen significance level of $\alpha = 0.05$ means that there is a 5% risk of inferring a statistically significant difference, even though there is no actual difference (type I error).

Statistical significance of the observed differences is encoded as $p < 0.001$ (***), $p < 0.01$ (**), $p < 0.025$ (*), $p < 0.1$ (').

8.1. Satterthwaite's approximate *t*-test

Table S5. Summary of Satterthwaite's approximate *t*-test for the values of the conditional macroscopic constants (log(K_1'$_m$) and log(K_2'$_m$)). All values and calculated statistics are archived and available for reference.[25]

pH	log(K_1'$_m$)				log(K_2'$_m$)			
	d	*df*	*p*-value	significance	*d*	*df*	*p*-value	significance
7.4	26.3	3.59	<0.001	***	49.7	4.00	<0.001	***
6.8[a]	4.12	2.22	0.054	·	1.06	2.54	0.400	
6.5	7.50	4.00	0.002	**	105	3.98	<0.001	***
6.2[b]	3.17	2.64	0.087	·	12.4	3.00	0.001	**
5.9	32.9	2.41	<0.001	***	87.7	3.82	<0.001	***

[a] At pH = 6.8, the calculated log(K_{1m}) and log(R) are not meaningful because the second iron ion binding event may dominate and possibly mask the effects of the first binding event, leading to incorrect values of the equilibrium constant.

[b] If a significant single-point outlier is omitted from the titration of Tf−S, the following adjusted values result: d = 7.76, df = 2.27, p-value = 0.016205, significance = *, for log(K_1'$_m$) and: d = 25.2, df = 3.00, p-value = 0.000137, significance = ***, for log(K_2'$_m$).

Table S6. Summary of Satterthwaite's approximate *t*-test for the fractional population of the intermediate at half saturation (F(FeTf)). All values and calculated statistics are archived and are available for reference.[25]

pH	F(FeTf)			
	d	*df*	*p*-value	significance
7.4	2.71	2.94	0.113	
6.8[a]	0.00	4.00	1.000	*
6.5	59.2	4.00	<0.001	***
6.2[b]	1.89	2.51	0.199	
5.9	1.07	2.06	0.395	

[a] At pH = 6.8, the calculated log(K_{1m}) and log(R) are not meaningful because the second iron ion binding event may dominate and possibly mask the effects of the first binding event, leading to incorrect values of the equilibrium constant.

[b] If a significant single-point outlier is omitted from the titration of Tf−S, the following adjusted values result: d = 6.12, df = 2.05, p-value = 0.026, significance = *.

9. Additional information

Table S7. Results of the mathematical model of the observed pH-dependence of the binding constants, defined by Chasteen and Williams.[26] f_{sp} is the site preference factor defined as K_{1m}/K_{2m}

	Tf+S		Tf−S	
pH	f_{sp}	f_{sp} (simulated)	f_{sp}	f_{sp} (simulated)
7.4	0.58	0.58	0.55	0.55
6.5	15.0	15.0	1.36	1.36
6.2	33.1	33.1	24.7	24.7
5.9	34.8	34.8	36.6	36.6

[a] If a significant single-point outlier is omitted from the titration of Tf−S, the following adjusted values result: f_{sp} = 23.9, f_{sp} (simulated) = 23.9.

Table S8. Parameters of the mathematical model of the observed pH-dependence of the binding constants, defined by Chasteen and Williams.[26]

Parameter	Tf+S	Tf−S
$f_{sp,\,min}$	0.58	0.55
$f_{sp,\,max}$	34.8	36.9
pK'_a	6.47	6.25
n'	4.73	6.45
R^2	>0.999	>0.999

[a] If a significant single-point outlier is omitted from the titration of Tf−S, the following adjusted values result: pK'_a = 6.24, n' = 6.32.

10. Conflicts of interest

There are no conflicts of interest to declare.

11. Acknowledgements

This work was supported by funding from the Croatian Science Foundation grant UIP-2017-05-9537 – Glycosylation as a factor in the iron transport mechanism of human serum transferrin (GlyMech). Valentina Borko was additionally financed by the Croatian Science Foundation grant DOK-2018-09-1042. Additional support was provided by the European Regional Development Fund grants for 'Strengthening of Scientific Research and Innovation Capacities of the Faculty of Pharmacy and Biochemistry at the University of Zagreb' (KK.01.1.1.02.0021), 'Development of methods for production and labelling of glycan standards for molecular diagnostics' (KK.01.1.1.07.0055) and 'Scientific center of excellence for personalized health care' (KK.01.1.1.01.0010).

12. Notes and references

1 V. Borko, T. Friganović and T. Weitner, *Anal. Methods*, 2023, **15**, 6499–6513.
2 T. Friganović, A. Tomašić, T. Šeba, I. Biruš, R. Kerep, V. Borko, D. Šakić, M. Gabričević and T. Weitner, *Heliyon*, 2021, **7**, e08030.
3 T. Friganović, V. Borko and T. Weitner, *Maced. Pharm. Bull.*, 2022, **68**, 415–416.
4 T. Weitner, T. Friganović and D. Šakić, *Anal. Chem.*, 2022, **94**, 7107–7114.
5 J. R. Lakowicz, Ed., in *Principles of Fluorescence Spectroscopy*, Springer US, Boston, MA, 2006, pp. 27–61.
6 T. Friganović and T. Weitner, *Anal. Chem.*, 2023, **95**, 13036–13045.
7 S. Kumar Panigrahi and A. Kumar Mishra, *Journal of Photochemistry and Photobiology C: Photochemistry Reviews*, 2019, **41**, 100318.
8 I. Jarmoskaite, I. AlSadhan, P. P. Vaidyanathan and D. Herschlag, *eLife*, 2020, **9**, e57264.
9 D. Jenkins, Solving Quadratic, Cubic, Quartic and higher order equations; examples, https://newtonexcelbach.com/2014/01/14/solving-quadratic-cubic-quartic-and-higher-order-equations-examples/, (accessed April 27, 2024).
10 M. A. Jenkins and J. F. Traub, *Commun. ACM*, 1972, **15**, 97–99.
11 H. D. B. Jenkins and K. P. Thakur, *J. Chem. Educ.*, 1979, **56**, 576.
12 A. Ralston and P. Rabinowitz, *A first Course in numerical analysis*, McGraw-Hill, Auckland, 2. ed., 1984.
13 A. Ringbom and E. Still, *Analytica Chimica Acta*, 1972, **59**, 143–146.
14 R. J. Motekaitis and A. E. Martell, *Journal of Coordination Chemistry*, 1994, **31**, 67–78.
15 J. Hegenauer, P. Saltman and G. Nace, *Biochemistry*, 1979, **18**, 3865–3879.
16 W. R. Harris and V. L. Pecoraro, *Biochemistry*, 1983, **22**, 292–299.
17 R. L. Anderson, W. E. Bishop, R. L. Campbell and G. C. Becking, *CRC Critical Reviews in Toxicology*, 1985, **15**, 1–102.
18 R. M. Smith and A. E. Martell, *Critical Stability Constants*, Springer US, Boston, MA, 1989.
19 T. Knepper, *TrAC Trends in Analytical Chemistry*, 2003, **22**, 708–724.
20 E. Repo, J. K. Warchoł, A. Bhatnagar, A. Mudhoo and M. Sillanpää, *Water Research*, 2013, **47**, 4812–4832.
21 D. C. Harris, *J. Chem. Educ.*, 1998, **75**, 119.
22 J. C. Dechaux, V. Zimmermann and V. Nollet, *Atmospheric Environment*, 1994, **28**, 195–211.
23 V. Borko, T. Friganović and T. Weitner, *Journal of Inorganic Biochemistry*, 2023, **244**, 112207.
24 P. Armitage, G. Berry and J. N. S. Matthews, *Statistical Methods in Medical Research*, Wiley, 1st edn., 2002.
25 T. Weitner, T. Friganovic and V. Borko, Protein sialylation affects the pH-dependent binding of ferric ion to human serum transferrin - experimental data, Zenodo, 2024, https://doi.org/10.5281/zenodo.10881688.
26 N. D. Chasteen and J. Williams, *Biochemical Journal*, 1981, **193**, 717–727.

6. RASPRAVA

6.1. Optimizacija enzimske desijalinizacije transferina

Napravljeno je istraživanje s ciljem optimizacije enzimske desijalinizacije ljudskog transferina (**Rad 1**). Kao što je prethodno navedeno, priprema asijalotransferina obično se provodi djelovanjem enzima sijalidaza (neuraminidaza) na nativni (visoko glikozilirani) transferin. Enzim uklanja sijalinsku kiselinu sa završetaka glikanskih ogranaka proteina. Alternativno, *de novo* sinteza asijalotransferina nije prikladna zbog visoke kompleksnosti procesa glikozilacije proteina.

Komercijalno je dostupno nekoliko različitih enzimskih pripravaka koji se koriste za desijalinizaciju proteina. Takvi pripravci uglavnom se sastoje od imobiliziranog enzima na površini agaroznih kuglica. U ponudi su i enzimske otopine, no ti pripravci obično imaju nisku iskoristivost te naknadno nije lako razdvojiti enzim od proteina, odnosno regenerirati enzim. S druge strane, enzim imobiliziran na agaroznim kuglicama lako se odvaja od proteinskog produkta centrifugiranjem, s obzirom na to da enzim ostaje deponiran na površini kuglica.

Proizvođači obično daju vrlo konzervativne procjene količina asijaloproteina koje se mogu pripraviti korištenjem pojedinog komercijalno dostupnog enzimskog pripravka. Razlozi za takve procjene vjerojatno su višestruki. Važno je napomenuti da su enzimski pripravci namijenjeni širokom spektru glikoziliranih proteina koji sadrže sijalinske završetke, pa je moguće da je enzim manje učinkovit za neke proteine u usporedbi, primjerice, s ljudskim transferinom. Također, nužno je osigurati da dobiveni produkt nakon djelovanja enzima ima vrlo nisku razinu glikozilacije.

S obzirom na visoku cijenu enzimskih pripravaka i potrebu za pripravljanjem većih količina asijalotransferina u svrhu daljnjih eksperimenata, prvi korak cjelokupnog istraživanja bila je optimizacija procesa enzimske desijalinizacije. U tu svrhu, ispitivanja su provedena koristeći dva komercijalno dostupna enzimska pripravka: GlycoCleave® i SialEXO®. Oba pripravka sadrže enzime imobilizirane na kuglicama agara. GlycoCleave® se prodaje u obliku suspenzije, dok SialEXO® dolazi u malim plastičnim kolonama prilagođenim za naknadno centrifugiranje. Proces enzimske desijalinizacije provodi se miješanjem otopine proteina sa suspenzijama enzima. Smjese se, određeno vrijeme i pri određenoj temperaturi, polagano i kontinuirano rotiraju okretanjem mikroepruveta (GlycoCleave®) ili malih kolona (SialEXO®) uz brzinu rotacije od 10 okretaja u minuti. Po završetku reakcije, protein se sakuplja kao

supernatant u mikroepruveti (GlycoCleave®) ili se izlučuje u mikroepruvetu prolaskom kroz odčepljenu plastičnu kolonu (SialEXO®). U oba slučaja, odvajanje je potpomognuto blažom rotacijom uz upotrebu centrifuge. Centrifuga se vrši 1 minutu pri 1000 RCF (engl. *Relative Centrifugal Force*).

U slučaju obaju enzimskih proizvoda, varirano je ukupno vrijeme reakcije, odnosno vrijeme kontakta proteinskog uzorka s kuglicama koje sadrže imobilizirani enzim. Optimizacijski eksperimenti provođeni su uz povišenje koncentracije početne otopine nativnog proteina. Eksperimenti desijalinizacije višestruko su ponovljeni koristeći već prethodno upotrijebljene enzimske kuglice. S obzirom na to da povišenjem koncentracije proteina dolazi i do porasta koncentracije slobodne sijalinske kiseline koja nastaje tijekom desijalinizacije, u eksperimentima je varirana i koncentracija pufera kako bi se postigli uvjeti minimalnih promjena pH tijekom cijelog procesa desijalinizacije. Naime, porast koncentracije proteina početnih otopina, bez odgovarajućeg prilagođavanja koncentracije pufera, može dovesti do značajnijeg zakiseljavanja reakcijske smjese tijekom desijalinizacijskog procesa. To, pak, može rezultirati smanjenom enzimskom aktivnošću i, posljedično, nižom učinkovitošću desijalinizacije.

Rezultati optimizacije inicijalno su validirani prikupljanjem i spajanjem manjih alikvota produkata (nakon višestrukih ciklusa desijalinizacije), te kromatofokusiranjem, odnosno FPLC kromatografijom pomoću pH gradijenta, korištenjem kolona za izmjenu aniona. Kromatografska metoda uz upotrebu ÄKTA Start FPLC instrumenta i HiTrap Q HP kolona povezanih u seriju podrobno je opisana u **Radu 2**. Kromatografska razdvajanja pomoću pH gradijenta također su provedena korištenjem ÄKTA Purifier 10 instrumenta i SOURCE™ 15Q 4.6/100 PE kolone. Ovaj napredniji kromatografski sustav omogućuje poboljšanje razlučivosti, jer se eksperiment može vršiti pri nešto višim tlakovima i uz upotrebu efikasnije kromatografske kolone. FPLC kromatografijom provedeno je preliminarno ispitivanje kvalitete desijalinizacije.

Potpuni glikanski profili dobiveni su upotrebom spregnutog UHPLC-MS/MS sustava (Synapt G2-Si ESI-QTOF-MS). Ukratko, eksperimenti su provedeni deglikozilacijom proteinskih uzoraka i obilježavanjem otpuštenih glikana fluorescentnim markerom. Obilježeni glikani zatim su propušteni kroz UHPLC uređaj, a pojedine frakcije detektirane su fluorescencijski. U konačnici se analiziraju profili masene fragmentacije pojedinih kromatografskih frakcija, čime je moguće precizno utvrditi i njihove glikanske sastave.

Optimizacijski eksperimenti pokazali su se veoma uspješnima, osobito u slučaju proizvoda SialEXO®. Što se tiče optimizacije enzima GlycoCleave®, masena koncentracija

proteina povećana je sa 2,5 mg / mL (prema protokolu proizvođača) na 6,25 mg / mL. Korišteni volumeni proteinske otopine iznosili su 800 µL, uz dodatak 200 µL agaroznih kuglica, čime je teorijska masa desijaliniziranog proteina dobivenog u jednom ciklusu bila jednaka 5 mg. Realne mase dobivenog asijaloproteina uvijek su bile nešto niže, vjerojatno zbog manjih gubitaka uslijed nepotpunog ispiranja i naknadnog centrifugiranja uzoraka kroz polupropusnu membranu. Vrijeme provođenja desijalinizacije produljeno je sa 6 sati na 24 ili 48 sati, a koncentracija acetatnog pufera povećana je četiri puta, s 0,05 mol / L na 0,2 mol / L. Ovim postupkom uklonjeno je nešto više od 90 % sijalinske kiseline s transferina, što je usporedivo s rezultatima objavljenim u **Radu 2**, gdje je korišten isti enzimski pripravak.

U slučaju SialEXO® kolona, desijalinizacijom je uklonjeno čak oko 99 % sijalinske kiseline vezane na protein. Masena koncentracija proteina povišena je četiri puta, s početnih 0,625 mg / mL na 2,5 mg / mL. Volumen je također povećan s 800 µL na 1000 µL, dok je trajanje desijalinizacijskog ciklusa produljeno s 30 minuta na 24 sata. Desijalinizacija je bila učinkovita nakon 19 uzastopno provedenih ciklusa. Primjenom optimiziranog protokola moguće je bilo proizvesti barem oko 50 mg (ili više) visoko (> 99 %) desijaliniziranog transferina po koloni. To je približno stotinu puta više od 0,5 mg, koliko je deklarirao proizvođač. Korištenjem ovog protokola na učinkovit i razmjerno brz način mogu se pripraviti velike količine asijalotransferina. Svrsishodno je istovremeno koristiti više kolona, čime se može proizvesti i po nekoliko desetaka miligrama asijalotransferina dnevno.

Nakon proizvodnje velike količine asijalotransferina, preporučljivo je testirati alikvote zadnjih pripremljenih frakcija iz svih korištenih kolona kako bi se provjerio uspjeh desijalinizacije. Potencijalni problemi uključuju gubitak enzima s površina kuglica te kontaminaciju enzima i posljedični razvoj mikroorganizama, čije prisustvo može negativno utjecati na sam proces enzimske desijalinizacije degradirajući enzim i onečišćujući proteinski pripravak.

6.2. Spektrofotometrijska karakterizacija nativnog i desijaliniziranog transferina

Poznato je da UV-Vis spektri različitih proteina često sadrže lokalni apsorpcijski maksimum pri $\lambda \approx 280$ nm. Ovaj spektralni maksimum proizlazi iz prisustva aromatskih aminokiselina, poput triptofana, tirozina i, u manjoj mjeri, fenilalanina (335,336). Ljudski transferin također sadrži značajnu količinu aromatskih aminokiselina, što rezultira relativno jakom apsorpcijom pri $\lambda \approx 280$ nm. Primarni doprinos potječe od tirozina i triptofana, ali je poznat i nezanemariv utjecaj cistina, oksidiranog oblika cisteina (337–340).

U svrhu provođenja raznih eksperimenata s glikoformama ljudskog transferina postoji potreba za preciznim određivanjem koncentracije proteina, posebno u eksperimentima čiji rezultati ovise o omjerima tvari, odnosno o koncentraciji proteina, kao što su, primjerice, eksperimenti određivanja konstanti ravnoteže vezanja transferina i željeza(III). U slučaju nativnog transferina, molarni apsorpcijski koeficijenti već su otprije poznati iz literature (340). Manja varijabilnost procijenjenih molarnih apsorpcijskih koeficijenata može biti posljedica eksperimentalne pogreške i/ili varijabilnosti u sastavu samog proteina, koji se u pravilu dobiva iz uzoraka prikupljenih od različitih populacija donora.

Molarni apsorpcijski koeficijenti asijalotransferina nisu bili poznati u literaturi prije istraživanja provedenih u sklopu ovog doktorskog rada te ih je stoga bilo potrebno odrediti. Određivanje molarnih apsorpcijskih koeficijenata moguće je provesti modificiranom Edelhochovom metodom, koja je detaljnije opisana u **Radu 2**. U osnovi, apsorbancije nativnog i denaturiranog proteina mjere se u otopini istog pufera, pri identičnim uvjetima pH. Denaturacija se postiže primjenom 6 M gvanidin hidroklorida u puferu korištenom za otapanje proteina. Određene spektralne promjene posljedica su denaturacije. Molarni apsorpcijski koeficijent izračunava se kao produkt molarnog apsorpcijskog koeficijenta denaturiranog proteina i omjera apsorbancija nativnog i denaturiranog proteina pri odgovarajućoj valnoj duljini ($\varepsilon_{\text{nativni}} = \varepsilon_{\text{denaturirani}} \cdot A_{\text{nativni}} / A_{\text{denaturirani}}$, $\lambda \approx 280$ nm). Referentni molarni apsorpcijski koeficijent (izračunati molarni apsorpcijski koeficijent denaturiranog proteina) za transferin iznosi 81,080 M^{-1} cm^{-1}. Ovaj koeficijent izračunava se zbrajanjem doprinosa pojedinih apsorbirajućih aminokiselina; u slučaju ljudskog transferina, to su 8 triptofana, 26 tirozina i 19 cistina (175).

U sklopu **Rada 2**, molarni apsorpcijski koeficijent nativnog transferina pri $\lambda \approx 280$ nm određen je kao $84{,}8 \pm 0{,}2 \cdot 10^3$ M^{-1} cm^{-1}. Molarni apsorpcijski koeficijent asijalotransferina također je određen te on iznosi $88{,}2 \pm 0{,}2 \cdot 10^3$ M^{-1} cm^{-1} (**Rad 2**, **Slika 4**). U **Radu 4**, molarni apsorpcijski koeficijent nativnog transferina ponovno je određen kao $84{,}4 \pm 0{,}8 \cdot 10^3$ M^{-1} cm^{-1}. U oba slučaja, vrijednosti molarnog apsorpcijskog koeficijenta nativnog transferina u dobroj su suglasnosti s prethodno poznatim literaturnim podacima (340). Razlika u molarnim apsorpcijskim koeficijentima između nativnog i asijalotransferina iznosi približno 4 %. Ova razlika vjerojatno je posljedica konformacijskih promjena proteina i/ili elektrostatskog učinka uklanjanja nabijenih skupina, odnosno sijalinske kiseline (175).

U sklopu **Rada 2** također je ispitan utjecaj pH i koncentracije kalijevog klorida u puferskoj otopini na apsorbanciju transferina pri 280 nm. Utvrđeno je da se apsorbancija proteinske otopine minimalno mijenja, čak i uz značajne promjene koncentracije kalijevog

klorida i pH vrijednosti (**Rad 2**, **Slika 5**). Ovaj pronalazak važan je za naredne eksperimente određivanja konstanti ravnoteže fluorimetrijskim titracijama, jer osigurava pouzdanost primijenjenih molarnih apsorpcijskih koeficijenata. Njihovom primjenom omogućena je precizna kvantifikacija transferina u ishodnim otopinama koje sadrže 0,2 M KCl pri različitim pH vrijednostima.

6.3. Odjeljivanje transferinskih glikoformi pH-gradijent FPLC kromatografijom

Kao što je prethodno spomenuto, djelovanjem prikladnog enzima na nativni transferin moguće je pripraviti asijalotransferin i određene niskosijalinizirane oblike transferina. Uzimajući u obzir da je sijalinska kiselina negativno nabijena pri fiziološkom pH, očekivano je da će uklanjanje sijalinske kiseline značajno utjecati na ukupni naboj proteina, a time i na položaj izoelektrične točke (pI vrijednosti).

U sklopu **Rada 2** izvršeni su kromatografski eksperimenti na ÄKTA Start FPLC sustavu s ciljem razdvajanja nativnog i desijaliniziranog proteina. Ovaj FPLC niskotlačni sustav predstavlja financijski relativno povoljnu opciju u usporedbi s (U)HPLC visokotlačnim sustavima. Kromatografski eksperimenti provedeni su metodom pH gradijenta, odnosno kromatofokusiranjem. Ovisno o vrsti kolone, eksperimenti se mogu provoditi variranjem pH od višeg ka nižem ili obrnuto. U slučaju eksperimenata prikazanih u **Radu 2**, korištene su HiTrap Q HP kolone s pozitivno nabijenom stacionarnom fazom, zbog čega je pH variran od višeg ka nižem. Za poboljšanje kromatografskog razlučivanja, dvije HiTrap Q HP kolone spojene su serijski. Povezivanje većeg broja kolona uzrokuje porast tlaka u sustavu iznad dopuštenih razina za ÄKTA Start FPLC uređaj. Međutim, korištenjem ÄKTA Purifier 10 FPLC uređaja, eksperimenti se mogu provoditi s do četiri HiTrap Q HP kolone povezane u seriju.

Kromatografsko odjeljivanje podrobnije opisano u **Radu 2** sastoji se od nekoliko ključnih koraka. Prvo, otopina proteina u prikladnom puferu unosi se u sustav injekcijom u tankocjevnu petlju za uzorak. Zatim se uzorak nanosi na kolonu ispiranjem petlje startnim puferom. U slučaju kromatofokusiranja s pH gradijentom od višeg ka nižem, kao što je opisano u **Radu 2**, važno je da pH uzorka bude malo iznad pH startnog pufera. Ako je pH uzorka niži od pH startnog pufera, postoji rizik da će proteinski uzorak biti djelomično ili potpuno ispran s kolone prije nego što započne eksperiment. Nakon što je proteinski uzorak nanesen na kolonu, proteinske forme, koje su u ovom slučaju negativno nabijene, nekovalentno su vezane za pozitivno nabijenu stacionarnu fazu kromatografske kolone. Nakon toga, započinje proces kromatografske separacije, tijekom kojeg se skupljaju frakcije. Pritom se pomoću UV-Vis

spektrofotometrije mjeri apsorbancija pri λ = 280 nm, što omogućuje praćenje proteinskih frakcija koje napuštaju kolonu.

U prvom koraku eksperimenta, kroz sustav se propušta manja količina ishodnog (bazičnijeg) pufera. Zatim se kroz sustav propušta smjesa ishodnog (bazičnijeg) i završnog (kiselijeg) pufera, pri čemu se omjer tih dvaju pufera linearno mijenja tijekom trajanja eksperimenta, odnosno postiže se linearni pH gradijent. Nakon završetka faze linearnog pH gradijenta, sustav se dodatno ispire završnim (kiselijim) puferom kako bi se osiguralo potpuno eluiranje proteina iz kolone. Ako se provode uzastopni eksperimenti, od ključne je važnosti temeljito isprati sustav početnim (bazičnijim) puferom prije pokretanja novog ciklusa. Ako u koloni slučajno zaostane kiseli pufer izgledno je da će se novi uzorak djelomično ili čak potpuno eluirati u prvoj fazi novog eksperimenta. Nakon višestrukih uzastopnih eksperimenata, poželjno je sustav isprati 0,1 M HCl. Tijekom ili odmah po završetku pojedinog kromatografskog eksperimenta, pH vrijednosti sakupljenih frakcija mjere se pomoću pH elektrode, koja se prethodno kalibrira.

Možda i najveći izazov u provođenju ovakvih eksperimenata jest postizanje stabilnog i pouzdanog pH gradijenta (341). U ovdje prikazanim eksperimentima, pH varira u širokom rasponu od 8 do 4. Kako bi se postigao dobar linearni pH gradijent, nužno je da puferske smjese imaju visok puferski kapacitet u cijelom ovom rasponu. Budući da se elucija pojedinih frakcija detektira mjerenjem apsorbancije pri λ = 280 nm, vrlo je važno da korišteni puferi minimalno apsorbiraju na toj valnoj duljini. Ako puferi ipak značajnije apsorbiraju, poželjno je da apsorbancija puferske smjese korištene za postizanje pH gradijenta ne ovisi o omjeru pojedinih komponenti smjese. Također je važno da puferi budu prikladni za rad s proteinima, kako bi se izbjegle neželjene interakcije između pufera i proteina. Primjena neprikladnih pufera mogla bi dovesti do djelomične proteinske denaturacije, deaminacije ili vezanja pufera na protein, čime bi se promijenila fizičko-kemijska svojstva proteina (341).

Preliminarni eksperimenti, u kojima su korištene smjese soli jednostavnih poliprotonskih baza/kiselina te komercijalno dostupne Servalyt™ i Pharmalyte™ puferske smjese, pokazali su se djelomično ili potpuno neuspješnima, prvenstveno zbog nemogućnosti postizanja dovoljnog puferskog kapaciteta u širokom pH rasponu. To je rezultiralo drastičnim promjenama u pH vrijednosti prilikom malih promjena omjera bazičnog i kiselog pufera, što može dovesti do istovremene elucije različitih komponenti uzorka, onemogućavajući time njihovo efikasno razdvajanje.

Korištenjem pISep© pufera (342,343), postignuto je značajno poboljšanje kvalitete pH gradijenta, što je ujedno omogućilo učinkovito razdvajanje nativnog i desijaliniziranog proteina

(**Rad 2**, **Slika 2**). Razlika u pI vrijednostima nativnog i desijaliniziranog transferina je očekivano značajna te ona iznosi oko 1,2 pH jedinice. pI nativnog transferina procijenjena je na 5,3, dok pI desijaliniziranog transferina iznosi približno 6,5. Ova razlika u pI vrijednostima omogućuje jasno razdvajanje visokosijaliniziranog (nativnog) i asijalotransferina, što je vidljivo sa **Slike 2** u **Radu 2**. Kromatografski signali pokazuju dobru razlučivost nativnog (S+) i asijalotransferina (S−).

Slični eksperimenti provedeni su u sklopu **Rada 4**, uz nešto uži pH raspon od 7,4 do 5,5. Također je korišten napredniji kromatografski sustav koji uključuje ÄKTA Purifier 10 FPLC instrument i Source 15Q 4.6/100 PE kolonu za izmjenu aniona. Dobiveni rezultati (**Rad 4**, **Dodatak**, **Slika S2**) u skladu su s onima iz **Rada 2**. Dodatna potvrda rezultata iz obje studije dobivena je glikanskom analizom proteina, koja je pokazala visok udio sijalinske kiseline u frakcijama pripisanim nativnom transferinu te vrlo nizak udio u frakcijama pripisanim asijalotransferinu.

Metoda pH gradijenta razvijena u sklopu **Rada 2** pokazala se prikladnom za preliminarno testiranje uspješnosti priprave asijalotransferina enzimskom desijalinizacijom. Ako kromatografski profil sadrži samo jedan snažniji signal pri pI ≈ 6,5, može se zaključiti da je desijalinizacija uspješno izvedena. Prisustvo dodatnih signala ukazuje na nepotpunu desijalinizaciju. Ova metoda je brza, zahtijeva relativno male količine proteina, a dobra razlučivost postignuta je s manje od pola miligrama uzorka. Iako je primarno korištena za validaciju desijalinizacijskog procesa, metoda se može primijeniti i za pročišćavanje različitih proteinskih glikoformi. U eksperimentima u kojima je uzorak namjerno nedovoljno desijaliniziran (skraćenjem vremena djelovanja enzima), uspješno su međusobno odijeljeni i neki niskosijalinizirani oblici transferina. Ovi rezultati još nisu objavljeni, ali su potvrđeni glikanskom analizom.

6.4. Razvoj metode korekcije IFE pogodne za čitače mikrotitarskih pločica

Jedan od ključnih preduvjeta za uspjeh fluorimetrijskih eksperimenata u svrhu određivanja konstanti ravnoteže vezanja željeza na glikoforme transferina jest pravilna korekcija učinka unutarnjeg filtera, IFE. Problem IFE-a općenito je značajan kod različitih fluorimetrijskih mjerenja, a primjena odgovarajućih korekcija često je nužna čak i kod relativno niskoapsorptivnih otopina (273,311,312). Prilikom mjerenja fluorescencije uzoraka transferina, primarni IFE posljedica je spektralnih doprinosa transferina i željezovog(III) kompleksa s nitrilotrioctenom kiselinom na valnoj duljini fluorescencijske pobude pri λ = 280 nm (28).

Određeni manji doprinosi i varijacije u apsorpciji emitiranog zračenja također su mogući, no izgledno je da u ovim sustavima sekundarni IFE nema velikoga značaja.

S obzirom na to da je većina IFE-korekcijskih metoda razvijena za klasičnu fluorimetriju koja se izvodi mjerenjem uzoraka u kiveti, pri čemu se detekcija emitiranog zračenja vrši pod kutom od 90 stupnjeva u odnosu na ulaznu zraku pobudnog zračenja, u poznatoj literaturi opažen je nedostatak metoda prilagođenih ili specifičnih za čitače mikrotitarskih pločica. Neke od postojećih metoda primjenjive su isključivo za razmjerno niskoapsorptivne (razrijeđene) uzorke, što ih čini neprimjenjivima za širi spektar mjerenja u mikrotitarskim pločicama. Zbog tih ograničenja, bilo je nužno razviti prikladnu IFE-korekcijsku metodu prije provođenja fluorimetrijskih eksperimenata titracija transferina i kompleksa nitrilotrioctene kiseline. U sklopu **Rada 3** razvijena je nova IFE-korekcijska metoda, pogodna za uzorke u veoma širokom rasponu apsorbancija, mjerene u mikrotitarskim pločicama. Ta metoda je stoga dobro primjenjiva i za fluorimetrijska mjerenja potrebna za izračunavanje konstanti ravnoteže kompleksiranja glikoformi transferina s željezom(III), koja su prikazana u **Radu 4**.

Prilikom preliminarnih fluorimetrijskih mjerenja uočena je značajna varijacija intenziteta fluorescencije s promjenom takozvane *z*-pozicije, odnosno visine (položaja na *z*-osi) optičkog elementa koji sadrži izvor zračenja i detektor. Ove varijacije intenziteta prije svega ovise o količini fluorescencije koja dopire do detektora, a to je uvjetovano internim geometrijskim parametrima uređaja i mikrotitarske pločice (273,310). Tehnički crtež s prikazom dimenzija mikrotitarskih jažica i relevantnih geometrijskih parametara pločice i instrumenta može se vidjeti na **Slici 1** u **Radu 3**.

U slučaju snažnog prigušenja fluorescencije uzrokovanog IFE mehanizmom uslijed prisustva apsorptivnog fluorofora, linearnost fluorescencije kao funkcije koncentracije očuvana je samo pri veoma niskim koncentracijama. S porastom koncentracije fluorofora i povećanom apsorpcijom pobudnog i/ili emitiranog zračenja, odnos postaje nelinearan. U nekim situacijama, zbog izrazito snažnog IFE-uvjetovanog prigušenja, može se čak dogoditi da više koncentracije fluorofora rezultiraju nižim intenzitetom fluorescencije u usporedbi s niže koncentriranim uzorcima (273,310). Zanimljivo je primijetiti da krivulje koje prikazuju odnos između fluorescencije i koncentracije, dobivene pri različitim *z*-pozicijama podesivog optičkog elementa (**Rad 3**, **Slika 2**), obično nisu kolinearne, već se njihovi profili značajno razlikuju. Visoka kolinearnost uočava se pretežno u linearnoj zoni niskih koncentracija ili kada su mjerenja izvedena uz minimalne pomake u *z*-poziciji, što rezultira malim međusobnim razlikama navedenih krivulja (**Rad 3**, **Dodatak**, **Slika S7**).

Iz navedenog se može naslutiti da snimanje fluorescencije na različitim *z*-pozicijama pruža dodatne informacije o sustavu u kontekstu IFE-a. Predložena korekcijska tehnika omogućuje snimanje fluorescencije na najmanje dvije *z*-pozicije kao potencijalno rješenje za procjenu i naknadno uklanjanje artefakata uzrokovanih IFE-om u različitim uzorcima.

Relativno sličan korekcijski princip već je primijenjen za klasični fluorimetar pomoću metode dijagonalnog pomaka kivete (329). Ta metoda koju su razvili Lutz i Luisi pokazala se relativno učinkovitom, no njezina primjena prilično je ograničena jer klasični fluorimetri obično nemaju mogućnost (preciznog i automatiziranog) dijagonalnog pomicanja kivete. Njihovi su eksperimenti stoga zahtijevali izradu specifičnog dijela aparature fluorimetra, koji je omogućavao precizno pomicanje kivete ručno, a u kasnijoj verziji uz pomoć pneumatskog sustava (329).

Za razliku od tipičnih fluorimetara, gotovo svi noviji čitači mikrotitarskih pločica omogućuju jednostavno i precizno podešavanje pozicije optičkog elementa (*z*-pozicije). Mjerenja na različitim visinama izvora/detektora ne zahtijevaju ručno podešavanje, dovoljno je unijeti parametar *z*-pozicije u postavke mjerenja, nakon čega uređaj automatski izvršava potrebna podešavanja i pripadajuća mjerenja fluorescencije.

Korekcijska metoda za mikrotitarske pločice (**Rad 3**) izvedena je prilagodbom korekcijskog modela temeljenog na metodi dijagonalnog pomicanja kivete. Izvedena je korekcijska jednadžba (**Rad 3**, **Jednadžba 5**), koja je primjenjiva za mjerenja provedena uz pomak optičkog elementa duž *z*-osi. U obzir su uzeti relevantni geometrijski parametri uređaja i mikrotitarske pločice potrebni za korekciju (**Rad 3**, **Slika 1** i **Jednadžba 4**). Za uspješnu primjenu ove metode dovoljna su fluorimetrijska mjerenja na dvjema *z*-pozicijama. Međutim, primijećeno je da je za najbolju korekciju ključno odabrati prikladan par *z*-pozicija pri kojima su fluorimetrijska mjerenja obavljena. Vrlo male razlike u *z*-pozicijama nisu adekvatne, a potencijalni problemi mogu se javiti i pri ekstremnim (visokim i niskim) *z*-pozicijama. Što se tiče intenziteta mjerene fluorescencije, najjači signali dobiveni su u rasponu srednjih *z*-pozicija, dok veliki pomaci prema višim ili nižim *z*- vrijednostima mogu rezultirati vrlo slabim signalima zbog smanjenog intenziteta fluorescencije koja dopire do detektora. Ovaj problem je posebno izražen kod izrazito apsorptivnih uzoraka (310). Primjerice, dodavanje velike količine apsorptivnog kromofora prvo uzrokuje degradaciju kvalitete mjerenja na *z*-pozicijama daleko od optimuma (visokim i niskim *z*-pozicijama). U tim slučajevima, zbog snažnog trnjenja već ishodno slabijih signala fluorescencije, brže se postiže nepovoljan omjer signala i šuma.

Metodologija primijenjena u **Radu 3** sastoji se od mjerenja fluorescencije na više (N) različitih *z*-pozicija. Broj mogućih IFE-korekcija jednak je broju kombinacija različitih *z*-

pozicija, odnosno jednak je $(N - 1) \cdot N$, s obzirom na to da dijagonalni elementi korekcijske matrice, gdje je $z_1 = z_2$, nisu definirani jer rezultiraju nultim nazivnikom eksponenta korekcijske jednadžbe (**Rad 3**, **Jednadžba 5**). Iz preliminarnih kalibracijskih eksperimenata moguće je odabrati par *z*-pozicija koje za određenu mikrotitarsku pločicu pružaju najbolju korekciju. Nakon toga, daljnja mjerenja potrebno je provoditi samo na tim dvjema *z*-pozicijama.

Eksponencijalni član korekcijske jednadžbe (**Rad 3**, **Jednadžba 5**), koji uključuje različite geometrijske parametre, moguće je dodatno numerički optimizirati iscrpnom pretragom (odnosno takozvanim *brute-force* pristupom) kako bi se postiglo određeno poboljšanje u korekcijskim rezultatima. Optimizirani eksponencijalni članovi vrlo su blizu vrijednostima dobivenim uvrštavanjem geometrijskih parametara, što dodatno potvrđuje točnost osnovne korekcijske metode. Kao dopuna znanstvenoj publikaciji (**Rad 3**), izrađena je mrežna stranica, dostupna na poveznici https://ninfe.science, koja široj znanstvenoj zajednici omogućuje jednostavnu primjenu korekcijske metode. Korekcije se mogu lako izvršiti učitavanjem MS Excel tablica s mjernim podacima, formatiranim na odgovarajući način. Mrežni servis generira IFE-korekcijske podatke koristeći pritom unesene geometrijske parametre za osnovne korekcije, uz dodatnu numeričku optimizaciju eksponenta. On također omogućuje izvoz različitih grafova i parametara, poput nagiba pravca, koeficijenta determinacije, 2D i 3D prikaza rezultata, granice detekcije i drugih relevantnih pokazatelja.

Metoda prikazana u **Radu 3** može se upotrijebiti za korekciju veoma apsorptivnih uzoraka. Vrlo linearni rezultati (koeficijent determinacije, $R^2 > 0.999$) postignuti su pri apsorbanciji pobudnog zračenja od $A_{ex} \approx 2$ i emitiranog zračenja $A_{em} \approx 0{,}5$. Normalizirano prema optičkom putu od 1 cm, te vrijednosti iznose $A_{ex} \approx 4$ i $A_{em} \approx 1$. Gornja granica metode u vidu apsorbancija pobudnog i/ili emitiranog zračenja nadilazi te vrijednosti (trenutno neobjavljeni rezultati). Većina postojećih metoda, prema znanju autora, nije primjenjiva na tako apsorptivne uzorke. Dodatni problem IFE-korekcija za klasične fluorimetre fizičko je ograničenje mjerenja visokoapsorptivnih uzoraka. Zbog specifične prirode mjerenja, pri kutu od 90 stupnjeva otklona između izvora pobudnog zračenja i detektora, mjeri se fluorescencija koja nastaje uglavnom u zoni blizu središta kivete. U slučaju vrlo apsorptivnih uzoraka, samo mala količina pobudnog zračenja dopire do centra kivete ako je primarni IFE izrazito jak, dok vrlo malen udio emitiranog zračenja dopire od približnog centra do detektora ako je sekundarni IFE veoma izražen. Prema tome, neovisno o korekcijskoj proceduri, nije moguće vršiti korekciju uslijed iznimne apsorpcije.

Mjerenja u mikrotitarskim pločicama nalikuju takozvanoj „*front-face*“ konfiguraciji za mjerenje fluorescencije, u kojoj su izvor zračenja i detektor smješteni s iste strane uzorka (310).

U slučaju čitača mikrotitarskih pločica to je najčešće iznad otopine, a može biti i ispod dna pločice. Čak i u slučaju iznimno apsorptivnih uzoraka, određena količina fluorescencije vjerojatno će biti detektirana. Većina relevantnih fluorescencijskih događaja tada se odvija u tankom sloju blizu površine tekućine, što samo po sebi ne predstavlja problem.

Velika prednost ove metode korekcije IFE njezina je primjenjivost u slučaju UV-Vis neprozirnih pločica. Fluorimetrijske pločice s dnom propusnim za UV-Vis zračenje obično su znatno skuplje od potpuno neprozirnih pločica. Budući da se većina poznatih IFE-korekcijskih metoda temelji na mjerenju apsorbancije uzoraka, primjena metode razvijene u **Radu 3** također omogućuje značajnu uštedu resursa. Efikasnost metode potvrđena je korištenjem različitih fluorofora, iako su u **Radu 3** objavljeni samo rezultati s upotrebom kinina kao fluorofora i kalijevog bikromata kao dodatnog (apsorbirajućeg) kromofora. Budući da je IFE-korigirana fluorescencija funkcija dviju fluorescencija izmjerenih na dvama *z*-pozicijama, te uzimajući u obzir manje nepouzdanosti u geometrijskim parametrima korištenim u izračunima, izvršena je temeljita propagacija pogreške (**Rad 3**, **Dodatak**, **Potpoglavlje 3.2**) kako bi se procijenili mogući intervali pogreške. Postignuti koeficijenti determinacije (R^2) vrlo blizu 1 (**Rad 3**, **Tablica 1**) ukazuju na snažnu linearnu ovisnost između korigirane fluorescencije (*y*-os) i koncentracije fluorofora (*x*-os) nakon provedenih korekcija (**Rad 3**, **Slika 2**). Osim toga, odstupanja u koeficijentima nagiba i odsječaka pravaca vrlo su mala, što dodatno potvrđuje visoku preciznost i točnost korekcijske metode (**Rad 3**, **Tablica 1**).

6.5. Fluorimetrijske titracije transferina s nitrilotrioctenim kompleksom željeza(III)

Prvi korak eksperimenata fokusiranih ka izračunima konstanti ravnoteže vezanja nativnog i asijalotransferina sa željezom(III) sastoji se u provođenju titracijskih eksperimenata. U sklopu **Rada 4** provedeno je ukupno 10 titracijskih eksperimenata, a svaki uzorak pripravljen je i izmjeren u triplikatu. Titracije su vršene pri 5 različitih pH vrijednosti: 7,4, 6,8, 6,5, 6,2 i 5,9, a pritom su korišteni su nativni (S+) i asijalotransferin (S−). S obzirom na pH osjetljivost istraživanih ravnoteža, svi eksperimenti vršeni su u puferskim radnim otopinama. Sve radne otopine sadržavale su 25 mM PIPES pufer, a osim toga i 0,2 M kalijev klorid te 10 mM kalijev karbonat. Prisustvo karbonata nužno je za normalno vezanje željeza u transferinski kompleks (100,104); dodatkom karbonatne soli povišena je količina karbonata prisutna u otopini te su na taj način postignuti uvjeti više koncentracije karbonata, slični fiziološkima. Prisustvo fiksne koncentracije kalijevog klorida primarno služi ujednačavanju ionske jakosti kroz sve točke titracije.

Otopina nitrilotrioctene kiseline (NTA) te visokokoncentrirani kompleks željeza(III) i nitrilotrioctene kiseline (FeNTA) pripremljeni su i standardizirani kako je opisano u prethodnom istraživanju (27). Kako bi FeNTA kompleks bio dugoročno stabilan, odnosno da se spriječi eventualna hidroliza željeza(III), on se pohranjuje se na temperaturi od −20 °C u kiseloj vodenoj otopini (pH ≈ 2,2). Otopina također sadrži i suvišak nitrilotiroctene kiseline prema željezu u približnom omjeru 2:1. Na taj način osigurava se da u otopini praktički nema slobodnog željeza(III) odnosno njegovog heksaakva kompleksa razmjerno podložnog hidrolizi.

Procjena kvalitete enzimske desijalinizacije, odnosno glikansko profiliranje asijalotransferina (S−) izvršeno je kako je ranije opisano u **Radu 2**. Inicijalna provjera kvalitete desijalinizacije obavljena je uz upotrebu naprednijeg kromatografskog FPLC sustava i kolone bolje razlučivosti nego u **Radu 2**, također i uz nešto uži pH gradijent.

Titracije su vršene dodatkom radnih otopina FeNTA i pufera u radnu otopinu transferina. pH vrijednosti početnih otopina podešene su na ciljane vrijednosti dodatkom vrlo malih količina baze ili kiseline. Početne puferske otopine pripravljene su u odmjernim tikvicama i precizno podešene na željeni pH, tako da je jedina manja pH promjena inicijalnih radnih otopina posljedica otapanja transferina odnosno FeNTA. Razrjeđenja otopina postignuta podešavanjem pH bila su manja od 1:1000, pa je njihov utjecaj praktički zanemariv. S obzirom na to da su koncentracije transferina i FeNTA određivane spektrofotometrijski u završnom koraku pripreme otopina, nakon finalnog podešavanja pH, vrlo mala pogreška u koncentracijama uslijed razrjeđenja ne obračunava se na ključne komponente transferin i FeNTA, već samo na koncentracije PIPES pufera, kalijevog klorida i kalijevog karbonata (i dodane NTA tamo gdje je ona dodavana). Ustanovljeno je također da su promjene pH uzoraka nakon titracije ili 24-satnog počeka bile minimalne. Molarni apsorpcijski koeficijenti transferina određeni su kao što je prethodno navedeno, a vrijednosti molarnih apsorpcijskih koeficijenata za FeNTA kompleks određene su u prethodnom istraživanju u kojem je također opažena mala ovisnost tih koeficijenata o varijacijama u koncentraciji kalijeva klorida i o varijacijama u pH (27). S obzirom na određenu dugoročnu nestabilnost FeNTA otopina, pogotovo pri povišenom pH, FeNTA otopine uvijek su pripremane iz kiselih i netom odleđenih koncentrata neposredno prije provođenja samih titracija. U prethodnom istraživanju ustanovljena je višednevna stabilnost FeNTA otopina u uvjetima vrlo sličnim onima u kojima su provedene titracije u **Radu 4** (27).

Same titracije vršene su dodatkom triju komponenti (otopina) u plastične mikroepruvete volumena 0,5 mL korištenjem robota za pipetiranje Opentrons OT-2. Robot je isprogramiran pomoću Python skripti. Tri korištene komponente su: otopina transferina, otopina FeNTA i osnovna otopina. Sve tri otopine sadrže 0,2 M kalijev klorid, 10 mM kalijev karbonat i fiksnu

količinu dodane nitrilotrioctene kiseline (NTA). Osnovna otopina sadrži samo ove komponente bez FeNTA i transferina te služi za nadopunjavanje tijekom titracije transferina s FeNTA. Dodana NTA korištena je u svim eksperimentima osim u onima koji nisu izravno služili za izračunavanje konstanti ravnoteže, već za postizanje uvjeta (gotovo) potpune saturacije i provjeru približne stehiometrije reakcije. Koncentracije dodane NTA podešavane su prema preliminarnim eksperimentima i njihove vrijednosti odabrane su ovisno o pH, jer je poznato da su konstante ravnoteže kojima je opisano vezanje željeza(III) na transferin pH-ovisne (28,96,308). Zbog nepovoljnih površinskih svojstava proteina i posljedične mogućnosti pogrešaka u pipetiranju uslijed stvaranja kapljica i mjehurića na vršku pipete robota, prvo su dodavane neproteinske komponente, a otopina proteina uvijek je dodana direktno u neproteinsku tekućinu uz višestruko miješanje usisavanjem i ispuštanjem smjese kroz vrh pipete. Mikroepruvete s uzorcima dobro su izmiješane i održavane 24 sata na 25 °C. Preliminarnim mjerenjima ustanovljeno je da je uravnoteženje kemijskog sustava postignuto unutar navedenog jednodnevnog intervala, jer nisu uočene značajne razlike u fluorescenciji istih uzoraka mjerenih više puta u kraćim vremenskim intervalima. Tomu u prilog idu i postojeća kinetička istraživanja u kojima se zaključuje da je prijenos željeza iz FeNTA kompleksa u ljudski transferin veoma brz proces (344,345). Navedeno općenito ne vrijedi za neke druge kelate željeza(III) koji mnogo sporije zasićuju transferin; u određenim slučajevima ravnoteže nisu uspostavljene niti nakon višednevnih počeka (346). Nakon 24-satnog počeka, uzorci su, koristeći robot za pipetiranje, preneseni iz mikroepruveta u jažice mikrotitarskih pločica. Ta procedura vršena je u (pseudo)nasumičnom poretku kako bi se umanjili eventualni sustavni učinci pogrešaka koji proizlaze iz anizotropije položaja uzorka u pločici i/ili iz nepravilnosti koje mogu utjecati na prostorno susjedne uzorke u pločici.

Fluorimetrijska mjerenja izvršena su upotrebom Tecan Spark M10 čitača mikrotitarskih pločica. Pobuda je vršena na 280 nm, a fluorescencija je snimana na 335 nm. Kako bi se dodatno osiguralo da nema detekcije pobudnog zračenja primijenjen je i pogodni optički filter. Osim fluorescencije izmjereni su i apsorpcijski spektri uzoraka.

Za korekcije IFE, primijenjena je metoda korekcija temeljena na snimanju uzoraka pri različitim visinama optičkog elementa koja je razvijena kao što je prikazano u **Radu 3**. Mjerenja su prvo vršena na optimalnoj *z*-poziciji, odnosno na onoj koja daje najintenzivniji fluorescencijski odziv, $z_{opt} \approx 17$ mm za sve titracijske eksperimente odnosno za sva navedena mjerenja. Izvršena su mjerenja i na devet drugih *z*-pozicija. Korekcije su vršene koristeći $z_1 \approx 17$ mm, $z_2 = 20$ mm. Za dodatnu verifikaciju korekcijske metode, usporedno je izvršena i spektroskopska korekcijska metoda na temelju mjerenih apsorbancija. Rezultati dvaju

korekcijskih metoda međusobno se vrlo malo razlikuju, kolinearni su za sve titracije ($R^2 > 0,99$), kao što se može vidjeti na **Slikama S5 i S6** (**Rad 4**, **Dodatak**).

Nelinearnost fluorescencijskog odziva koja je posljedica IFE nije direktno uvjetovana visokim apsorbancijama odnosno značajnim gubicima zračenja uslijed apsorpcije. Ona je pak posljedica varijabilnosti u relevantnim apsorbancijama odnosno u nejednolikim gubicima pobudnog ili emitiranog zračenja između različitih uzoraka. Ukoliko je prisutna fiksna količina snažno apsorbirajuće tvari u svim uzorcima, tada njezino prisustvo ujednačuje IFE gubitke i efektivno umanjuje ili anulira IFE artefakte. Ta metodologija iskorištena je za razvoj nove metode korekcija IFE u mikrotitarskim pločicama dodatkom (nefluorescentnog) apsorbera (310). Ideja je i na neki način primijenjena u samom dizajnu titracijskih eksperimenata u **Radu 4**. Naime, titracije je u teoriji moguće provoditi varijacijom koncentracije FeNTA uz održavanje koncentracije transferina fiksnom ili obrnuto, uz fiksnu koncentraciju FeNTA i variranje koncentracije transferina. Prva opcija odabrana je uglavnom zbog toga što je transferin primarni doprinositelj apsorbancije pri fluorescencijskoj pobudi na λ = 280 nm. Određene manje promjene apsorpcije proteinskih komponenti pri λ = 280 nm posljedica su vezanja jer se UV-Vis spektri i molarni apsorpcijski koeficijenti transferina donekle razlikuju ovisno o tome je li na njega vezano željezo (340). Također, FeNTA ima manji ali nezanemariv apsorpcijski doprinos pri λ = 280 nm (27). Spomenutim dizajnom eksperimenta minimizirane su IFE varijacije, premda su one i dalje prisutne. Neovisno o dizajnu eksperimenta, dobrim IFE korekcijama dobit će se kvalitetni rezultati, ali je vjerojatno dobra praksa pokušati umanjiti taj učinak eksperimentalno, tako da eventualne nesavršenosti korekcija u konačnici imaju manji utjecaj na rezultate.

Fluorimetrijske titracije vršene su izmjenom željeza iz FeNTA kompleksa i transferina. Zbog vrlo visokih konstanti ravnoteže vezanja željeza(III) u glikoforme transferina, nužno je vršenje eksperimenata izmjene na način da se u titraciji koristi stabilan kompleks željeza(III), ali niže stabilnosti nego u slučaju s transferinom. Također, nekelirano („slobodno“) željezo(III), odnosno ono dobiveno otapanjem jednostavnih soli poput $FeCl_3$, nije pogodno za ovu vrstu eksperimenata, prvenstveno zato što se takvim reagensima ne može uvijek postići dovoljno zasićenje proteina željezom (347). Drugi važan razlog jest taj što kelati štite željezo(III) od hidrolize u vodenoj otopini, tvoreći vrlo stabilne komplekse, što je značajno pri neutralnom i bazičnom pH, gdje hidroliza iona željeza može biti vrlo izražena (348,349). Kako bi se osigurao povoljan titracijski režim, odnosno kako bi vezanje željeza na transferin bilo dovoljno postupno, a samim time i promjene mjerene fluorescencije, određene fiksne količine NTA bile su prisutne u otopinama (0,1 mM do 50 mM). U slučaju eksperimenata pri višim pH

vrijednostima, afinitet transferina prema željezu raste te je stoga potrebno dodati veće količine NTA; pri nižim pH slučaj je obrnut. Bez vezanog željeza NTA ima zanemarive spektralne doprinose pri valnoj duljini pobude na λ = 280 nm i u (obližnjem) spektralnom području te u području emisije (28).

Provedeni su eksperimenti bez dodatka NTA kako bi se izvršila procjena aktivne frakcije proteina koja veže na sebe željezo. Rezultati tih eksperimenata dobar su pokazatelj nepostupnog vezanja željeza, odnosno primjera kada nije postignut dobar titracijski režim potreban za određivanje konstanti ravnoteže. Rezultati tih fluorimetrijskih titracija prikazani su na **Slici S7** i **Slici S9** (**Rad 4**, **Dodatak**). Bez dodane NTA, promjena fluorescencije kao funkcije dodanog FeNTA kompleksa prilično je linearna, a gašenje fluorescencije potpuno prestaje u trenutku postizanja zasićenja cjelokupnog transferina željezom, jer su mjerene promjene fluorescencije posljedica gašenja intrinzične fluorescencije transferina prilikom vezanja željeza u dva aktivna mjesta proteina. Dobivene krivulje sadrže točke prilično naglog pregiba, koje su blizu stehiometrijskih omjera 2:1 u korist željeza naspram transferina. Te točke će očekivano biti blizu ciljanje stehiometrije, ali ne točno pri toj točki jer je u završnim fazama titracije prisutna i značajnija količina NTA koja konkurira za željezo. Dodatna korist ovih eksperimenata dokaz je da dodatkom suvišaka FeNTA kompleksa ne dolazi do dodatnog gašenja fluorescencije transferina. Naime, u točkama u kojima je transferin praktički potpuno zasićen željezom, daljnji dodaci FeNTA neće primjetno povećati saturaciju transferina željezom, a samim time ne bi trebali dodatno gasiti intrinzičnu fluorescenciju proteina. S obzirom na to da ti dodaci suviška FeNTA ne produciraju promjene fluorescencije na ovaj ili neki drugi način, može se dokazati da u sklopu provedenih eksperimenata nema drugih značajnih mehanizama gašenja fluorescencije poput kolizijskog gašenja ili FRET-a. Ukoliko bi navedeni učinci bili prisutni, nema valjanog razloga zašto se oni ne bi nastavili ispoljavati i nakon što je postignuto potpuno (stehiometrijsko) zasićenje proteina željezom. Pojavnost navedenih efekata vjerojatno bi bilo teško uočiti iz uobičajenih titracijskih krivulja, jer se zbog dovoljne količine dodane NTA, koja konkurira za željezo(III), transferin ne zasićuje u potpunosti tijekom tih eksperimenata, pa se plato na kraju titracijskih krivulja nikad ne postiže.

Za pojedini eksperiment, koncentracije transferina bile su poznate i međusobno jednake (do na malu eksperimentalnu pogrešku titracije) za svaku titracijsku točku. Ukupne koncentracije željeza i NTA također su precizno određene i poznate za svaku točku. Međutim, s obzirom da su konstante ravnoteže kojima se opisuje raspodjela željeza u sustavu nepoznate, raspodjela željeza između pojedinih vrsta (slobodno željezo, željezo vezano na transferin i željezo u FeNTA kompleksu) nije bila unaprijed poznata. U **Poglavlju 6 Dodatka** (**Rad 4**)

detaljno su opisane pH-ovisne ravnoteže nitrilotrioctenog kompleksa, što je važno za točno određivanje koncentracije slobodnog željeza u sustavu. Temeljita karakterizacija ravnoteža nitrilotrioctene kiseline (NTA) i pripadajućih kompleksa željeza(III) (FeNTA) opisana je u prethodnoj publikaciji (27).

Ovisnost izmjerene fluorescencije o koncentraciji dodanog FeNTA kompleksa modelirana je korištenjem polinoma vezanja (engl. *binding polynomial*) inicijalno izvedenog za dva neovisna vezna mjesta za željezo na ljudskom transferinu, što pruža opći statističko-termodinamički okvir za proučavanje vezanja liganada na makromolekule. U postupku modeliranja, prvo je definiran polinom vezanja za spomenuta dva mjesta kojim se opisuje kako se različiti oblici transferina, apotransferin (bez vezanog željeza), jednostruko zasićeni transferin (FeTf) i dvostruko zasićeni transferin (Fe_2Tf, odnosno holotransferin), formiraju u odnosu na koncentraciju slobodnog željeza. Za svaku eksperimentalnu točku izračunate su ukupne koncentracije proteina i željeza(III). Jednadžba bilance mase za željezo(III) analitički je riješena za svaku točku, uz pretpostavljene vrijednosti makroskopskih konstanti vezanja. Ove konstante, označene kao K_{1m} i K_{2m}, predstavljaju konstante ravnoteže vezanja željeza na prvo i drugo vezno mjesto transferina. K_{1m} opisuje afinitet prvog veznog mjesta transferina prema željezu, dok K_{2m} opisuje afinitet drugog veznog mjesta. U prvom koraku cjelokupnog iterativnog procesa, vrijednosti tih konstanti su pretpostavljene.

U drugom koraku, izračunate su koncentracije različitih kompleksa (apoTf, FeTf, Fe_2Tf) za svaku točku koristeći pretpostavljene konstante ravnoteže. Relativne koncentracije različitih oblika transferina izračunate su koristeći jednadžbe koje opisuju njihove frakcijske udjele u otopini (**Rad 4**, **Jednadžbe 9-11**). Sumirajući navedene jednadžbe, lako se može dokazati da je zbroj svih frakcijskih udjela jednak *n*, odnosno da je jednak broju veznih mjesta. Ukupna normalizirana relativna fluorescencija za svaku eksperimentalnu točku izračunata je prema **Jednadžbi 12** (**Rad 4**).

Očekivani fluorescencijski signal izračunat je pretpostavljajući određene vrijednosti molarnih fluorescencija pojedinih oblika transferina, koje su bile promjenjivi parametri u nelinearnoj analizi metodom najmanjih kvadrata. Ovom metodom minimiziraju se razlike između eksperimentalnih i izračunatih vrijednosti fluorescencije. Te vrijednosti predstavljaju relativni doprinos svakog oblika ukupnom intenzitetu fluorescencije. Iterativnom metodom dobiven je optimalni skup makroskopskih ravnotežnih konstanti koji najbolje reproducira eksperimentalne podatke.

Glavni korak izračuna konstanti ravnoteže proveden je pomoću VBA (engl. *Visual Basic for Applications*) rutine u programu Microsoft Excel. Rješenja kubne jednadžbe, kojom je

opisana koncentracija slobodnog željeza(III) (**Jednadžba 5** u **Radu 4**), dobivena su primjenom Jenkins-Traub algoritma, koristeći koeficijente iz **Jednadžbi 6-8** definiranih u **Radu 4**.

Razlike između izračunatih vrijednosti fluorescencije (F_{calc}) i normaliziranih eksperimentalnih vrijednosti (F_{norm}) kvadrirane su i zbrojene za sve eksperimentalne točke kako bi se dobila ponderirana suma kvadrata reziduala (engl. *Weighted Residual Sum of Squares*, WRSS). Za izračun WRSS-a izvršeno je uteževanje inverznom varijancijom ($1 / \sigma^2$, gdje je σ^2 varijancija mjerenja fluorescencije trostruko repliciranih mjerenih uzoraka). Ovaj pristup učinkovito minimizira utjecaj slučajnih pogrešaka u skupu podataka i osigurava da algoritam prilagodbe najveću statističku težinu pridodaje najpouzdanijim i najreproducibilnijim podacima. Vrijednost WRSS-a potom je minimizirana kroz iterativni postupak kako bi se dobio optimalni skup konstanti ravnoteže, koristeći alat Solver u Microsoft Excelu.

Kako bi se poboljšala konvergencija, primijenjeno je nekoliko strategija. Korištene su normalizirane vrijednosti fluorescencije umjesto izvornih vrijednosti, što omogućuje konzistentno skaliranje podataka i olakšava proces prilagodbe. Umjesto izravnog određivanja nominalnih vrijednosti konstanti ravnoteže, prilagođavane su logaritamske vrijednosti $\log(K_{1m})$ i $\log(R)$, gdje je $R = K_{2m} / K_{1m}$; odgovarajuća vrijednost K_{2m} izračunata je kao $\log(K_{2m}) = \log(K_{1m}) + \log(R)$. Korištenje logaritamskih vrijednosti pomaže u osiguravanju pozitivnih, nenultih vrijednosti za konstante ravnoteže i poboljšava numeričku stabilnost tijekom optimizacije. Također, podaci su raspoređeni u nasumičnom poretku prije optimizacijskog procesa kako bi se spriječilo da redoslijed podataka utječe na konvergenciju algoritma; nasumično svrstavanje provedeno je generiranjem (pseudo)nasumičnih brojeva koristeći funkciju RAND() i sortiranjem podataka prema dobivenim vrijednostima.

Stupnjevi disocijacije α za FeNTA i NTA uključeni su u konačne izračune kako bi se uzeli u obzir različiti protonacijski oblici ovih spojeva pri varijabilnim pH uvjetima. Precizno određeni α(NTA) i α(FeNTA) omogućuju točne procjene koncentracija slobodne NTA i FeNTA kompleksa u otopini, što je u konačnici ključno za točno izračunavanje koncentracije slobodnog željeza(III). Nitrilotrioctena kiselina poliprotonska je kiselina, a pH ravnoteže sa željezom(III) razmjerno su kompleksne te u otopini, između ostalog, mogu biti prisutni i različiti miješani hidroksidi kao i dimeri (**Rad 4**, **Poglavlje 6** i prethodna publikacija) (27).

Konstante K'_{1m} i K'_{2m} su uvjetne (kondicionalne) konstante ravnoteže pri datim uvjetima pH; one uključuju stupnjeve disocijacije α(NTA) i α(FeNTA). Te konstante dobivene su iz konstanti ravnoteže (K_{1m} i K_{2m}) izračunatih iterativnim postupkom i K'_{110}, konstante kojom je karakterizirana interakcija željeza(III) i NTA (**Jednadžbe 13** i **14** u **Radu 4**, **Poglavlja 6** i **7**,

Dodatak). Uključivanje K'_{110} ključno je za točniji opis sustava, jer stupnjevi protonacije liganada značajno utječu na spomenute kemijske ravnoteže.

U daljnjoj analizi rezultata proračuna, uveden je faktor preferencije veznog mjesta (f_{sp}), definiran kao omjer konstanti ravnoteže K_{1m} / K_{2m} (308). Ovim faktorom opisana je relativna preferencija pojedinih veznih mjesta ka vezanju željeza(III).

Izračunat je i faktor F(FeTf), koji definira frakcijsku populaciju jednostruko zasićenog transferina (FeTf) pri polovičnoj saturaciji (350). Taj faktor predstavlja udio oblika FeTf u ukupnoj populaciji proteina kada je ukupno zasićenje željezom 50 %. Vrijednosti F(FeTf) niže od 0,5 ukazuju na pozitivnu kooperativnost, a vrijednosti više od 0,5, sukladno, ukazuju na (prividnu) negativnu kooperativnost. Pojam "prividna" u kontekstu negativne kooperativnosti koristi se jer se njezino postojanje ne može nedvosmisleno potvrditi samo na temelju fluorimetrijskih mjerenja; slični efekti mogu se ispoljiti zbog nezavisnog vezanja liganda na dva mjesta s različitim afinitetima (351,352). Za definitivnu potvrdu vjerojatno je nužno provesti dodatne kinetičke studije (351,352).

U sklopu **Rada 4** provedena je detaljnija analiza pogreške. Propagacija pogreške podrobno je opisana u **Potpoglavlju 7.3** (**Rad 4**, **Dodatak**). Ukratko, u procjeni standardnih devijacija fluorescencijskih mjerenja uračunati su i manji doprinosi standardnih devijacija baznih linija. Izvedeni su izrazi propagacije pogreške IFE-korigirane fluorescencije dobivene primjenom korekcijske metode razvijene u sklopu **Rada 3**. Kao što je prethodno navedeno, K_{1m} i R dobiveni su iterativnim postupkom prilagodbe odnosno optimizacije. Zbog složenosti samog postupka, dobivanje analitičkih izraza za propagaciju pogreške tih parametara vrlo je teško rješiv problem. Stoga su nesigurnosti u podesivim parametrima $\log(K_{1m})$ i R procijenjene upotrebom takozvanog „*jackknife*“ pristupa (353). U tom pristupu izostavlja se pojedina titracijska točka prilikom izračuna WRSS, $\log(K_{1m})$ i R. Za svaku pojedinačno izostavljenu točku izračunati su $\log(K_{1m})$ i R, te su iz rasapa svih dobivenih vrijednosti procijenjene njihove standardne devijacije. S obzirom na linearnu zavisnost $\log(K_{2m})$ vrijednosti ($\log(K_{2m}) = \log(K_{1m}) + \log(R)$), procjena pogreške K_{2m} lako se izračuna prema procjenama pogrešaka K_{1m} i R.

Statistička značajnost razlika između rezultata nativnog i desijaliniziranog proteina za svaku pH vrijednost procijenjena je korištenjem Satterthwaiteovog približnog t-testa, metode iz Behrens-Welchove obitelji koja se temelji na robusnijoj t-statistici s približnim stupnjevima slobode. Satterthwaiteov odnosno Welchov t-test koristi se za usporedbu srednjih vrijednosti dviju grupa kako bi se utvrdilo postoji li statistički značajna razlika između njih, posebno kada grupe imaju različite varijancije i/ili različite veličine uzorka i/ili kada su varijancije

heteroskedastične (354–356). Sve vrijednosti s $p \leq 0,05$ smatrane su statistički značajnima. Osim prikaza samih rezultata optimizacije, odnosno procijenjenih (i mjerenih) rezultata fluorescencije kao funkcije dodanog FeNTA, prikazani su i reziduali (**Rad 4**, **Slika 2** i **Potpoglavlje 5.3**, **Dodatak**).

Rezultati dobiveni pri fiziološkom pH (7,4) u skladu su s rezultatima prethodnih studija (357,358), što potvrđuje valjanost modela i ujedno validira primijenjenu fluorimetrijsku metodu. Uklanjanje sijalinske kiseline rezultiralo je približno trostrukim porastom konstanti ravnoteže koje opisuju vezanje željeza na oba vezna mjesta asijalotransferina (K_{1m} i K_{2m}). Ti rezultati su u razmjernom skladu s prethodnim kalorimetrijskim istraživanjem (84). Određene razlike u rezultatima vjerojatno se barem djelomično mogu pripisati različitim uvjetima u otopini, odnosno vrsti korištenog pufera i razmjerno višoj ionskoj jakosti postignutoj prisustvom 0,2 M kalijevog klorida u otopinama korištenim u **Radu 4**. Također je važno napomenuti da se u slučaju fluorimetrijskih mjerenja sama mjerenja vrše s odgodom od 24 sata, što omogućuje eventualnu preraspodjelu željeza između veznih mjesta glikoproteina. S druge strane, kod brzih ITC mjerenja, relevantna diferencijalna snaga bilježi se odmah po dodatku FeNTA otopine, kroz trenutni titracijski signal. To upućuje na to da ITC rezultati vjerojatno djelomično odražavaju i kinetičku preferenciju veznih mjesta. U svakom slučaju, rezultati obaju istraživanja ukazuju na statistički značajno više konstante ravnoteže vezanja željeza(III) na oba vezna mjesta u slučaju asijalotransferina u odnosu na nativni transferin.

U literaturi je poznato da su konstante ravnoteže koje opisuju vezanje željeza(III) na transferin pri kiselim uvjetima u endosomu značajno niže nego pri fiziološkom pH, što je uglavnom posljedica konformacijskih promjena uslijed varijabilnosti protonacije aminokiselina (115,308,359). U sklopu **Rada 4**, kroz mjerenja pri različitim pH vrijednostima, uključujući međuvrijednosti između fiziološkog i endosomskog pH, dokazana je ovisnost tih konstanti o pH kako za nativni tako i za desijalinizirani protein. Sniženjem pH, izračunate konstante za oba vezna mjesta sustavno se smanjuju u oba slučaja, odnosno i kod nativnog i kod asijalotransferina (**Rad 4**, **Slika 3**). Zanimljivo je da su pri najnižem pH od 5,9, na kojem su provedeni eksperimenti, konstante ravnoteže za vezanje željeza(III) na asijalotransferin približno deset puta veće nego za nativni transferin. Drugim riječima, pri tim kiselijim uvjetima, utjecaj desijalinizacije na povećanu sposobnost proteina da veže željezo(III) još je izraženiji nego pri fiziološkom pH.

Opaženo je da varijacija pH ima značajan utjecaj i na faktore f_{sp} i F(FeTf). Ustanovljeno je da je vezanje na drugo vezno mjesto asijalotransferina manje ovisno o pH nego u slučaju nativnog transferina (**Rad 4**, **Slika 4**). Pri fiziološkom pH, odnosno pri pH = 7,4, vrijednosti

F(FeTf) nativnog i asijalotransferina vrlo su slične i nešto niže od 0,3 (**Rad 4**, **Slika 5**)**.** Budući da su te vrijednosti ispod 0,5, to upućuje na pozitivnu kooperativnost. Drugim riječima, vezanje prvog iona željeza(III) pospješuje vezanje sljedećeg iona željeza(III), što rezultira nešto većom količinom Fe_2Tf kompleksa i nešto manjom količinom FeTf kompleksa od onoga što bi se očekivalo u slučaju vezanja na dva međusobno neovisna vezna mjesta.

Sniženjem pH trend se mijenja, te pri pH 6,2 i 5,9, *F*(FeTf) vrijednosti asijalotransferina i nativnog transferina ponovno su međusobno slične, ali su znatno više od 0,5, što upućuje na promjenu kooperativnosti, odnosno vezanje željeza postaje prividno negativno kooperativno. Pri pH 6,5, razlike *F*(FeTf) faktora nativnog i asijalotransferina vrlo su velike; zanimljivo je da je vezanje pozitivno kooperativno u slučaju asijalotransferina, a negativno kooperativno u slučaju nativnog proteina. Pri pH 6,8 (vrijednosti su izostavljene iz grafičkih prikaza rezultata u **Radu 4**), rezultati upućuju na vrlo visoku kooperativnost, do te mjere da je izgledno kako su tijekom cijele titracije prisutne samo male količine jednostruko zasićenih formi (FeTf), jer rezultati upućuju na to da dodano željezo preferencijalno dodatno zasićuje FeTf. Prema tome, vezanje se uglavnom odvija skoro kao da iz apoTf direktno nastaje Fe_2Tf, bez prethodne akumulacije značajnijih količina jednostruko zasićene forme. Navedena pojava uzrokovala je problem prilikom preciznog određivanja konstanti K_{1m} i K_{2m}, i posljedično kumulativnih konstanti K'_{1m} i K'_{2m}, jer dominantno vezanje drugog iona željeza efektivno maskira prisutnost i učinak vezanja prvog iona. Opažena vrlo izražena pozitivna kooperativnost vjerojatno je posljedica specifičnih uvjeta pH i ionske jakosti, premda bi se navedene utjecaje vjerojatno isplatilo dodatno istražiti prije donošenja konkretnijih zaključaka koji bi nedvojbeno objasnili tu anomaliju.

Rezultati dobiveni u **Radu 4** mogu pomoći u uspostavljanju korelacije između promjena u strukturi glikana transferina, koje su povezane s različitim fiziološkim uvjetima, i uočenih promjena u ravnotežama vezanja željeza. Uočeno je da asijalotransferin veže željezo učinkovitije od nativnog transferina u cjelokupnom analiziranom rasponu pH, a razlike u afinitetu pogotovo su izražene u kiselim uvjetima (pH = 5,9). To naglašava potencijalni značaj asijalotransferina u regulaciji dostupnosti željeza i toksičnosti u ishemičkim tkivima. Povišene količine asijalotransferina u organizmu mogle bi značajno utjecati na dinamiku labilnog bazena (odjeljka) željeza (engl. *Labile Iron Pool*, LIP) i posljedično na patofiziološke učinke ishemijskih događaja. Eksperimenti provedeni pri pH nižem od tipičnog fiziološkog (≈ 7,4) također mogu biti od fiziološkog značaja. Najkiseliji uvjeti ostvareni u eksperimentima bliski su pH endosoma, u kojem se uslijed sniženog pH i dodatne interakcije transferina s receptorom u organizmu događa otpuštanje željeza (115). pH vrijednosti između najviše i najniže korištene

u eksperimentima mogu biti ostvarene tijekom acidoze tkiva, koja može biti posljedica brojnih patoloških stanja, a nerijetko je i direktni rezultat hipoksije (360,361).

Nadalje, u sklopu ove studije razvijen je predložak za numeričko rješavanje problema kemijske ravnoteže koristeći Microsoft Excel. Ovaj pristup, koji se temelji na polinomu vezanja, služi kao moguća osnova za sveobuhvatna i modelno-neovisna istraživanje konstanti ravnoteže.

7. ZAKLJUČCI

Uspješna optimizacija procesa enzimske desijalinizacije transferina provedena je korištenjem komercijalno dostupnih enzimskih pripravaka za uklanjanje sijalinske kiseline s krajeva glikanskih lanaca glikoproteina. Variranjem uvjeta u otopini i trajanja procesa postignut je približno stotinu puta veći prinos od onog deklariranog od strane proizvođača. Kvaliteta desijalinizacijskog procesa precizno je potvrđena korištenjem spregnutog UHPLC-MS/MS sustava. Ovo istraživanje je značajno jer je omogućilo učinkovitu pripremu velikih količina asijalotransferina uz minimalne troškove, s obzirom na visoku cijenu enzimskih pripravaka. Primjenom slične metodologije vjerojatno je moguće značajno unaprijediti pripravu i nekih drugih desijaliniziranih proteina osim samog transferina.

Nova kromatografska procedura razvijena je za razdvajanje nativnog transferina od asijalotransferina pomoću pH gradijenta. Metoda se pokazala posebno prikladnom za preliminarno testiranje kvalitete enzimske desijalinizacije. Također je perspektivna za preparativno pročišćavanje različitih oblika transferina, a preliminarni rezultati pokazali su da se uz manje modifikacije metode mogu razmjerno dobro razdvojiti različite transferinske glikoforme dobivene nepotpunom desijalinizacijom. Kombinacijom manje efikasnog („istrošenog“) enzimskog pripravka, koji ima nižu enzimsku aktivnost zbog pretjeranog korištenja, i navedene kromatografske tehnike, potencijalno je moguće pripraviti i međusobno razdvojiti različite, rijetke transferinske glikoforme koje nisu potpuno desijalinizirane. Dodatna prednost metode je to što se vrši upotrebom FPLC sustava koji su u pravilu razmjerno jeftini u usporedbi s visokotlačnim (U)HPLC sustavima. To omogućuje širu primjenu metode s obzirom na niže troškove samih uređaja i njihovog rada. Također je zanimljivo poboljšanje kromatografske razlučivosti postignuto povezivanjem višestrukih kolona u seriju. Navedeni pristup može općenito biti koristan za niskotlačne FPLC sustave kod kojih je moguće takvo serijsko povezivanje kolona bez ekstremnog porasta ukupnog tlaka unutar kromatografskog sustava. Za uspješno razdvajanje sijaloformi u pH-gradijentu ključan je bio odabir pogodnih pufera. To je posebno značajno ako se želi razdvajati više različitih glikoformi. U takvim slučajevima, gdje je potrebno postići razmjerno širok pH raspon, puferski kapacitet mora biti dovoljno visok u širem području. To uglavnom nije slučaj kod većine jednostavnijih pufera. Brzina i jednostavnost predočene metode dodatne su prednosti koje je čine još prikladnijom za širu upotrebu.

Zbog opaženog nedostatka potencijalnih IFE korekcijskih metoda koje se mogu primijeniti na mjerenja izvršena u mikrotitarskim pločicama, razvijena je nova korekcijska metoda primjenjiva za te uređaje. Primjena takve metode nužan je preduvjet za kvalitetu narednih fluorimetrijskih istraživanja, jer ako IFE artefakti nisu pravilno uklonjeni, određivanje konstanti ravnoteže iz titracijskih krivulja može biti pogrešno. Štoviše, budući da su tipične fluorimetrijske titracijske krivulje nelinearne, a IFE uzrokuje dodatnu nelinearnost u odzivu fluorescencije kao funkcije koncentracije fluorofora, nije lako razlučiti ta dva utjecaja u kombiniranim krivuljama. IFE artefakti mogu se "maskirati" kao nešto snažnije ili slabije vezanje, ovisno o tome dolazi li prilikom vezanja do porasta ili pada intrinzične fluorescencije proteina. Bez prikladne korekcije moguće je stoga dobiti potpuno pogrešne procjene konstanti ravnoteže premda to možda nije očito iz izgleda fluorimetrijskih profila.

Razvijena metoda korekcije IFE temelji se na mjerenju fluorescencije uzoraka pri različitim visinama optičkog elementa. Prednosti metode su višestruke. Metodu je vrlo jednostavno primijeniti na većini modernijih čitača mikrotitarskih pločica, s obzirom da takvi uređaji omogućuju jednostavno podešavanje visine optičkog elementa. Metoda je također primjenjiva za vrlo apsorptivne uzorke, što često nije slučaj kod tipičnih IFE metoda dizajniranih za klasične fluorimetre. Dodatna prednost metode je to što ona zahtijeva samo mjerenja fluorescencije, odnosno nije potrebno mjeriti apsorbanciju. S obzirom da su fluorimetrijske mikrotitarske pločice s UV-Vis propusnim dnom u pravilu višestruko skuplje od neprozirnih (crnih) fluorimetrijskih pločica, primjena ove metode omogućuje potencijalne uštede u vidu potrošnog materijala, odnosno pločica. Metoda je široko primjenjiva, odnosno može se koristiti za različite vrste fluorimetrijskih eksperimenata i tvari, a ne samo specifično za titracije transferina s kompleksom FeNTA ili slične eksperimente. Zanimljivo je dodati da je vršenje IFE korekcija navedenom metodom dodatno olakšano postojanjem mrežne stranice koja omogućuje jednostavan unos nekorigiranih podataka i brzo dobivanje korekcijskih rezultata uz mogućnost izvoza raznih grafova i relevantnih numeričkih parametara.

Titracije transferinskih glikoformi kompleksom FeNTA provedene su sa svrhom određivanja konstanti ravnoteže vezanja željeza(III) na nativni i asijalotransferin pri različitim pH uvjetima. Titracijski eksperimenti provedeni su pomoću OT-2 robota, a fluorescencija je mjerena pomoću čitača mikrotitarskih pločica. Navedeni pristup omogućava visokoprotočna mjerenja uz niske utroške skupih proteinskih uzoraka. Takvom procedurom omogućeno je jednostavno vršenje mjerenja u replikatima, čime se poboljšava statistička snaga dobivenih rezultata. Automatiziranim postupkom jednostavno se vrši randomizacija prostornih pozicija

pojedinih uzoraka u mikrotitarskoj pločici, čime se umanjuju eventualne sustavne pogreške koje se mogu ispoljiti zbog nepravilnosti pločica i/ili anizotropije položaja.

Usporedbom rezultata za nativni transferin dobivenih pri fiziološkom pH (7,4), validirana je metoda fluorimetrijskog određivanja konstanti ravnoteže. Vrijednosti izračunatih konstanti bliske su vrijednostima iz referentnih studija. Obradom fluorimetrijskih rezultata, nakon primjene nove IFE korekcijske metode, izračunate su koncentracijske konstante ravnoteže vezanja željeza(III) na oba vezna mjesta proteina, za nativni i asijalotransferin, pri pet različitih pH vrijednosti (7,4, 6,8, 6,5, 6,2 i 5,9). Iz tih konstanti izračunate su i kondicionalne konstante, uzimajući u obzir utjecaj pH na protonaciju svih FeNTA i NTA vrsta prisutnih u otopini. Ustanovljeno je da su pri svim pH vrijednostima konstante ravnoteže vezanja željeza(III) na oba vezna mjesta proteina statistički značajno više u slučaju asijalotransferina (u odnosu na nativni protein). U slučaju fiziološkog pH = 7,4, razlika je približno trostruka za oba vezna mjesta. To je, uz manje odstupanje, u skladu s rezultatima postignutim ITC mjerenjima, pri nešto različitim uvjetima u otopini, ali pri istom pH. Navedena razlika u konstantama nativnog i asijalotransferina najznačajnija je pri najnižem pH = 5,9, gdje su konstante za asijalotransferin približno deset puta veće od onih za nativni. Očekivano, sa sniženjem pH dolazi i do smanjenja konstanti ravnoteže za oba vezna mjesta, i to u slučaju i nativnog i desijaliniziranog transferina. Pri pH = 6,8 izračun konstanti ravnoteže pokazao se neuspješnim, najvjerojatnije uslijed visoke pozitivne kooperativnosti i efektivnog maskiranja vezanja na prvo vezno mjesto vezanjem željeza na drugo vezno mjesto. Zbog navedenih učinaka, primijenjena fluorimetrijska metoda očito nije dovoljno osjetljiva za precizno određivanje konstanti ravnoteže u ovom specifičnom slučaju. Ova konkretna anomalija, prema znanju autora, nije prethodno opisana u literaturi. Razlog tome vjerojatno leži u činjenici da su istraživanja kompleksiranja transferina uglavnom provođena pri fiziološkom pH ili pH vrijednostima endosoma, dok je ponašanje sustava pri međuvrijednostima pH slabo ispitano. Premda se kondicionalne konstante K'_{1m} i K'_{2m} međusobno razlikuju za oko tri puta između nativnog i asijalotransferina pri fiziološkom pH = 7,4, međusobne razlike između konstanti K'_{1m} i K'_{2m} unutar svake vrste transferina su znatno manje. To znači da su međusobne razlike u afinitetima prvog i drugog veznog mjesta za željezo male i u slučaju nativnog i u slučaju asijalotransferina pri fiziološkom pH. Sniženjem pH te razlike postaju značajnije, no pri pH = 6,5 razlike su vrlo značajne samo u slučaju nativnog transferina. Chasteen i Williams istraživali su utjecaj pH i prisutnosti soli (0,5 M NaCl) na vezanje željeza na nativni transferin u pH rasponu od 6,0 do 9,0 (308). Otkrili su da je faktor preferencije vezanja ovisan o pH te da prisutnost NaCl značajno utječe na afinitet prema željezu. Pri nižim pH vrijednostima željezo se preferencijalno veže na C- terminalno vezno

mjesto, neovisno o soli. Povećanjem pH, ta se preferencija mijenja, a prisutnost NaCl dodatno modulira ravnotežu vezanja. Opaženi značajan utjecaj soli u otopini na navedene ravnoteže može djelomično objasniti određene manje nesrazmjere rezultata dobivenih ITC eksperimentima (bez prisustva dodane soli) i fluorimetrijskih eksperimenata prikazanih u sklopu **Rada 4** uz 0,2 M KCl.

Uklanjanje ostataka sijalinske kiseline vjerojatno značajno utječe na konformaciju proteina, stabilizirajući mjesto koje je tipično osjetljivije na promjene pH. Elektrostatske i konformacijske razlike nastale modifikacijom transferina uklanjanjem sijalinske kiseline mogle bi utjecati i na endocitozu posredovanu transferinskim receptorom. Naime, transferinski receptori TfR_1 i TfR_2 preferencijalno se vežu na zasićeni holotransferin (Fe_2Tf). Povećano formiranje holo-formi asijalotransferina (Fe_2Tf) može imati implikacije na mehanizme staničnog unosa željeza. Opažena preferencija asijalotransferina ka formiranju holo-formi može utjecati na njegovu interakciju s transferinskim receptorima, utječući time na unos željeza u stanice. Ovo bi moglo biti posebno relevantno u brzo dijelećim stanicama, poput stanica raka, koje imaju visoke potrebe za željezom.

Poznato je da se u ljudskom organizmu vrši značajna i brza desijalinizacija transferina tijekom sepse i drugih upalnih procesa. Viši afinitet asijalotransferina za željezo(III) vjerojatno pridonosi "izgladnjivanju" bakterija željezom, s obzirom da metabolizam patogenih bakterija obično zahtijeva veliku potrošnju i unos željeza. S obzirom da je acidoza tkiva česta popratna pojava ozljeda tkiva, upala i ishemije (362), povišeni afinitet asijalotransferina prema željezu(III) u tim kiselim uvjetima može biti od velikog fiziološkog značaja. Primjerice, u ishemičnim tkivima, gdje nedostatak kisika vodi do acidoze, pojačana sposobnost vezanja željeza asijalotransferinom mogla bi utjecati na distribuciju i dostupnost željeza. Ovo bi moglo utjecati na stanične odgovore na ishemiju, uključujući preživljavanje stanica, apoptozu ili oksidativni stres.

Razumijevanje međuodnosa sijalilacije transferina i njegovog afiniteta za vezanje željeza ne samo da rasvjetljava temeljne biokemijske procese, već ima i potencijalne kliničke implikacije. Otvaraju se mogućnosti za istraživanje novih strategija u upravljanju poremećajima povezanim sa željezom i naglašava se važnost posttranslacijskih modifikacija u regulaciji funkcije proteina.

8. LITERATURNI IZVORI

1. Holmes RJ, Lu Y, Lu L. Introduction: Overview of the global iron ore industry. In: Iron Ore [Internet]. Elsevier; 2022 [cited 2024 Oct 27]. p. 1–56. Available from: https://linkinghub.elsevier.com/retrieve/pii/B9780128202265000239
2. Aisen P. Chemistry and biology of eukaryotic iron metabolism. The International Journal of Biochemistry & Cell Biology. 2001 Oct;33(10):940–59.
3. Baumgartner J, Faivre D. Iron solubility, colloids and their impact on iron (oxyhydr)oxide formation from solution. Earth-Science Reviews. 2015 Nov;150:520–30.
4. McCafferty E, Hackerman N. Kinetics of Iron Corrosion in Concentrated Acidic Chloride Solutions. J Electrochem Soc. 1972;119(8):999.
5. Pehkonen S. Determination of the oxidation states of iron in natural waters. A review. Analyst. 1995;120(11):2655.
6. Tomyn S, Shylin SI, Bykov D, Ksenofontov V, Gumienna-Kontecka E, Bon V, et al. Indefinitely stable iron(IV) cage complexes formed in water by air oxidation. Nat Commun. 2017 Jan 19;8(1):14099.
7. Mayer M, Vankova N, Stolz F, Abel B, Heine T, Asmis KR. Identification of a Two-Coordinate Iron(I)–Oxalate Complex. Angew Chem Int Ed. 2022 Apr 11;61(16):e202117855.
8. Keilwerth M, Mao W, Malischewski M, Jannuzzi SAV, Breitwieser K, Heinemann FW, et al. The synthesis and characterization of an iron(VII) nitrido complex. Nat Chem. 2024 Apr;16(4):514–20.
9. King RB, Crabtree RH, Lukehart CM, Atwood DA, Scott RA, editors. Encyclopedia of Inorganic Chemistry [Internet]. 1st ed. Wiley; 2005 [cited 2024 Oct 27]. Available from: https://onlinelibrary.wiley.com/doi/book/10.1002/0470862106
10. Cotton SA. Some aspects of the coordination chemistry of iron(III). Coordination Chemistry Reviews. 1972 Oct;8(3):185–223.
11. Grau M, England J, Torres Martin De Rosales R, Rzepa HS, White AJP, Britovsek GJP. Coordination Equilibria Between Seven- and Five-coordinate Iron(II) Complexes. Inorg Chem. 2013 Oct 21;52(20):11867–74.
12. Pascualini ME, Di Russo NV, Thuijs AE, Ozarowski A, Stoian SA, Abboud KA, et al. A high-spin square-planar Fe(II) complex stabilized by a trianionic pincer-type ligand and conclusive evidence for retention of geometry and spin state in solution. Chem Sci. 2015;6(1):608–12.
13. Goodenough JB. Jahn-Teller distortions induced by tetrahedral-site Fe2+ ions. Journal of Physics and Chemistry of Solids. 1964 Feb;25(2):151–60.
14. Zheng Y, Xie H, Li J, Hui KS, Yu Z, Xu H, et al. Insights into the Jahn-Teller Effect in Layered Oxide Cathode Materials for Potassium-Ion Batteries. Advanced Energy Materials. 2024 Apr;14(14):2400461.
15. Toledo S, Poon PCY, Gleaves M, Rees J, Rogers DM, Kaminsky W, et al. Increasing reactivity by incorporating π-acceptor ligands into coordinatively unsaturated thiolate-ligated iron(II) complexes. Inorganica Chimica Acta. 2021 Sep;524:120422.
16. Moreland AC, Rauchfuss TB. Binding of π-Acceptor Ligands to (Triamine)iron(II) Complexes. Inorg Chem. 2000 Jul 1;39(14):3029–36.
17. Vinod Kumar Vashistha, Kumar A, Tevatia P, Das DK. Synthesis, Characterization, Electrochemical and Antimicrobial Studies of Iron(II) and Nickel(II) Macrocyclic Complexes. Russ J Electrochem. 2021 Apr;57(4):348–56.

18. Jones PL, Jeffery JC, McCleverty JA, Ward MD. Dinuclear and tetranuclear oxo-bridged iron(III) complexes of the ambidentate ligand 3-(2-pyridyl)-pyrazole. Polyhedron. 1997 Jan;16(9):1567–71.
19. Ibrahim O, O'Sullivan J. Iron chelators in cancer therapy. Biometals. 2020 Oct;33(4–5):201–15.
20. Entezari S, Haghi SM, Norouzkhani N, Sahebnazar B, Vosoughian F, Akbarzadeh D, et al. Iron Chelators in Treatment of Iron Overload. Abd Elhakim Y, editor. Journal of Toxicology. 2022 May 5;2022:1–18.
21. Casado CM, Alonso B, García-Armada MP. Ferrocenes and Other Sandwich Complexes of Iron. In: Comprehensive Organometallic Chemistry IV [Internet]. Elsevier; 2022 [cited 2024 Oct 27]. p. 3–45. Available from: https://linkinghub.elsevier.com/retrieve/pii/B9780128202067000834
22. Astruc D, Ruiz J. On the Redox Chemistry of Ferrocenes and Other Iron Sandwich Complexes and Its Applications. J Inorg Organomet Polym. 2015 May;25(3):330–8.
23. Astruc D. Why is Ferrocene so Exceptional? Eur J Inorg Chem. 2017 Jan 3;2017(1):6–29.
24. Martin RL, Hay PJ, Pratt LR. Hydrolysis of Ferric Ion in Water and Conformational Equilibrium. J Phys Chem A. 1998 May 1;102(20):3565–73.
25. Millero FJ, Yao W, Aicher J. The speciation of Fe(II) and Fe(III) in natural waters. Marine Chemistry. 1995 Aug;50(1–4):21–39.
26. Guimarães L, De Abreu HA, Duarte HA. Fe(II) hydrolysis in aqueous solution: A DFT study. Chemical Physics. 2007 Mar;333(1):10–7.
27. Borko V, Friganović T, Weitner T. Preparation and characterization of iron(III) nitrilotriacetate complex in aqueous solutions for quantitative protein binding experiments. Anal Methods. 2023;15(46):6499–513.
28. Friganović T, Borko V, Weitner T. Protein sialylation affects the pH-dependent binding of ferric ion to human serum transferrin. Dalton Trans. 2024;53(25):10462–74.
29. Jomova K, Valko M. Importance of Iron Chelation in Free Radical-Induced Oxidative Stress and Human Disease. CPD. 2011 Oct 1;17(31):3460–73.
30. Waters SE, Robb BH, Marshak MP. Effect of Chelation on Iron–Chromium Redox Flow Batteries. ACS Energy Lett. 2020 Jun 12;5(6):1758–62.
31. Quintero-Gutiérrez AG, González-Rosendo G, Sánchez-Muñoz J, Polo-Pozo J, Rodríguez-Jerez JJ. Bioavailability of Heme Iron in Biscuit Filling Using Piglets as an Animal Model for Humans. Int J Biol Sci. 2008;58–62.
32. Abbaspour N, Hurrell R, Kelishadi R. Review on iron and its importance for human health. J Res Med Sci. 2014 Feb;19(2):164–74.
33. Guerinot ML. MICROBIAL IRON TRANSPORT. Annu Rev Microbiol. 1994 Oct;48(1):743–72.
34. Miethke M, Marahiel MA. Siderophore-Based Iron Acquisition and Pathogen Control. Microbiol Mol Biol Rev. 2007 Sep;71(3):413–51.
35. Khan A, Singh P, Srivastava A. Synthesis, nature and utility of universal iron chelator – Siderophore: A review. Microbiological Research. 2018 Jul;212–213:103–11.
36. Stoj CS, Augustine AJ, Zeigler L, Solomon EI, Kosman DJ. Structural Basis of the Ferrous Iron Specificity of the Yeast Ferroxidase, Fet3p. Biochemistry. 2006 Oct 1;45(42):12741–9.
37. Bonaccorsi Di Patti MC, Miele R, Eugenia Schininà M, Barra D. The yeast multicopper oxidase Fet3p and the iron permease Ftr1p physically interact. Biochemical and Biophysical Research Communications. 2005 Jul;333(2):432–7.

38. Severance S, Chakraborty S, Kosman DJ. The Ftr1p iron permease in the yeast plasma membrane: orientation, topology and structure-function relationships. Biochemical Journal. 2004 Jun 1;380(2):487–96.
39. Radisky D, Kaplan J. Regulation of Transition Metal Transport across the Yeast Plasma Membrane. Journal of Biological Chemistry. 1999 Feb;274(8):4481–4.
40. Schröder I, Johnson E, De Vries S. Microbial ferric iron reductases. FEMS Microbiol Rev. 2003 Jun;27(2–3):427–47.
41. Jhurry ND, Chakrabarti M, McCormick SP, Holmes-Hampton GP, Lindahl PA. Biophysical Investigation of the Ironome of Human Jurkat Cells and Mitochondria. Biochemistry. 2012 Jul 3;51(26):5276–84.
42. Attieh ZK, Mukhopadhyay CK, Seshadri V, Tripoulas NA, Fox PL. Ceruloplasmin Ferroxidase Activity Stimulates Cellular Iron Uptake by a Trivalent Cation-specific Transport Mechanism. Journal of Biological Chemistry. 1999 Jan;274(2):1116–23.
43. Chifman J, Laubenbacher R, Torti SV. A Systems Biology Approach to Iron Metabolism. In: Corey SJ, Kimmel M, Leonard JN, editors. A Systems Biology Approach to Blood [Internet]. New York, NY: Springer New York; 2014 [cited 2024 Oct 27]. p. 201–25. (Advances in Experimental Medicine and Biology; vol. 844). Available from: https://link.springer.com/10.1007/978-1-4939-2095-2_10
44. Buzała M, Janicki B, Buzała M, Słomka A. Heme iron in meat as the main source of iron in the human diet. J Elem [Internet]. 2015 Dec 3 [cited 2024 Oct 27];(1/2016). Available from: http://jsite.uwm.edu.pl/articles/view/850/
45. Piskin E, Cianciosi D, Gulec S, Tomas M, Capanoglu E. Iron Absorption: Factors, Limitations, and Improvement Methods. ACS Omega. 2022 Jun 21;7(24):20441–56.
46. Pietrangelo A. Hereditary Hemochromatosis: Pathogenesis, Diagnosis, and Treatment. Gastroenterology. 2010 Aug;139(2):393-408.e2.
47. Powell LW. Diagnosis of Hemochromatosis. Ann Intern Med. 1998 Dec 1;129(11_Part_2):925.
48. Cappellini MD, Musallam KM, Taher AT. Overview of Iron Chelation Therapy with Desferrioxamine and Deferiprone. Hemoglobin. 2009 Jan;33(sup1):S58–69.
49. Ahmed MH, Ghatge MS, Safo MK. Hemoglobin: Structure, Function and Allostery. In: Hoeger U, Harris JR, editors. Vertebrate and Invertebrate Respiratory Proteins, Lipoproteins and other Body Fluid Proteins [Internet]. Cham: Springer International Publishing; 2020 [cited 2024 Oct 27]. p. 345–82. (Subcellular Biochemistry; vol. 94). Available from: http://link.springer.com/10.1007/978-3-030-41769-7_14
50. Thomas C, Lumb AB. Physiology of haemoglobin. Continuing Education in Anaesthesia Critical Care & Pain. 2012 Oct;12(5):251–6.
51. Gell DA. Structure and function of haemoglobins. Blood Cells, Molecules, and Diseases. 2018 May;70:13–42.
52. Nascimento ALA, Guimarães AS, Rocha TDS, Goulart MOF, Xavier JDA, Santos JCC. Structural changes in hemoglobin and glycation. In: Vitamins and Hormones [Internet]. Elsevier; 2024 [cited 2024 Oct 27]. p. 183–229. Available from: https://linkinghub.elsevier.com/retrieve/pii/S0083672924000049
53. Baldwin JM. The structure of human carbonmonoxy haemoglobin at 2.7 Å resolution. Journal of Molecular Biology. 1980 Jan;136(2):103–28.
54. Baldwin J, Chothia C. Haemoglobin: The structural changes related to ligand binding and its allosteric mechanism. Journal of Molecular Biology. 1979 Apr;129(2):175–220.
55. Marengo-Rowe AJ. Structure-Function Relations of Human Hemoglobins. Baylor University Medical Center Proceedings. 2006 Jul;19(3):239–45.
56. Habler OP, Messmer KFW. The physiology of oxygen transport. Transfusion Science. 1997 Sep;18(3):425–35.

57. Hsia CCW. Respiratory Function of Hemoglobin. Epstein FH, editor. N Engl J Med. 1998 Jan 22;338(4):239–48.
58. Yu S. Hemoglobin: Physiology and Hemoglobinopathy. In: Liu H, Kaye AD, Jahr JS, editors. Blood Substitutes and Oxygen Biotherapeutics [Internet]. Cham: Springer International Publishing; 2022 [cited 2024 Oct 27]. p. 45–51. Available from: https://link.springer.com/10.1007/978-3-030-95975-3_4
59. Wittenberg JB, Wittenberg BA. Myoglobin function reassessed. Journal of Experimental Biology. 2003 Jun 15;206(12):2011–20.
60. Schlichting I, Berendzen J, Phillips GN, Sweet RM. Crystal structure of photolysed carbonmonoxy-myoglobin. Nature. 1994 Oct;371(6500):808–12.
61. Scott Mathews F. The structure, function and evolution of cytochromes. Progress in Biophysics and Molecular Biology. 1985;45(1):1–56.
62. Yamanaka T, Okunuki K. CYTOCHROMES. In: Microbial Iron Metabolism [Internet]. Elsevier; 1974 [cited 2024 Oct 27]. p. 349–400. Available from: https://linkinghub.elsevier.com/retrieve/pii/B9780125152501500199
63. Ghosh A, Mitchell DA, Chanda A, Ryabov AD, Popescu DL, Upham EC, et al. Catalase−Peroxidase Activity of Iron(III)−TAML Activators of Hydrogen Peroxide. J Am Chem Soc. 2008 Nov 12;130(45):15116–26.
64. Bai J, Cederbaum AI. Mitochondrial Catalase and Oxidative Injury. Neurosignals. 2001;10(3–4):189–99.
65. Michiels C, Raes M, Toussaint O, Remacle J. Importance of SE-glutathione peroxidase, catalase, and CU/ZN-SOD for cell survival against oxidative stress. Free Radical Biology and Medicine. 1994 Sep;17(3):235–48.
66. Nordlund P, Reichard P. Ribonucleotide reductases. Annu Rev Biochem. 2006;75:681–706.
67. Lundin D, Berggren G, Logan D, Sjöberg BM. The Origin and Evolution of Ribonucleotide Reduction. Life. 2015 Feb 27;5(1):604–36.
68. Ahmad MdF, Dealwis CG. The Structural Basis for the Allosteric Regulation of Ribonucleotide Reductase. In: Progress in Molecular Biology and Translational Science [Internet]. Elsevier; 2013 [cited 2024 Oct 27]. p. 389–410. Available from: https://linkinghub.elsevier.com/retrieve/pii/B9780123869319000143
69. Shakoury-Elizeh M, Protchenko O, Berger A, Cox J, Gable K, Dunn TM, et al. Metabolic Response to Iron Deficiency in Saccharomyces cerevisiae. Journal of Biological Chemistry. 2010 May;285(19):14823–33.
70. Higashida K, Inoue S, Nakai N. Iron deficiency attenuates protein synthesis stimulated by branched-chain amino acids and insulin in myotubes. Biochemical and Biophysical Research Communications. 2020 Oct;531(2):112–7.
71. Song CC, Pantopoulos K, Chen GH, Zhong CC, Zhao T, Zhang DG, et al. Iron increases lipid deposition via oxidative stress-mediated mitochondrial dysfunction and the HIF1α-PPARγ pathway. Cell Mol Life Sci. 2022 Jul;79(7):394.
72. Rockfield S, Chhabra R, Robertson M, Rehman N, Bisht R, Nanjundan M. Links Between Iron and Lipids: Implications in Some Major Human Diseases. Pharmaceuticals. 2018 Oct 22;11(4):113.
73. Schiffer L, Barnard L, Baranowski ES, Gilligan LC, Taylor AE, Arlt W, et al. Human steroid biosynthesis, metabolism and excretion are differentially reflected by serum and urine steroid metabolomes: A comprehensive review. The Journal of Steroid Biochemistry and Molecular Biology. 2019 Nov;194:105439.
74. Acconcia F, Marino M. Steroid Hormones: Synthesis, Secretion, and Transport. In: Belfiore A, LeRoith D, editors. Principles of Endocrinology and Hormone Action [Internet].

Cham: Springer International Publishing; 2018 [cited 2024 Oct 27]. p. 43–72. (Endocrinology). Available from: http://link.springer.com/10.1007/978-3-319-44675-2_4
75. Doerge DR, Chang HC. Inactivation of thyroid peroxidase by soy isoflavones, in vitro and in vivo. Journal of Chromatography B. 2002 Sep;777(1–2):269–79.
76. Gierach M, Rudewicz M, Junik R. Iron and ferritin deficiency in women with hypothyroidism and chronic lymphocytic thyroiditis — systematic review. Endokrynol Pol. 2024 Jun 26;VM/OJS/J/97860.
77. Dichtl S, Haschka D, Nairz M, Seifert M, Volani C, Lutz O, et al. Dopamine promotes cellular iron accumulation and oxidative stress responses in macrophages. Biochemical Pharmacology. 2018 Feb;148:193–201.
78. Wu Q, Ren Q, Meng J, Gao WJ, Chang YZ. Brain Iron Homeostasis and Mental Disorders. Antioxidants. 2023 Nov 13;12(11):1997.
79. Xiong L, Helm EY, Dean JW, Sun N, Jimenez-Rondan FR, Zhou L. Nutrition impact on ILC3 maintenance and function centers on a cell-intrinsic CD71–iron axis. Nat Immunol. 2023 Oct;24(10):1671–84.
80. Nairz M, Weiss G. Iron in infection and immunity. Molecular Aspects of Medicine. 2020 Oct;75:100864.
81. Pakdaman R, Chahine JMEH. A Mechanism for Iron Uptake by Transferrin. European Journal of Biochemistry. 1996 Mar 1;236(3):922–31.
82. Yu Y, Jiang L, Wang H, Shen Z, Cheng Q, Zhang P, et al. Hepatic transferrin plays a role in systemic iron homeostasis and liver ferroptosis. Blood. 2020 Aug 6;136(6):726–39.
83. Gkouvatsos K, Papanikolaou G, Pantopoulos K. Regulation of iron transport and the role of transferrin. Biochimica et Biophysica Acta (BBA) - General Subjects. 2012 Mar;1820(3):188–202.
84. Borko V, Friganović T, Weitner T. Glycoproteomics meets thermodynamics: A calorimetric study of the effect of sialylation and synergistic anion on the binding of iron to human serum transferrin. Journal of Inorganic Biochemistry. 2023 Jul;244:112207.
85. Kim BJ, Zhou J, Martin B, Carlson OD, Maudsley S, Greig NH, et al. Transferrin Fusion Technology: A Novel Approach to Prolonging Biological Half-Life of Insulinotropic Peptides. J Pharmacol Exp Ther. 2010 Sep;334(3):682–92.
86. Miljuš G, Penezić A, Pažitná L, Gligorijević N, Baralić M, Vilotić A, et al. Glycosylation and Characterization of Human Transferrin in an End-Stage Kidney Disease. IJMS. 2024 Apr 24;25(9):4625.
87. Clerc F, Reiding KR, Jansen BC, Kammeijer GSM, Bondt A, Wuhrer M. Human plasma protein N-glycosylation. Glycoconj J. 2016 Jun;33(3):309–43.
88. Gomme PT, McCann KB, Bertolini J. Transferrin: structure, function and potential therapeutic actions. Drug Discovery Today. 2005 Feb 15;10(4):267–73.
89. Yang N, Zhang H, Wang M, Hao Q, Sun H. Iron and bismuth bound human serum transferrin reveals a partially-opened conformation in the N-lobe. Sci Rep. 2012 Dec;2(1):999.
90. MacGillivray RTA, Moore SA, Chen J, Anderson BF, Baker H, Luo Y, et al. Two High-Resolution Crystal Structures of the Recombinant N-Lobe of Human Transferrin Reveal a Structural Change Implicated in Iron Release [†,‡]. Biochemistry. 1998 Jun;37(22):7919–28.
91. Rinaldo D, Field MJ. A Density Functional Theory Study of the Iron-Binding Site of Human Serum Transferrin. Aust J Chem. 2004;57(12):1219.
92. Byrne SL, Chasteen ND, Steere AN, Mason AB. The Unique Kinetics of Iron Release from Transferrin: The Role of Receptor, Lobe–Lobe Interactions, and Salt at Endosomal pH. Journal of Molecular Biology. 2010 Feb;396(1):130–40.

93. Steere AN, Byrne SL, Chasteen ND, Mason AB. Kinetics of iron release from transferrin bound to the transferrin receptor at endosomal pH. Biochimica et Biophysica Acta (BBA) - General Subjects. 2012 Mar;1820(3):326–33.
94. Edwards KC, Kim H, Ferguson R, Lockart MM, Vincent JB. Significance of conformation changes during the binding and release of chromium(III) from human serum transferrin. Journal of Inorganic Biochemistry. 2020 May;206:111040.
95. Zurita C, Tsushima S, Solari PL, Menut D, Dourdain S, Jeanson A, et al. Interaction Between the Transferrin Protein and Plutonium (and Thorium), What's New? Chemistry A European J. 2023 Oct 2;29(55):e202300636.
96. Moshtaghie AA, Badii A, Fazilati M, Hassanzadeh T, Kharazi H. Manganese and Iron Binding to Human Transferrin. Iranian Journal of Pharmaceutical Research. 2010;101–6.
97. Aisen P, Aasa R, Redfield AG. The Chromium, Manganese, and Cobalt Complexes of Transferrin. Journal of Biological Chemistry. 1969 Sep;244(17):4628–33.
98. Campos-Escamilla C, Siliqi D, Gonzalez-Ramirez LA, Lopez-Sanchez C, Gavira JA, Moreno A. X-ray Characterization of Conformational Changes of Human Apo- and Holo-Transferrin. IJMS. 2021 Dec 13;22(24):13392.
99. Hirose M. The Structural Mechanism for Iron Uptake and Release by Transferrins. Bioscience, Biotechnology, and Biochemistry. 2000 Jan 1;64(7):1328–36.
100. Bates GW, Graham G. Carbonate: Key to Transferrin Chemistry. In: Yasunodu KT, Mower HF, Hayaishi O, editors. Iron and Copper Proteins [Internet]. Boston, MA: Springer US; 1976 [cited 2024 Oct 27]. p. 400–7. (Advances in Experimental Medicine and Biology; vol. 74). Available from: http://link.springer.com/10.1007/978-1-4684-3270-1_34
101. Chung MCM. Structure and function of transferrin. Biochem Educ. 1984 Oct 1;12(4):146–54.
102. Silva AMN, Moniz T, De Castro B, Rangel M. Human transferrin: An inorganic biochemistry perspective. Coordination Chemistry Reviews. 2021 Dec;449:214186.
103. Aisen P, Aasa R, Malmström BG, Vänngård T. Bicarbonate and the Binding of Iron to Transferrin. Journal of Biological Chemistry. 1967 May;242(10):2484–90.
104. Schlabach MR, Bates GW. The synergistic binding of anions and Fe3+ by transferrin. Implications for the interlocking sites hypothesis. J Biol Chem. 1975 Mar 25;250(6):2182–8.
105. Kumar R, Sharma D, Kumar N, Kumari B, Shabnam, Kumar S, et al. Substitution of carbonate by non-physiological synergistic anion modulates the stability and iron release kinetics of serum transferrin. Biochimica et Biophysica Acta (BBA) - Proteins and Proteomics. 2023 Jan;1871(1):140856.
106. Halbrooks PJ, Mason AB, Adams TE, Briggs SK, Everse SJ. The Oxalate Effect on Release of Iron from Human Serum Transferrin Explained. Journal of Molecular Biology. 2004 May;339(1):217–26.
107. Dassanayake U, Gnanathasan C. Acute renal failure following oxalic acid poisoning: a case report. Journal of Occupational Medicine and Toxicology. 2012;7(1):17.
108. Pomara C, Fiore C, D'Errico S, Riezzo I, Fineschi V. Calcium oxalate crystals in acute ethylene glycol poisoning: A confocal laser scanning microscope study in a fatal case. Clinical Toxicology. 2008 Jan;46(4):322–4.
109. James LF. Oxalate Toxicosis. Clinical Toxicology. 1972 Jan;5(2):231–43.
110. Ghanbari Z, Housaindokht MR, Bozorgmehr MR, Izadyar M. Effects of synergistic and non-synergistic anions on the iron binding site from serum transferrin: A molecular dynamic simulation analysis. Journal of Molecular Graphics and Modelling. 2017 Nov;78:176–86.
111. Byrne SL, Steere AN, Chasteen ND, Mason AB. Identification of a Kinetically Significant Anion Binding (KISAB) Site in the N-Lobe of Human Serum Transferrin. Biochemistry. 2010 May 18;49(19):4200–7.

112. Garcia YS, Barros MR, Ventura GT, De Queiroz RM, Todeschini AR, Neves JL. Probing the interaction of carbonaceous dots with transferrin and albumin: Impact on the protein structure and non-synergetic metal release. Journal of Molecular Liquids. 2019 Oct;292:111460.
113. Bertini I, Hirose J, Kozlowski H, Luchinat C, Messori L, Scozzafava A. Effect of nonsynergistic anions on copper transferrin. Inorg Chem. 1988 Mar;27(6):1081–6.
114. Baldwin DA, De Sousa DM, Von Wandruszka RM. The effect of pH on the kinetics of iron release from human transferrin. Biochimica et Biophysica Acta (BBA)-General Subjects. 1982;719(1):140–6.
115. Lee DA, Goodfellow JM. The pH-Induced Release of Iron from Transferrin Investigated with a Continuum Electrostatic Model. Biophysical Journal. 1998 Jun;74(6):2747–59.
116. Giannetti AM, Halbrooks PJ, Mason AB, Vogt TM, Enns CA, Björkman PJ. The Molecular Mechanism for Receptor-Stimulated Iron Release from the Plasma Iron Transport Protein Transferrin. Structure. 2005 Nov;13(11):1613–23.
117. Dautry-Varsat A. Receptor-mediated endocytosis: The intracellular journey of transferrin and its receptor. Biochimie. 1986 Mar;68(3):375–81.
118. Testi C, Boffi A, Montemiglio LC. Structural analysis of the transferrin receptor multifaceted ligand(s) interface. Biophysical Chemistry. 2019 Nov;254:106242.
119. Jian J, Yang Q, Huang X. Src Regulates Tyr20 Phosphorylation of Transferrin Receptor-1 and Potentiates Breast Cancer Cell Survival. Journal of Biological Chemistry. 2011 Oct;286(41):35708–15.
120. Candelaria PV, Leoh LS, Penichet ML, Daniels-Wells TR. Antibodies Targeting the Transferrin Receptor 1 (TfR1) as Direct Anti-cancer Agents. Front Immunol. 2021 Mar 17;12:607692.
121. Kawabata H. Transferrin and transferrin receptors update. Free Radical Biology and Medicine. 2019 Mar;133:46–54.
122. Miyazawa M, Bogdan AR, Hashimoto K, Tsuji Y. Regulation of transferrin receptor-1 mRNA by the interplay between IRE-binding proteins and miR-7/miR-141 in the 3′-IRE stem–loops. RNA. 2018 Apr;24(4):468–79.
123. Cabrera C, Frisk C, Löfström U, Lyngå P, Linde C, Hage C, et al. Relationship between iron deficiency and expression of genes involved in iron metabolism in human myocardium and skeletal muscle. International Journal of Cardiology. 2023 May;379:82–8.
124. Li H, Blanc L, Choesang T, Chen H, Feola M, Bao W, et al. Changes in TfR1 Expression and Trafficking Correlate with Erythroid Effectiveness in β-Thalassemic Mice. Blood. 2014 Dec 6;124(21):51–51.
125. Wang S, He X, Wu Q, Jiang L, Chen L, Yu Y, et al. Transferrin receptor 1-mediated iron uptake plays an essential role in hematopoiesis. Haematologica. 2020 Aug;105(8):2071–82.
126. Worthen CA, Enns CA. The role of hepatic transferrin receptor 2 in the regulation of iron homeostasis in the body. Front Pharmacol [Internet]. 2014 Mar 6 [cited 2024 Apr 24];5. Available from: http://journal.frontiersin.org/article/10.3389/fphar.2014.00034/abstract
127. Trinder D, Baker E. Transferrin receptor 2: a new molecule in iron metabolism. The International Journal of Biochemistry & Cell Biology. 2003 Mar;35(3):292–6.
128. Pantopoulos K. TfR2 links iron metabolism and erythropoiesis. Blood. 2015 Feb 12;125(7):1055–6.
129. Kleven MD, Jue S, Enns CA. Transferrin Receptors TfR1 and TfR2 Bind Transferrin through Differing Mechanisms. Biochemistry. 2018 Mar 6;57(9):1552–9.

130. Pardridge WM. Kinetics of Blood–Brain Barrier Transport of Monoclonal Antibodies Targeting the Insulin Receptor and the Transferrin Receptor. Pharmaceuticals. 2021 Dec 21;15(1):3.
131. Klausner RD, Ashwell G, Van Renswoude J, Harford JB, Bridges KR. Binding of apotransferrin to K562 cells: explanation of the transferrin cycle. Proc Natl Acad Sci USA. 1983 Apr;80(8):2263–6.
132. Eckenroth BE, Steere AN, Chasteen ND, Everse SJ, Mason AB. How the binding of human transferrin primes the transferrin receptor potentiating iron release at endosomal pH. Proc Natl Acad Sci USA. 2011 Aug 9;108(32):13089–94.
133. Kumar R, Mauk AG. Protonation and Anion Binding Control the Kinetics of Iron Release from Human Transferrin. J Phys Chem B. 2012 Mar 29;116(12):3795–807.
134. Gelb MH, Harris DC. Correlation of proton release and ultraviolet difference spectra associated with metal binding by transferrin. Archives of Biochemistry and Biophysics. 1980 Mar;200(1):93–8.
135. Indrakumar S, Kulakova A, Harris P, Peters GHJ. Dynamics of Human Serum Transferrin in Varying Physicochemical Conditions Explored by Using Molecular Dynamics Simulations. Mol Pharmaceutics. 2022 Aug 1;19(8):2795–806.
136. Beatty EJ, Zhong W, Kubal G, Houldershaw D, Goodfellow JM, Sadler PJ. Histidine pKa values for the N-lobe of human transferrin: effect of substitution of binding site Asp by Ser (D63S). Journal of Inorganic Biochemistry. 2002 Feb;88(3–4):403–9.
137. Ohgami RS, Campagna DR, Greer EL, Antiochos B, McDonald A, Chen J, et al. Identification of a ferrireductase required for efficient transferrin-dependent iron uptake in erythroid cells. Nat Genet. 2005 Nov;37(11):1264–9.
138. Dhungana S, Taboy CH, Zak O, Larvie M, Crumbliss AL, Aisen P. Redox Properties of Human Transferrin Bound to Its Receptor. Biochemistry. 2004 Jan;43(1):205–9.
139. Reily C, Stewart TJ, Renfrow MB, Novak J. Glycosylation in health and disease. Nat Rev Nephrol. 2019 Jun;15(6):346–66.
140. Reynders E, Foulquier F, Annaert W, Matthijs G. How Golgi glycosylation meets and needs trafficking: the case of the COG complex. Glycobiology. 2011 Jul 1;21(7):853–63.
141. Zhang X, Wang Y. Glycosylation Quality Control by the Golgi Structure. Journal of Molecular Biology. 2016 Aug;428(16):3183–93.
142. Xu C, Ng DTW. Glycosylation-directed quality control of protein folding. Nat Rev Mol Cell Biol. 2015 Dec;16(12):742–52.
143. Parodi AJ. Protein Glucosylation and Its Role in Protein Folding. Annu Rev Biochem. 2000 Jun;69(1):69–93.
144. Jayaprakash NG, Surolia A. Role of glycosylation in nucleating protein folding and stability. Biochemical Journal. 2017 Jul 15;474(14):2333–47.
145. Boscher C, Dennis JW, Nabi IR. Glycosylation, galectins and cellular signaling. Current Opinion in Cell Biology. 2011 Aug;23(4):383–92.
146. J. B. The Role of Glycosylation in Receptor Signaling. In: Petrescu S, editor. Glycosylation [Internet]. InTech; 2012 [cited 2024 Oct 28]. Available from: http://www.intechopen.com/books/glycosylation/the-role-of-glycosylation-in-receptor-signaling
147. Lin B, Qing X, Liao J, Zhuo K. Role of Protein Glycosylation in Host-Pathogen Interaction. Cells. 2020 Apr 20;9(4):1022.
148. Conroy LR, Hawkinson TR, Young LEA, Gentry MS, Sun RC. Emerging roles of N-linked glycosylation in brain physiology and disorders. Trends in Endocrinology & Metabolism. 2021 Dec;32(12):980–93.
149. Zhai X, Yuan Y, He WT, Wu Y, Shi Y, Su S, et al. Evolving roles of glycosylation in the tug-of-war between virus and host. National Science Review. 2024 Apr 3;11(5):nwae086.

150. Mellquist JL, Kasturi L, Spitalnik SL, Shakin-Eshleman SH. The Amino Acid Following an Asn-X-Ser/Thr Sequon Is an Important Determinant of N-Linked Core Glycosylation Efficiency. Biochemistry. 1998 May 1;37(19):6833–7.
151. Shakin-Eshleman SH, Spitalnik SL, Kasturi L. The Amino Acid at the X Position of an Asn-X-Ser Sequon Is an Important Determinant of N-Linked Core-glycosylation Efficiency. Journal of Biological Chemistry. 1996 Mar;271(11):6363–6.
152. Aebi M. N-linked protein glycosylation in the ER. Biochimica et Biophysica Acta (BBA) - Molecular Cell Research. 2013 Nov;1833(11):2430–7.
153. Schwarz F, Aebi M. Mechanisms and principles of N-linked protein glycosylation. Current Opinion in Structural Biology. 2011 Oct;21(5):576–82.
154. Fisher P, Thomas-Oates J, Wood AJ, Ungar D. The N-Glycosylation Processing Potential of the Mammalian Golgi Apparatus. Front Cell Dev Biol. 2019 Aug 13;7:157.
155. Wang P, Wang H, Gai J, Tian X, Zhang X, Lv Y, et al. Evolution of protein N-glycosylation process in Golgi apparatus which shapes diversity of protein N-glycan structures in plants, animals and fungi. Sci Rep. 2017 Jan 11;7(1):40301.
156. Breitling J, Aebi M. N-Linked Protein Glycosylation in the Endoplasmic Reticulum. Cold Spring Harbor Perspectives in Biology. 2013 Aug 1;5(8):a013359–a013359.
157. Fischer K, Topallar S, Kraatz F, Groschup MH, Diederich S. The role of N-linked glycosylation in proteolytic processing and cell surface transport of the Cedar virus fusion protein. Virol J. 2022 Aug 23;19(1):136.
158. Esmail S, Manolson MF. Advances in understanding N-glycosylation structure, function, and regulation in health and disease. European Journal of Cell Biology. 2021 Sep;100(7–8):151186.
159. Crispin M, Scanlan CN, Bowden TA. Structure and Biosynthesis of Glycoprotein Carbohydrates. In: Comprehensive Biotechnology [Internet]. Elsevier; 2011 [cited 2024 Oct 28]. p. 73–90. Available from: https://linkinghub.elsevier.com/retrieve/pii/B978008088504900009X
160. Jensen PH, Kolarich D, Packer NH. Mucin-type O-glycosylation – putting the pieces together. The FEBS Journal. 2010 Jan;277(1):81–94.
161. Thompson N, Wakarchuk W. O-glycosylation and its role in therapeutic proteins. Bioscience Reports. 2022 Oct 28;42(10):BSR20220094.
162. Zhang L, Ten Hagen KG. Extracellular O-Glycans. In: Encyclopedia of Cell Biology [Internet]. Elsevier; 2023 [cited 2024 Oct 28]. p. 577–85. Available from: https://linkinghub.elsevier.com/retrieve/pii/B9780128216187000523
163. Tit-oon P, Wonglangka A, Boonkanta K, Ruchirawat M, Fuangthong M, Sasisekharan R, et al. Intact mass analysis reveals the novel O-linked glycosylation on the stalk region of PD-1 protein. Sci Rep. 2023 Jun 14;13(1):9631.
164. Chen SA, Lee TY, Ou YY. Incorporating significant amino acid pairs to identify O-linked glycosylation sites on transmembrane proteins and non-transmembrane proteins. BMC Bioinformatics. 2010 Dec;11(1):536.
165. Hanisch FG. O-Glycosylation of the Mucin Type. Biological Chemistry [Internet]. 2001 Jan 12 [cited 2024 Oct 28];382(2). Available from: https://www.degruyter.com/document/doi/10.1515/BC.2001.022/html
166. Tran DT, Ten Hagen KG. Mucin-type O-Glycosylation during Development. Journal of Biological Chemistry. 2013 Mar;288(10):6921–9.
167. Nason R, Büll C, Konstantinidi A, Sun L, Ye Z, Halim A, et al. Display of the human mucinome with defined O-glycans by gene engineered cells. Nat Commun. 2021 Jul 1;12(1):4070.
168. Lauc G, Trbojević-Akmačić I, editors. The Role of Glycosylation in Health and Disease [Internet]. Cham: Springer International Publishing; 2021 [cited 2024 Oct 28].

(Advances in Experimental Medicine and Biology; vol. 1325). Available from: https://link.springer.com/10.1007/978-3-030-70115-4
169. Rudman N, Gornik O, Lauc G. Altered N-glycosylation profiles as potential biomarkers and drug targets in diabetes. FEBS Letters. 2019 Jul;593(13):1598–615.
170. Shkunnikova S, Mijakovac A, Sironic L, Hanic M, Lauc G, Kavur MM. IgG glycans in health and disease: Prediction, intervention, prognosis, and therapy. Biotechnology Advances. 2023 Oct;67:108169.
171. Krištić J, Vučković F, Menni C, Klarić L, Keser T, Beceheli I, et al. Glycans Are a Novel Biomarker of Chronological and Biological Ages. The Journals of Gerontology: Series A. 2014 Jul;69(7):779–89.
172. Sanznebot V, Gonzalez P, Toro I, Ribes A, Barbosa J. Characterization of human transferrin glycoforms by capillary electrophoresis and electrospray ionization mass spectrometry. Journal of Chromatography B. 2003 Dec 5;798(1):1–7.
173. Cheng Y, Zak O, Aisen P, Harrison SC, Walz T. Structure of the human transferrin receptor-transferrin complex. Cell. 2004;116(4):565–76.
174. De Jong G, Van Eijk HG. Microheterogeneity of human serum transferrin: A biological phenomenon studied by isoelectric focusing in immobilized pH gradients. Electrophoresis. 1988 Jan;9(9):589–98.
175. Friganović T, Tomašić A, Šeba T, Biruš I, Kerep R, Borko V, et al. Low-pressure chromatographic separation and UV/Vis spectrophotometric characterization of the native and desialylated human apo-transferrin. Heliyon. 2021 Sep;7(9):e08030.
176. Paul A, Padler-Karavani V. Evolution of sialic acids: Implications in xenotransplant biology. Xenotransplantation. 2018 Nov;25(6):e12424.
177. Wada Y, Okamoto N. Electrospray Ionization Mass Spectrometry of Transferrin: Use of Quadrupole Mass Analyzers for Congenital Disorders of Glycosylation. Mass Spectrometry. 2022 Apr 15;11(1):A0103–A0103.
178. Petrén S, Vesterberg O. The N-acetylneuraminic acid content of five forms of human transferrin. Biochimica et Biophysica Acta (BBA) - Protein Structure and Molecular Enzymology. 1989 Feb;994(2):161–5.
179. Edwards M, McKenzie F, O'Callaghan S, Somerset D, Woodford P, Spilsbury J, et al. Prenatal Diagnosis of congenital disorder of glycosylation type Ia (CDG-Ia) by cordocentesis and transferrin isoelectric focussing of serum of a 27-week fetus with non-immune hydrops. Prenat Diagn. 2006 Oct;26(10):985–8.
180. Gornik O, Gornik I, Gašparović V, Lauc G. Change in transferrin sialylation is a potential prognostic marker for severity of acute pancreatitis. Clinical Biochemistry. 2008 May;41(7–8):504–10.
181. Goreta SS, Dabelic S, Dumic J. Insights into complexity of congenital disorders of glycosylation. Biochem Med (Zagreb). 2012 Jun 15;22(2):156–70.
182. Raynor A, Bruneel A, Vermeersch P, Cholet S, Friedrich S, Eckenweiler M, et al. "Hide and seek": Misleading transferrin variants in PMM2-CDG complicate diagnostics. Proteomics Clinical Apps. 2024 Mar;18(2):2300040.
183. Hall PL, Liedke K, Turgeon C, White A, Pino GB, Peck D, et al. Sensitivity of transferrin isoform analysis for PMM2-CDG. Molecular Genetics and Metabolism. 2024 Sep;143(1–2):108564.
184. Lebredonchel E, Duvet S, Douillard C, Foulquier F, Klein A. Variation of the serum *N* -glycosylation during the pregnancy of a MPI-CDG patient. JIMD Reports. 2021 Nov;62(1):22–9.
185. Poskanzer SA, Schultz MJ, Turgeon CT, Vidal-Folch N, Liedtke K, Oglesbee D, et al. Immune dysfunction in MGAT2-CDG : A clinical report and review of the literature. American J of Med Genetics Pt A. 2021 Jan;185(1):213–8.

186. Lefeber DJ, Morava E, Jaeken J. How to find and diagnose a CDG due to defective N-glycosylation. J of Inher Metab Disea. 2011 Aug;34(4):849–52.
187. Lipiński P, Tylki-Szymańska A. Congenital Disorders of Glycosylation: What Clinicians Need to Know? Front Pediatr. 2021 Sep 3;9:715151.
188. Westphal V, Xiao M, Kwok PY, Freeze HH. Identification of a frequent variant inALG6, the cause of Congenital Disorder of Glycosylation-Ic. Hum Mutat. 2003 Nov;22(5):420–1.
189. Mochel F, Sedel F, Vanderver A, Engelke UFH, Barritault J, Yang BZ, et al. Cerebellar ataxia with elevated cerebrospinal free sialic acid (CAFSA). Brain. 2009 Mar;132(3):801–9.
190. Vanderver A, Wolf NI. Genetic and Metabolic Disorders of the White Matter. In: Swaiman's Pediatric Neurology [Internet]. Elsevier; 2017 [cited 2024 Oct 28]. p. 747–58. Available from: https://linkinghub.elsevier.com/retrieve/pii/B9780323371018000990
191. Schauer R, Kamerling JP. Exploration of the Sialic Acid World. In: Advances in Carbohydrate Chemistry and Biochemistry [Internet]. Elsevier; 2018 [cited 2024 Oct 28]. p. 1–213. Available from: https://linkinghub.elsevier.com/retrieve/pii/S0065231818300015
192. Prolo LM, Vogel H, Reimer RJ. The Lysosomal Sialic Acid Transporter Sialin Is Required for Normal CNS Myelination. J Neurosci. 2009 Dec 9;29(49):15355–65.
193. Gornik O, Gornik I, Kolednjak IZ, Lauc G. Change of transferrin sialylation differs between mild sepsis and severe sepsis and septic shock. Internal medicine. 2011;50(8):861–9.
194. Piagnerelli M, Boudjeltia KZ, Nuyens V, De Backer D, Su F, Wang Z, et al. RAPID ALTERATIONS IN TRANSFERRIN SIALYLATION DURING SEPSIS: Shock. 2005 Jul;24(1):48–52.
195. Ganapathy S. R, Levová K, Kotačková L, Trnka J, Zogala D, Rusz J, et al. Increased Transferrin Sialylation Predicts Phenoconversion in Isolated REM Sleep Behavior Disorder. Movement Disorders. 2022 May;37(5):983–92.
196. Van Kamp GJ, Mulder K, Kuiper M, Wolters ECh. Changed transferrin sialylation in Parkinson's disease. Clinica Chimica Acta. 1995 Mar;235(2):159–67.
197. König P, Niederhofer H, Steurer H, Haller R, Wölfle R, Fritzsche H, et al. Changes of Carbohydrate-Deficient Transferrin in Chronic Alcoholism. Neuropsychobiology. 1995;32(4):192–6.
198. Fiorelli D, Romani L, Treglia M, Pallocci M, Passalacqua P, Coppeta L, et al. Carbohydrate-Deficient Transferrin (CDT) as a Biomarker of Alcohol Abuse: A Retrospective Study of the Italian Drinking Trend among Drivers from 2016 to 2022. Toxics. 2023 Nov 7;11(11):914.
199. Fleming MF, Anton RF, Spies CD. A Review of Genetic, Biological, Pharmacological, and Clinical Factors That Affect Carbohydrate-Deficient Transferrin Levels. Alcoholism Clin & Exp Res. 2004 Sep;28(9):1347–55.
200. Gonzalo P, Radenne S, Gonzalo S. Biomarkers of chronic alcohol misuse. CBF. 2014 Jan;9.
201. Arndt T. Carbohydrate-deficient Transferrin as a Marker of Chronic Alcohol Abuse: A Critical Review of Preanalysis, Analysis, and Interpretation. Clinical Chemistry. 2001 Jan 1;47(1):13–27.
202. del Castillo Busto ME, Montes-Bayón M, Blanco-González E, Meija J, Sanz-Medel A. Strategies To Study Human Serum Transferrin Isoforms Using Integrated Liquid Chromatography ICPMS, MALDI-TOF, and ESI-Q-TOF Detection: Application to Chronic Alcohol Abuse. Analytical Chemistry. 2005 Sep;77(17):5615–21.
203. De Jong G, Feelders R, Van Noort WL, Van Eijk HG. Transferrin microheterogeneity as a probe in normal and disease states. Glycoconj J. 1995 Jun;12(3):219–26.

204. Beck-Sickinger AG, Mörl K. Posttranslational Modification of Proteins. Expanding Nature's Inventory. By Christopher T. Walsh. Angew Chem Int Ed. 2006 Feb 6;45(7):1020–1020.
205. Silva AMN, Vitorino R, Domingues MRM, Spickett CM, Domingues P. Post-translational Modifications and Mass Spectrometry Detection. Free Radical Biology and Medicine. 2013 Dec;65:925–41.
206. Illiano A, Pinto G, Melchiorre C, Carpentieri A, Faraco V, Amoresano A. Protein Glycosylation Investigated by Mass Spectrometry: An Overview. Cells. 2020 Aug 28;9(9):1986.
207. Fernández-Tejada A, Brailsford J, Zhang Q, Shieh JH, Moore MAS, Danishefsky SJ. Total Synthesis of Glycosylated Proteins. In: Liu L, editor. Protein Ligation and Total Synthesis I [Internet]. Cham: Springer International Publishing; 2014 [cited 2024 Oct 28]. p. 1–26. (Topics in Current Chemistry; vol. 362). Available from: https://link.springer.com/10.1007/128_2014_622
208. Link AJ, Fleischer TC, Weaver CM, Gerbasi VR, Jennings JL. Purifying protein complexes for mass spectrometry: applications to protein translation. Methods. 2005 Mar;35(3):274–90.
209. Ryan BJ, Henehan GT. Avoiding Proteolysis During Protein Purification. In: Walls D, Loughran ST, editors. Protein Chromatography [Internet]. New York, NY: Springer New York; 2017 [cited 2024 Oct 28]. p. 53–69. (Methods in Molecular Biology; vol. 1485). Available from: http://link.springer.com/10.1007/978-1-4939-6412-3_4
210. Tang S, Tao J, Li Y. Challenges and solutions for the downstream purification of therapeutic proteins. Antibody Therapeutics. 2024 Jan 16;7(1):1–12.
211. D'Imprima E, Floris D, Joppe M, Sánchez R, Grininger M, Kühlbrandt W. Protein denaturation at the air-water interface and how to prevent it. eLife. 2019 Apr 1;8:e42747.
212. Bondos SE, Bicknell A. Detection and prevention of protein aggregation before, during, and after purification. Analytical Biochemistry. 2003 May;316(2):223–31.
213. Burgess RR. Protein Purification. In: Meyers RA, editor. Encyclopedia of Molecular Cell Biology and Molecular Medicine [Internet]. Weinheim, Germany: Wiley-VCH Verlag GmbH & Co. KGaA; 2006 [cited 2024 Oct 28]. p. mcb.200400065. Available from: https://onlinelibrary.wiley.com/doi/10.1002/3527600906.mcb.200400065
214. Kim MS, Leahy D. Enzymatic Deglycosylation of Glycoproteins. In: Methods in Enzymology [Internet]. Elsevier; 2013 [cited 2024 Oct 28]. p. 259–63. Available from: https://linkinghub.elsevier.com/retrieve/pii/B9780124200678000192
215. Hägglund P, Matthiesen R, Elortza F, Højrup P, Roepstorff P, Jensen ON, et al. An Enzymatic Deglycosylation Scheme Enabling Identification of Core Fucosylated *N* -Glycans and O-Glycosylation Site Mapping of Human Plasma Proteins. J Proteome Res. 2007 Aug 1;6(8):3021–31.
216. Baker HM, Day CL, Norris GE, Baker EN. Enzymatic deglycosylation as a tool for crystallization of mamalian binding proteins. Acta Crystallogr D Biol Crystallogr. 1994 Jul 1;50(4):380–4.
217. Kamerling JP, Gerwig GJ. Strategies for the Structural Analysis of Carbohydrates. In: Comprehensive Glycoscience [Internet]. Elsevier; 2007 [cited 2024 Oct 28]. p. 1–68. Available from: https://linkinghub.elsevier.com/retrieve/pii/B9780444519672000325
218. Nakakita S ichi, Sumiyoshi W, Miyanishi N, Hirabayashi J. A practical approach to N-glycan production by hydrazinolysis using hydrazine monohydrate. Biochemical and Biophysical Research Communications. 2007 Oct;362(3):639–45.
219. Friganović T, Borko V, Weitner T. Optimization of enzymatic desialylation of human serum transferrin. Maced Pharm Bull. 2022 Dec 31;68(03):415–6.

220. Kishino S, Miyazaki K. Separation methods for glycoprotein analysis and preparation. Journal of Chromatography B: Biomedical Sciences and Applications. 1997 Oct;699(1–2):371–81.
221. Freeze HH. Lectin Affinity Chromatography. CP Protein Science [Internet]. 1995 Jun [cited 2024 Oct 28];00(1). Available from: https://currentprotocols.onlinelibrary.wiley.com/doi/10.1002/0471140864.ps0901s00
222. Wuhrer M, Deelder A, Hokke C. Protein glycosylation analysis by liquid chromatography–mass spectrometry. Journal of Chromatography B. 2005 Oct 25;825(2):124–33.
223. Willey DG, Rosenthal MA, Caldwell S. Glycosylated haemoglobin and plasma glycoprotein assays by affinity chromatography. Diabetologia [Internet]. 1984 Jul [cited 2024 Oct 28];27(1). Available from: http://link.springer.com/10.1007/BF00253503
224. Pedrali A, Tengattini S, Marrubini G, Bavaro T, Hemström P, Massolini G, et al. Characterization of Intact Neo-Glycoproteins by Hydrophilic Interaction Liquid Chromatography. Molecules. 2014 Jun 30;19(7):9070–88.
225. Ahamed T, Nfor BK, Verhaert PDEM, Van Dedem GWK, Van Der Wielen LAM, Eppink MHM, et al. pH-gradient ion-exchange chromatography: An analytical tool for design and optimization of protein separations. Journal of Chromatography A. 2007 Sep;1164(1–2):181–8.
226. Kaliszan R, Wiczling P, Markuszewski MJ. pH gradient high-performance liquid chromatography: theory and applications. Journal of Chromatography A. 2004 Dec;1060(1–2):165–75.
227. Kröner F, Hubbuch J. Systematic generation of buffer systems for pH gradient ion exchange chromatography and their application. Journal of Chromatography A. 2013 Apr;1285:78–87.
228. Reinmuth-Selzle K, Tchipilov T, Backes AT, Tscheuschner G, Tang K, Ziegler K, et al. Determination of the protein content of complex samples by aromatic amino acid analysis, liquid chromatography-UV absorbance, and colorimetry. Anal Bioanal Chem. 2022 Jun;414(15):4457–70.
229. Stoscheck CM. [6] Quantitation of protein. In: Methods in Enzymology [Internet]. Elsevier; 1990 [cited 2024 Oct 28]. p. 50–68. Available from: https://linkinghub.elsevier.com/retrieve/pii/007668799082008P
230. Albahri Z, Marklová E, Vaníček H, Minxová L, Dédek P, Skálová S. Genetic variants of transferrin in the diagnosis of protein hypoglycosylation. J of Inher Metab Disea. 2005 Dec;28(6):1184–8.
231. Caslavska J, Lanz C, Burda P, Tobler M, Thormann W. Analysis of genetic variants of transferrin in human serum after desialylation by capillary zone electrophoresis and capillary isoelectric focusing. J of Separation Science. 2017 Jun;40(11):2488–97.
232. Trbojević-Akmačić I, Vučković F, Pribić T, Vilaj M, Černigoj U, Vidič J, et al. Comparative analysis of transferrin and IgG N-glycosylation in two human populations. Commun Biol. 2023 Mar 23;6(1):312.
233. Plummer TH, Elder JH, Alexander S, Phelan AW, Tarentino AL. Demonstration of peptide:N-glycosidase F activity in endo-beta-N-acetylglucosaminidase F preparations. Journal of Biological Chemistry. 1984 Sep;259(17):10700–4.
234. Norris GE, Stillman TJ, Anderson BF, Baker EN. The three-dimensional structure of PNGase F, a glycosyl asparaginase from Flavobacterium meningosepticum. Structure. 1994 Nov;2(11):1049–59.
235. Hua L, Gao X, Yang X, Wan D, He C, Cao J, et al. Highly efficient production of peptides: N-glycosidase F for N-glycomics analysis. Protein Expression and Purification. 2014 May;97:17–22.

236. Štambuk T, Cvetko A, Weitner T. Protocol for ultra performance liquid chromatography-mass spectrometry N-glycan analysis of the native and desialylated human apo-transferrin [Internet]. Zenodo; 2020 Aug [cited 2024 Oct 28]. Available from: https://zenodo.org/record/4006017
237. Saldova R, Asadi Shehni A, Haakensen VD, Steinfeld I, Hilliard M, Kifer I, et al. Association of N-Glycosylation with Breast Carcinoma and Systemic Features Using High-Resolution Quantitative UPLC. J Proteome Res. 2014 May 2;13(5):2314–27.
238. Zhao S, Walsh I, Abrahams JL, Royle L, Nguyen-Khuong T, Spencer D, et al. GlycoStore: a database of retention properties for glycan analysis. Kelso J, editor. Bioinformatics. 2018 Sep 15;34(18):3231–2.
239. Cooper CA, Gasteiger E, Packer NH. GlycoMod - A software tool for determining glycosylation compositions from mass spectrometric data. Proteomics. 2001 Feb;1(2):340–9.
240. Ceroni A, Maass K, Geyer H, Geyer R, Dell A, Haslam SM. GlycoWorkbench: A Tool for the Computer-Assisted Annotation of Mass Spectra of Glycans. J Proteome Res. 2008 Apr 1;7(4):1650–9.
241. Ramanujam N. Fluorescence Spectroscopy In Vivo. In: Meyers RA, editor. Encyclopedia of Analytical Chemistry [Internet]. 1st ed. Wiley; 2000 [cited 2024 Oct 28]. Available from: https://onlinelibrary.wiley.com/doi/10.1002/9780470027318.a0102
242. Bright FV. Bioanalytical applications of fluorescence spectroscopy. Anal Chem. 1988 Sep 15;60(18):1031A-1039A.
243. Valeur B, Berberan-Santos MN. Molecular Fluorescence: Principles and Applications [Internet]. 1st ed. Wiley; 2012 [cited 2023 Mar 13]. Available from: https://onlinelibrary.wiley.com/doi/book/10.1002/9783527650002
244. Kuyper CL, Fujimoto BS, Zhao Y, Schiro PG, Chiu DT. Accurate Sizing of Nanoparticles Using Confocal Correlation Spectroscopy. J Phys Chem B. 2006 Dec 1;110(48):24433–41.
245. Basic Properties and Measuring Methods of Nanoparticles. In: Nanoparticle Technology Handbook [Internet]. Elsevier; 2018 [cited 2024 Jul 7]. p. 3–47. Available from: https://linkinghub.elsevier.com/retrieve/pii/B9780444641106000019
246. Wolfbeis OS. An overview of nanoparticles commonly used in fluorescent bioimaging. Chem Soc Rev. 2015;44(14):4743–68.
247. Xiao D, Qi H, Teng Y, Pierre D, Kutoka PT, Liu D. Advances and Challenges of Fluorescent Nanomaterials for Synthesis and Biomedical Applications. Nanoscale Res Lett. 2021 Nov 27;16(1):167.
248. Moerner WE (William E). Single-Molecule Spectroscopy, Imaging, and Photocontrol: Foundations for Super-Resolution Microscopy (Nobel Lecture). Angew Chem Int Ed. 2015 Jul 6;54(28):8067–93.
249. Weiss S. Fluorescence Spectroscopy of Single Biomolecules. Science. 1999 Mar 12;283(5408):1676–83.
250. Volpato A, Ollech D, Alvelid J, Damenti M, Müller B, York AG, et al. Extending fluorescence anisotropy to large complexes using reversibly switchable proteins. Nat Biotechnol. 2023 Apr;41(4):552–9.
251. Zhao J. Studying the physics of charged macromolecules by single molecule fluorescence spectroscopy. The Journal of Chemical Physics. 2020 Nov 7;153(17):170903.
252. Schwille P, Haupts U, Maiti S, Webb WW. Molecular Dynamics in Living Cells Observed by Fluorescence Correlation Spectroscopy with One- and Two-Photon Excitation. Biophysical Journal. 1999 Oct;77(4):2251–65.
253. Lakowicz JR, editor. Instrumentation for Fluorescence Spectroscopy. In: Principles of Fluorescence Spectroscopy [Internet]. Boston, MA: Springer US; 2006 [cited 2023 Mar 13]. p. 27–61. Available from: https://link.springer.com/10.1007/978-0-387-46312-4_2

254. Mathies RA, Peck Konan, Stryer Lubert. Optimization of high-sensitivity fluorescence detection. Anal Chem. 1990 Sep 1;62(17):1786–91.
255. Dos Santos Rodrigues FH, Delgado GG, Santana Da Costa T, Tasic L. Applications of fluorescence spectroscopy in protein conformational changes and intermolecular contacts. BBA Advances. 2023;3:100091.
256. Wang F, Wen J, Huang L, Huang J, Ouyang J. A highly sensitive "switch-on" fluorescent probe for protein quantification and visualization based on aggregation-induced emission. Chem Commun. 2012;48(59):7395.
257. Wang C, Zhou Y, Zhang KX, Nie XG, Xia XH. Fast and sensitive detection of protein concentration in mild environments. Talanta. 2015 Apr;135:102–7.
258. Gao Z, Hao Y, Zheng M, Chen Y. A fluorescent dye with large Stokes shift and high stability: synthesis and application to live cell imaging. RSC Adv. 2017;7(13):7604–9.
259. Shcherbakova DM, Hink MA, Joosen L, Gadella TWJ, Verkhusha VV. An Orange Fluorescent Protein with a Large Stokes Shift for Single-Excitation Multicolor FCCS and FRET Imaging. J Am Chem Soc. 2012 May 9;134(18):7913–23.
260. Baird FJ, Wadsworth MP, Hill JE. Evaluation and optimization of multiple fluorophore analysis of a Pseudomonas aeruginosa biofilm. Journal of Microbiological Methods. 2012 Sep;90(3):192–6.
261. Meagher JL, Beechem JM, Olson ST, Gettins PGW. Deconvolution of the Fluorescence Emission Spectrum of Human Antithrombin and Identification of the Tryptophan Residues That Are Responsive to Heparin Binding. Journal of Biological Chemistry. 1998 Sep;273(36):23283–9.
262. Djikanović D, Devečerski A, Steinbach G, Simonović J, Matović B, Garab G, et al. Comparison of macromolecular interactions in the cell walls of hardwood, softwood and maize by fluorescence and FTIR spectroscopy, differential polarization laser scanning microscopy and X-ray diffraction. Wood Sci Technol. 2016 May;50(3):547–66.
263. Lamb JJ, Røkke G, Hohmann-Marriott MF. Chlorophyll fluorescence emission spectroscopy of oxygenic organisms at 77 K. Photosynt. 2018 Mar 1;56(SPECIAL ISSUE):105–24.
264. Boens N, Qin W, Basarić N, Hofkens J, Ameloot M, Pouget J, et al. Fluorescence Lifetime Standards for Time and Frequency Domain Fluorescence Spectroscopy. Anal Chem. 2007 Mar 1;79(5):2137–49.
265. Kuznetsov NA. Conformational Dynamics of Biopolymers in the Course of Their Interaction: Multifaceted Approaches to the Analysis by the Stopped-Flow Technique with Fluorescence Detection. Photonics. 2023 Sep 8;10(9):1033.
266. Trepman E, Chen RF. Fluorescence stopped-flow study of the o-phthaldialdehyde reaction. Archives of Biochemistry and Biophysics. 1980 Oct;204(2):524–32.
267. Alvarez-Pez JM, Ballesteros L, Talavera E, Yguerabide J. Fluorescein Excited-State Proton Exchange Reactions: Nanosecond Emission Kinetics and Correlation with Steady-State Fluorescence Intensity. J Phys Chem A. 2001 Jul 1;105(26):6320–32.
268. Itoh T. Fluorescence and Phosphorescence from Higher Excited States of Organic Molecules. Chem Rev. 2012 Aug 8;112(8):4541–68.
269. Salas Redondo C, Kleine P, Roszeitis K, Achenbach T, Kroll M, Thomschke M, et al. Interplay of Fluorescence and Phosphorescence in Organic Biluminescent Emitters. J Phys Chem C. 2017 Jul 13;121(27):14946–53.
270. Cannon TM, Shah AT, Walsh AJ, Skala MC. High-throughput measurements of the optical redox ratio using a commercial microplate reader. J Biomed Opt. 2015 Jan 29;20(1):010503.

271. Hidayat MA, Fitri A, Kuswandi B. Scanometry as microplate reader for high throughput method based on DPPH dry reagent for antioxidant assay. Acta Pharmaceutica Sinica B. 2017 May;7(3):395–400.
272. Galgani F, Bocquene G. Semi-automated colorimetric and enzymatic assays for aquatic organisms using microplate readers. Water Research. 1991 Feb;25(2):147–50.
273. Weitner T, Friganović T, Šakić D. Inner Filter Effect Correction for Fluorescence Measurements in Microplates Using Variable Vertical Axis Focus. Anal Chem. 2022 May 17;94(19):7107–14.
274. Ennis C. Corning® 384 Well Low Volume Microplate Performance in Miniaturized Assays. Journal of the Association for Laboratory Automation. 2001 May 1;6(2):33–5.
275. Kolb AJ, Neumann K. Beyond the 96-Well Microplate: Instruments and Assay Methods for the 384-Well Format. SLAS Discovery. 1997 Mar;2(2):103–9.
276. Novikov E, Stobiecka A, Boens N. Analysis of Fluorometric Titration Curves. J Phys Chem A. 2000 Jun 1;104(22):5388–95.
277. Kowalczyk A, Boens N, Van Den Bergh V, De Schryver FC. Determination of the Ground-State Dissociation Constant by Fluorometric Titration. J Phys Chem. 1994 Aug;98(34):8585–90.
278. Sadlej-Sosnowska N. Fluorometric determination of association constants of three estrogens with cyclodextrins. J Fluoresc. 1997 Sep;7(3):195–200.
279. Naik DV, Paul WLarry, Threatte RM, Schulman SG. Fluorometric determination of drug-protein association constants. Binding of 8-anilino-1-naphthalenesulfonate by bovine serum albumin. Anal Chem. 1975 Feb 1;47(2):267–70.
280. Rockey JH, Li W, Eccleston JF. Binding of fluorescein and carboxyfluorescein by human serum proteins: Significance of kinetic and equilibrium parameters of association in ocular fluorometric studies. Experimental Eye Research. 1983 Nov;37(5):455–66.
281. Loukas YL. Multiple Complex Formation of Fluorescent Compounds with Cyclodextrins: Efficient Determination and Evaluation of the Binding Constant with Improved Fluorometric Studies. J Phys Chem B. 1997 Jun 1;101(24):4863–6.
282. Naik DV, Larry Paul W, Schulman SG. Fluorometric Determination of Drug-Protein Association Constants: Binding of Pamaquine by Bovine Serum Albumin. Journal of Pharmaceutical Sciences. 1975 Oct;64(10):1677–80.
283. Kashanian S, Javanmardi S, Chitsazan A, Paknejad M, Omidfar K. Fluorometric study of fluoxetine DNA binding. Journal of Photochemistry and Photobiology B: Biology. 2012 Aug;113:1–6.
284. Rothwarf DM, Scheraga HA. Equilibrium and kinetic constants for the thiol-disulfide interchange reaction between glutathione and dithiothreitol. Proc Natl Acad Sci USA. 1992 Sep;89(17):7944–8.
285. Bhaumik ML. Quenching and Temperature Dependence of Fluorescence in Rare-Earth Chelates. The Journal of Chemical Physics. 1964 Jun 15;40(12):3711–5.
286. Parkhomenko AI, Shalagin AM. Effect of collisions on the resonance fluorescence spectrum. J Exp Theor Phys. 2008 May;106(5):858–68.
287. Fairchild PW, Smith GP, Crosley DR. Collisional quenching of *A* 2Σ+ OH at elevated temperatures. The Journal of Chemical Physics. 1983 Aug 15;79(4):1795–807.
288. Fedunov RG, Yermolenko IP, Nazarov AE, Ivanov AI, Rosspeintner A, Angulo G. Theory of fluorescence spectrum dynamics and its application to determining the relaxation characteristics of the solvent and intramolecular vibrations. Journal of Molecular Liquids. 2020 Jan;298:112016.
289. Albani JR. Fluorescence Quenching. In: Structure and Dynamics of Macromolecules: Absorption and Fluorescence Studies [Internet]. Elsevier; 2004 [cited 2024 Oct 28]. p. 141–92. Available from: https://linkinghub.elsevier.com/retrieve/pii/B9780444514493500046

290. Kim IJ, Xu Y, Nam KH. Metal-Induced Fluorescence Quenching of Photoconvertible Fluorescent Protein DendFP. Molecules. 2022 May 3;27(9):2922.
291. Varnes AW, Dodson RB, Wehry EL. Interactions of transition-metal ions with photoexcited states of flavines. Fluorescence quenching studies. J Am Chem Soc. 1972 Feb;94(3):946–50.
292. Gehlen MH. The centenary of the Stern-Volmer equation of fluorescence quenching: From the single line plot to the SV quenching map. Journal of Photochemistry and Photobiology C: Photochemistry Reviews. 2020 Mar;42:100338.
293. Park HR, Oh CH, Lee HC, Choi JG, Jung BI, Bark KM. Quenching of Ofloxacin and Flumequine Fluorescence by Divalent Transition Metal Cations. Bulletin of the Korean Chemical Society. 2006 Dec 20;27(12):2002–10.
294. Lovell JF, Chen J, Jarvi MT, Cao WG, Allen AD, Liu Y, et al. FRET Quenching of Photosensitizer Singlet Oxygen Generation. J Phys Chem B. 2009 Mar 12;113(10):3203–11.
295. Dworak L, Reuss AJ, Zastrow M, Rück-Braun K, Wachtveitl J. Discrimination between FRET and non-FRET quenching in a photochromic CdSe quantum dot/dithienylethene dye system. Nanoscale. 2014;6(23):14200–3.
296. Jiang L, Xiong Z, Song Y, Lu Y, Chen Y, Schultz JS, et al. Protein–Protein Affinity Determination by Quantitative FRET Quenching. Sci Rep. 2019 Feb 14;9(1):2050.
297. Van Drogen F, Peter M. Revealing Protein Dynamics by Photobleaching Techniques. In: Signal Transduction Protocols [Internet]. New Jersey: Humana Press; 2004 [cited 2024 Oct 28]. p. 287–306. Available from: http://link.springer.com/10.1385/1-59259-816-1:287
298. Houtsmuller AB. Fluorescence Recovery after Photobleaching: Application to Nuclear Proteins. In: Rietdorf J, editor. Microscopy Techniques [Internet]. Berlin, Heidelberg: Springer Berlin Heidelberg; 2005 [cited 2024 Oct 28]. p. 177–99. (Advances in Biochemical Engineering/Biotechnology; vol. 95). Available from: http://link.springer.com/10.1007/b102214
299. Klonis N, Rug M, Harper I, Wickham M, Cowman A, Tilley L. Fluorescence photobleaching analysis for the study of cellular dynamics. Eur Biophys J. 2002 Mar;31(1):36–51.
300. Eggeling C, Widengren J, Rigler R, Seidel CAM. Photobleaching of Fluorescent Dyes under Conditions Used for Single-Molecule Detection: Evidence of Two-Step Photolysis. Anal Chem. 1998 Jul 1;70(13):2651–9.
301. Kenworthy AK. Photobleaching FRET Microscopy. In: Molecular Imaging [Internet]. Elsevier; 2005 [cited 2024 Oct 28]. p. 146–64. Available from: https://linkinghub.elsevier.com/retrieve/pii/B9780195177206500171
302. Waters JC. Live-Cell Fluorescence Imaging. In: Methods in Cell Biology [Internet]. Elsevier; 2013 [cited 2024 Oct 28]. p. 125–50. Available from: https://linkinghub.elsevier.com/retrieve/pii/B9780124077614000063
303. Thordarson P. Determining association constants from titration experiments in supramolecular chemistry. Chem Soc Rev. 2011;40(3):1305–23.
304. Wortmann A, Jecklin MC, Touboul D, Badertscher M, Zenobi R. Binding constant determination of high-affinity protein–ligand complexes by electrospray ionization mass spectrometry and ligand competition. J Mass Spectrom. 2008 May;43(5):600–8.
305. Stootman FH, Fisher DM, Rodger A, Aldrich-Wright JR. Improved curve fitting procedures to determine equilibrium binding constants. Analyst. 2006;131(10):1145.
306. Barbieri B, Terpetschnig E, Jameson DM. Frequency-domain fluorescence spectroscopy using 280-nm and 300-nm light-emitting diodes: Measurement of proteins and protein-related fluorophores. Analytical Biochemistry. 2005 Sep;344(2):298–300.

307. Ghisaidoobe A, Chung S. Intrinsic Tryptophan Fluorescence in the Detection and Analysis of Proteins: A Focus on Förster Resonance Energy Transfer Techniques. IJMS. 2014 Dec 5;15(12):22518–38.
308. Chasteen ND, Williams J. The influence of pH on the equilibrium distribution of iron between the metal-binding sites of human transferrin. Biochemical Journal. 1981 Mar 1;193(3):717–27.
309. Elving PJ, Markowitz JM, Rosenthal Isadore. Preparation of Buffer Systems of Constant Ionic Strength. Anal Chem. 1956 Jul 1;28(7):1179–80.
310. Friganović T, Weitner T. Reducing the Inner Filter Effect in Microplates by Increasing Absorbance? Linear Fluorescence in Highly Concentrated Fluorophore Solutions in the Presence of an Added Absorber. Anal Chem. 2023 Sep 5;95(35):13036–45.
311. Fonin AV, Sulatskaya AI, Kuznetsova IM, Turoverov KK. Fluorescence of Dyes in Solutions with High Absorbance. Inner Filter Effect Correction. Permyakov EA, editor. PLoS ONE. 2014 Jul 29;9(7):e103878.
312. Kubista M, Sjöback R, Eriksson S, Albinsson B. Experimental correction for the inner-filter effect in fluorescence spectra. Analyst. 1994;119(3):417–9.
313. Wang T, Zeng LH, Li DL. A review on the methods for correcting the fluorescence inner-filter effect of fluorescence spectrum. Applied Spectroscopy Reviews. 2017 Nov 26;52(10):883–908.
314. Kumar Panigrahi S, Kumar Mishra A. Inner filter effect in fluorescence spectroscopy: As a problem and as a solution. Journal of Photochemistry and Photobiology C: Photochemistry Reviews. 2019 Dec;41:100318.
315. Luciani X, Mounier S, Redon R, Bois A. A simple correction method of inner filter effects affecting FEEM and its application to the PARAFAC decomposition. Chemometrics and Intelligent Laboratory Systems. 2009 Apr;96(2):227–38.
316. Kothawala DN, Murphy KR, Stedmon CA, Weyhenmeyer GA, Tranvik LJ. Inner filter correction of dissolved organic matter fluorescence: Correction of inner filter effects. Limnol Oceanogr Methods. 2013 Dec;11(12):616–30.
317. Holland JF, Teets RE, Kelly PM, Timnick Andrew. Correction of right-angle fluorescence measurements for the absorption of excitation radiation. Anal Chem. 1977 May 1;49(6):706–10.
318. Panigrahi SK, Mishra AK. Study on the dependence of fluorescence intensity on optical density of solutions: the use of fluorescence observation field for inner filter effect corrections. Photochem Photobiol Sci. 2019 Feb;18(2):583–91.
319. Albani JR. Fluorescence: Principles and Observables. In: Structure and Dynamics of Macromolecules: Absorption and Fluorescence Studies [Internet]. Elsevier; 2004 [cited 2024 Oct 28]. p. 55–98. Available from: https://linkinghub.elsevier.com/retrieve/pii/B9780444514493500022
320. Cardoso MC. Fluorescence Microscopy: Spectral Imaging vs. Filter-based Imaging. In: Encyclopedic Reference of Genomics and Proteomics in Molecular Medicine [Internet]. Berlin, Heidelberg: Springer Berlin Heidelberg; 2005 [cited 2024 Oct 28]. p. 583–6. Available from: https://link.springer.com/10.1007/3-540-29623-9_5560
321. Yappert MC, Ingle JD. Correction of Polychromatic Luminescence Signals for Inner-Filter Effects. Appl Spectrosc. 1989 Jul;43(5):759–67.
322. Ficek Z, Freedhoff HS. VI Spectroscopy in polychromatic fields. In: Progress in Optics [Internet]. Elsevier; 2000 [cited 2024 Oct 28]. p. 389–441. Available from: https://linkinghub.elsevier.com/retrieve/pii/S0079663800800347
323. Ceresa L, Kimball J, Chavez J, Kitchner E, Nurekeyev Z, Doan H, et al. On the origin and correction for inner filter effects in fluorescence. Part II: secondary inner filter effect -the

proper use of front-face configuration for highly absorbing and scattering samples. Methods Appl Fluoresc. 2021 Jul 1;9(3):035005.
324. Chen S, Yu YL, Wang JH. Inner filter effect-based fluorescent sensing systems: A review. Analytica Chimica Acta. 2018 Jan;999:13–26.
325. Winkelman JW, Grossman Judith. Quantitative fluorescence analysis in opaque suspensions using front face optics. Anal Chem. 1967 Jul 1;39(8):1007–9.
326. Sádecká J, Tóthová J. Fluorescence spectroscopy and chemometrics in the food classification - a review. Czech J Food Sci. 2007 Aug 31;25(4):159–74.
327. McGown EL. UV Absorbance Measurements of DNA in Microplates. BioTechniques. 2000 Jan;28(1):60–4.
328. Zeng LH, Wang C, Wang T, Li DL. The correction fluorescence inner filter effect using a single excitation and dual-emission fiber optic probe. Analyst. 2016;141(18):5339–45.
329. Lutz HP, Luisi PL. Correction for Inner Filter Effects in Fluorescence Spectroscopy. Helv Chim Acta. 1983 Nov 2;66(7):1929–35.
330. Larsson T, Wedborg M, Turner D. Correction of inner-filter effect in fluorescence excitation-emission matrix spectrometry using Raman scatter. Analytica Chimica Acta. 2007 Feb;583(2):357–63.
331. Nettles CB, Hu J, Zhang D. Using Water Raman Intensities To Determine the Effective Excitation and Emission Path Lengths of Fluorophotometers for Correcting Fluorescence Inner Filter Effect. Anal Chem. 2015 May 5;87(9):4917–24.
332. Bauer N, Fröhlich DR, Panak PJ. Interaction of Cm(III) and Am(III) with human serum transferrin studied by time-resolved laser fluorescence and EXAFS spectroscopy. Dalton Trans. 2014 Mar 14;43(18):6689–700.
333. Sturzbecher-Hoehne M, Goujon C, Deblonde GJP, Mason AB, Abergel RJ. Sensitizing Curium Luminescence through an Antenna Protein To Investigate Biological Actinide Transport Mechanisms. J Am Chem Soc. 2013 Feb 20;135(7):2676–83.
334. Chikh Z, Hémadi M, Miquel G, Ha-Duong NT, El Hage Chahine JM. Cobalt and the Iron Acquisition Pathway: Competition towards Interaction with Receptor 1. Journal of Molecular Biology. 2008 Jul;380(5):900–16.
335. Mach H, Middaugh CR, Lewis RV. Statistical determination of the average values of the extinction coefficients of tryptophan and tyrosine in native proteins. Analytical Biochemistry. 1992 Jan;200(1):74–80.
336. Simonian(spectrophotometric Methods) MH, Smith(colorimetric Methods) JA. Spectrophotometric and Colorimetric Determination of Protein Concentration. CP Toxicology [Internet]. 2001 Nov [cited 2024 Oct 28];10(1). Available from: https://currentprotocols.onlinelibrary.wiley.com/doi/10.1002/0471140856.txa03gs10
337. MacGillivray RT, Mendez E, Sinha SK, Sutton MR, Lineback-Zins J, Brew K. The complete amino acid sequence of human serum transferrin. Proc Natl Acad Sci USA. 1982 Apr;79(8):2504–8.
338. Baldwin GS. Comparison of transferrin sequences from different species. Comparative Biochemistry and Physiology Part B: Comparative Biochemistry. 1993 Sep;106(1):203–18.
339. Gill SC, Von Hippel PH. Calculation of protein extinction coefficients from amino acid sequence data. Analytical Biochemistry. 1989 Nov;182(2):319–26.
340. James NG, Mason AB. Protocol to determine accurate absorption coefficients for iron-containing transferrins. Analytical Biochemistry. 2008 Jul;378(2):202–7.
341. Bobály B, Sipkó E, Fekete J. Challenges in liquid chromatographic characterization of proteins. Journal of Chromatography B. 2016 Oct;1032:3–22.

342. Tsonev LI, Hirsh AG. Theory and applications of a novel ion exchange chromatographic technology using controlled pH gradients for separating proteins on anionic and cationic stationary phases. Journal of Chromatography A. 2008 Jul;1200(2):166–82.
343. Hirsh AG, Tsonev LI. Multiple, simultaneous, independent gradients for a versatile multidimensional liquid chromatography. Part II: Application 2: Computer controlled pH gradients in the presence of urea provide improved separation of proteins: Stability influenced anion and cation exchange chromatography. Journal of Chromatography A. 2017 Apr;1495:22–30.
344. Bates GW, Billups C, Saltman P. The Kinetics and Mechanism of Iron(III) Exchange between Chelates and Transferrin. Journal of Biological Chemistry. 1967 Jun;242(12):2810–5.
345. Bates GW, Wernicke J. The Kinetics and Mechanism of Iron (III) Exchange between Chelates and Transferrin IV. THE REACTION OF TRANSFERRIN WITH IRON(III) NITRILOTRIACETATE. J Biol Chem. 1971 Jun 10;246(11):3679–85.
346. Harmuth-Hoene AE, Vladár M, Ohrtmann R. Iron(III)-exchange between transferrin and chelates in vitro. Chemico-Biological Interactions. 1970 Feb;1(3):271–83.
347. Bates GW, Schlabach MR. The Reaction of Ferric Salts with Transferrin. Journal of Biological Chemistry. 1973 May;248(9):3228–32.
348. Ahrland S, Dahlgren Å, Persson I. Stabilities and Hydrolysis of Some Iron(III) and Manganese(III) Complexes with Chelating Ligands. Acta Agriculturae Scandinavica. 1990 Jan;40(2):101–11.
349. Stefánsson A. Iron(III) Hydrolysis and Solubility at 25 °C. Environmental Science & Technology. 2007 Sep;41(17):6117–23.
350. Freire E, Schön A, Velazquez-Campoy A. Chapter 5 Isothermal Titration Calorimetry. In: Methods in Enzymology [Internet]. Elsevier; 2009 [cited 2024 Apr 27]. p. 127–55. Available from: https://linkinghub.elsevier.com/retrieve/pii/S0076687908042055
351. Cattoni DI, Chara O, Kaufman SB, González Flecha FL. Cooperativity in Binding Processes: New Insights from Phenomenological Modeling. Papaleo E, editor. PLoS ONE. 2015 Dec 30;10(12):e0146043.
352. Sevlever F, Di Bella JP, Ventura AC. Discriminating between negative cooperativity and ligand binding to independent sites using pre-equilibrium properties of binding curves. Finley S, editor. PLoS Comput Biol. 2020 Jun 4;16(6):e1007929.
353. Harris DC. Nonlinear Least-Squares Curve Fitting with Microsoft Excel Solver. J Chem Educ. 1998 Jan;75(1):119.
354. Jan SL, Shieh G. A systematic approach to designing statistically powerful heteroscedastic 2 × 2 factorial studies while minimizing financial costs. BMC Med Res Methodol. 2016 Dec;16(1):114.
355. Armitage P, Berry G, Matthews JNS. Statistical Methods in Medical Research [Internet]. 1st ed. Wiley; 2002 [cited 2024 Apr 27]. Available from: https://onlinelibrary.wiley.com/doi/book/10.1002/9780470773666
356. Satterthwaite FE. An Approximate Distribution of Estimates of Variance Components. Biometrics Bulletin. 1946 Dec;2(6):110.
357. Martin RB, Savory J, Brown S, Bertholf RL, Wills MR. Transferrin binding of Al3+ and Fe3+. Clinical Chemistry. 1987 Mar 1;33(3):405–7.
358. Aisen P, Leibman A, Zweier J. Stoichiometric and site characteristics of the binding of iron to human transferrin. J Biol Chem. 1978 Mar 25;253(6):1930–7.
359. To Yue K, Lee M, Zheng J, Callender R. The determination of the pKa of histidine residues in proteins by Raman difference spectroscopy. Biochimica et Biophysica Acta (BBA) - Protein Structure and Molecular Enzymology. 1991 Jun;1078(2):296–302.

360. Galley HF, Webster NR. Acidosis and Tissue Hypoxia in the Critically III: How to Measure it and What Does it Mean. Critical Reviews in Clinical Laboratory Sciences. 1999 Jan;36(1):35–60.
361. Emmett M. Review of Clinical Disorders Causing Metabolic Acidosis. Advances in Chronic Kidney Disease. 2022 Jul;29(4):355–63.
362. Hung CH, Chin Y, Fong YO, Lee CH, Han DS, Lin JH, et al. Acidosis-related pain and its receptors as targets for chronic pain. Pharmacology & Therapeutics. 2023 Jul;247:108444.

9. ŽIVOTOPIS

Tomislav Friganović rođen je 10. 1. 1992. godine u Zagrebu, gdje ujedno završava osnovnoškolsko i srednjoškolsko obrazovanje. Nakon polaganja državne mature upisuje istraživački smjer kemije na Prirodoslovno-matematičkom fakultetu. Na diplomskom studiju odabire smjerove fizikalne i anorganske kemije. Tijekom diplomskog studija, zajedno s kolegom Jurjem Nikolićem, biva nagrađen Rektorovom nagradom za rad pod nazivom „Utjecaj aminskih kompleksa kobalta(III) na nastajanje polioksomolibdata“. Rad je izrađen pod stručnim vodstvom prof. dr. sc. Marine Cindrić. Diplomirao je radom pod naslovom „Kompleksni spojevi nikla(II) s hidrazonskim ligandima: sinteza, karakterizacija i kvantno-kemijski proračuni“ izrađenim pod mentorstvom prof. dr. sc. Višnje Vrdoljak (eksperimentalni dio rada) i prof. dr. sc. Tomice Hrenara (kvantno-kemijski proračuni). 2018. godine zapošljava se na Farmaceutsko-biokemijskom fakultetu kao doktorand na projektu „Glikozilacija serumskog transferina kao faktor u mehanizmu prijenosa željeza“ vođenom od strane prof. dr. sc. Tina Weitnera i sufinanciranog od strane Hrvatske zaklade za znanost. Tijekom rada na fakultetu sudjeluje u izvođenju obveznog kolegija Opća kemija sa stehiometrijom, kao i izbornog kolegija Metaloproteini: struktura i mehanizam. Neposredno je vodio izradu jednog diplomskog rada. Ostvario je višestruka sudjelovanja na raznim znanstvenim konferencijama/skupovima. 2023. zapošljava se u svojstvu stručnog suradnika na Zavodu za eksperimentalnu fiziku na Prirodoslovno-matematičkom fakultetu. Do pisanja ovog životopisa, objavio je 8 znanstvenih radova, od kojih je 7 uvršteno u *Web of Science Core Collection* bazu. Rad pod nazivom „Protein sialylation affects the pH-dependent binding of ferric ion to human serum transferrin“ uvršten je u kolekciju „Dalton Transactions HOT Articles,“ koja obuhvaća 10 % najboljih radova u tromjesečju, prema odabiru urednika i/ili recenzenata.

Popis znanstvenih radova (WoSCC):

1. **Friganović T**, Borko V, Weitner T. Protein sialylation affects the pH-dependent binding of ferric ion to human serum transferrin. Dalton Trans. 2024;53(25):10462–74.
2. Borko V, **Friganović T**, Weitner T. Glycoproteomics meets thermodynamics: A calorimetric study of the effect of sialylation and synergistic anion on the binding of iron to human serum transferrin. J Inorg Biochem. 2023 Jul;244:112207.
3. **Friganović T**, Weitner T. Reducing the Inner Filter Effect in Microplates by Increasing Absorbance? Linear Fluorescence in Highly Concentrated Fluorophore Solutions in the Presence of an Added Absorber. Anal Chem. 2023 Sep 5;95(35):13036–45.
4. Borko V, **Friganović T**, Weitner T. Preparation and characterization of iron(III) nitrilotriacetate complex in aqueous solutions for quantitative protein binding experiments. Anal Methods. 2023;15(46):6499–513.
5. Vrdoljak V, Hrenar T, Rubčić M, Pavlović G, **Friganović T**, Cindrić M. Ligand-Modulated Nuclearity and Geometry in Nickel(II) Hydrazone Complexes: From Mononuclear Complexes to Acetato- and/or Phenoxido-Bridged Clusters. Int J Mol Sci. 2023 Jan 18;24(3):1909.
6. Weitner T, **Friganović T**, Šakić D. Inner Filter Effect Correction for Fluorescence Measurements in Microplates Using Variable Vertical Axis Focus. Anal Chem. 2022 May 17;94(19):7107–14.
7. **Friganović T**, Tomašić A, Šeba T, Biruš I, Kerep R, Borko V, et al. Low-pressure chromatographic separation and UV/Vis spectrophotometric characterization of the native and desialylated human apo-transferrin. Heliyon. 2021 Sep;7(9)

Popis ostalih znanstvenih radova:

1. **Friganović T**, Borko V, Weitner T. Optimization of enzymatic desialylation of human serum transferrin. Maced Pharm Bull. 2022 Dec 31;68(03):415–6.

Temeljna dokumentacijska kartica

Sveučilište u Zagrebu
Farmaceutsko-biokemijski fakultet
Zavod za opću i anorgansku kemiju
A. Kovačića 1, 10000 Zagreb, Hrvatska

Doktorski rad

UTJECAJ STUPNJA SIJALINIZACIJE LJUDSKOG SERUMSKOG TRANSFERINA NA TERMODINAMIKU VEZANJA ŽELJEZA

Tomislav Friganović

SAŽETAK

Ljudski transferin je glikoprotein koji prenosi željezo u krvi i tkivima; sastoji se od dvije domene s veznim mjestima za željezo(III). Željezo(III) tvori vrlo stabilan kompleks s transferinom putem koordinacije s aminokiselinama i sinergističkim karbonatnim ionom. Otpuštanje željeza iz transferina potpomognuto je sniženim pH endosoma i vezanjem na transferinski receptor. Transferin je visokoglikozilirani glikoprotein s vezanom sijalinskom kiselinom; u zdravih osoba najčešća glikoforma ima dva oligosaharidna lanca s četiri sijalinske kiseline. Smanjena sijalinizacija transferina opažena je u patološkim stanjima poput alkoholizma, genetskih poremećaja i tijekom sepse. Promjene u sijalinizaciji nisu nužno vezane uz patološka stanja; primjerice, tijekom trudnoće povećava se udio visoko sijaliniziranog transferina, što se nakon poroda normalizira. Utjecaj sijalinizacije transferina može značajno utjecati na prijenos i metabolizam željeza u ljudskom organizmu. U ovom radu optimizirana je priprava asijalotransferina i razvijena pH-gradijent kromatografska metoda za testiranje kvalitete desijalinizacije i razdvajanje glikoformi transferina. Viskoprotočnim fluorimetrijskim mjerenjima određene su konstante ravnoteže kojima je kvantificiran afinitet dvaju veznih mjesta nativnog i asijalotransferina prema željezu(III). Razvijena je i nova metoda korekcije učinka unutarnjeg filtra za čitače mikrotitarskih pločica, nužna za kvalitetna fluorimetrijska istraživanja. Optimizacijom enzimske desijalinizacije dobiveno je oko 100 puta više asijalotransferina nego što deklarira proizvođač. pH-gradijent kromatografija uspješno je detektirala i razdvojila nativni i asijalotransferin. Nova metoda IFE-korekcije, omogućena podešavanjem visine optičkog elementa čitača, pokazala se pogodnom za fluorimetrijske titracije transferina i kompleksa željeza(III) s nitrilotrioctenom kiselinom, bez potrebe za mjerenjem apsorbancije. Metoda je također primjenjiva i u neprozirnim mikrotitarskim pločicama. Fluorimetrijskim titracijama određene su konstante ravnoteže (pri različitim pH) formiranja kompleksa željeza(III) s transferinom. Utvrđeno je da asijalotransferin ima veći afinitet prema željezu od nativnog transferina, oko tri puta veći pri fiziološkom pH i oko deset puta veći pri približnom pH endosoma. Povećana efikasnost asijalotransferina u kiselim uvjetima može biti povezana s brzim desijalinizacijom tijekom sepse, kao odgovorom organizma koji uskraćuje željezo bakterijama. Snižavanje pH smanjuje konstante ravnoteže za obje forme transferina i oba vezna mjesta. Zapažene su promjene kooperativnosti pri vezanju, posebno je zanimljiva iznimna pozitivna kooperativnost opažena pri pH = 6,8.

Rad je pohranjen u Centralnoj knjižnici Farmaceutsko-biokemijskog fakulteta Sveučilišta u Zagrebu.

Rad sadrži:	201 stranica, 66 slika, 24 tablica i 362 literaturna navoda. Izvornik je na hrvatskom jeziku.
Ključne riječi:	ljudski transferin, željezo(III), glikozilacija, neuraminidaza, kromatografija, fluorimetrija, IFE-korekcije, konstante ravnoteže
Mentor:	**Dr. sc. Tin Weitner**, *izvanredni profesor Sveučilišta u Zagrebu Farmaceutsko-biokemijskog fakulteta*.
Ocjenjivači:	**Dr. sc. Mario Gabričević**, *redoviti profesor Sveučilišta u Zagrebu Farmaceutsko-biokemijskog fakulteta.* **Dr. sc. Viktor Pilepić**, *izvanredni profesor Sveučilišta u Zagrebu Farmaceutsko-biokemijskog fakulteta.* **Dr. sc. Vladislav Tomišić**, *redoviti profesor Sveučilišta u Zagrebu Prirodoslovno-matematičkog fakulteta.*

Rad prihvaćen: dan. mjesec 2025.

Basic documentation card

University of Zagreb
Faculty of Pharmacy and Biochemistry
Department of General and Inorganic Chemistry
A. Kovačića 1, 10000 Zagreb, Croatia

Doctoral thesis

THE INFLUENCE OF THE DEGREE OF SIALYLATION OF HUMAN SERUM TRANSFERRIN ON THE THERMODYNAMICS OF IRON BINDING

Tomislav Friganović

SUMMARY

Human transferrin is a glycoprotein responsible for iron transport in the blood and tissues; it consists of two domains with binding sites for iron(III). Iron(III) forms a very stable complex with transferrin through coordination with amino acids and a synergistic carbonate ion. The release of iron from transferrin is facilitated by the lowered pH of endosomes and by binding of transferrin to the transferrin receptor. Transferrin is a highly glycosylated glycoprotein with bound sialic acid; in healthy individuals, the most common glycoform has two oligosaccharide chains with four sialic acids. Reduced sialylation of transferrin has been observed in pathological conditions such as alcoholism, genetic disorders, and during sepsis. Changes in sialylation are not necessarily linked to pathological conditions; for example, during pregnancy, the proportion of highly sialylated transferrin increases, and normalizes postpartum. The effect of transferrin sialylation can significantly influence the transport and metabolism of iron in the human body. In this work, the preparation of asialotransferrin was optimized, and a pH-gradient chromatographic method was developed for testing the quality of desialylation and for separating transferrin glycoforms. High-throughput fluorimetric measurements were used to calculate equilibrium constants that quantify the affinity of the two binding sites of native and asialotransferrin for iron(III). A novel inner filter effect correction method suitable for microtiter plate readers was also developed, as it is necessary for high-quality fluorimetric studies. By optimizing enzymatic desialylation, approximately 100 times more asialotransferrin was obtained than declared by the manufacturer. pH-gradient chromatography successfully detected and separated native and asialotransferrin. The new IFE-correction method, enabled by adjusting the height of the optical element of the reader, proved suitable for fluorimetric titrations of transferrin and iron(III) complexes with nitrilotriacetic acid, without the need for absorbance measurement. The method is also applicable in opaque microtiter plates. Equilibrium constants for the formation of iron(III) complexes with transferrin were determined by fluorimetric titrations at different pH. It was found that asialotransferrin has a higher affinity for iron than native transferrin, about three times higher at physiological pH and about ten times higher at the approximate pH of endosomes. The increased efficiency of asialotransferrin in acidic conditions may be related to rapid desialylation during sepsis, as a response of the organism in its attempt for depriving bacteria of iron. Lowering the pH decreases the equilibrium constants for both forms of transferrin and both binding sites. Changes in binding cooperativity were observed, particularly notable is the exceptional positive cooperativity seen at pH = 6,8.

The thesis is deposited in the Central Library of the University of Zagreb Faculty of Pharmacy and Biochemistry.

Thesis contains: 201 pages, 66 figures, 24 tables and 362 references. The original was written in Croatian.
Keywords: Human transferrin, iron(III), glycosylation, neuraminidase, chromatography, fluorimetry, IFE-corrections, equilibrium constants
Mentor: **Dr. sc. Tin Weitner**, *Associate Professor, University of Zagreb Faculty of Pharmacy and Biochemistry*
Reviewers: **Dr. sc. Mario Gabričević**, *Full professor, University of Zagreb Faculty of Pharmacy and Biochemistry*
Dr. sc. Viktor Pilepić, *Associate Professor, University of Zagreb Faculty of Pharmacy and Biochemistry*
Dr. sc. Vladislav Tomišić, *Full professor, University of Zagreb Faculty of Faculty of Science*

The thesis was accepted: day month 2025.